Doctoral School in Environmental Engineering

On the effects of hydrological uncertainty in assessing the impacts of climate change on water resources

Mauricio Zambrano-Bigiarini

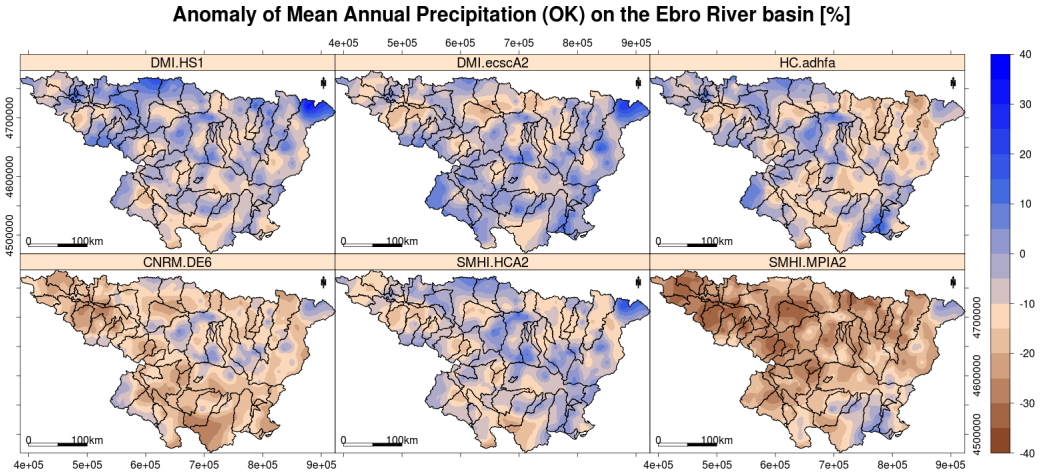

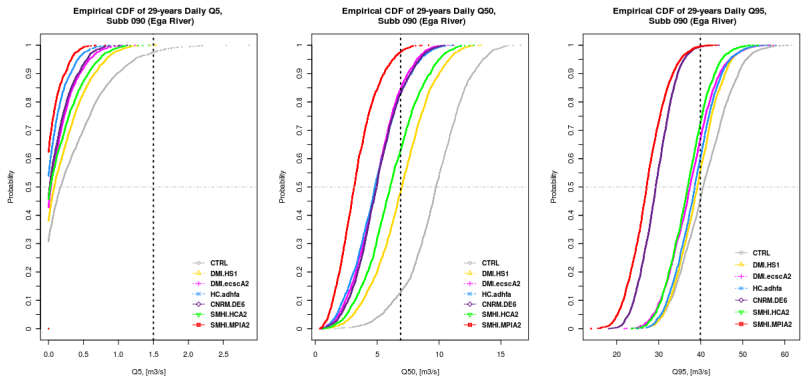

UNIVERSITÀ DEGLI STUDI DI TRENTO
Dipartimento di Ingegneria Civile e Ambientale

March 2010

Doctoral thesis in **Environmental Engineering**, **XXII** cycle
Faculty of Engineering, **University of Trento**
Academic year **2009/2010**

Advisor: **Alberto Bellin**,
Department of Civil and Environmental Engineering,
Università degli Studi di Trento,
Trento, Italy

External Advisor: **Jan Seibert**,
Department of Geography
University of Zurich - Irchel
Zürich, Switzerland

University of Trento
Trento, Italy
2010

A Carolina, mi compañera en el sendero de la vida...

Acknowledgements

"To get the full value of joy
you must have someone to divide it with".

(Mark Twain)

Seven years ago, while working at the Studies and Planning Department of the Chilean Water Office, the idea of applying to a Ph.D programme came to my mind, but I was not ready yet to take that decision. Today, after three years and a couple of months travelling through the steep and sinuous road of a Ph.D, it is hard to believe that I'm writing this acknowledgements. I thank God for giving me the courage to take the decision that bring me here, and for giving me the strength to finish it.

I would like to thank my advisor, Alberto Bellin, for challenging every decision I took during this programme, for always demanding better results, and for providing the necessary funds to attend conferences, meetings, summer schools and other research activities that contributed very much to my formation as hydrologist. I really appreciate his guidance, his example as a researcher, the freedom he gave me and the trust he put on me to discuss the due course of this research. I also want to thank Jan Seibert, for giving very valuable comments in some crucial moments of this research, for encouraging me to go forward, and for pushing me to leave the office and go to the field (even if I could not make it within the limited time of this research), to look for physical links to the mathematical results.

During all this period I have put a lot of effort to learn about hydrological processes and the appropriate methodologies for facing some of the many challenges they pose. Therefore, I am very grateful to Isabella Bovolo, and Stephen Blenkinsop for providing a more climatic point of view to the results of this work, and for giving me full support during a short visiting period to the Newcastle University during the last part of this research. At the other hand, I also want to thank Karim Abbaspour for his rapid and very valuable support for solving some issues raised during the implementation of the GLUE analysis within SWAT-CUP. At the same time, I'm grateful to Nancy Sammons and other members of the SWAT team, that always were available for giving a fast answer to my questions regarding the implementation of the SWAT model.

A special mention deserves my friend and ex-colleague Rodrigo Rojas Mujica, who introduced me to the GLUE methodology, and grasped in my mind the importance of dealing with the unavoidable uncertainty in the best way possible. A word of gratitude to Bruno Majone, for the useful discussion about the meaning of the main parameters adopted for the conceptual model in SWAT.

Many thanks to Riccardo Rigon for his honest and timely advice, and to all his "*GEO-boys*" for allowing me to share with them some GEOframe caffè and other useful technical conversations. It could sound a little bit strange, but I would like to express my most sincere gratitude to the *R* Core development team and to the entire *R* community, for creating such an efficient and powerful statistical environment, that with time become the cornerstone of all the analysis carried out in this dissertation.

Special thanks the Confederación Hidrográfica del Ebro for their availability during the data collection process. In particular, I would like to thank Rogelio Galván and all the people working in the Departamento de Hydrología for providing daily time series of precipitation, air temperature and streamflows, and to Joseé Losada, for his valuable help with the GIS data. I also want to thank the EU Aquaterra project that provided an excellent interdisciplinary framework for carrying out this dissertation.

Thanks are due to Laura Martuscelli, the secretary of the DICA department, that helped me a lot with the administrative issues during the application to this doctoral programme, and by the constant effort she put into organizing the Doctoral School. At the same time, I'm deeply grateful to Jorge Troncoso, who unselfishly offered to be my guarantor during the written and oral examinations of this doctoral programme, and to Álvaro San Martín that built the bridge between Jorge and me.

More than four years have passed, but I can still remember a friend's lunch in the summer of 2006, on the corner of Paris and Londres street in Santiago de Chile, when Rodrigo Rojas -after finishing

his M.Sc- told us "*why to try one single model if we can try them all ?*". In that moment I was far away from realising what he was talking about, but today, I know he was completely right.

Fortunately, not all in life is work, even if for me this fact was hard to be experienced during the Ph.D journey. Therefore, I want to thank all those people that shared part of their lives with me during this period. Firstly, I'm deeply grateful to Corrado, who helped me so much at the beginning of this programme, mainly to get used to the Italian academic system, and after the first year of courses, he become a friend that could visit my family in Chile before me. Impossible is not to mention Danielle, who offered himself to be holder of an Internet contract for me and my wife, in a period in which Internet was forbidden for a foreign student without an Italian credit card. I also want to thank him for introducing me to the Italian folk of Modena City Ramblers, whose melodies and social lyrics were at my side during many hours of study. Special thanks goes for Chiara and Roberta, two Ph.D candidates that after sharing many last-time quasi-Latin American lunches become friends I can count on. Thanks Francesco, Marco, and Simonetta for your help in finding an apartment, and for always being there when I needed.

I am also infinitely grateful to Gisella and Hugo, for becoming the closest family during this period, and to their children Renata and Matteo for adding fantasy and imagination to our lives, and becoming our best little friends. Thanks to Marcos, Jorge, Ingrid, Philip, Cristina, and Fabiola for transforming "*Al Son de la Guitarra*" in a group of friends that -beyond a common nationality- shared many funny and happy weekends, birthdays and New Year's Eve. Many thanks also to my Bigiarini family in Badia Prataglia, for introducing us to the delicious Tuscan cuisine, for sharing Easter and summer holidays, and for being a real family for me and Carolina.

To all my Chilean friends, those who have given me precious moments of their lives, especially to those I met while working at the DGA in Santiago: Anita, Adrian, Álvaro, Guille and Miguel Ángel, who significantly contributed to my professional formation. In particular, I'm grateful to Liliana and Rodrigo, whose determination in applying to a Ms.C programme in 2003 become an important example to follow when I have to take a similar decision. I also want to thank my in-laws for treating me like a son, and in particular, I am greatly indebted to Mónica, whose birthday celebration in 2005 allowed me to know her sister Carolina, who become my wife.

Any thankful phrase will be unable to fully convey how much of this achievement belongs to my family, for whom the physical distance was never an obstacle to feel their great affection and permanent support. The infinite love and tenderness of my mother has been fundamental for me during all my educational process, and this period has not been the exception. My father is an example of hard-work and discipline, and I will always be an admirer of him. The years have passed and today I can truly say that I have found in Loreto, Felipe, Francisco and Soledad friends more than brothers and sisters. To the "*little*" Matías, who hardly pronounced my name when I left Chile, and today he regales me every weekend enjoyable adventures. And to Antonella, for having such a beautiful smile with two teeth only.

As it usually happens with those you love the most, I want to thank Carolina, for so many things that no single book could keep inside my eternal gratitude. She encouraged me to do not give up during the application process to this Ph.D programme and helped me with the collection of the mountain of documents needed to apply. I still admire the courage she had for abandoning her work in Chile, getting married and come with me to face an uncertain future. Carolina, you have been the emotional support that have allowed me to overcome all the discouraging moments experienced during these years. For allowing me to devote part of "*your*" time to this dissertation, for your infinite love and patience, and for all the beautiful moments, I just can say "*te amo*".

Finally, I would like to thank again God for keeping our families alive and safe during the big earthquake that on last Saturday (February 27^{th}) hit Chile and took the lives of many countrymen away.

Mauricio Zambrano-Bigiarini

March, 2010

Table of Contents

$\overline{O}$	Mean of the observed values, page 17
σ_i^2	error variance associated to the i^{th} model, page 21
σ_{obs}^2	variance of the observation for the period under consideration, page 21
$\underline{\theta_i}$	i^{th} model, page 21
$\underline{Y}$	Set of observations, page 21
a_m, b_m, c_m	Monthly coefficients used for the computation of daily maximum and minimum air temperature., page 27
$Elevation$	Elevation of the gauging station, [m.a.s.l.], page 27
T_{max}	Maximum daily temperature, [°C], page 27
T_{mean}	Mean daily temperature, [°C], page 27
T_{min}	Minimum daily temperature, [°C], page 27
95PPU	95% of predictive uncertainty, computed at the 2.5% and 97.5% levels of the cumulative distribution of of every simulated streamflow, page 36
b	Slope of the linear regression between observations and simulations, page 17
p-factor	Percentage of measured data bracketed by the 95% of predicted uncertainty., page 36
r-factor	Average thickness of the 95PPU band divided by the standard deviation of the measured data., page 36
ALPHA_BF	Baseflow alpha factor, [days]., page 33
AOGCM	Atmosphere-Ocean General Circulation Models., page 52
AR4	Fourth Assessment Report., page 51
ARS	Agricultural Research Service, page 22
bR^2	Weighted coefficient of determination, page 18
CEDEX	Centro de Estudios y Experimentación de Obras Públicas [Centre of Studies and Experimentation of Public Works], page 10
CHE	Confederación Hidrográfica del Ebro [Hydrological Confederation of Ebro River], page 7
CN2	Initial Soil Conservation Service (SCS) runoff curve number for moisture condition II., page 33
CTRL	Time period from 01/Jan/1961 to 31/Dec/1990, page 25
d	Index of agreement, page 18
DEM	Digital elevation model, page 7
DMI	Danish Meteorological Institute., page 54
ECDF	Empirical cumulative density function., page 92
EMIC	Earth-System Models of Intermediate Complexity, page 52

FDC Flow Duration Curve., page 43

GCM General Circulation Model, page 52

GIS Geographical Information System, page 23

GLUE Generalized Likelihood Uncertainty Estimation, page 20

GW_DELAY Groundwater delay time, [days], page 33

GW_REVAP roundwater *revap* coefficient., page 33

GWQMN Threshold depth of water in the shallow aquifer required for return flow to occur, [mm H_2O]., page 33

HRU Hydrological Response Units, page 22

IDW Inverse distance weighted, page 55

INE Instituto Nacional de Estadísticas [National Institute of Statistics], page 5

IPCC Intergovernmental Panel on Climate Change., page 51

LAM Limited-Area Model., page 53

LBIDW Local block inverse distance weighted interpolation algorithm, page 29

LH Latin Hypercube sampling, page 17

LH-OAT Latin Hypercube One-factor-At-a-Time, page 17

MAE Mean absolute error, page 18

N Shape parameter, page 21

n Number of observations, page 17

O_i Observed value at time step i, page 17

OAT One-factor-At-a-Time sensitivity method, page 17

OK Ordinary kriging., page 58

OPH Oficina de Planificación Hidrológica [Hydrological Planning Office] of the CHE, page 8

P Coefficient of persistence, page 18

PET Potential evapotranspiration, page 22

PRUDENCE Prediction of Regional scenarios and Uncertainties for Defining EuropeaN Climate change risks and Effects, an EU Fifth Framework Programme (FP5) project., page 53

r Pearson's product-moment correlation coefficient, page 18

R^2 Coefficient of determination, page 18

RCHRG_DP Deep aquifer percolation fraction., page 33

RCM Regional Climate Model, page 52

REVAPMN Threshold depth of water in the shallow aquifer for *revap* or percolation to the deep aquifer to occur, [mm H_20]., page 33

RMSE	Root mean squared error, page 18
RSR	Ratio of the mean squared error to the standard deviation of observations, page 18
S_i	Simulated value at time step *i*, page 17
SAIH	Sistema Automático de Información Hidrológica y de Comunicación Fónica de la Cuenca Hidrográfica del Ebro [Automatic Hydrologic Information System of the Ebro Basin], page 10
SCM	Simple Climate Models., page 52
SCS	Soil Conservation Service, page 22
SMHI	Swedish Meteorological and Hydrological Institute., page 54
SOL_AWC	Available water capacity of the soil layer [mm H_20/mm soil]., page 33
SOL_K	Saturated hydraulic conductivity, [mm/hr]., page 33
SOL_Z	Depth from soil surface to bottom of a layer, [mm]., page 33
SRES	Special Report on Emissions Scenarios., page 53
SWAT	Soil and Water Assessment Tool, page 21
TAR	Third Assessment Report., page 51
USDA	US Department of Agriculture, page 22

List of Figures

List of Tables

Abstract

This dissertation focuses on the assessment of projected changes on water resources by the end of this century (2071-2100), considering an ensemble of high resolution future climate scenarios, the effects of hydrological parameterisation, and the bias of the hydrological model in representing different streamflow magnitudes.

Quantification of the impacts of climate change on water resources will depend on the emission scenario, climate model, downscaling technique and impact model used to drive the impact study. In particular, hydrological impact studies involve important decisions (e.g., model structure, parameterisation, input data) whose effects are reflected into the final impacts. As a result, quantification of impacts of climate change have to be seen as a "*cascade of uncertainty*", in which decisions taken in every step of the assessment process convey uncertainties that are unavoidably propagated to subsequent levels. At the other hand, uncertainties in projections of climate models and those involved in the quantification of their hydrological response limit the understanding of those future impacts and hamper the assessment of mitigation policies.

The Soil and Water Assessment Tool (SWAT) hydrological model was set up for daily simulations of the western part of the Ebro River basin ($\sim$ 42000 km^2) in Spain, during the control period 01/Jan/1961 to 31/Dec/1990, and two subcatchments were selected for testing the methodology proposed in this dissertation. A sensitivity analysis with Latin Hypercube One-factor-At-a-Time (LH-OAT) was carried out in order to identify parameters with a high effect on simulated streamflows. Then, an uncertainty analysis was carried out using the Generalized Likelihood Uncertainty Estimation (GLUE) methodology, in order to select parameter sets that can be considered as acceptable simulators of the system, adopting a re-scaled Nash-Sutcliffe efficiency as "*less formal*" likelihood, and a cut-off threshold equal to zero to discriminate between behavioural and non-behavioural simulators. Afterwards, a Latin Hypercube (LH) sampling strategy was implemented within GLUE, in order to reduce the number of model runs required to obtain a good exploration of the parameter space. The 95% of the cumulative distribution of each predicted output, weighted by the re-scaled likelihood of each behavioural parameter set, was used to compute the predictive uncertainty bounds, both during the control and future scenarios.

Bias-corrected daily time series of precipitation and air temperature, for the future period 2071-2100, were derived from an ensemble of six high-resolution climate change scenarios, selected from the EU FP5 PRUDENCE project. Long-term averages of precipitation and air temperature fields were computed for the control period, and projected anomalies for the future scenarios were computed as well, in an annual, seasonal and monthly basis, including expected changes for different elevation bands within the basin. The same bias-corrected time series were then used to drive daily hydrological simulations during the future period on the two selected catchments. For each climate scenario, a number of simulations equal to the number of behavioural parameter sets obtained during the uncertainty analysis was carried out. Resulting streamflows were used to compute daily flow duration curves (FDCs) to provide a qualitative assessment of the relative importance of uncertainties coming from the choice of the driving RCM and from hydrological parameterisation. In addition, streamflows derived from running each climate scenario with its corresponding behavioural parameter sets, were used to compute empirical cumulative density functions (ECDFs) of three selected percentiles, representing different flow magnitudes, in order to provide a quantitative assessment of the projected changes in streamflows.

We observed that the hydrological parametric uncertainty was larger than the uncertainty coming from the driving RCM, during the complete future period and each one of the four seasons, for the two selected catchments. However, this result can not be generalised, because it is conditional to decisions taken during the uncertainty analysis and to the ensemble of RCMs considered. Empirical CDFs computed for projected values of low (Q5), medium (Q50) and high (Q95) flows show that there is a general projected decrease in all the streamflow magnitudes, but bias in the representation of the streamflows during the control period 1961-1990 hamper the assessment of reliable quantitative projections for low and medium flows, whereas projected decreases for high flows range from 0 to 60%, depending on the catchment and the climate scenario considered.

"The aim of science is to seek the simplest explanation of complex facts... seek simplicity and distrust it".

(A. N. Whitehead)

1 Introduction

This chapter provides a brief introduction about the context and motivation of the present dissertation. Section 1.1 describes projected changes in climate and their links with expected hydrological impacts. Section 1.2 provides an overview about the current approaches used for assessing the hydrological impacts of climate change. The aforementioned topics are covered in detail in further chapters. The research aim and its specific objectives are presented in section 1.3. Finally, section 1.4 presents an outline of the present dissertation.

1.1 Climate Change

Global mean surface temperatures have risen by $0.74°C \pm 0.18°C$ over the last 100 years (1906-2005) and eleven of the last twelve years (1995-2006) are among the 12 warmest years since 1850, as mentioned in the Fourth Assessment Report (AR4) of the Intergovernmental Panel on Climate Change (IPCC) (*Trenberth et al.*, 2007). The warming of our climate system seems unequivocal (*Bates et al.*, 2008), and it may lead to changes in the overall Earth's hydrological cycle, in particular, changes in regional water availability and frequency/intensity of extreme events (*Trenberth et al.*, 2007). Such hydrological changes will have implications of societal importance, from agricultural productivity and energy production to flood control, highlighting the necessity of a better understanding about how those changes in global climate will affect local water resources (*Xu*, 1999).

Changes are undergoing globally, but mitigation policies have to been applied locally. In Europe, the mean annual temperatures are likely to increase more than the global mean, with the largest warming in summer for the Mediterranean area, and in particular, the highest summer temperatures are expected to increase more than the average for central and southern Europe (*Christensen et al.*, 2007a). In the Mediterranean area, annual precipitation is very likely to decrease, whereas the annual number of precipitation days is very likely to decrease as well (*Christensen et al.*, 2007a). Consequently, significant hydrological changes are expected for southern Europe, in particular, a likely decrease in annual runoff, by 0 to 23% up to 2020s and by 6 to 36% up to 2070s; accompanied with a decrease by up to 80% of low summer flows, making the risk of drought particularly important. Moreover, projected increase of water withdrawals in southern Europe would amplify the risks associated to climate change, being the Mediterranean (Spain and Portugal) the region more exposed to drought risk (*Alcamo et al.*, 2007).

Nowadays, climate models are the best available tools for quantifying the global climate response to different future development scenarios of our society, represented by different atmospheric concentrations of carbon dioxide and other trace gases. Climate models use well-known physical principles to simulate the interactions among atmosphere, oceans, land surface and ice, through different numerical schemes and/or different parameterisations. Up to now, the assessment of potential impacts of climate change has generally relied on data from Atmosphere-Ocean General Circulation Models (AOGCM), which are dynamical three-dimensional representation of the atmosphere, land surface, oceans and sea ice processes, with a spatial resolution not suitable for accurately reproducing precipitation and temperature fields, especially in areas of complex topography and land use distribution (*Christensen et al.*, 2007b), hampering their direct application into

hydrological impact assessment. To overcome these limitations, spatial and temporal downscaling techniques are carried out for limited areas and run for shorter periods, aiming at producing climate information with a spatial resolution finer than the large-scale GCM outputs.

1.2 Hydrological Impacts of Climate Change

Once the climatological fields have been downscaled, conceptual rainfall-runoff models have been -to date- the preferred tools of many climate-change researchers worldwide to assess the likely impacts of climate change (e.g. *Arnell*, 2003a; *Booij*, 2005; *Gosain et al.*, 2006; *Thodsen*, 2007; *Graham et al.*, 2007a; *Steele-Dunne et al.*, 2008; *Abbaspour et al.*, 2009; *Chiew et al.*, 2009), in spite of their known limitations, related to parameter identifiability, equifinality and predictive uncertainty (e.g. *Johnston and Pilgrim*, 1976; *Sorooshian and Dracup*, 1980; *Sorooshian et al.*, 1983; *Sorooshian and Gupta*, 1983; *Kuczera*, 1983; *Hornberger et al.*, 1985; *Duan et al.*, 1992; *Beven and Binley*, 1992; *Freer et al.*, 1996; *Seibert*, 1997; *Beven and Freer*, 2001; *Beven*, 2006). The main reasons for this preference are: (i) relative low data-requirements, (ii) computation time suited for long-term hydrological simulations, and (iii) a large amount of models are available, already calibrated and verified during years of application to water management and related problems.

According to *Xu* (1999), the assessment of the hydrological impacts of climate change can be carried out with different approaches, among them: using hypothetical scenarios as input to hydrological models, direct use of GCM-derived hydrological output, coupling General Circulation Models (GCMs) and macroscale hydrological models, and downscaling GCM climate outputs to drive a hydrological model, the later being the approach adopted in this dissertation.

1.2.1 Aquaterra Project

Driven by the precautionary principle and anticipating risks caused by upcoming priority threats, the 6th EU RTD Framework Programme started, in June of 2004, the Aquaterra project (http://www.eu-aquaterra.de/). This European project aimed at providing the scientific basis for an improved river basin management, enhanced soil and groundwater monitoring programs and the early identification and forecasting of impacts on water quantity and quality during this century; through a better understanding of the river-sediment-soil-groundwater system as a whole, by integrating both natural and socio-economics aspects at different temporal and spatial scales. This should be applicable to European contexts facing modifications or changes due to climate change, land use change and pollution of soil and water. The Aquaterra project consisted of several sub-projects with different specific objectives, which integrates the key biogeochemical, climatic and hydrological processes over relevant scales in time and space. In particular, this dissertation was carried out within the work package C3 COMPUTE, which had to collect and organise results from different work packages in order to provide a quantitative assessment of the likely hydrological impacts of climate change on the Ebro River basin.

1.2.2 Uncertainty in Hydrological Impacts of Climate Change

Hydrology is a highly uncertain science, in which complex dynamics of many hydrological processes, physical domains that evolve in time, data scarcity, and measurement errors hamper the theoretical treatment of the phenomenon under study. Uncertainty, ignorance, error, and risk are defined in different ways by different authors (see *Refsgaard et al.*, 2007; *Walker et al.*, 2003). We want to emphasise the difference between *ignorance* and *uncertainty*, in which the former represents a lack of awareness regarding imperfect knowledge, and the latter stands for a degree of confidence in the possible outcomes. The uncertainty treatment adopted in this dissertation correspond to the general definition given by *Walker et al.* (2003), in which uncertainty is "*any deviation from the unachievable ideal of completely deterministic knowledge of the real system*". In this way, uncertainty is an unavoidable fact when dealing with real catchments, and hydrologists and water

management agencies have to get use to include it into their every-day decisions.

Projected impacts of climate change will depend on the combination of emissions scenarios, climate forcings, and impact model used to assess the local impacts (*Viner*, 2003; *Olesen et al.*, 2007). In particular, quantification of impacts of climate change should be seen as a "*cascade of uncertainty*" (*New and Hulme*, 2000; *Mearns et al.*, 2001; *Schneider*, 2002; *Viner*, 2003; *Giorgi*, 2005; *Wilby*, 2005), in which decisions taken in every step of the assessment process, going from emissions scenario to projected impacts, convey uncertainties that are unavoidably propagated to subsequent levels. So far, most of the studies providing an assessment of the impacts of climate change on water resources have relied on a single hydrological model, i.e, a unique combination of model structure and parameter set, overlooking the relative importance of hydrological uncertainties into the final impacts. Comparatively, only few quantitative studies have looked at the propagation of the aforementioned uncertainties into the final hydrological impacts (e.g. *Jakeman et al.*, 1993; *Wilby*, 2005; *Dibike and Coulibaly*, 2005; *Cameron*, 2006; *Wilby and Harris*, 2006; *Prudhomme and Davies*, 2009a,b).

Most of the studies indicate that the greatest source in the cascade of uncertainty is the GCM chosen to drive the simulations (e.g. *Wilby and Harris*, 2006; *Graham et al.*, 2007b; *Prudhomme and Davies*, 2009b), whereas some few claim that the relative importance of the uncertainty may be dependent on the scale of the study (*Abbaspour et al.*, 2009), with hydrological model uncertainty being larger and uncertainties due to emissions scenarios becoming smaller as the scale of the study increases. This dissertation attempt to provide new insights about the relative magnitudes of uncertainties derived from the driving climate model and hydrological parameterisation, and its implications for hydrological impact assessment.

1.3 Research Aim

To develop a methodology that allows the probabilistic assessment of the likely impacts of climate change on surface water resources of the Ebro River basin (NE Spain), taking into account uncertainties coming from the driving climate scenario and from hydrological parameterisation.

Specific objectives are:

- To select a modelling approach that allows the assessment of the hydrological impacts of climate change on the chosen study area.
- To implement a suitable hydrological model that allows the integration of all the available data within an uncertainty framework, aiming at the probabilistic assessment of the hydrological impacts of climate change.
- To carry out an uncertainty analysis of the streamflows computed by the hydrological model during the control period 1961-1990, in order to select parameter sets that lead to reliable predictive uncertainty bounds.
- To select an ensemble of future climate scenarios that can be used as drivers of the hydrological simulations during the future period 2071-2100.
- To provide an assessment of the projected changes in climate (precipitation and air temperature) expected on the study area by the end of this century.
- To assess the likely impacts of climate change on water resources of the study area by the end of this century (2071-2100), taking into account possible bias of the hydrological model in representing the catchment response.

1.4 Outline of the Dissertation

Each chapter of this dissertation was though to be an independent readable unit, and notwithstanding a great deal of effort was put in avoiding repetition among them, some overlapping was unavoidable. The rest of the dissertation is organised as follow: Chapter 2 describes the study area and the procedure used to select data to be used in the hydrological simulations; Chapter 3 describes the implementation of a semi-distributed modelling approach on the north-western part of Ebro River basin, and the uncertainty analysis carried out for the predicted streamflows; Chapter 4 presents projected changes for precipitation and temperature fields on the Ebro River basin by the end of this century (2071-2100), based on bias-corrected daily precipitation and temperature fields, downscaled from an ensemble of six regional climate models; Chapter 5 presents projected changes for streamflows in two selected subcatchments of the Ebro River basin by the end of this century (2071-2100), considering the effects of hydrological parameterisation and the bias of the hydrological model in representing different streamflow magnitudes; and the last chapter provides a discussion of the main findings, and further research needed in this area. In order to save paper, **all the Appendixes are not available in the printed copies of this dissertation, but only in the electronic version of this document**.

"A journey of a thousand miles begins with a single step".

(Lao Tse)

2 Study Area and Data Selection

This chapter provides a description of the study area selected in this dissertation to analyse the hydrological impacts of climate change, and a summary of the data collection/selection stage used to set up the hydrological model in Chapter 3.

2.1 Study Area

The Ebro River basin is located between latitudes 40.5°N - 43°N and longitudes 4.5°W - 2°E at the north-eastern part of Iberian Peninsula, with a total area of 85362 km^2, 502 belonging to France, 445 belonging to Andorra and all the rest located in Spain. Its natural limits are: the Vasco-Cantabrian and Pyrenean mountains range by the north, the Iberian System by the south-east and the Coastal-Catalan mountain range by the east (http://www.chebro.es/cuencaDescripcion.htm). The Ebro River basin is the largest basin of Spain (17.3% of the total peninsular Spanish territory) and it was selected as a case study within the FP6 EU Aquaterra project (http://www.eu-aquaterra.de/) because this basin achieved a good balance between data availability, climatic situation representativeness, size, functioning conditions and pollution profile. It is drained by the Ebro River, with a total length of 910 km, flowing by a roughly plain central valley from the Cantabrian Mountains to its delta in the Mediterranean sea (direction NW to SE). During its path, it collects water from the Cantabrian and Pyrenean mountain ranges by its left bank and from the Iberian system by the right one. Elevations in the left bank of the basin are higher than in the right one, giving place to higher annual precipitation and consequently higher availability of water resources. The total length of the rivers within this basin is ∼12000 km, with ∼50000 km^2 belonging to its left bank and 30000 km^2 to the right one. Northwestern rivers are strongly influenced by the ocean, but snow retention in their heads defines a pluvial-nival regime. Going to the southeast, the nival and Atlantic influence disappears and the Mediterranean one starts, giving place to a pluvial-Mediterranean regime. Population living within this basin is around 3019176 inhabitants[1], which is mainly concentrated in the central valley. The total water resources are estimated in 18200 Mm^3/year for the period 1940-1986, comparatively high and important with respect to other watersheds in the Iberian Peninsula, whereas the estimated total water demand comprises 6310 Mm^3/year for agriculture, 414 Mm^3/year for industrial use, and 313 Mm^3/year for drinking water supply (http://oph.chebro.es/DatosBasicosCHE.html).

Figure 2.1 shows the location of the Ebro River basin and the study area selected for the hydrological simulations. Topography exerts a continental effect over the Mediterranean climate in a large area of the basin, with a clear semi-arid condition in its centre. Precipitations are scarce, with exception of the northern mountain ranges and the northern part of the Iberian one, mainly concentrated during the spring and autumn. Precipitation, besides its scarcity, presents a strong inter-monthly and inter-annual variability, with long periods without any precipitation, specially in wintertime and at the end of autumn. Mean annual precipitation on the entire basin is 622 mm/year, from 1920 to 2002, and the minimum and maximum annual precipitations are 452 and 840 mm/year, respectively, being 3813 mm/year the individual observed maximum, at station P9269I in 1964/65 (*Ministerio del Medio Ambiente y Confederación Hidrográfica del Ebro*, 2007). Mean

[1] I.N.E. 2005

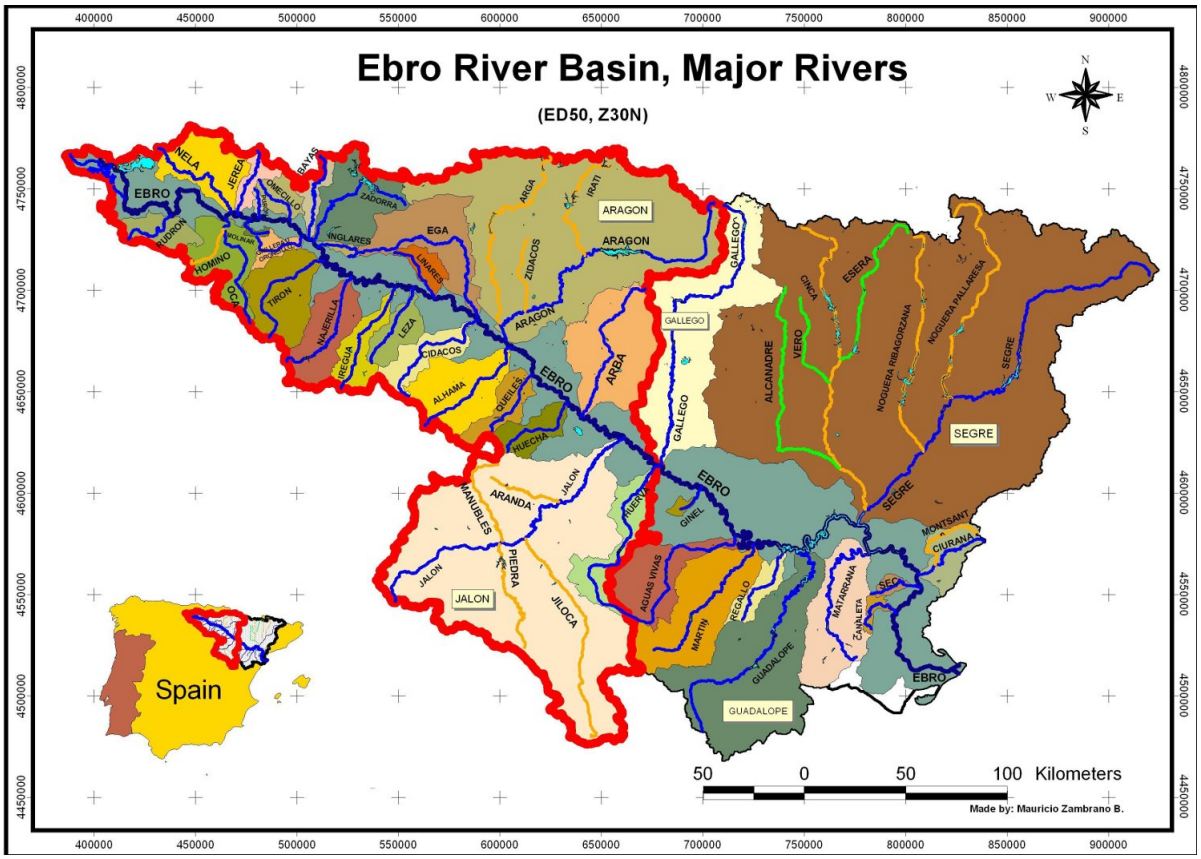

FIGURE 2.1: Ebro River basin, in the north-western part of Spain, and the red polygon shows the extent of the study area selected for the hydrological simulations, with a total area of 42000 km^2 (see section 3.3).

annual temperature is $\sim$12°C, over the period 1961-1990, and the mean winter minimum and summer maximum temperatures are $\sim$5°C and $\sim$20°C respectively, for the same period. Potential evapotranspiration is estimated in 700 mm/year (http://www.chebro.es/).

Within the Ebro River basin there are three large groundwater areas: pyreneian, alluvial and iberian. The pyreneain aquifers are karstic, with many springs with a highly variable flow, covering from the Pyreneian mountain range to the headwaters of the Ebro River, through the Basque and Cantabrian mountains. The alluvial aquifers are located following the course of the most important rivers, and they are strongly related to the surface rivers, varying its behaviour according to the season, with a medium to high regulation capacity, and a weekly-based response to infiltration recharges. The Iberian aquifers cover from La Demanda Mountains to the Puertos de Beceite, to finally connect the Coastal-Catalan range. The presence of several layers of karstificated limestones, mixed with low hydraulic conductivity loam, makes them to be considered as multilayer aquifers (http://www.chebro.es/cuencaGeoMedio.htm).

A more detailed description about the climate, hydrology and hydrogeological units is provided by *Zambrano-Bigiarini et al.* (2007).

2.2 Data Selection

2.2.1 Topography

A digital elevation model (DEM) with 20x20 m of spatial resolution was provided by the Confederación Hidrográfica del Ebro [Hydrological Confederation of Ebro River] (CHE), the public office responsible for the administration and control the Ebro River basin. This DEM is depicted in Figure 2.2 and it was used in section 3.3 to derive the spatial parameters required by the hy-

drological model. Elevations within the basin range from 0 to 3394 m.a.s.l., with a mean value of ∼760 m.a.s.l. and 75% of the basin below the 1010 m.a.s.l. As watershed delineation and stream network extraction is affected by DEM resolution (e.g. *Wang et al.*, 2000; *Defourny et al.*, 1999), we tried different spatial resolutions (100x100m, 80x80m and 60x60m) up to find the coarsest resolution that allowed the correct identification of the drainage network, catchment borders, reservoirs and withdrawals that had to be included in the hydrological simulations, by using an automated procedure implemented in the AVSWAT-X GIS interface (*Di Luzio et al.*, 2002a, 2004). The final resolution used for the hydrological simulations was 60x60m, and the same resolution was automatically set by AVSWAT-X as the cell size for the land use and soil maps. Additional information about the effect of input data resolution on hydrologic simulations might be found in *Chaubey et al.*, 2005; *Di Luzio et al.*, 2005; *Kumar and Merwade*, 2009; *Peschel et al.*, 2006; *Geza and Mccray*, 2008; *Cotter et al.*, 2003; *Le Coz et al.*, 2009; *Bosch et al.*, 2004; *Cochrane and Flanagan*, 2005; *Wang and Melesse*, 2006, and *Chaplot et al.*, 2005.

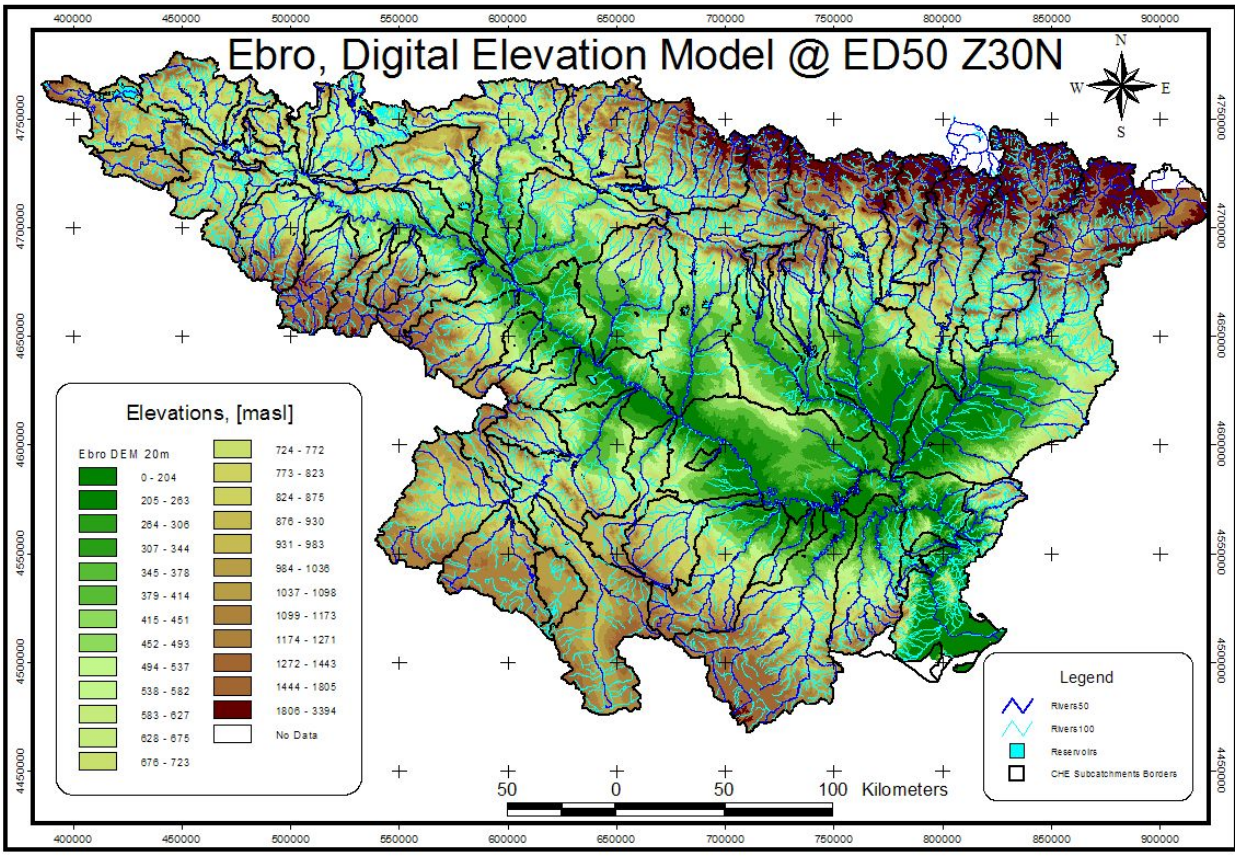

FIGURE 2.2: Digital elevation model (DEM) of the Ebro River basin, with a spatial resolution of 20x20 m.

2.2.2 Land Use

The land use cover was downloaded from the CHE website (http://oph.chebro.es/ContenidoCartoApoyo.htm), with information for the years 1984, 1991 and 1995, at a 1:100000 scale. The land use cover corresponding to the year 1984 (field 'USOS84') was selected as representative of the historical period considered for the hydrological simulations (1961-1990), as shown in Figure 2.3. For all the cells in which the land use identifier was missing, i.e. without a value in the field 'USOS84', a pasture land use was assigned, based on visual comparison with current satellite land covers provided by Google Earth (http://earth.google.com/). The five major land covers within the area are: pasture (64.2%), forest (24.8%), agriculture (8.9%), rocks (1.7%) and urban areas (0.4%). The full list of land use classes is presented in Table 2.1.

TABLE 2.1: Land uses on the Ebro River basin, based on information for the year 1984 at 1:100000 scale, with the eight classes identified.

GRID Value	LandCover	% Basin Area	Original Name	A84
1	Rocks	1.69	Roquedo	20
2	Forest	24.83	Bosques	13, 14, 15, 16, 17
3	Pasture	64.21	Praderas	1, 2, 3, 10, 11, 12, 16, 18, 19, 20, 24, 25, 26, 27, 31
4	Urban	0.35	Suelo Artificial	28, 29, 30
5	Water	0.04	Lagos Interiores	21
6	Agriculture	8.88	Regadíos	4, 4a, 4b, 4c, 5, 5b, 5c, 6, 6b, 6c, 7, 7a, 7b, 7c, 8, 9, 9b, 9c
7	Coastal Lakes	0.02	Lagunas Costeras	22
8	Marshlands	0.00	Marismas	23

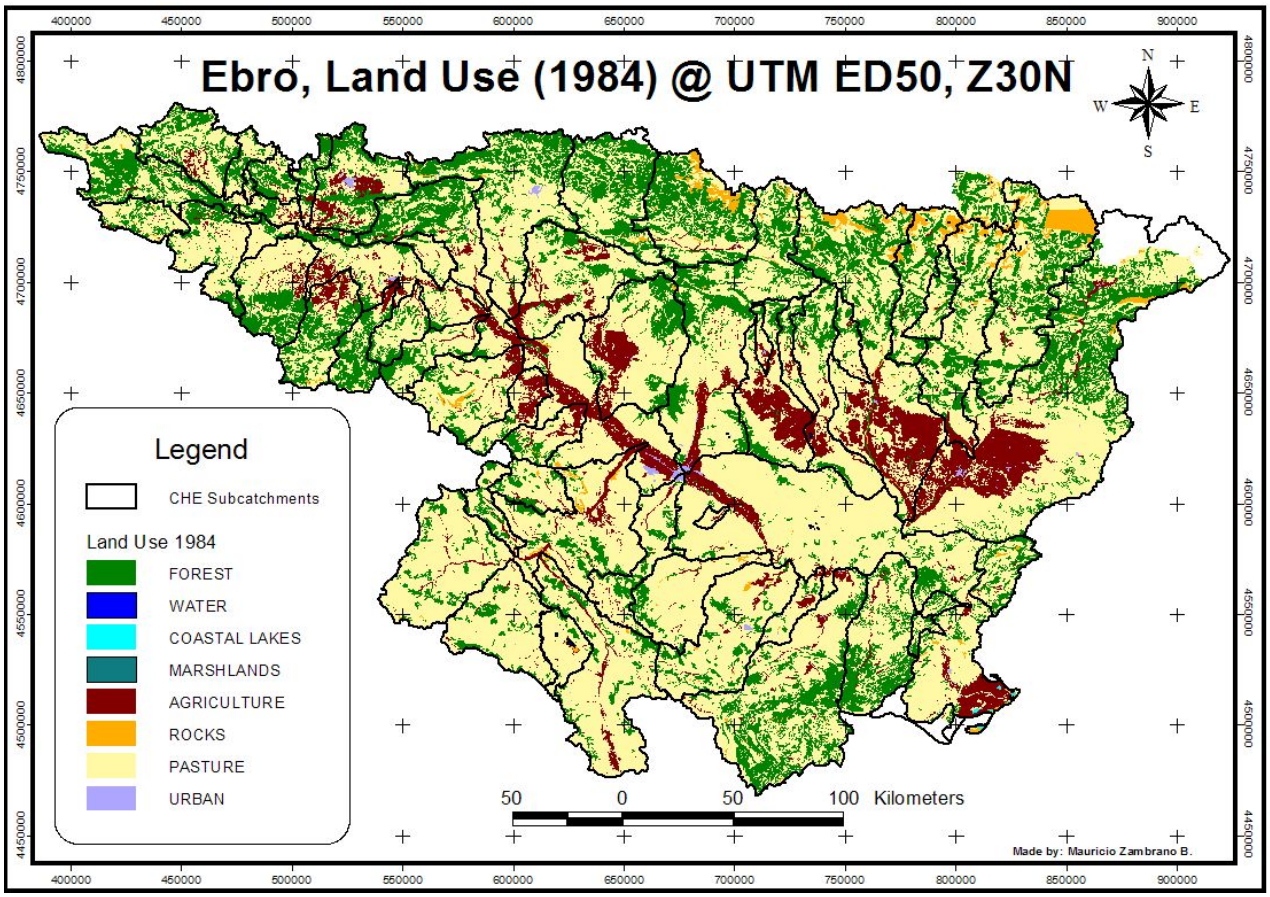

FIGURE 2.3: Land uses on the Ebro River basin, based on information for the year 1984 at 1:100000 scale.

2.2.3 Soil Types

Information about the soil types was provided by the Oficina de Planificación Hidrológica [Hydrological Planning Office] of the CHE, in March 2009 (*Confederación Hidrográfica del Ebro & Ministerio de Medio Ambiente y Medio Rural y Marino*, 2009) as an under-construction shapefile ('geoebrop') created by merging Arc Info files from http://oph.chebro.es/ContenidoCartoGeologia.htm. This information was used for defining the initial soil properties required for the hydrological simulations. The original 150 lithological classes were first aggregated into 23 major classes, as shown in Figure 2.4, and described in Table 2.2.

TABLE 2.2: Original 150 soil classes for the Ebro River basin, provided by the Oficina de Planificación Hidrológica (OPH) (*Confederación Hidrográfica del Ebro & Ministerio de Medio Ambiente y Medio Rural y Marino*, 2009) and the 23 aggregated classes.

VALUE	Aggregated Class	Original IDDOM's ID
1	Arcillas	315, 7347, 7348, 7349, 7358
2	Arenas	451
3	Arenas y otros	310, 360, 370, 990, 1010, 1040, 7212, 7213, 7224
4	Areniscas	100, 110, 330, 400, 540, 660, 661, 721, 722, 723, 7236
5	Brechas	210, 491
6	Calcarenitas, margas y calizas arenosas	622
7	Calizas	3, 6, 121, 123, 230, 240, 250, 260, 280, 312, 316, 320, 340, 341, 350, 410, 421, 440, 470, 490, 620, 650, 651, 752, 753, 754, 758, 970, 7513
8	Cantos	910, 920, 940, 950, 980
9	Conglomerados	311, 711, 713, 714, 716, 900, 7113, 7123, 7124, 7134, 7136, 7145, 7146, 7147, 7148, 7149, 7179, 7248
10	Cuarcitas y pizarras	1, 4, 10
11	Dolomias	120, 200, 290, 621
12	Facies lagunares con sales potasicas	662
13	Flysch: Areniscas y lutitas en facies turbiditicas	630
14	Grauvacas y pizarras. Arenitas, pelitas y conglomerados	5
15	Gravas	930, 960, 1030
16	Intercalaciones de calizas lacustres y lignitos	611
17	Limolitas y Limos	313, 728, 1060, 7246
18	Lutitas	7, 122, 380, 610, 733, 734, 7313, 7335, 7346, 7359
19	Margas	130, 220, 270, 314, 342, 422, 441, 450, 460, 480, 530, 640, 641, 743, 7446, 7449, 7456
20	Megabrechas carbonatadas, ofitas, pizarras ampeliticas, rocas filonianas, rocas metamorficas, Sales, serie mixta detritico-terrigena	2, 140, 430, 631, 1050, 3000, 4000
24	Rocas Intrusivas	2000
26	Rocas volcanicas	5000
29	Yesos	761, 763, 7623, 7636, 7646, 7656

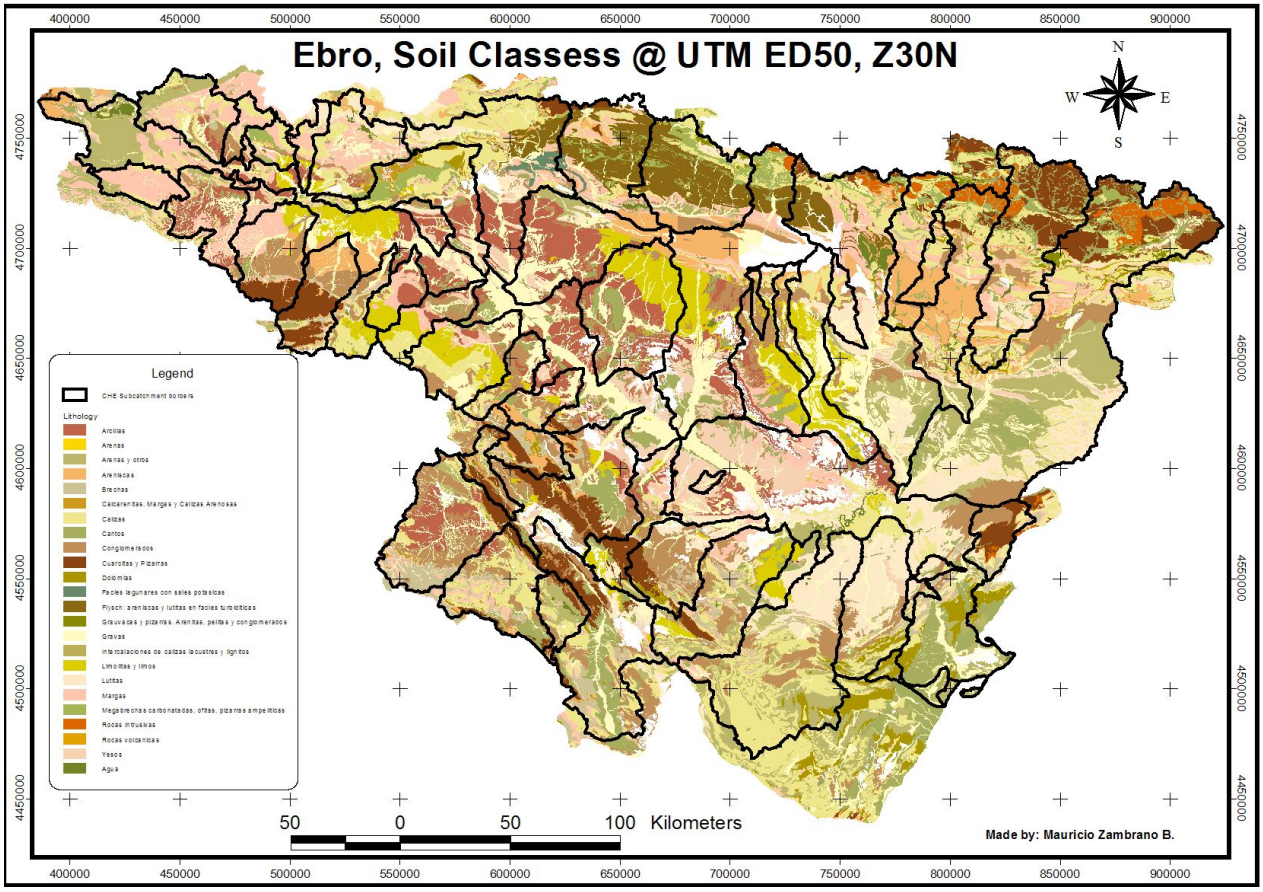

FIGURE 2.4: Soil classes on the Ebro River basin, provided by the Oficina de Planificación Hidrológica [Hydrological Planning Office] of the CHE (*Confederación Hidrográfica del Ebro & Ministerio de Medio Ambiente y Medio Rural y Marino*, 2009).

2.2.4 Reservoirs and Infrastructures

Within the study area there are numerous infrastructures that severely modify the natural flow regime. These infrastructures are summarized by *Zambrano-Bigiarini et al.* (2008), and comprise more than 45 reservoirs with a capacity larger than 1 Mm^3 (http://oph.chebro.es/DatosBasicosCHE.html), equivalent to a total regulation capacity of 4055 Mm^3; 380 hydropower plants; 90 fish farms; and 51 main irrigation systems, spread over ∼10% of the total area of Ebro River basin up to year 2004. Among all the water uses, the influence of reservoirs on the hydrological regime is one often difficult to predict, even in the presence of a good data record, because their behaviour change on a daily/weekly/monthly basis according to variations in the relationship between water availability and demand. Daily stored volumes and releases for reservoirs were downloaded from the web site of the Centro de Estudios y Experimentación de Obras Públicas (CEDEX) [Centre of Studies and Experimentation of Public Works] (http://hercules.cedex.es/anuarioaforos/), for the period 01/Jan/1961 - 31/Dec/1990. Notwithstanding the simulation of reservoirs is not presented in this dissertation, additional reservoir information was collected in early stages of this work, in order to allow a further representation of these infrastructures in the hydrological simulations. In this context, daily data of water depth and stored volume were downloaded from the web site Sistema Automático de Información Hidrológica y de Comunicación Fónica de la Cuenca Hidrográfica del Ebro (SAIH) [Automatic Hydrologic Information System of the Ebro Basin] (http://195.55.247.237/saihebro/index.php), for the period Sep/2003[2] - Dec/2008, and this information was used for reconstructing the curve of stored volume versus surface area of some test reservoirs. These curves might be used in further studies for calibrating the feeding catchment to each reservoir, by using the water balance equation of each reservoir to compute its daily

[2] Available information starts on September 1^{st}, 2003

inflows, and then using those inflows as the outflows of the corresponding feeding catchment.

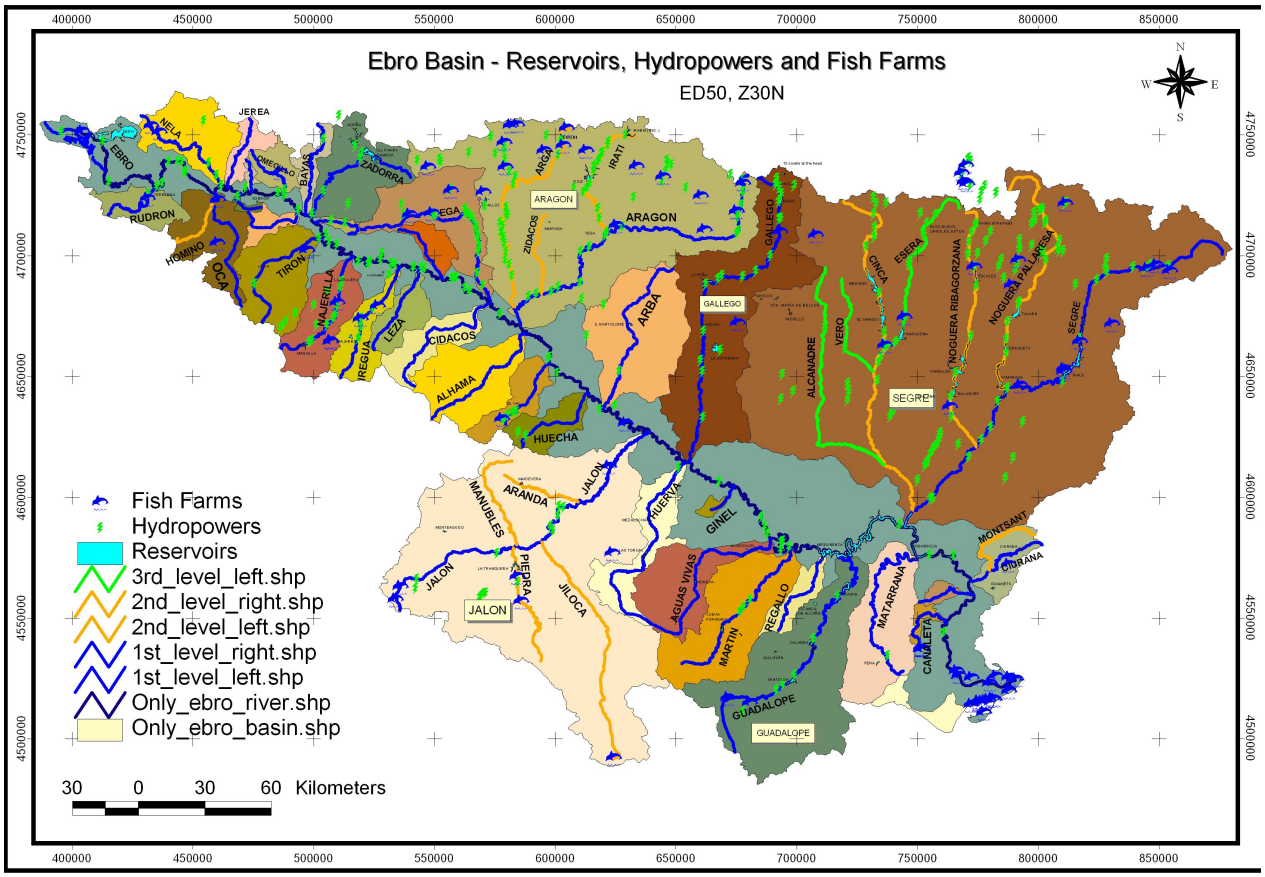

FIGURE 2.5: Main reservoirs, hydropower plants and fish farms existing on the Ebro River basin.

2.2.5 Weather and Streamflow Data

Time series and spatial location of monthly precipitation, temperature, and computed potential evapotranspiration were downloaded from http://oph.chebro.es/ContenidoClimatologicoD.htm, for the period Oct/1940 - Sep/1991. However, in order to provide the hydrological model with the required daily data of precipitation and air temperature, daily precipitation in 1569 rain gauges and daily mean temperature in 859 stations were provided in April/2008 by the OPH, for the period 1900-2004. At the other hand, daily streamflows in 318 stream gauges, for the water years Oct/1912 - Sep/2004, were collected from the website of the CHE (http://oph.chebro.es/documentacion/CaudalEA/CaudalEA.htm) for stations located in the main course of rivers, and from the OPH for those stations measuring reservoir deliveries. These data are summarized by *Zambrano-Bigiarini et al.* (2007).

Additionally, in order to provide the hydrological model with the required maximum/minimum daily temperature, hourly data in 34 stations of the HidroEbro database (stations 0016A, 0034C, 0076, 0149D, 0158O, 0162C, 0189E, 0200E, 0208, 0222, 0321, 0341, 0367, 0421E, 1014, 1024E, 1082, 1109, 1111, 2030, 2331, 3013, 3168C, 8368U, 8500A, 9091O, 9170, 9263D, 9381I, 9390, 9434, 9771C, 9898, 9981A) were provided in April 2008 by the OPH, for the period 01/Jan/2003 - 16/Oct/2006. These hourly data were used to derive monthly relationships between the maximum/minimum daily temperature and the daily mean temperature, as described in section 3.3.4.

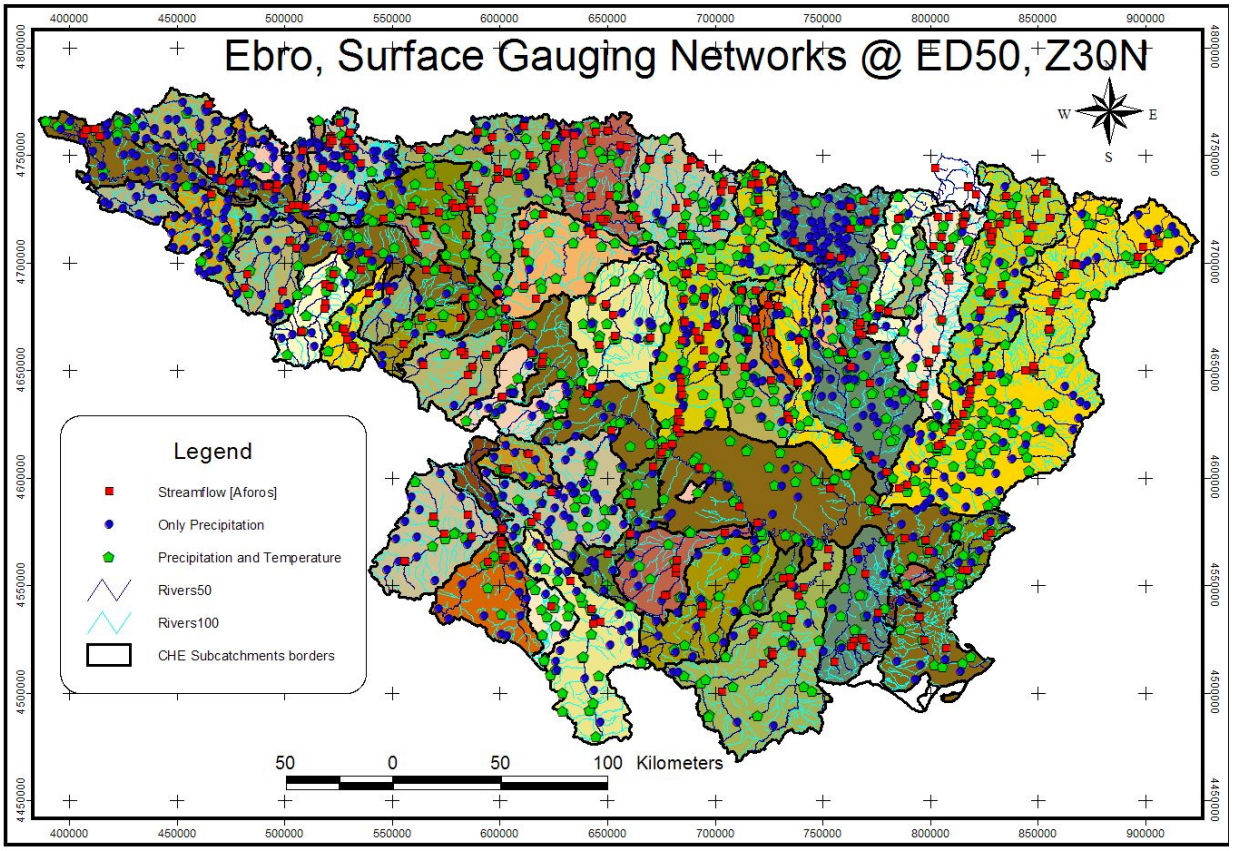

FIGURE 2.6: Gauging networks on the Ebro River basin, showing the spatial location of stations measuring streamflow (red squares), precipitation and temperature (green boxes) and only precipitation (blue circles).

2.2.5.1 Selection of Gauging Stations

The large amount of collected time series vary in length and quality, with many missing values unevenly distributed in space and time. In order to reduce the amount of information to be managed during the hydrological simulations, and to avoid the use of non-representative gauges, only stations with a long-data record, i.e., an amount of daily information above a given threshold, were selected for the simulations. The threshold for each gauging type was selected trying to meet a balance between the number of stations with a long-data record, and the number of stations necessary to (i) describe the spatial variability of the meteorological fields, in the case of precipitation and air temperature gauging stations, and (ii) to calibrate and validate the hydrological model in some representative points, in the case of stream gauges. In particular, for the control period 01/Jan/1961 - 31/Dec/1990, we plotted different desired threshold values, representing the percentage of days with no- missing values in each station, versus the number of gauging stations in which the percentage of days with non-missing values was above the desired threshold, as shown in Figure 2.7. Based on the previous plots, we selected a threshold of 70% for precipitation, 65% for temperature and 65% for streamflow, resulting in 349, 146 and 182 gauging stations of precipitation, temperature and streamflow, respectively. The complete list of stations is reported in the Appendix A, and a summary with the distribution of days with information per year in each station is depicted in Figure 2.8.

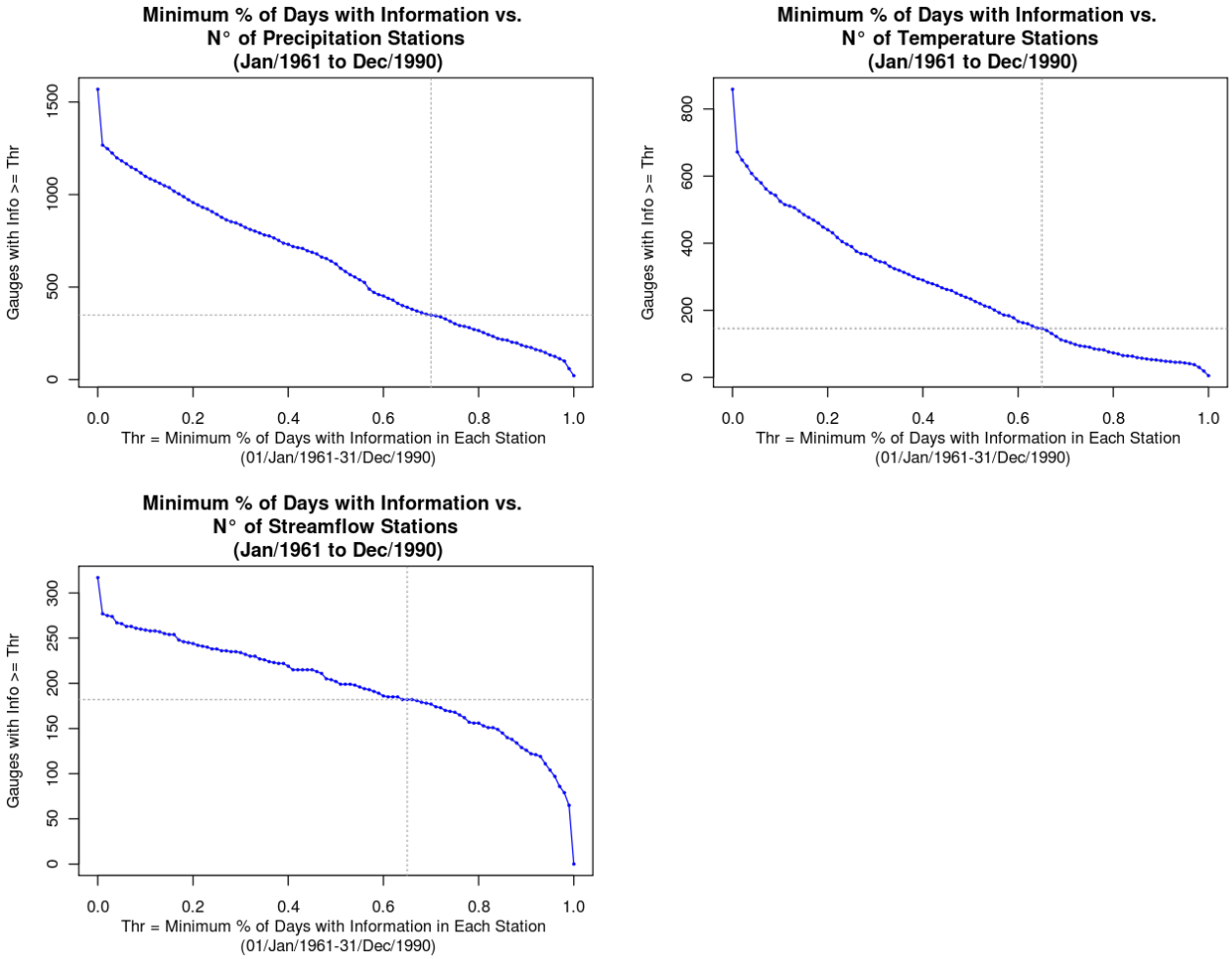

FIGURE 2.7: Desired minimum percentage of days with information in the gauging stations, during the control period 01/Jan/1961 - 31/Dec/1990, versus the number of stations satisfying that criterion. Vertical lines show the selected thresholds of 70%, 65% and 65% of days with information for precipitation, temperature and stream gauges, respectively.

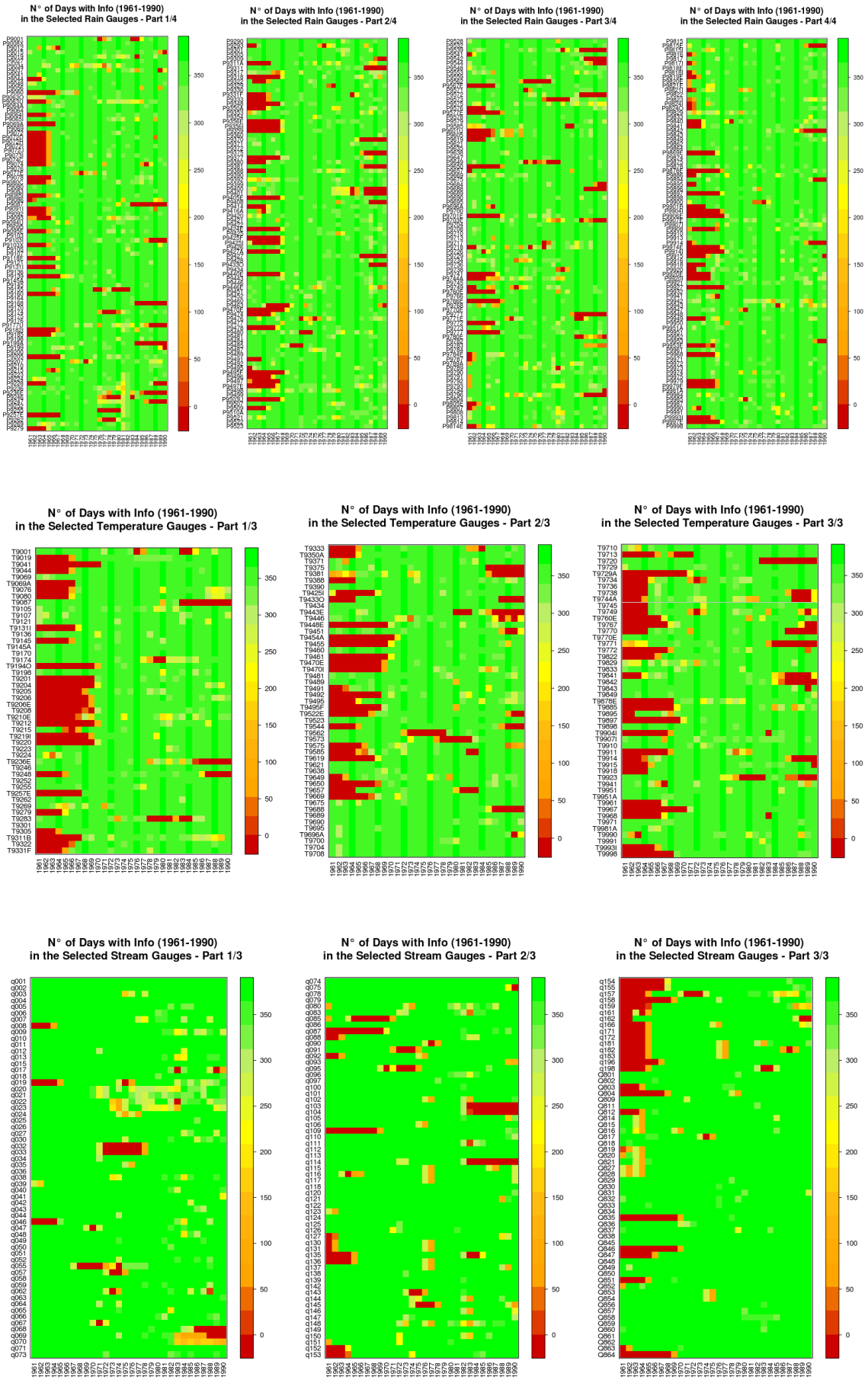

FIGURE 2.8: Days with information per year in the selected gauges, during the period Jan/1961-Dec/1990, considering only those stations with more than 70%, 65% and 65% of days with information for precipitation, temperature and stream gauges, respectively.

"To know one's ignorance
is the best part of knowledge"
(Lao Tse)

3

Hydrological Modelling (1961-1990)

This chapter describes the implementation of a semi-distributed modelling approach on the north-western part of Ebro River basin, and the uncertainty analysis carried out for the streamflows predicted with the hydrological simulations. Section 3.1 provides a brief introduction about conceptual rainfall-runoff modelling, parameter identifiability, equifinality, sensitivity and uncertainty analysis, in order to provide the required background for this chapter. In section 3.2 the selected hydrological model, Soil and Water Assessment Tool (SWAT), is described along with its set up in a 42000 km^2 catchment area in the Northern Spain, in order to carry out daily simulations during the control period 1961 - 1990. In section 3.4, a Latin-Hypercube One-factor-At-a-Time (LH-OAT) sensitivity analysis method is used to identify parameters with the highest impact on simulated streamflows; whereas the Generalized Likelihood Uncertainty Estimation (GLUE) methodology was used, in combination with a Latin Hypercube (LH) sampling, to carry out the uncertainty analysis and to select parameter sets that better represent the catchment behaviour during the calibration period 1962-1980. Parameter sets deemed as good simulators of the catchment during calibration were then tested during the verification period 1981-1990. The large number of simulations required to assess the combined effect of uncertainties in hydrological parameterisation and driving climate scenario, in the next chapters of this dissertation, leads to consider only two study catchments for testing the proposed methodology, and similar approaches can then be used for the entire area, already set up. Finally, section 3.6 presents the results and a brief summary of the main findings, at the end of this chapter.

3.1 Introduction

3.1.1 Conceptual Rainfall-Runoff Modelling

Hydrological models have been increasingly used during the last decades (tightly tied to the development of computer power) for a variety of purposes, including water resources assessment and management, flood forecasting, runoff estimation in ungauged basins, impact assessment of land use and climate change, point and diffuse pollution assessment, support to policy making, and better understanding of some hydrological process. Hydrological models are *simplified* representations of interlinked complex processes undergoing in real catchments, in which the hydrological cycle is represented through a mathematical formulation of the most relevant and well-known physical process. The resulting set of equations are embedded into a computer code, and some *parameters* are used to characterize properties of the catchment that are constant under some circumstances (*Wheater*, 2008). The characteristics and data requirements of each model will depend on the particular aim that led to its development. Therefore, they could be grouped in different ways: deterministic/stochastic, surface runoff/groundwater; water-quantity/water-quality; metric (black/box)/parametric/mechanistic (physically-based) (*Wagener et al.*, 2004; *Wheater*, 2008); lumped/distributed/semi-distributed, or many combinations among them. In principle, the modelling approach should be decided according to the spatio-temporal scale of the problem, model and data availability, the objective of modelling task, and the type of catchment. Although the choice of the modelling approach is a very interesting and in some

cases a controversial topic, this is not the main focus of the present dissertation. Despite the fact that the physical laws governing the hydrological cycle involve complex relationships, evidence indicates that the information content in a rainfall-runoff record is sufficient to support models of only very limited complexity (*Jakeman and Hornberger*, 1993). Conceptual rainfall-runoff models are relatively simple and easy to use tools in which the model structure is specified prior to any modelling being undertaken, and at least one of the model parameters does not have a direct physical interpretation, in the sense of being independently measurable; hence it have to be estimated through calibration against observed data (*Wheater*, 2008; *Wagener et al.*, 2004).

3.1.2 Parameter Identifiability, Uniqueness and Equifinality

Some parameters used in conceptual models to represent the hydrological properties of the catchments do not have direct physical meaning and are usually estimated by a trial-an-error (calibration) procedure (*Wheater*, 2008; *Wagener et al.*, 2004), using one or more goodness-of-fit between observed and simulated values within the catchment. Even though computer power has been continuously increasing during the last decades, the exploration of the high-dimensional parameter space is undermined by several well-known problems (e.g. *Johnston and Pilgrim*, 1976; *Sorooshian and Dracup*, 1980; *Sorooshian et al.*, 1983; *Sorooshian and Gupta*, 1983; *Kuczera*, 1983; *Hornberger et al.*, 1985; *Duan et al.*, 1992; *Beven and Binley*, 1992; *Uhlenbrook et al.*, 1999): (a) more than one main convergence region; (b) multiple local optima on the objective function surface; (c) rough and non-convex response surface (d) non-linear interaction and interdependence of parameters; (e) selection of the objective function used to measure the agreement between observed and simulated values; (f) interactions between boundaries of different parameter values; (e) saddle points, where first derivatives vanish, but minima are not reached; (g) different scales for different parameters; (h) non-informative data (*Yapo et al.*, 1996), and (i) bias, autocorrelation and heteroscedasticity in the residuals (*Sorooshian and Dracup*, 1980; *Feyen et al.*, 2007). One important consequence of the aforementioned problems is the impossibility to find a unique *best* parameter set, i.e., many parameter sets might provide equally good fit to the observations (for a given performance criterion) (e.g. *Beven and Binley*, 1992; *Duan et al.*, 1992; *Freer et al.*, 1996; *Seibert*, 1997), leading to a *non-identifiability* and *equifinality* (*Beven*, 2006), arising from over-parametrized models, data limitations, and structural flaws in the conceptualization of the system. According to *Wheater* (2008), two major limitations for hydrological modelling arise from equifinality: (a) if parameters can not be uniquely defined, they can not be associated to catchment characteristics; hampering the application in ungauged catchments; and (b) if physical significance of parameters is ambiguous, representation of catchment change can be difficult to achieve.

3.1.3 Sensitivity Analysis and Calibration Techniques

Over-parameterisation of complex models is a well-known concern in hydrological modelling and it may turn into a challenge the assessment of the parameter values to be used for a given modelling task. The number of parameters involved in hydrological simulations will depend on the selected modelling approach and the spatial detail used for describing catchment's characteristics. Sensitivity analyses are valuable tools for identifying parameters with a high impact on model outputs, and for testing the selected model structure; allowing a better planning of future field measurements (*Sieber and Uhlenbrook*, 2005). The correct identification of sensitive parameters allows to reduce the amount of parameters subject to calibration. A short overview of existing methods for sensitivity analysis and their role in the model-building process is given by *Campolongo et al.* 2000; *Sieber and Uhlenbrook* 2005; *Francos et al.* 2003, and a full review can be found in *Saltelli et al.* (2000). Random One-factor-At-a-Time (OAT) (*Morris*, 1991) is a local sensitivity method integrated into a global one, where only one parameter is modified between two successive model runs, to obtain the partial effect of each parameter, allowing the unambiguous attribution of changes in model outputs to such a parameter (*Holvoet et al.*, 2005). Considering P parameters this analysis involves $P+1$ model runs to obtain the partial effect of each parameter. The partial effects obtained through

this method may depend on the nominal values chosen for the remaining parameters, and hence this procedure is repeated with several random sets of nominal values of the parameters, allowing the final effect of each parameter be obtained as the average of the partial effects (*van Griensven et al.*, 2006). The random sampling underlying the OAT procedure can lead to a significant computational cost. Latin-Hypercube (LH) sampling (*McKay et al.*, 1979) is an efficient technique to perform random sampling without requiring too many runs as the normal Monte-Carlo approach, in which each parameter range is divided into *N* strata with the same *1/N* probability of occurrence (uniform distributions within parameter ranges leads to *N* equal intervals). For each parameter, only one random value is generated from each stratum. *van Griensven et al.* (2006) developed an efficient Latin-Hypercube One-factor-At-a-Time (LH-OAT) method, used in the present dissertation. This approach combines the efficiency of LH sampling (ensuring that the full range of all the parameters has been sampled) with the OAT sensitivity analysis, by taking the LH samples as initial points for the OAT analysis, with a total of $N(p+1)$ required runs, where *N* is the number of strata used for each parameter, and *P* is the number of parameters under consideration. At the end of the analysis, LH-OAT provides a ranking of parameter sensitivity based on the final effects.

After a decision has been taken about which model parameters have to be estimated, a calibration procedure has to be selected for carrying out the parameter estimation. A great deal of research has been devoted to the development of calibration procedures, ranging from semi-intuitive/manual (*Janssen and Heuberger*, 1995) to fully automatic methods (e.g. *Duan et al.*, 1992; *Cooper et al.*, 1997; *Franchini et al.*, 1998; *Madsen et al.*, 2002; *van Griensven and Bauwens*, 2003; *Vrugt et al.*, 2003a; *Lin and Radcliffe*, 2006; *Vrugt et al.*, 2006; *Kuczera et al.*, 2006; *Zhang et al.*, 2009a); the former are very time-consuming processes that depends on the modeller's accumulated experience; and the latter are much faster and objective approaches, in the sense that explicit rules for changing the parameters are included in the algorithms implemented for carrying out the automatic search. Early developments in automated calibration methods were focused mainly on the selection of a single-objective index/criteria for measuring the distance between observed and simulated values, and the selection of an automatic optimization algorithm to find the parameter set that minimize that index/criteria within a pre-defined model structure (*Freer et al.*, 1996; *Yapo et al.*, 1998).

Automatic calibration procedures require the selection of an objective function to measure how close simulated values are to observations, and its quantitative assessment is used to provide an evaluation of the predictive capabilities of the model (*Legates and McCabe Jr.*, 1999). Despite the Pearson's product-moment correlation coefficient *r* and its square, the coefficient of determination R^2, are over-sensitive to outliers and are insensitive to additive and proportional differences between observed and simulated values (*Willmott*, 1981, 1984; *Legates and McCabe Jr.*, 1999), they are commonly used to assess the "goodness-of-fit" of hydrological models. To circumvent problems associated to correlation-based measures, some relatively new descriptive statistics have been proposed, for looking at the agreement between observed and simulated values with an emphasis on different aspects of the hydrological response. Among the previously mentioned statistics, some widely used are: the Nash-Sutcliffe efficiency NS_{eff} (*Nash and Sutcliffe*, 1970), the percent bias *PBIAS* (*Yapo et al.*, 1996), the index of agreement *d* (*Willmott*, 1981, 1984), the coefficient of persistence *P* (*Kitanidis and Bras*, 1980), the ratio of the root mean squared error to the standard deviation of the observations *RSR* (*Moriasi et al.*, 2007), and the weighted coefficient of determination bR^2 (*Krause et al.*, 2005). For a given number of observations, *n*, the aforementioned goodness-of-fit are defined in equations 3.1, 3.2, 3.3, 3.4, 3.5 and 3.6 as follow:

$$NS_{eff} = 1 - \left[\frac{\sum_{i=1}^{n} (S_i - O_i)^2}{\sum_{i=1}^{n} \left(O_i - \overline{O}\right)^2} \right] \qquad (3.1)$$

$$PBIAS = \left[\frac{\sum_{i=1}^{n} (S_i - O_i)}{\sum_{i=1}^{n} O_i} \right] \cdot 100 \qquad (3.2)$$

$$d = 1 - \left[\frac{\sum_{i=1}^{n} (S_i - O_i)^2}{\sum_{i=1}^{n} \left(|S_i - \overline{O}| + |O_i - \overline{O}| \right)^2} \right] \quad (3.3)$$

$$P = 1 - \left[\frac{\sum_{i=1}^{n} (O_i - S_i)^2}{\sum_{i=2}^{n} (O_i - O_{i-1})^2} \right] \quad (3.4)$$

$$RSR = \frac{\sqrt{\sum_{i=1}^{n} (S_i - O_i)^2}}{\sqrt{\sum_{i=1}^{n} \left(O_i - \overline{O} \right)^2}} \quad (3.5)$$

$$bR^2 = \begin{cases} |b| \cdot R^2 & , b \leq 1 \\ |b|^{-1} \cdot R^2 & , b > 1 \end{cases} \quad (3.6)$$

in which O_i and S_i correspond to the observed and simulated values at time step *i*, $\overline{O}$ is the arithmetic mean of all the observations, and *b* is the slope of the linear regression between observations and simulations.

The NS_{eff} measures the fraction of the variance of the observed flows explained by the model, its optimal value is 1.0, and values less than 0 indicates unacceptable performance, because the mean of the observed values is a better predictor than the simulations. Although the NS_{eff} is an improvement over the coefficient of determination for evaluation purposes, it is markedly sensitive to extreme values, as is R^2 (*Legates and McCabe Jr.*, 1999). The index of agreement *d* is a measure of the degree to which model predictions are error free, it varies between 0.0 and 1.0, the latter indicating a perfect agreement, and a the former representing a variety of complete disagreements. The *PBIAS* measures the tendency of the simulated variable to be larger or smaller than the corresponding observed value, its optimal value is 0.0, positive values indicate a tendency to over-estimation whereas negative values indicate a tendency to under-estimation. The coefficient of persistence *P* is commonly used for real-time forecasting models, it compares the predictions of the model with predictions obtained in a Wiener process (a linear increment of variance with time), where the best estimation for a future value is given by the last measurement, its optimal value is 1.0 and lower values indicates lower performance. The ratio of the RMSE to the standard deviation of the observations *RSR* standardizes RMSE using the observations, it varies from an optimal value of 0 (which means RMSE=0) to a large positive value. The bR^2 is an error index designed for dealing with systematic under- or over-predictions, where the coefficient of determination is weighted by the slope of the linear regression between observations and simulations, it varies from an optimal value of 1 to zero.

Legates and McCabe Jr. (1999) examined the use of goodness-of-fit measures for validation assessment of hydrological models, and they concluded that reporting a single goodness-of-fit measure is inappropriate for assessing the predictive capabilities of a model, because they are but single tools in assessing model performance. *Legates and McCabe Jr.* (1999) and *Krause et al.* (2005) also encouraged the use of absolute error measures (e.g., mean absolute error *MAE* and/or root mean squared error *RMSE*) in the units of the simulated variable, along with additional statistics and graphical tools (*Willmott*, 1984; *Willmott et al.*, 1985), in order to gain insights about systematic problems in the model. *Moriasi et al.* (2007) reviewed reported ranges for the previously described statistics, and recommended the use of the NS_{eff}, the *PBIAS* and *RSR*, along with graphical techniques for model evaluation, and suggested that streamflow simulations can be deemed acceptable when $NS_{eff} > 0.5$, $RSR < 0.7$ and $-25\% \leq PBIAS \leq +25\%$, *ME*, *MAE*, *RMSE*, are close to zero; and *d*, *P*, R^2 and bR^2 are close to 1.

However, practical experience with the calibration of hydrological models suggests that single-objective functions, no matter how carefully chosen, are often unable to properly capture all the main characteristics of the observed data, and therefore, parameter sets obtained with such single-objective calibration methods are seldom deemed acceptable by practitioners (*Yapo et al.*, 1998; *Vrugt et al.*, 2003b). Furthermore, multi-objective (e.g. *Yapo et al.*, 1998; *Boyle et al.*, 2000; *Wagener et al.*, 2001; *Seibert and McDonnell*, 2002; *Engeland et al.*, 2006; *van Griensven and Bauwens*, 2003; *Bekele and Nicklow*, 2007; *Pokhrel et al.*, 2008) and/or multi-site (e.g. *Zhang et al.*, 2008; *Cao et al.*, 2006)

optimization strategies might be needed to adequately represent the trade-offs among the different incommensurable and often conflicting objectives, and to better understand the limitations of the selected model structure (*Vrugt et al.*, 2003b).

Notwithstanding automatic calibration procedures are able to find parameter sets that reproduce reasonably well -according to one or more goodness-of-fit criterion- the observations, a good fit between observed and simulated streamflows might be obtained with different and even unrealistic concepts (e.g. *Uhlenbrook et al.*, 1999; *Mroczkowski et al.*, 1997), and therefore a good fit only ensures that the model under evaluation is *one* of many possible representations of the real system. Additionally, parameter optimization might result in biased parameter values, where errors in the estimated parameters are compensated with errors in the model structure (e.g. *Refsgaard et al.*, 2006), leading to fit the noise in the target signal instead of capturing the underlying physical process. Consequently, model predictions should be presented as ranges or probability distributions instead of single best predictions (*Freer et al.*, 1996; *Beven and Binley*, 1992; *Uhlenbrook and Sieber*, 2005; *Refsgaard et al.*, 2007). Moreover, *Wheater et al.* (2008) states that "*it will soon no longer be adequate to present a simulation output as a single best estimate, with no attempt to specify the associated confidence intervals*".

Recently, *Yilmaz et al.* (2008) suggested a diagnostic approach to model evaluation which abandon the classical approach to find parameter sets that optimize some aggregated measure of model performance, whereas it propose the use of *signature* patterns present in data to identify model inadequacies. The use of such signatures; related to the overall water balance, vertical soil moisture redistribution, long-term baseflow behaviour, and timing of flows at fine time scales; can help to avoid achieving better model performance due to wrong reasons, and to assist a semi-automated approach to detect model flaws, for resolving the failures through modifications to the corresponding model component/parameter group. Some of the signatures and concepts proposed by *Yilmaz et al.* (2008) are used during the uncertainty analysis of this dissertation (section 3.4.2).

3.1.4 Uncertainty in Hydrological Modelling

In contrast to other sciences in which it is possible to obtain an exact solution for the phenomenon under study, hydrology is a highly uncertain science, in which complex dynamics of many hydrological processes, physical domains that evolve in time, data scarcity, and errors in measurements hamper the theoretical treatment of the aforementioned problems. Uncertainty, ignorance, error, risk and other related terms widely used in hydrology are defined in a different way by different authors. Brief definitions and taxonomies can be found in *Refsgaard et al.* (2007), whereas *Walker et al.* (2003) provides a conceptual basis for the treatment of uncertainty in policy-making and other model-based activities. We want to emphasise the difference between *ignorance* and *uncertainty*, in which the former represents a lack of awareness regarding imperfect knowledge, and the latter stands for a degree of confidence in the possible outcomes. The uncertainty treatment adopted in this dissertation correspond to the general definition given by *Walker et al.* (2003), in which uncertainty is "*any deviation from the unachievable ideal of completely deterministic knowledge of the real system*". In this way, uncertainty is an unavoidable fact when dealing with real catchments, and hydrologists have to get use to include it into their every-day decisions.

3.1.4.1 Sources and Nature of Uncertainty

The sources of uncertainty can be identified under the umbrella of different -and not always consistent- classification schemes (*Matott et al.*, 2009). In this dissertation we adopted the following main sources of uncertainty: (a) input data (e.g. *Vrugt et al.*, 2008; *Ajami et al.*, 2007; *Kuczera et al.*, 2006), used to drive hydrological simulations; (b) model parameter values, used to represent some features of the real system, within the selected model structure; and (c) model structure or conceptual model (e.g *Smith et al.*, 2008a; *Beven et al.*, 2008; *Ajami et al.*, 2007; *Refsgaard et al.*, 2006; *Butts et al.*, 2004; *Wagener et al.*, 2003; *Sorooshian and Gupta*, 1985), used as a simplified representa-

tion of the real system under study. However, some authors identify additional sources: modeller uncertainty (*Linkov and Burmistrov*, 2003), initial system state uncertainty (*Beck*, 1987), context and technical uncertainty (*Refsgaard et al.*, 2007), and outcome uncertainty (*Walker et al.*, 2003).

According to *Matott et al.* (2009), uncertainty may also be classified as *reducible* or *irreducible*, depending on its nature[1]. Reducible uncertainty comes from imperfect knowledge, conceptualizations, data, etc., and can be reduced by more studies; whereas irreducible uncertainty originates in the natural variability of the phenomenon under study (e.g, rainfall, streamflows). The quest for a reasonably good representation of the real catchments is often affected by both types of uncertainty.

3.1.4.2 Uncertainty Assessment

Hydrological predictions are commonly used to support the introduction of a new environmental regulation policy, to design mitigation plans for climate change impacts, etc. Therefore, quantification of the reliability of hydrological predictions has a societal importance. Uncertainty assessment is a research topic with an increasing number of contributions in the recent years. Methodologies for uncertainty assessment are numerous, ranging from objective/analytical approaches (e.g., error propagation equations, sensitivity analysis, inverse modelling) to subjective judgements (e.g., expert elicitation, extended peer-review). *Refsgaard et al.* (2007) provides a brief review of 14 methodologies used in uncertainty assessment and characterization, within a framework tailored to the role of uncertainty in model-assisted water management practices. Recently, *Matott et al.* (2009) provided a summary of concepts related to characterization, quantification and propagation of uncertainty in integrated environmental models, presented a list of relevant tools, and gave some guidelines for both practitioners and tool developers.

3.1.4.3 Generalized Likelihood Uncertainty Estimation (GLUE)

In a way of providing a realistic assessment of the uncertainties in model predictions, coming from imperfect knowledge about model structure, parameter sets and forcing data, *Beven and Binley* (1992) proposed the Generalized Likelihood Uncertainty Estimation (GLUE), an uncertainty analysis methodology developed as an extension of the Generalized Sensitivity Analysis (*Beven*, 2006) of Hornberger, Spear and Young (*Whitehead and Young*, 1979; *Hornberger and Spear*, 1981; *Young*, 1983), to assess the confidence in model predictions of complex real-world applications (*Beven et al.*, 2008), where new block of data are not always informative for formal likelihood measures (*Beven et al.*, 2007). From that point on, GLUE has been widely used in hydrological applications (e.g *Freer et al.*, 1996; *Beven and Freer*, 2001; *Beven*, 2006; *Blasone et al.*, 2008a; *Yang et al.*, 2008). *Beven and Binley* (1992) argue that "*prior to the introduction of any quantitative or qualitative information to a modelling exercise, any model/parameter set combination that predict the variable or variables of interest must be considered equally likely simulator of the system*".

The GLUE methodology rejects the idea of a unique "*best*" representation of real system in favour of all the possible acceptable (or "*behavioural*" in the GLUE terminology) model structures and parameter sets within model structures (*Beven*, 2006; *Beven et al.*, 2000), on the basis of available data and knowledge. The selection of behavioural parameters is made on the basis of a performance cut-off threshold, whereas the distribution of model predictions are computed using a "*less formal*" likelihood function. Simulators that performs below the cut-off threshold are assigned a likelihood of zero, whereas all the simulators with a performance higher than the cut-off threshold are retained as acceptable representations of the system, and hence used to compute the predictive uncertainty. The selection of both the cut-off threshold and the less formal likelihood is modeller's dependent, and expresses his/her understanding of the uncertainties involved in the modelling process. The GLUE methodology can be summarized as follow:

[1] *Walker et al.* (2003) refers to the reducible uncertainty as *epistemic*, and to the irreducible uncertainty as *stochastic* or *ontological*.

1. Selection of a prior probability distribution for each parameter within each model structure under consideration.
2. Definition of a methodology for sampling the parameter space.
3. Formal definition of a likelihood measure or set of likelihood measures, for assessing the goodness-of-fit between observed and simulated values.
4. Performance assessment of each simulator, using the likelihood function.
5. Selection of behavioural parameter sets, using a cut-off threshold.
6. Rescaling the likelihood of the behavioural parameter sets, such they sum to 1.
7. Compute predictive uncertainty, by using quantiles of the cumulative distribution of each predicted output, weighted by its corresponding likelihood.

GLUE uses the term *likelihood* as a fuzzy concept that represent the degree of confidence of the modeller in each parameter set within a particular model structure, instead of using the restricted sense of maximum likelihood theory, which assumes errors with zero mean and normally distributed (*Beven and Binley*, 1992). Requirements for the chosen likelihood measure are: (i) it should be zero for all the simulators that do not represent the real behaviour of the system, and (ii) it should increases monotonically for better representations of the system (*Beven and Binley*, 1992). Following *Freer et al.* (1996), results presented in this study make use of the following likelihood measure:

$$L[\underline{\theta}_i|\underline{Y}] = \left(1 - \frac{\sigma_i^2}{\sigma_{obs}^2}\right)^N \quad ; \quad \sigma_i^2 < \sigma_{obs}^2 \tag{3.7}$$

where $L[\underline{\theta}_i|\underline{Y}]$ is the likelihood of the $\underline{\theta}_i$ model conditioned on the $\underline{Y}$ set of observations, σ_i^2 is the error variance associated to the $\underline{\theta}_i$ model, σ_{obs}^2 is the variance of the observations during the analysis period, and N is a shape parameter. The higher the value of N the higher will be the weight associated with better simulations. When N is equal to 1, equation 3.7 is equivalent to the Nash-Sutcliffe efficiency criterion (*Nash and Sutcliffe*, 1970). Other likelihood measures are discussed in *Smith et al.* (2008b); *Beven and Freer* (2001); *Beven et al.* (2000), and *Beven and Binley* (1992). Consequently, predicted uncertainties obtained with GLUE will be conditional to the data used as input, to the selected model structure, to the models parameter sets evaluated through the sampling strategy, and to the *less formal* likelihood measure used to assess the model performance. Therefore, all of these decisions have to be made explicit to the end users, in order to allow them to decide if those choices are in agreement with the objectives of the modelling study (*Beven*, 2001; *Beven et al.*, 2008).

The subjective decisions ("*less formal*" likelihood and behavioural threshold) required to implement the GLUE methodology have been the focus of some recent debate (*Montanari*, 2005; *Mantovan and Todini*, 2006; *Beven et al.*, 2007; *Mantovan et al.*, 2007; *Beven et al.*, 2008; *Stedinger et al.*, 2008). In this dissertation, we subscribe what expressed by *Beven et al.* (2007): "*the use of a formal Bayes likelihood function is essentially a special case of GLUE where the user is prepared to make strong assumptions about the nature of the errors*". We also support that a correct estimation of the nature of the errors in real hydrological problems is undermined by "*(unknown) input errors that are processed non-linearly through hydrological models that are subject to model structure errors*" (*Beven et al.*, 2008), limiting the correct application of a formal Bayesian approach. Moreover, making such strong assumptions can yield to an apparent sensation of having the right result when those assumptions might not be fulfilled (*Beven et al.*, 2007). Consequently, we chose the GLUE methodology as a framework for assessing the uncertainty in the model predictions subject to our imperfect knowledge, and to assist in the identification of conceptual model inadequacies and errors in the data used to drive the simulations. Recently, *Vrugt et al.* (2009a), including the discussion given by

Beven (2009) and *Vrugt et al.* (2009b), showed that formal Bayesian methods and GLUE can lead to very similar values of total predictive uncertainty, even when they are based on completely different error representation approaches.

3.2 Model Description (SWAT)

Among the plethora of hydrological models available (see *Singh and Frevert*, 2006; *Wagener et al.*, 2004; *Singh and Frevert*, 2001; *Singh*, 1995), the Soil and Water Assessment Tool (SWAT) version 2005, (*Arnold et al.*, 1998; *Arnold and Fohrer*, 2005), was selected for carrying out the hydrological simulations, for the following four reasons. Firstly, the hydrological modules of SWAT have been used for assessing water quantity and quality evolution in a wide range of spatial scales (e.g. *Arnold et al.*, 2005; *Cao et al.*, 2006; *Fontaine et al.*, 2002; *Schuol et al.*, 2008a; *Zhang et al.*, 2009b), climates (e.g. *Van Liew and Garbrecht*, 2003) and hydrogeologic conditions (e.g. *Mapfumo et al.*, 2004; *Arnold et al.*, 2005; *Abbaspour et al.*, 2007; *Gosain et al.*, 2005; *Wu and Johnston*, 2007; *Thomson et al.*, 2005; *Krysanova et al.*, 2007) worldwide (e.g. *Abbaspour et al.*, 2009; *Setegn et al.*, 2009; *Schuol et al.*, 2008b; *Ndomba et al.*, 2008; *Yang et al.*, 2007; *Arnold et al.*, 1999; *Borah and Bera*, 2004). A comprehensive review of SWAT model applications, strengths and weaknesses can be found on *Gassman et al.* (2007). Secondly, its GIS interface allows the modeller a relatively fast implementation of the data involved in the simulation of a large river basin, and it is computationally efficient to operate on a large scale in a reasonable time. Thirdly, its inputs are commonly available from government agencies. Fourthly, the source code of its hydrological routines have been recoded into Fortran 90 (*Arnold and Fohrer*, 2005), are well documented and freely available on the web, allowing further customization for tackling particular needs (e.g. *Holvoet et al.*, 2008; *Haverkamp et al.*, 2005; *Eckhardt et al.*, 2002; *Sophocleous et al.*, 1999; *Krysanova et al.*, 1998). An advantage of SWAT is its modular structure, where different process (water quality, sediments, pesticides, etc.) can be activated or excluded during the simulations, depending on the amount of available data.

SWAT is a public domain (http://www.brc.tamus.edu/swat), basin scale, physically based, conceptual, continuous-time model that operates on a daily time step. SWAT integrates more than 30 years of model developments, within the US Department of Agriculture's (USDA) Agricultural Research Service (ARS) (*Arnold and Fohrer*, 2005) into a single model, developed to support water managers in assessing the impacts of climate and management practices on water supplies, sediments, non-point source loadings, and pesticide contamination in ungauged watersheds and large complex river basins, with varying soils, land use and management conditions over long periods of time (*Arnold et al.*, 1998; *Neitsch et al.*, 2005a). Upland model components of the latest version (2005) include weather, hydrology, erosion/sedimentation, soil temperature, plant growth, nutrients, pesticides, agricultural management, sediment and nutrient loadings from urban areas, bacteria growth/die-off, and modified dormancy calculations for tropical areas. Stream process allow for routing of water, sediment, nutrient and organic chemicals in the main channel and transport of bacteria from land areas to the stream network. Pond/reservoir components include water balance (considering inflow, outflow, rainfall on the surface, evaporation, seepage from the reservoir bottom, and diversions), routing, sediment settling, and simplified nutrient and pesticide transformation algorithms. Water diversion into, out of, or within the basin might be modelled to represent irrigation, water supply and other withdrawals from the system (*Arnold and Fohrer*, 2005; *Neitsch et al.*, 2005a).

In SWAT, the spatial hetereogeneity of the study area is represented by dividing the main basin into a large number of subbasins or subwatersheds connected by a stream network. Each subbasin is further subdivided into several homogeneous Hydrological Response Units (**HRUs**), unique combinations of land use and soil type, based on threshold percentages thereof (*Arnold et al.*, 1998; *Neitsch et al.*, 2005a,b). Subdividing the main catchment into HRUs allows the model to reflect differences in evapotranspiration and other hydrologic conditions for different land cover/crops and soils, increasing the accuracy of load computations (*Fitzhugh and Mackay*, 2000) and providing a much better physical description of the water balance (*Neitsch et al.*, 2005a) . Alternatively, for

studies involving large spatial or long-term scales, a single HRU can be used for characterizing each subcatchmet, with the dominant land use, soil type and management combination. Soil water content, surface runoff, nutrient cycle, sediment yield, crop growth and management practices are simulated for each HRU and then aggregated for the subbasin by a weighted average (*Abbaspour et al.*, 2007). Computed flow, sediment yield and nutrient loading obtained for each subbasin are then routed through the river network to the watershed outlet, using the variable storage or Muskingum method, both of them variations of the kinematic wave model (*Neitsch et al.*, 2005a).

The water balance in each HRU is computed in four storages: snow, soil profile, shallow aquifer, and deep aquifer, including canopy interception of precipitation; partitioning of precipitation, snowmelt water, and irrigation water between surface runoff and infiltration; redistribution of water within the soil profile, and return flow from shallow aquifers, as depicted in Figure 3.1. Surface runoff from daily rainfall is estimated using a modified SCS curve number method, which takes into account the antecedent moisture condition; or the Green-Ampt infiltration equation, which requires measured or generated sub-daily precipitation inputs. Potential evapotranspiration can be computed with the Hargreaves (*Hargreaves et al.*, 1985), Priestey-Taylor (*Priestey and J.*, 1972) or Penman-Monteith (*Monteith*, 1965) method depending on the available data[2], or it can be read from daily potential evapotranspiration (PET) values computed by a different method. Peak runoff predictions are computed with a modified rational formula, whereas the concentration time of the watershed is estimated using Manning's formula, considering both overland and channel flow. Up to ten elevation bands can be used for representing orographic precipitation and/or snowmelt, based on the routines developed by *Fontaine et al.* (2002). Snow melts on days when the average between the snowpack and maximum air temperature exceeds a threshold value, allowing for seasonal variations, and melted snow is treated as rainfall for the computation of runoff and percolation.

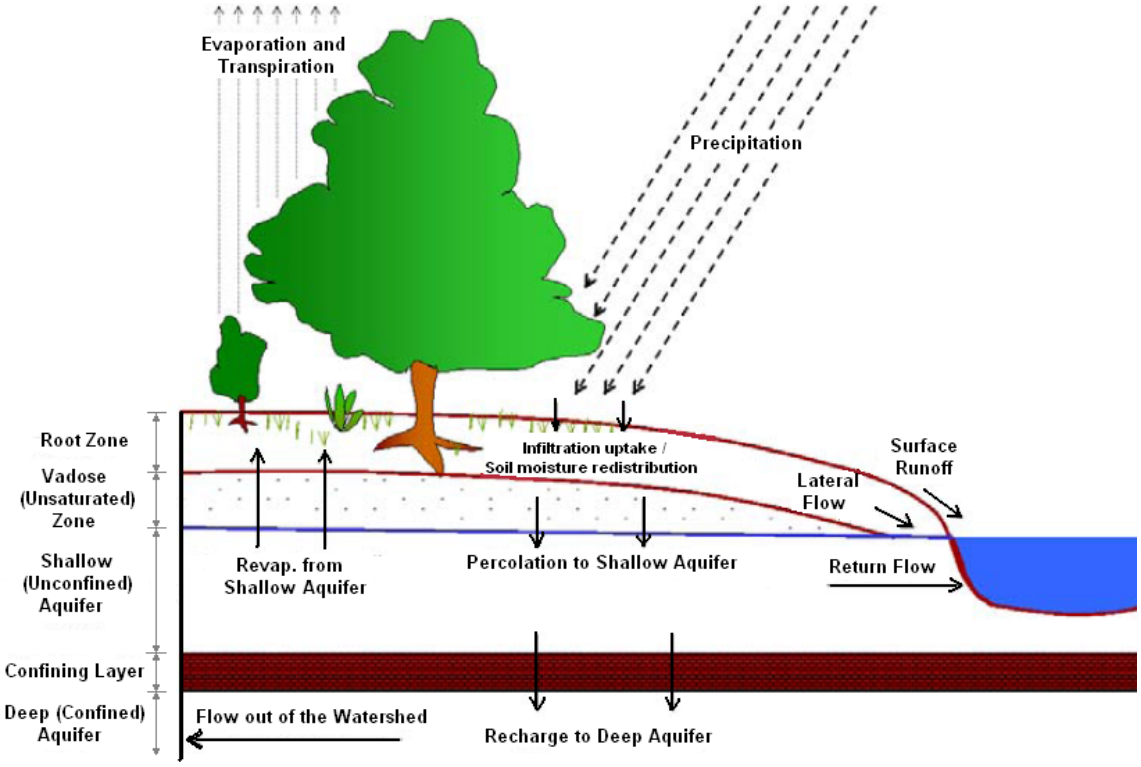

FIGURE 3.1: Schematic representation of the hydrologic cycle in SWAT. After *Neitsch et al.* (2005a), with permission.

Water in the soil can flows under saturated or unsaturated conditions, and SWAT directly simulates saturated flow only, assuming that water is uniformly distributed within each layer. This

[2]Hargreaves method requires air temperature only; the Priestey-Taylor method additionally requires solar radiation and relative humidity; whereas the Penman-Monteith requires wind speed as well.

assumption eliminates the need to model the saturated flow in the horizontal direction (*Neitsch et al.*, 2005a). The soil profile might be divided into multiple layers in which infiltration, evaporation, plant uptake, lateral flow, and vertical redistribution process to other layers can take place. A storage routing is used to compute redistribution of water between layers in the soil profile. Saturated flow occurs when the water content of a soil layer surpasses the field capacity of that layer, and the water in excess is available for percolation, lateral flow or tile flow drainage, unless the temperature of the soil layer is below $0°C$, in which case no water movement is computed[3]. Unsaturated flow between layers is indirectly simulated with the depth distribution of plant water uptake and the depth distribution of soil water evaporation (*Neitsch et al.*, 2005a). Lateral flow is simulated through the kinematic storage model for subsurface flow developed by *Sloan et al.* (1983) and summarized by *Sloan and Morre* (1984). Percolation from each soil layer in the root zone is allowed when the water content of that layer exceeds its field capacity and the layer below is not saturated (*Neitsch et al.*, 2005a). Percolation from the bottom of the soil profile recharges the shallow aquifer, which is conceptualized as an unconfined aquifer that contributes to flow in the main channel or reach of the subbasin (*Neitsch et al.*, 2005a). The deep aquifer is a confined one, and water entering to it is considered a loss that contributes to streamflow somewhere outside the main watershed (*Arnold et al.*, 1993).

A complete description of the model components and their associated equations can be found in *Arnold et al.* (1998) and *Neitsch et al.* (2005a).

3.3 Model Setup

Data required for this study were compiled from different sources as described in section 2.2. Application of SWAT to the Ebro River basin requires topographic, soil, land use, and climate data, as well as streamflow data for calibration, verification, and uncertainty analysis. Discretization of the main basin into subbasins and HRUs requires several input files in ASCII format. Each subbasin requires six files to specify the subbasin (.sub), weather (.wgn), water use (.wus), water quality (.swq), main channel (.rte), and impoundments (.pnd) parameters; whereas each HRU requires five files to describe soil (.sol), groundwater (.gw), management (.mgt), topography and water cycle (.hru), and chemistry (.chm) main properties. All the previous files can be input manually, but this is a very time-consuming and prone-to-error task.

Nowadays there are three main GIS interfaces available to speed up the creation of the input files required by SWAT, all of them developed for the © Windows operative system: (a) ArcSWAT (*Olivera et al.*, 2006; *Winchell et al.*, 2007), ESRI ArcGIS extension that works over © ArcGIS-ArcView 9.x; (b) AVSWAT-X (*Di Luzio et al.*, 2002b,a, 2004), ESRI ArcView extension that works over © Arc-View 3.x; and (c) MWSWAT (*George and Leon*, 2007), free and open source interface that works over MapWindow. We tried MWSWAT in 2008, but it was unable to handle an area of 41000 km^2 with a spatial resolution of 60 x 60 m. Finally, we chose AVSWAT-X (http://swatmodel.tamu.edu/software/avswat) because it was fast and stable for setting up initial parameters values and generating the corresponding ASCII input files required for the hydrological simulations, from the available map layers.

3.3.1 Conceptual Model

An adequate representation of the water availability in a catchment strongly affected by anthropogenic disturbances, as the Ebro River basin, not only requires that the main hydrological process be "well" represented, but also needs the main abstractions, reservoirs, and water transfers be considered in the hydrological modelling task; which implies to collect, analyse and simplify its main spatio-temporal features before they can be included into the hydrological model. In order to spend the available time in developing and testing the proposed methodology instead of

[3]Daily average soil temperature is simulated as a function of the maximum and minimum air temperature.

collecting and analysing raw data, only the western part of the Ebro River basin, shown in Figures 2.1 and 3.2, was selected as study area for the hydrological simulations, with a total area of 42000 km^2. Elevations within this western area range from 185 to 2875 m.a.s.l., with an average elevation of 790 m.a.s.l., and 50% of the area below 770 m.a.s.l.

The size, scale, and number of subbasins used in the SWAT simulations may impact the modelling process and its subsequent results (*Jha et al.*, 2004). *Tripathi et al.* (2006) showed that the number and size of sub-watersheds used in SWAT do not appreciably affect runoff, but it has a significant effect on the water balance components. *Jha et al.* (2004) also concluded that the number of sub-watersheds has very little effect on streamflow, but they found that the opposite result is verified for sediment, nitrate, and inorganic phosphorus. In principle, the use of subbasins in a simulation is beneficial when different areas within the main basin are different enough in properties to impact its hydrological behaviour (*Neitsch et al.*, 2005a), but the larger the number of subbasins the larger the input data preparation effort and the subsequent computational evaluation (*Tripathi et al.*, 2006). Additional information about the effect of watershed delineation on SWAT outputs can be found in *Jha et al.*, 2004; *Tripathi et al.*, 2006; *Arabi et al.*, 2006; *Muleta et al.*, 2007; *Fitzhugh and Mackay*, 2000; *Binger et al.*, 1997. The DEM described in section 2.2.1 was used to divide the study area into 120 subcatchments, as shown in Figure 3.2, taking into account: (a) the original watershed subdivision provided by CHE, in which water balances are computed for planning purposes; (b) the presence of gauging stations with long-term data; and (c) the existence of important withdrawals/infrastructures (e.g. reservoirs, channels). The resulting catchment boundaries and drainage network were in close visual agreement with the corresponding vectorial maps available at the the CHE website . The total and accumulated drainage area; overland field slope and length; and channels dimensions, slope and length were derived with the AVSWAT-X GIS interface (*Di Luzio et al.*, 2002b,a, 2004) for each sub-watershed, and this information was used at a sub-watershed level.

Climate change projections are now based on multi-model ensembles to span as much as possible the possible range of uncertainties associated to the likely future climate (e.g. *Tebaldi and Knutti*, 2007; *Meehl et al.*, 2007; *Christensen et al.*, 2007b; *Giorgi and Mearns*, 2003). At the other hand, calibration and uncertainty analysis of any hydrological model involves a large number of runs, in order to examine the performance of different parameter sets in representing the target observed values. Consequently, the propagation of the uncertainties coming from hydrological parameterisation into the ensemble of likely future climates leads to a very large number of runs of the hydrological model[4], considering both the historical period and the future scenarios. In this way, to test the feasibility of the developed methodology, two test catchments were first selected within the study area, in order to allow similar approaches be applied afterwards on the remaining subbasins. The selected subcatchments were chosen since they represent two different climatic conditions of the Ebro River basin, and because they have an amount of data that is enough for implementing the hydrological simulations, as shown in Table 3.1. The location of the selected catchments, and the main elements involved in the hydrological simulations are shown in Figure 3.2. The selected subcatchments were:

1. Sub-basin 090: It correspond to the Ega River basin, located in the central part of the study area, with 1004 m of elevation range (420 to 1424 m.a.s.l.). The mean annual precipitation is 817.5 mm $year^{-}1$, computed with the values observed during the control period 01/Jan/1961 - 31/Dec/1990 in the four raingauges located within this catchment (P9175, P9176, P9095, P9177U). It is representative of catchments with an intermediate climatological regime.

2. Sub-basin 115: It corresponds to the Homino River basin, located in the north-eastern part of the catchment, with 680 m of elevation range (570 to 1250 m.a.s.l.). The mean annual precipitation is 543.0 mm $year^{-1}$, computed with the values observed during the control period

[4] which depends on the uncertainty analysis procedure and the amount of climate models considered for the future scenarios.

01/Jan/1961 - 31/Dec/1990 in the two raingauges located within this catchment (P9034, P9037). It represents catchments with a clear semi-arid condition.

TABLE 3.1: Main characteristics of the two selected subcatchments, including ID in the SWAT project, draining area, elevation range, streamgauge station name, period with streamflow data, the number of days with missing data, the mean annual streamflow ($\overline{Q}$) and the mean annual precipitation ($\overline{P}$) of each catchment, the latter two computed for the control period 1961-1990.

Subb. ID	Draining Area [km^2]	Elevation Range [m.a.s.l.]	Station ID	Q Station Name	Period with Q Data	N° missing daily Q data	$\overline{Q}$ [m^3/s]	$\overline{P}$ [mm]
90	808.07	420-1424	Q071	Ega en Estella	1931-2002	7	12.51	817.5
115	1040.34	570-1250	Q093	Oca en Oña	1959-2002	480	5.03	542.9

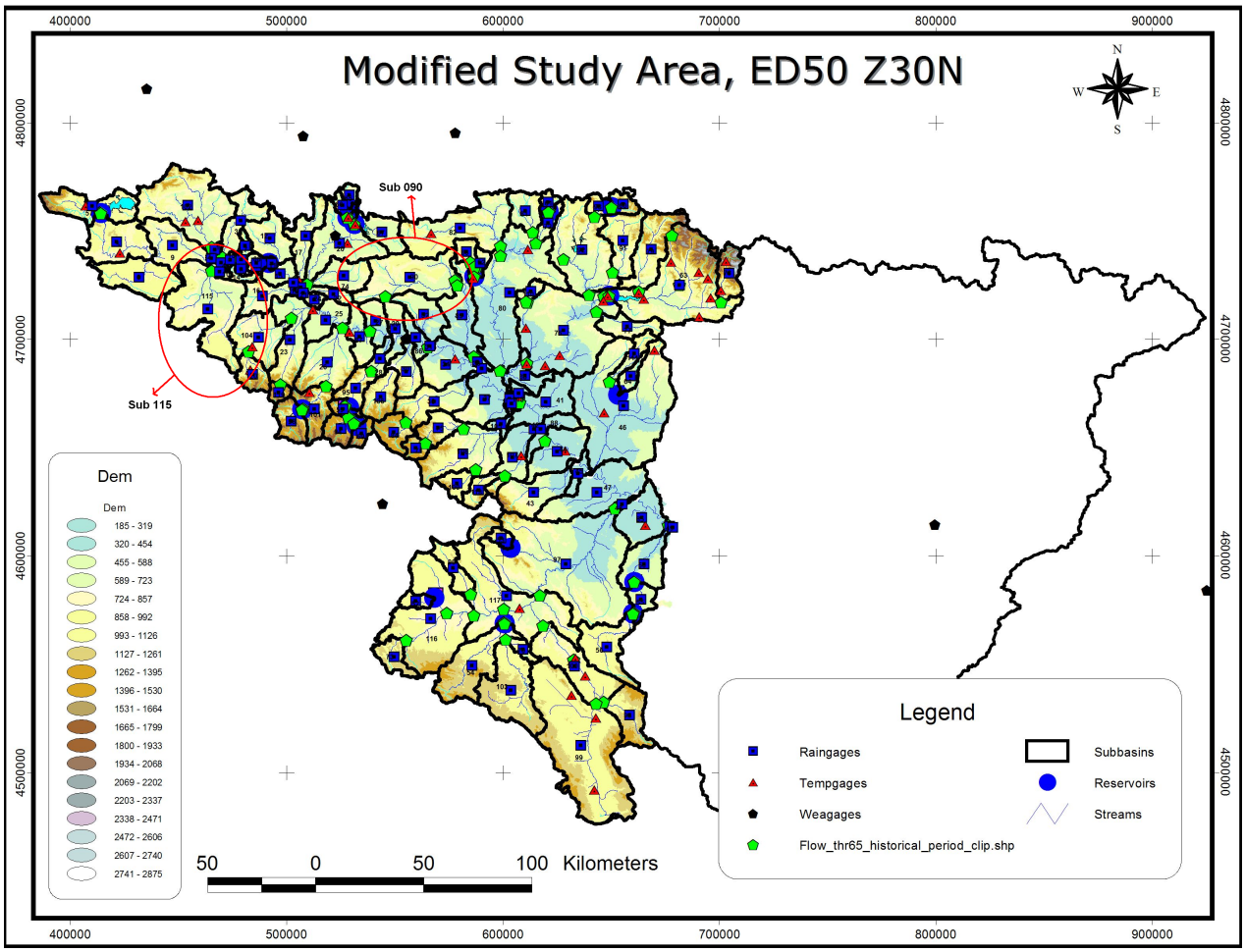

FIGURE 3.2: Map of the study area showing the location of the 120 sub-catchments adopted in the present dissertation. The red circles indicate the location of the two subwatersheds selected for carrying out the hydrological simulations during the control and future scenarios.

In this dissertation the subbasins were characterized by the dominant land use and soil type combination, instead of considering several HRUs for each subbasin. This decision was taken in order to: (a) obtain the simplest yet realistic description of the catchment that allows a reasonably good representation of the flows thereof, or in other words, to obtain a parsimonious structure for each subcatchment, in order to reduce the number of parameters involved in the further stages of calibration and uncertainty analysis; and (b) to reduce the time needed for carrying out the large

amount of simulations involved in the uncertainty analysis and future climate scenarios.

According to the document "Caracterización de las Alteraciones del Régimen Hidrológico Sufridas en las estaciones de Aforos de la Cuenca del Ebro" [Characterization of the Disturbances to the Hydrological Regime on the Streamflow Stations of the Ebro Basin] (*CHE*, 2008) gauging stations located at the outlet of the selected catchments (Q071 and Q093) are only slightly modified by withdrawals, hence no consumptive use was incorporated in the simulations of their corresponding catchments.

3.3.2 Land Use

The available land use cover was described in section 2.2.2, and Table 3.2 presents the six major land use classes identified within the study area and the corresponding names used in SWAT.

TABLE 3.2: Land uses within the study area and adopted for the hydrological simulations, based on information for the year 1984 at 1:100000 scale

GRID Value	SWAT ID	SWAT LandCover/Plant Class	% Study Area	Original Name
1	SPAS	Summer Pasture	0.91	Roquedo
2	FRST	Forest-Mixed	26.12	Bosques
3	PAST	Pasture	64.48	Praderas
4	URML	Urban, Medium Density	0.42	Suelo Artificial
5	WATR	Water	0.038	Lagos Interiores
6	AGRL	Agricultural Land-Generic	8.04	Regadíos

3.3.3 Soil Types

The original soil cover information was described in section 2.2.3. Each one of the 23 major soil classes was "*assimilated*" to one available in the SWAT soil database, as included in the SWAT Editor v.2.1.4, in order to have a rough initial estimation of the soil properties, but considering only one layer for each soil class, as shown in Table 3.3. This simplified assimilation responds to the following two criteria: (a) this classification should give an idea about the spatial distribution of the major soil classes within the study area; (b) the values of most important effective parameters of each soil class will be provided by the calibration procedure in a further stage.

TABLE 3.3: Soil classes within the study area and adopted for the hydrological simulations with SWAT 2005.

VALUE	Adopted STMUID	NAME	Adopted S5ID	Fitted Class	Original IDDOM's ID
1	VT023	LIVINGSTON	VT0018	Arcillas	315, 7347, 7348, 7349, 7358
2	VT027	DUANE	NY0034	Arenas	451
3	VT002	POOTATUCK	CT0064	Arenas y otros	310, 360, 370, 990, 1010, 1040, 7212, 7213, 7224
4	VT025	STETSON	ME0021	Areniscas	100, 110, 330, 400, 540, 660, 661, 721, 722, 723, 7236
5	VT002	HERO	CT0047	Brechas	210, 491
6	AL253	HUMPHREYS	TN0026	Calcarenitas, margas y calizas arenosas	622
7	VT065	HADLEY	MA0022	Calizas	3, 6, 121, 123, 230, 240, 250, 260, 280, 312, 316, 320, 340, 341, 350, 410, 421, 440, 470, 490, 620, 650, 651, 752, 753, 754, 758, 970, 7513
8	VT081	MACHIAS	ME0033	Cantos	910, 920, 940, 950, 980

Continued on next page...

Table 3.3 – Continued

VALUE	Adopted STMUID	NAME	Adopted S5ID	Fitted Class	Original IDDOM's ID
9	AL003	BODINE	TN0064	Conglomerados	311, 711, 713, 714, 716, 900, 7113, 7123, 7124, 7134, 7136, 7145, 7146, 7147, 7148, 7149, 7179, 7248
10	VT016	MIDDLEBURY	NY0045	Cuarcitas y pizarras	1, 4, 10
11	VT059	NINIGRET	CT0018	Dolomias	120, 200, 290, 621
12	VT082	ONDAWA	ME0010	Facies lagunares con sales potasicas	662
13	VT072	NICHOLVILLE	NY0099	Flysch: Areniscas y lutitas en facies turbiditicas	630
14	VT004	BERKSHIRE	MA0030	Grauvacas y pizarras. Arenitas, pelitas y conglomerados	5
15	VTPIT	PITS	NY0029	Gravas	930, 960, 1030
16	VT033	MELROSE	ME0034	Intercalaciones de calizas lacustres y lignitos	611
17	VT079	HOWLAND	ME0005	Limolitas y Limos	313, 728, 1060, 7246
18	VT082	CHARLES	ME0082	Lutitas	7, 122, 380, 610, 733, 734, 7313, 7335, 7346, 7359
19	VT068	MOOSILAUKE	NH0043	Margas	130, 220, 270, 314, 342, 422, 441, 450, 460, 480, 530, 640, 641, 743, 7446, 7449, 7456
20	VT082	LOVEWELL	ME0081	Megabrechas carbonatadas, ofitas, pizarras ampeliticas, rocas filonianas, rocas metamorficas, Sales, serie mixta detritico-terrigena	2, 140, 430, 631, 1050, 3000, 4000
24	VT096	ROCK OUTCROP	DC0015	Rocas Intrusivas	2000
26	VT088	OAKVILLE	MI0038	Rocas volcanicas	5000
29	VT007	RIPPOWAM	CT0065	Yesos	761, 763, 7623, 7636, 7646, 7656

3.3.4 Daily Maximum and Minimum Temperature on Gauging Stations

As described in section 3.2, computation of ETP requires -at least- measurements of air temperature, and in particular, SWAT requires daily maximum and minimum air temperature in all the selected temperature stations, data that were not available during the control period 1961-1990. However, as mentioned in section 2.2.5, hourly data were available in the HidroEbro database, were provided by the (OPH) in April 2008, for the period 01/Jan/2003 - 16/Oct/2006 in 34 stations within the Ebro River basin and surroundings (stations 0016A, 0034C, 0076, 0149D, 0158O, 0162C, 0189E, 0200E, 0208, 0222, 0321, 0341, 0367, 0421E, 1014, 1024E, 1082, 1109, 1111, 2030, 2331, 3013, 3168C, 8368U, 8500A, 9091O, 9170, 9263D, 9381I, 9390, 9434, 9771C, 9898, 9981A). These hourly data were used to compute multivariate monthly linear relationships between daily maximum/minimum temperature and elevation and daily mean temperature. The resulting regression equations for the daily minimum and maximum temperature are as follows:

$$T_{min} = a_m + b_m \cdot Elevation + c_m \cdot T_{mean} \quad (3.8)$$

$$T_{max} = a_m + b_m \cdot Elevation + c_m \cdot T_{mean} \quad (3.9)$$

The computed coefficients a_m, b_m and c_m of the linear regressions (3.8) and (eq:Tmax) are shown in Tables 3.3a and 3.3b. A leave-one-out cross validation procedure was used for testing the goodness-of-fit between the values computed with these relationships and the observed ones.

TABLE 3.3: Monthly values of the coefficients a, b and c for the relationship between minimum and maximum daily temperature with mean daily temperature

(A) Minimum daily temperature

Month	a	b	c
Jan	-3.573	-0.001	1.031
Feb	-3.263	-0.002	0.985
Mar	-3.621	-0.002	0.959
Apr	0.351	-0.004	0.687
May	2.330	-0.004	0.624
Jun	2.496	-0.005	0.696
Jul	3.250	-0.006	0.699
Aug	2.771	-0.005	0.713
Sep	-0.746	-0.004	0.858
Oct	-1.345	-0.002	0.873
Nov	-3.903	-0.001	1.050
Dec	-3.727	-0.000	1.074

(B) Maximum daily temperature.

Month	a	b	c
Jan	4.981	0.000	0.864
Feb	3.762	0.002	1.019
Mar	3.996	0.003	1.049
Apr	0.174	0.004	1.305
May	-1.460	0.004	1.349
Jun	-1.754	0.005	1.290
Jul	-2.548	0.005	1.292
Aug	-1.970	0.005	1.277
Sep	0.889	0.005	1.169
Oct	1.631	0.003	1.146
Nov	5.287	0.001	0.877
Dec	5.306	-0.000	0.803

The indexes used for measuring the goodness-of-fit were: the mean error (*ME*), the mean absolute error (*MAE*), the root mean squared error (*RMSE*), the normalised[5] RMSE (*NRMSE*), the percent bias (*PBIAS*, *Yapo et al.*, 1996), the Nash-Sutcliffe efficiency (NS_{eff}, *Nash and Sutcliffe*, 1970), the index of agreement (*d*, *Willmott*, 1981, 1984), the coefficient of persistence (*P*, *Kitanidis and Bras*, 1980), the Pearson's product-moment coefficient of correlation (*r*) and the coefficient of determination (R^2), most of them discussed in *Moriasi et al.* (2007). Tables 3.4 and 3.5 summarize the overall performance (aggregating the results of the 34 stations for all the available days) for T_{max} and T_{min}, respectively. The mean Nash-Sutcliffe efficiency larger than 0.75 indicates that the simulated values were close enough to the observed ones, whereas a mean error of 0.00 and a percent bias of 0.00% for all the months, for both T_{max} and T_{min}, indicate that the computed values are unbiased.

TABLE 3.4: Monthly goodness-of-fit for T_{min} obtained with the monthly relationships, using a leave-one-out cross validation for all the 34 stations and all the days within the time period

Index	Jan	Feb	Mar	Apr	May	Jun	Jul	Aug	Sep	Oct	Nov	Dec	Mean
ME, [°C]	0.00	0.00	0.00	0.00	0.00	0.00	0.00	0.00	0.00	0.00	0.00	0.00	0.00
MAE, [°C]	1.51	1.64	1.85	1.75	1.76	1.75	1.53	1.67	1.74	1.58	1.49	1.35	1.64
RMSE, [°C]	1.83	1.99	2.25	2.15	2.18	2.17	1.92	2.05	2.15	1.95	1.81	1.64	2.01
RMSEnorm, [%]	5.20	6.70	6.60	8.70	8.70	7.70	8.20	8.40	8.20	7.40	6.20	6.10	7.34
PBIAS, [%]	0.00	0.00	0.00	0.00	0.00	0.00	0.00	0.00	0.00	0.00	0.00	0.00	0.00
NSeff, [-]	0.86	0.81	0.80	0.70	0.68	0.68	0.76	0.75	0.76	0.81	0.85	0.87	0.78
d, [-]	0.96	0.94	0.94	0.90	0.90	0.90	0.93	0.92	0.93	0.95	0.96	0.96	0.93
P, [-]	0.65	0.49	0.54	0.33	0.31	-0.01	0.16	0.13	0.13	0.52	0.61	0.67	0.38
r, [-]	0.93	0.90	0.89	0.83	0.82	0.82	0.87	0.87	0.87	0.90	0.92	0.94	0.88
R^2, [-]	0.86	0.81	0.80	0.70	0.68	0.68	0.76	0.75	0.76	0.81	0.85	0.87	0.78

Equations 3.8 and 3.9 were used afterwards for generating the daily time series of maximum and minimum air temperature in each one of the 146 temperature gauging stations selected for the hydrological simulations (see section 2.2.5.1), both during the control period 01/Jan/1961 - 31/Dec/1990 and the future time slice 01/Jan/2071 - 31/Dec/2100.

[5]Normalized by the difference between the maximum and minimum observed value.

TABLE 3.5: Monthly goodness-of-fit for T_{max} obtained with the monthly relationships, using a leave-one-out cross validation for all the 34 stations and all the days within the time period

Index	Jan	Feb	Mar	Apr	May	Jun	Jul	Aug	Sep	Oct	Nov	Dec	Mean
ME, [°C]	0.00	0.00	0.00	0.00	0.00	0.00	0.00	0.00	0.00	0.00	0.00	0.00	0.00
MAE, [°C]	2.02	2.11	1.98	1.65	1.57	1.57	1.47	1.58	1.80	1.75	1.96	1.74	1.77
RMSE, [°C]	2.51	2.59	2.43	2.03	1.93	1.94	1.80	1.93	2.25	2.17	2.43	2.19	2.18
RMSEnorm, [%]	8.10	8.80	8.90	7.20	6.70	7.90	7.20	7.70	8.40	8.30	10.00	8.10	8.11
PBIAS, [%]	0.00	0.00	0.00	0.00	0.00	0.00	0.00	0.00	0.00	0.00	0.00	0.00	0.00
NSeff, [-]	0.68	0.64	0.74	0.81	0.85	0.83	0.86	0.82	0.70	0.79	0.63	0.68	0.75
d, [-]	0.90	0.88	0.92	0.94	0.96	0.95	0.96	0.95	0.91	0.94	0.88	0.90	0.92
P, [-]	0.25	0.20	0.52	0.71	0.74	0.67	0.65	0.57	0.45	0.59	0.22	0.32	0.49
r, [-]	0.82	0.80	0.86	0.90	0.92	0.91	0.93	0.91	0.84	0.89	0.79	0.82	0.87
R^2, [-]	0.68	0.64	0.74	0.81	0.85	0.83	0.86	0.82	0.70	0.79	0.63	0.68	0.75

3.3.5 Mean Daily Precipitation on Subbasins

Precipitation is a key driver of the hydrological cycle, and should be accurately reproduced in simulations, since a wrong representation of the precipitation volumes over a catchment might lead to significant errors in reproducing observations. *Moulin et al.* (2009) analysed the influence of mean areal precipitation estimation errors on the flood hydrographs computed by two lumped conceptual rainfall-runoff models, for three small to medium-size catchments (60 to 3200 km^2) and concluded that a large part of the rainfall-runoff modelling errors can be explained by uncertainty in rainfall estimates, especially in the case of smaller catchments; whereas *Kuczera and Williams* (1992) found that the 90% prediction interval of the 100-year design flood increased by about 100% when uncertainty in the calibration event rainfall was taken into account.

SWAT uses the gauging station closest to the centroid of each subcatchment as representative of the daily precipitation over it, even if within the subcatchment were more than one raingauge. In order to avoid loosing precipitation information, due to the fact that the hydrological model described in section 3.3.1 has 120 main subcatchments but we had information on 349 raingauges with -at least- 70% of days with information within the control period 1961-1990, we used the *hydroTSM*[6] *R* (*R Development Core Team*, 2009) package, developed by the author of this dissertation throughout his Ph.D programme, for computing the mean daily precipitation for each subcatchment, based on information of the neighbouring stations. A local block inverse distance weighted (*LBIDW*) procedure, with a weight of 2, was implemented. Figure 3.3 depicts an example for a single day, and this procedure can be summarized as follow:

1. All the subbcatchments within the study area are sampled using a squared grid with cells of 1 km^2.
2. All the stations with a measured value in the current day are used of the analysis, whereas all the other are discarded (only for the current day).
3. For each cell, an interpolated value of precipitation is computed using the LBIDW, considering only the closest 10 neighbouring stations within a maximum searching radius of 50 km.
4. For each subcatchment, the mean daily precipitation is computed, averaging over all the precipitation values of the cells belonging to each subcatchment.

This procedure was applied for each day within both the control period 01/Jan/1961 to 31/Dec/1990 and the future scenarios 01/Jan/2071 - 31/Dec/2100. The resulting time series of mean

[6] in particular, the *hydrokrige* function, a wrapper to some geostatistical functions of the *gstat* (*Pebesma*, 2004) and *automap* (*Hiemstra et al.*, 2008) packages of *R*.

daily precipitation were assigned to one fictitious station for each subcatchment, located in the spatial centroid thereof and at elevation computed with the same LBIDW procedure applied to the elevations of the raingauges. Preliminary hydrological simulations (not shown here) for subcatchment 90 (see Table 3.1) during the control period revealed that computed streamflows driven by the LBIDW interpolated precipitations were much closer to the observed ones than those computed by simulations driven by the use of a single raingauge.

Notwithstanding the use of the LBIDW algorithm improved the quality of the precipitation drivers used in SWAT, we observed that the computed daily values not always provide a realistic estimate of the total volume of precipitation entering to each catchment. In particular, preliminary simulations (not presented here) showed that the daily values computed for subcatchment 90 underestimated the precipitation volume that allowed the reproduction of the observed streamflows in the catchment. This underestimation was due to the fact that all the four raingauges within this subcatchment (P9175, P9176, P9177U and P9095) were located within elevations ranging from 600 to 785 m.a.s.l., whereas the elevations within the catchment arrive up to 1424 m.a.s.l., leading to an underestimation of the precipitation values at high elevations. For overcoming this drawback, a precipitation lapse rate was computed based on annual precipitation derived from 71 raingauges located in a buffer area of 75 km around the catchment border, and within elevations ranging from 300 to 1223 m.a.s.l. The computed lapse rate was 0.522 ± 0.136 mm m^{-1}, which was found statistically significant at $\alpha = 0.1\%$ (p-value < 0.001).

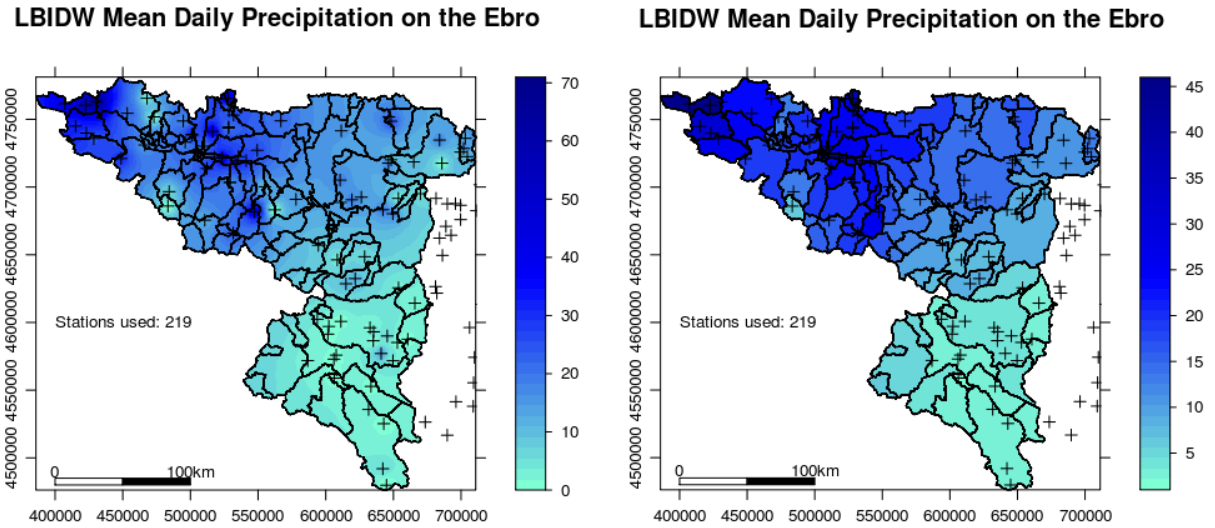

FIGURE 3.3: Example of the block inverse distance weighted (LBIDW) computation of the mean daily precipitation over the study area, for the 18-Oct-1961. The left figure shows the interpolated values in each cell of 1 km^2, whereas the right figure shows the mean values over each subcatchment. Crosses represent raingauges.

3.3.6 Selected Model Options

Section 3.2 described the options available in SWAT for setting up different model structures, including different runoff, evapotranspiration, snow accumulation, snowmelting, and flow routing algorithms. Among them, we selected the modified SCS curve number for computing runoff, due to the absence of subdaily rainfall data; the Priestey-Taylor method for computing the ETP, based on preliminary comparisons of the monthly ETP provided by the CHE office (http://oph.chebro.es/ContenidoClimatologicoD.htm) with those computed with Hargreaves and Priestey-Taylor methods; and the the Muskingum procedure for the routing through the channel network. For a comparison among the 3 different ETP methods, the 2 routing procedures, and 3 snowfall and melt algorithms included in SWAT2005, in a context of calibration and uncertainty, see *Zhang et al.* (2009b).

3.4 Sensitivity and Uncertainty Analysis

3.4.1 Sensitivity Analysis

As mentioned in section 3.1.3, sensitivity analysis allows to identify those parameters that exerts a strong influence on the model outputs. The sensitivity analysis in the present dissertation was divided in two stages: (i) an automatic procedure for a preliminary identification of the most sensitive parameters; (ii) a manual analysis of the sensitive parameters identified during the automatic approach.

The automatic analysis was carried out with the Latin Hypercube One-factor-At-a-Time (LH-OAT) algorithm described by *van Griensven et al.* (2006) and included in the AVSWAT-X GIS interface (*Di Luzio et al.*, 2002b,a, 2004) for SWAT2005. Parameter values can be modified in a lumped way (over the entire catchment) or in a distributed one (for selected subbasins and/or HRUs), and we changed them in a lumped way. Parameters can be modified by replacement, by addition of an absolute change, or by a multiplication of a relative change within the predefined parameter ranges (see *van Griensven and Meixner*, 2003; *van Griensven et al.*, 2006). Currently, the implemented procedure is not able to analyse the sensitivity of all the parameters used in SWAT, instead, it analyses the behaviour of a pre-defined set of 27 parameters, most of them included in sensitivity analyses and calibration procedures of other studies (e.g. *Lenhart et al.*, 2002; *Francos et al.*, 2003; *White and Chaubey*, 2005; *Kannan et al.*, 2007; *Holvoet et al.*, 2005; *Muleta and Nicklow*, 2005; *Eckhardt and Arnold*, 2001; *Abbaspour et al.*, 2007; *Zhang et al.*, 2009b). Preliminary trials (not shown here) made clear that the final sensitivity for each parameter depends on the number of strata used in the LH sampling, so different number of strata (10, 100, 300, 700, 1000) were tried until finding a stabilization of the final sensitivity ranking, which was found after 1000 strata for subcatchments 090 and 115. The final rankings for the two selected catchments are presented in Table 3.6.

The results of the automatic sensitivity analysis were used just as a guideline in the selection of the parameters with a high impact on the streamflows simulated by the model, because no automatic routine can replace the understanding of the physical effects of parameters in the response of complex hydrological models (*Abbaspour et al.*, 2007). The sixteen parameters shown in Table 3.6 where then subject to a "*manual*" sensitivity analysis, in which the value of each parameter was changed within its physical range, while keeping all the others constant, in order to visually observe the effects of those changes in the simulated streamflows. *Abbaspour et al.* (2007) suggests using five simulations for each parameter, dividing the physical range in equal strata, and using the midpoint of each interval as representative of it.

After the sensitivity analysis, 10 parameters were selected for the uncertainty analysis described in the next section. Most of those parameters has been previously identified as sensitive parameters of the SWAT model (e.g. *Kannan et al.*, 2007; *Holvoet et al.*, 2005; *Muleta and Nicklow*, 2005; *van Griensven et al.*, 2006).

TABLE 3.6: Parameters selected as significant after the automatic sensitivity analysis, including a short description, the extension of files in which they are located, the option used for carrying out the changes, the parameter range, and the final ranking after the sensitivity analysis.

					Ranking	
Parameter	Short Description	Location	Change Option	Range	Sub090	Sub115
CN2	Initial SCS CN II value	*.mgt	relative	[-50, 50]	1	1
RCHRG_DP	Deep aquifer percolation factor	*.gw	absolute	[0, 1]	2	2
GWQMN	Threshold water depth in the shallow aquifer for flow, [mm]	*.gw	absolute	[0, 5000]	3	3
SLOPE	Average slope steepness, [m/m]	*.hru	relative	[-50, 50]	4	4
SOL_K	Saturated hydraulic conductivity, [mm/hr]	*.sol	relative	[-50, 50]	5	5
GW_REVAP	Groundwater "*revap*" coefficient	*.gw	absolute	[0.02, 0.2]	6	6
ESCO	Soil evaporation compensation factor	*.hru	absolute	[0, 1]	7	7
SOL_AWC	Available water capacity, [mm H2O/mm soil]	*.sol	relative	[-50, 50]	8	8
SOL_Z	Soil depth, [mm]	*.sol	relative	[-50, 50]	9	9
REVAVMN	Threshold water depth in the shallow aquifer for "*revap*", [mm]	*.gw	absolute	[0, 500]	10	10
SURLAG	Surface runoff lag time, [days]	*.bsn	absolute	[0, 10]	11	11
ALPHA_BF	Baseflow alpha factor, [days]	*.gw	absolute	[0, 1]	12	13
SMTMP	Snowmelt base temperature, [°C]	*.bsn	absolute	[0, 5]	13	12
SOL_ALB	Moist soil albedo	*.sol	absolute	[0, 1]	14	15
TIMP	Snowpack temperature lag factor	*.bsn	absolute	[0.01, 1]	15	14
GW_DELAY	Groundwater delay time, [days]	*.gw	absolute	[0, 100]	16	17

3.4.2 Uncertainty Analysis

The hydrological SWAT model was calibrated and validated based on daily discharges for the period 01/Jan/1961 - 31/Dec/1990 at the outlet of the two selected catchments. An attempt was made in order to maintain the number of calibration parameter as small as possible, because according to *Jakeman and Hornberger* (1993) "*only a handful of parameters can be reliably estimated from rainfall-runoff data*". The final 10 parameters used during the calibration and uncertainty analysis are schematically presented in Figure 3.4. These parameters are briefly summarized next, and a detailed description can be found in *Neitsch et al.* (2005a,b):

- **CN2**: Initial Soil Conservation Service (SCS) runoff curve number for moisture condition II. The SCS curve number is a function of the soil's permeability, land use and antecedent soil water conditions.

- **RCHRG_DP**: Deep aquifer percolation fraction. The amount of water that will be diverted from the shallow aquifer to percolate into the deep aquifer (out of the main catchment). The value for RCHRG_DP should be between 0.0 and 1.0

- **GWQMN**: Threshold depth of water in the shallow aquifer required for return flow to occur, [mm H_2O]. Groundwater flow to the reach is allowed only if the depth of water in the shallow aquifer is equal to or greater than GWQMN. The value for GWQMN should be between 0 and 5000 [mm H_2O].

- **SOL_K**: Saturated hydraulic conductivity, [mm/hr]. It relates soil water flow rate (flux density) to the hydraulic gradient, and is a measure of the ease of water movement through the soil.

- **GW_REVAP**: Groundwater *"revap"* coefficient. This process is significant in watersheds where the saturated zone is not very far below the surface or where deep-rooted plants are growing. GW_REVAP can vary between 0 and 1, with low values indicating that the movement of water from the shallow aquifer to the root zone is restricted, whereas high values indicates that the rate of transfer from the shallow aquifer to the root zone approaches the rate of potential evapotranspiration. According to *Neitsch et al.* (2005a) its value should be between 0.02 and 0.2.

- **SOL_AWC**: Available water capacity of the soil layer [mm H_20/mm soil]. The plant available water is calculated by subtracting the fraction of water present at permanent wilting point from that present at field capacity. AWC= FC - WP, where AWC is the plant available water content, FC is the water content at field capacity and WP is the water content at permanent wilting point.

- **SOL_Z**: Depth from soil surface to bottom of a layer, [mm]. Since all the sub-catchments were conceptualized as single layer units, SOL_Z is equal to SOLZMX, the maximum rooting depth of soil profile [mm]. If no SOLZMX is specified, the model assumes the roots can develop throughout the entire depth of the soil profile.

- **REVAPMN**: Threshold depth of water in the shallow aquifer for *"revap"* or percolation to the deep aquifer to occur, [mm H_20].

- **ALPHA_BF**: Baseflow alpha factor, [days]. The baseflow recession constant is a direct index of groundwater flow response to changes in recharge. Values vary from 0.1-0.3 for catchments with slow response to recharge, to 0.9-1.0 for catchments with a rapid response.

- **GW_DELAY**: Groundwater delay time, [days]. It represents the lag between that water exits the soil profile and enters the shallow aquifer.

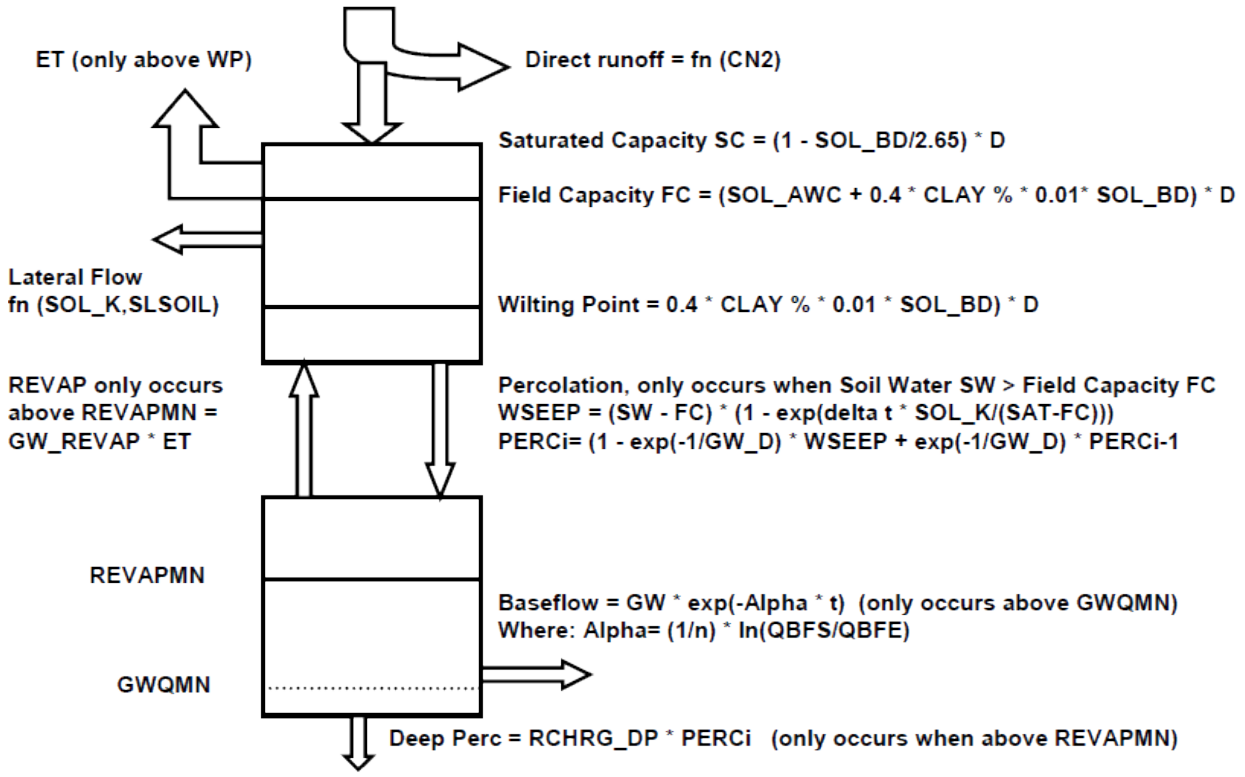

FIGURE 3.4: Main parameters related to the water balance components in SWAT 2005 (after *MRC*, 2006, with permission).

3.4.2.1 Sampling Strategy

One of the major shortcomings of the GLUE methodology is the time needed to obtain a number of parameter sets that provides a good characterization of the likelihood response in the model space. The traditional GLUE methodology uses uniform prior distributions of each parameter with a simple random sampling strategy, which is very easy to implement but unlikely to densely sample the high-dimensional parameter space in the region where the high likelihood parameter sets are found (*Beven et al.*, 2000). Therefore, we implemented a Latin Hypercube (LH) sampling strategy, which allows an efficient exploration of the model response to different parameter sets. This sampling strategy can be summarized as follow: (i) equi-probable subdivision, in which the range of each parameter is subdivided in *N* strata with the same probability of occurrence *1/N*; (ii) stratified sampling, where a single parameter value is sampled within each interval; (iii) random pairing, in which *N* parameter sets are created from randomly pairing the samples of each strata. Non informative uniform prior distributions for each parameter were chosen due to the absence of prior knowledge of the individual probability distributions.

3.4.2.2 Methodology

As mentioned in section 3.3.1, in this dissertation subbasins were characterized by the dominant land use and soil combination, with a single layer through the soil profile, in order to keep the complexity of the analysis at a practical limit for the propagation of the hydrological uncertainties into the projected climate impacts. If this simple configuration can be deemed acceptable will depend on the results of the uncertainty analysis.

The efficiency of the uncertainty analysis is a crucial issue when dealing with computationally intensive, complex, long-term and large-scale hydrological models, in particular when the results of the analysis will be used to propagate hydrological uncertainties into the projected impacts of climate change. Therefore, the uncertainty analysis used in this dissertation was implemented in three stages:

1. **Exploration of the surface response and derivation of a prior large parameters range**. The complete physical range of each parameter is used to explore the surface response, using a Latin Hypercube sampling with a few runs (300), and to select a prior large range for each parameter, a range large enough for encompassing good simulators of the system, but smaller than the physical one;

2. **Derivation of a reduced parameters range**. The GLUE methodology is used with a Latin Hypercube sampling within the large range defined in the previous step, using 2000 strata and uniform distributions for each parameter. The Nash-Sutcliffe efficiency, described in equation 3.7 with a shape factor *N* equal to 1, is used as "*less formal*" likelihood, in order to select the behavioural parameter sets. A cut-off threshold equal to zero is used to discriminate between behavioural and non-behavioural parameter sets, in order to consider as acceptable simulators of the system all the parameter sets leading to a NS_{eff} performance better than using the mean of the observed values. A new reduced range for each one of the 10 selected parameters is obtained from the 95% of their cumulative distribution, weighted by their corresponding re-scaled likelihood;

3. **Derivation of predictive uncertainty**. GLUE is used with a Latin Hypercube sampling within the previously defined reduced range, using 2000 strata and uniform distributions for each parameter. Behavioural parameter sets are then selected with the same criteria of the previous step. Predictive uncertainty is computed by using the 95% of the cumulative distribution of each predicted output, weighted by the re-scaled likelihood of each behavioural parameter set. It is worth to mention that uncertainty bounds are not confidence bounds in the formal statistical sense, because they are quantiles of the model predictions and not nec-

essarily have to include a given percentage of the observations (*Beven and Freer*, 2001; *Blasone et al.*, 2008b).

The aforementioned procedure was carried out by using a combination of algorithms included in the SWAT-CUP software (*Abbaspour et al.*, 2008; *Abbaspour*, 2008), which provides a suite of stand-alone tools able to interoperate via standardized I/O procedures, allowing to change the 10 selected parameters in a lumped way for each subcatchment.

TABLE 3.7: Parameters used in the uncertainty analysis, including a short description, the extension of files in which they are located, the prior large range used to reduce the size of the parameter space, and the reduced range used to compute the predictive uncertainty

			Prior Large Range		Reduced Range	
Parameter	Short Description	Location	Sub090	Sub115	Sub090	Sub115
CN2	Initial SCS CN II value	*.mgt	U[30, 95]	U[25, 95]	U[31, 77.3]	U[28.64, 71.03]
RCHRG_DP	Deep aquifer percolation factor	*.gw	U[0, 0.3]	U[0.01, 0.9]	U[0, 0.293]	U[0.15, 0.86]
GWQMN	Threshold water depth in the shallow aquifer for flow, [mm]	*.gw	U[0, 100]	U[0, 200]	U[2.5, 97]	U[12, 199]
SOL_K	Saturated hydraulic conductivity, [mm/hr]	*.sol	U[10, 1000]	U[0.1, 500]	U[15, 256]	U[6.1, 152.5]
GW_REVAP	Groundwater "*revap*" coefficient	*.gw	U[0, 0.3]	U[0, 0.2]	U[0, 0.295]	U[0.017, 0.19]
SOL_AWC	Available water capacity, [mm H2O/mm soil]	*.sol	U[0, 0.35]	U[0.05, 0.5]	U[0.05, 0.342]	U[0.077, 0.429]
SOL_Z	Soil depth, [mm]	*.sol	U[200, 2000]	U[10, 2500]	U[251, 1958]	U[224, 2493]
REVAVMN	Threshold water depth in the shallow aquifer for "*revap*", [mm]	*.gw	U[1, 400]	U[1, 400]	U[10, 391]	U[40, 389]
ALPHA_BF	Baseflow alpha factor, [days]	*.gw	U[0, 0.9]	U[0, 0.9]	U[0.028, 0.88]	U[0.045, 0.87]
GW_DELAY	Groundwater delay time, [days]	*.gw	U[0, 50]	U[0, 100]	U[2.5, 49]	U[12.8, 98.6]

In order to get rid of the unknown initial conditions of the system, the first year (1961) was used as a warm-up period for all the simulations.

For calibration, usually half of the observed data record is used to be compared against the simulated values, whereas the other half is used to perform an assessment of the predictive capabilities of the model (frequently referred as "*validation*"). *Yapo et al.* (1996) studied the sensitivity of the Shuffled Complex Evolution global optimization algorithm (*Duan et al.*, 1992, 1994) to the input data used for the calibration, and concluded that at least 8 years of data are required to obtain results relatively insensitive to the length of the selected period, and that the use of the wettest data period greatly reduced the uncertainty in the parameter values. In this dissertation we decided to use 19 years for the calibration (01/Jan/1962 - 31/Dec/1980) and the last ten years (01/Jan/1981 - 31/Dec/1990) for verification, because exploratory data analysis revealed a decreasing trend in the daily streamflows of subcatchment 090, with mean daily values of 15.8, 12.5 and 9.2 $m^3 s^{-1}$ for the first, second and third decade of the observation record, respectively; whereas in subcatchment 115 the wettest year was measured in 1978. Therefore, we decided to use the first 19 years to capture as much as possible the observed variability, but preserving a reasonably long verification period.

3.4.2.3 Performance Evaluation

In order to use the behavioural parameter sets found during the uncertainty analysis in the propagation of the hydrological uncertainty into the projected impacts of climate change, the uncertainty associated to the behavioural parameter sets is carefully examined during the 10 years used for verification (01/Jan/1981 - 31/Dec/1990).

Based on previous recommendations (*Legates and McCabe Jr.*, 1999; *Krause et al.*, 2005; *Moriasi et al.*, 2007), a combination of graphical techniques and error index statistics was used for evaluating the goodness-of-fit between the simulated and observed values, both during the calibration and verification period. The used index statistics are briefly described in section 3.1.3: the mean error (*ME*), the mean absolute error (*MAE*), the root mean squared error (*RMSE*), the percent bias

(*PBIAS*, *Yapo et al.*, 1996), the Nash-Sutcliffe efficiency (*NSeff*, *Nash and Sutcliffe*, 1970), the index of agreement (*d*, *Willmott*, 1981, 1984; *Willmott et al.*, 1985), the coefficient of persistence (*P*, *Kitanidis and Bras*, 1980), the ratio of the root mean squared error to the standard deviation of the observations (*RSR*, *Moriasi et al.*, 2007), the coefficient of determination (R^2), and the weighted coefficient of determination (bR^2, *Krause et al.*, 2005). In particular, according to *Yilmaz et al.* (2008), indices related to the long-term water balance, as PBIAS, are very sensitive to climatic variability of evapotranspiration, and almost insensitive to process operating at shorter time scales, therefore PBIAS is expected to be most sensitive to parameters controlling evapotranspiration.

Regarding the uncertainty in the simulated outputs, coming from the direct effect of hydrological parameterisation but also implicitly from uncertainties in input data and model structure, we used the 95% of predictive uncertainty (95PPU), computed at the 2.5% and 97.5% of the cumulative distribution of every simulated streamflow. Two main indexes, proposed by *Abbaspour et al.* (2009, 2007), were used to quantify the performance of the uncertainty analysis: (i) the *P-factor*, which represents the percentage of observed data embraced by the 95PPU; and (ii) the *R-factor*, which measures how wide the uncertainty bounds are with respect to the variability of the observations, computed as the average width of the 95PPU divided by the standard deviation of the observations. Ideally, i.e., with a combination of model structure and parameter values that perfectly represents the catchment under study, and in absence of measurement errors and other additional sources of uncertainty, all the simulated values should be in a perfect match with the observations, leading to a *P-factor* equal to 1, and an *R-factor* equal to zero. However, in real-world applications we aim at encompassing as much observations as possible within the 95PPU (*P-factor* $\rightarrow$ 1) while keeping the width of the uncertainty bounds as small as possible (*R-factor* $\rightarrow$ 0), in order to avoid obtaining a good bracketing of observations at expense of uncertainty bounds too wide to be informative for the decision-making process. In this dissertation, a minimum P-factor close to or higher than 0.75 during the the calibration and verification period will be considered as acceptable. Regarding the width of the uncertainty bounds, *Abbaspour et al.* (2009); *Schuol et al.* (2008a) and *Abbaspour* (2008), argue that an *R-factor* close to or smaller than 1 can be deemed acceptable. There is an implicit assumption: parameter sets classified as behavioural during the calibration period will be behavioural also during the verification one, i.e., errors in the prediction period will be similar to those observed during the calibration one (*Beven*, 2006). Therefore, any significant change in the *P-factor* and/or *R-factor* is carefully examined.

3.5 Results

3.5.1 Parameter Distributions

Figures 3.5 and 3.6 show, for subcatchments 090 and 115 respectively, dotty plots with the values of each one of the 10 aggregated parameters defined in section 3.4.2 versus their corresponding Nash-Sutcliffe efficiency (*Nash and Sutcliffe*, 1970), where the parameter values were obtained from a Latin Hypercube sampling of the prior large range defined in Table 3.7, using 2000 strata for subcatchment 090 (Ega River) and 300 strata for subcatchment 115 (Homino River). They show that most of the sampled parameters are associated to NS_{eff} lower than zero, which is expected due to the sampling procedure that covered almost the complete physical range of each parameter. However, the proportion of parameter values with a NS_{eff} lower than zero is much higher in subcatchmetn 115 than in 090. At the other hand, in both catchments there are only two parameters with a strong influence on the predicted streamflows: the initial Soil Conservation Service (SCS) runoff curve number for moisture condition II (*CN2*), and the saturated hydraulic conductivity of the soil profile (*SOL_K*), whereas the remaining eight parameters present NS_{eff} greater than zero all along their complete range. Parameter sets with a NS_{eff} higher than zero were selected as behavioural (1948 for subcatchment 090 and 1464 for subcatchment 115), and their corresponding NS_{eff} were rescaled such they sum to 1, in order to be used as "*less formal*" likelihood. The 95% of the cumulative distribution of each one of the 10 selected parameters, weighted by their corre-

sponding likelihood, was used as prior reduced range for computing the predictive uncertainties with GLUE in the next step.

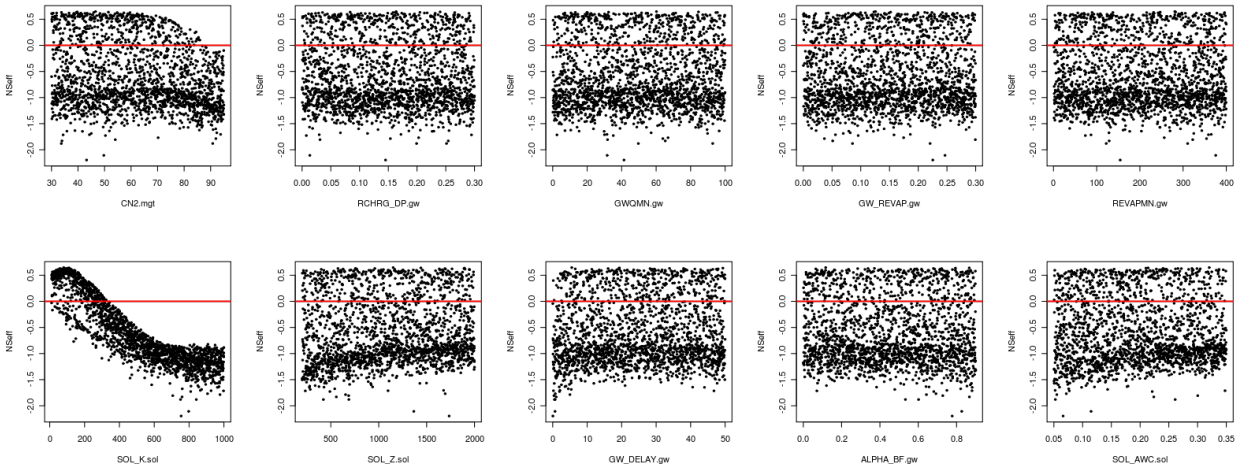

FIGURE 3.5: Dotty plots with the values of the 10 aggregated parameters of subcatchment 090 (Ega River) versus their corresponding Nash-Sutcliffe efficiency, obtained from a Latin Hypercube sampling of the prior large range, using 2000 strata. The red line shows the cut-off threshold used to select the prior reduced range.

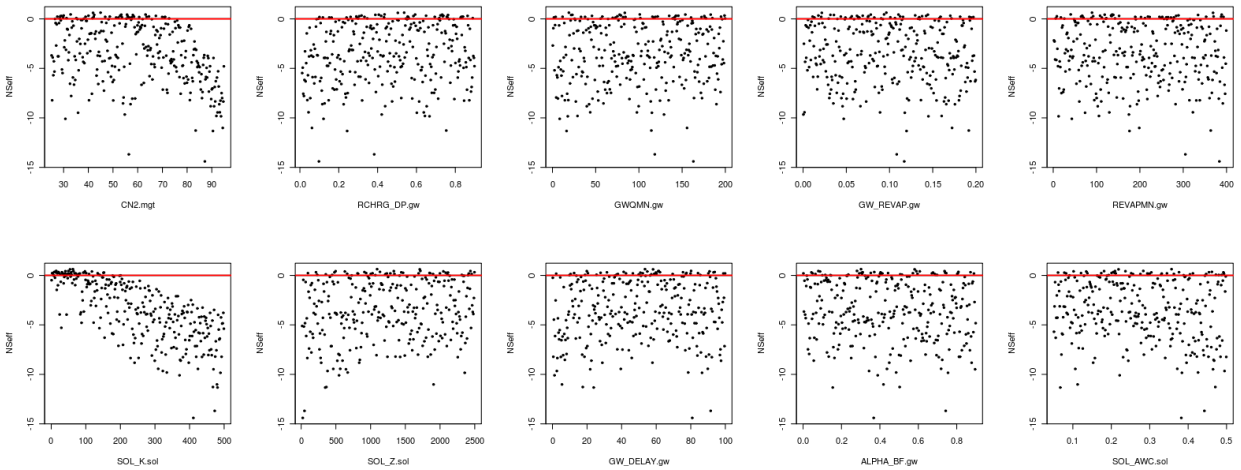

FIGURE 3.6: Dotty plots with the values of the 10 aggregated parameters of subcatchment 115 (Homino River) versus their corresponding Nash-Sutcliffe efficiency, obtained from a Latin Hypercube sampling of the prior large range, using 300 strata. The red line shows the cut-off threshold used to select the prior reduced range for computing the predictive uncertainties obtained with GLUE.

The resulting reduced ranges for each parameter were used as prior uniform distributions in a GLUE procedure with a Latin Hypercube sampling with 2000 strata for both catchments, in order to obtain the predictive uncertainties. Figures 3.7 and 3.8 present, for subcatchments 090 and 115 respectively, dotty plots with the values of each one of the 10 aggregated parameters defined in section 3.4.2 versus their corresponding Nash-Sutcliffe efficiency (*Nash and Sutcliffe*, 1970). The figures show that the use of the reduced range obtained at the end of the previous stage, significantly increased the amount of parameter values with a NS_{eff} higher than zero in both catchments, but this proportion was much higher in subcatchment 090 than in subcatchment 115, what may be

a preliminary indication of the existence of structural problems in the conceptualization of subcatchment 115 and/or data errors that have not been considered. Again, in both catchments there are only few parameters with a strong influence in the predicted streamflows: in subcathcment 090 they are the initial Soil Conservation Service (SCS) runoff curve number for moisture condition II (*CN2*), and the saturated hydraulic conductivity of the soil profile (*SOL_K*), whereas in the subcatchment with more semi-arid regime (115) two additional parameter are needed to explain the slow response of the catchment: (a) the deep aquifer percolation factor (*RCHRG_DP*), which controls the fraction of water that is lost from the shallow aquifer to recharge the deep aquifer (out of the catchment); and (b) the groundwater delay time *GW_DELAY*,which represents the lag between the water exit the soil profile and enters to the shallow aquifer. As can be seen in Figure 3.4, the *CN2* controls the partitioning of precipitation into runoff and infiltration, *SOL_K* takes part in the production of lateral flow and percolation to the shallow aquifer; whereas *GW_DELAY* affects the slope of the recession curve, and *RCHRG_DP* control the losses of the system. The remaining parameters present NS_{eff} greater than zero all along their analysed range, and their interactions contribute to partially compensate by deficiencies in the simplified representation of the catchment.

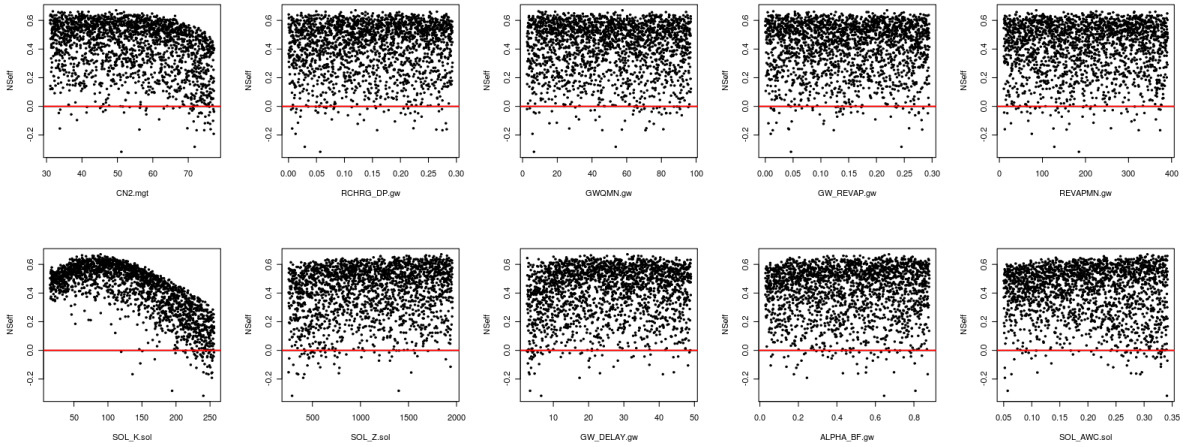

FIGURE 3.7: Dotty plots with the values of the 10 aggregated parameters of subcatchment 090 (Ega River) versus their corresponding Nash-Sutcliffe efficiency, obtained from a Latin Hypercube sampling of the prior reduced range, using 2000 strata. The red line shows the cut-off threshold used to select the behavioural parameter sets of GLUE.

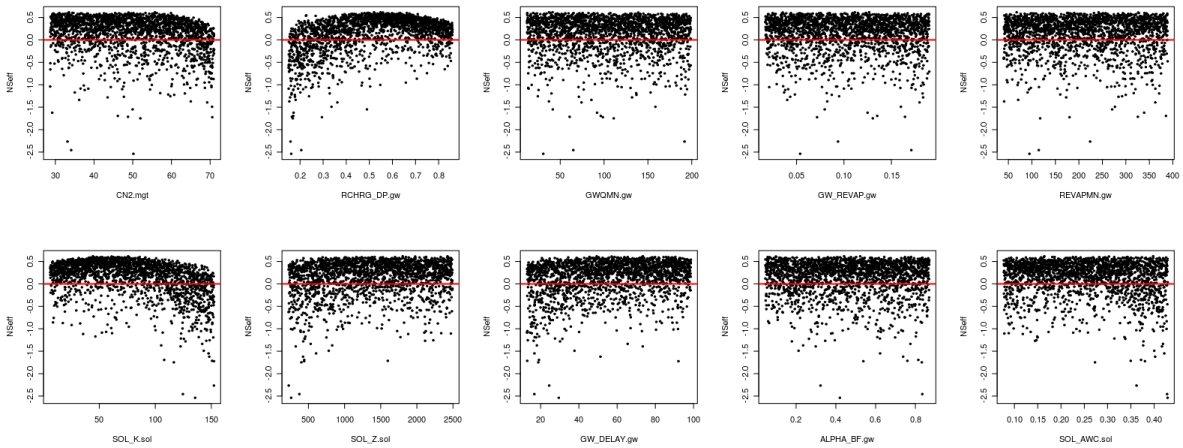

FIGURE 3.8: Dotty plots with the values of the 10 aggregated parameters of subcatchment 115 (Homino River) versus their corresponding Nash-Sutcliffe efficiency, obtained from a Latin Hypercube sampling of the prior reduced range, using 2000 strata. The red line shows the cut-off threshold used to select the behavioural parameter sets of GLUE.

Tables 3.8 and 3.9 show the correlation matrix of the parameter values used in the application of GLUE with the reduced parameter ranges of subcatchment 090 and 115, respectively. The correlations between all the parameters were very small, and none of them was statistically significant at $\alpha = 10\%$ (p-values were larger than 0.1). Table 3.8 shows that in subcatchment 090 (Ega, River), three parameters were statistically correlated to the NS_{eff} (at $\alpha = 0.1\%$, p-value < 0.001), with the highest correlations corresponding to *CN2* and *SOL_K* ; whereas for subcatchment 115, six parameters were found statistically correlated to the NS_{eff} (at $\alpha = 0.1\%$, p-value < 0.001), with the highest correlations corresponding to *RCHRG_DP*, *SOL_K*, *CN2*, *GW_DELAY* and *SOL_Z*. The previous results are in partial agreement with the sensitivity analysis summarized in Table 3.6. Differences between the relative sensitivity of each parameter obtained by these two procedures are very likely due to: (i) the way in which parameters were changed, because in the sensitivity analysis carried out with LH-OAT some parameters were changed in a relative way with respect to their initial values obtained from the GIS analysis, whereas in the GLUE procedure all the parameters were changed in an absolute way within the reduced range; and (ii) the LH-OAT was carried out with 1000 strata for each parameter, whereas the GLUE procedure used 2000.

TABLE 3.8: Correlation matrix of the parameter values used in the application of GLUE with the reduced parameter ranges of subcatchment 090 (Ega River). Numbers in blue (and with an asterisk for the B&W version) are those statistically significant (p-value $<$ 2e-16). GW_DELAY was found statistically significant at $\alpha = 0.1\%$ (p-value < 0.001).

Aggregated Parameter											
CN2.mgt	1.00										
RCHRG_DP.gw	0.03	1.00									
GWQMN.gw	-0.01	-0.03	1.00								
GW_REVAP.gw	-0.02	0.02	0.01	1.00							
REVAPMN.gw	-0.01	0.03	-0.03	0.03	1.00						
SOL_K.sol	0.03	0.01	-0.01	0.01	-0.00	1.00					
SOL_Z.sol	0.02	0.03	-0.05	0.02	0.01	0.03	1.00				
GW_DELAY.gw	0.02	0.02	-0.03	-0.04	-0.00	-0.01	-0.04	1.00			
ALPHA_BF.gw	0.02	0.02	0.04	0.02	-0.01	-0.00	0.02	-0.01	1.00		
SOL_AWC.sol	0.03	-0.01	0.00	-0.01	0.00	0.05	-0.01	0.04	-0.01	1.00	
NS_{eff}	-0.22*	-0.01	0.01	-0.00	-0.00	-0.88*	0.08*	0.06	-0.02	-0.03	1.00

TABLE 3.9: Correlation matrix of the parameter values used in the application of GLUE with the reduced parameter ranges of subcatchment 115 (Homino River). Numbers in blue (and with an asterisk for the B&W version) are those statistically significant (p-value $<$ 2e-16).

Aggregated Parameter											
CN2.mgt	1.00										
RCHRG_DP.gw	-0.04	1.00									
GWQMN.gw	-0.00	-0.00	1.00								
GW_REVAP.gw	0.03	-0.01	-0.03	1.00							
REVAPMN.gw	0.01	0.02	0.00	-0.00	1.00						
SOL_K.sol	0.02	-0.01	-0.01	0.02	-0.00	1.00					
SOL_Z.sol	0.00	0.00	-0.01	-0.01	0.02	-0.02	1.00				
GW_DELAY.gw	0.02	0.00	-0.01	0.00	-0.01	-0.02	-0.02	1.00			
ALPHA_BF.gw	0.01	0.00	-0.00	0.00	-0.01	-0.04	-0.01	0.02	1.00		
SOL_AWC.sol	-0.02	0.01	0.03	-0.01	0.04	0.06	0.02	-0.02	0.01	1.00	
NS_{eff}	-0.22*	0.40*	-0.00	-0.02	0.02	-0.39*	0.17*	0.22*	-0.03	-0.10*	1.00

3.5.2 Future Streamflows and Predictive Uncertainty

During the implementation of the GLUE procedure with the reduced parameter ranges, 1948 and 1464 parameter sets were selected as behavioural for subcatchments 090 (Ega River) and 115 (Homino River), respectively, considering a NS_{eff} equal to zero as cut-off threshold. Afterwards,

the NS_{eff} were rescaled such they sum to 1, in order to be used as "*less formal*" likelihood. The predictive uncertainties were finally computed as the 95% of the cumulative distribution of each predicted streamflow, weighted by the likelihood of the corresponding behavioural parameter set.

Figures 3.9 and 3.10 show the results of the daily and monthly uncertainty analysis carried out in subcatchments 090 (Ega River) and 115 (Homino River), respectively. The shaded area represent the 95% of predictive uncertainty (95PPU), whereas black dotted lines correspond to the observed discharges at the basin outlet. Tables 3.10 and 3.11 present daily and monthly summaries, respectively, with the *P-factor* and *R-factor* obtained during the uncertainty analysis carried out with GLUE. Additionally, some goodness-of-fit measures between observations and values simulated with the parameter set with the highest NS_{eff} are also presented, just to look at how close those "*best*" simulated values match the observations. It is worth mentioning that in both catchments, the parameter set that achieved the highest NS_{eff} during calibration was not the same that achieved the highest efficiency during the verification period, emphasizing the importance of not considering only one single "*best*" simulation, but considering several acceptable simulators of the system. Moreover, when comparing observations to a single "*best*" simulation, the goodness-of-fit used to measure the performance of the simulations may indicate different behaviours during calibration and verification periods (e.g., the PBIAS in subcatchment 090 indicated a slight underestimation of the streamflows by the model during calibration, whereas it indicates a clear over-estimation during the calibration period), making less reliable predictions with such "*best*" parameter set outside the calibration period.

Regarding the daily simulations, it is possible to observe that for both catchments the selected behavioural parameter sets led to uncertainty bounds that bracket most of the observations, both during calibration and verification period, as shown by *P-factors* larger than 0.73 and 0.9 in subcatchment 090 (Ega River) and 115 (Homino River), respectively. However, the relative magnitude of the uncertainty bounds for both catchments are very different, as evident in their corresponding *R-factors*. In subcatchment 090, the R-factor in calibration was $0.95 < 1$, what is deemed acceptable according to what mentioned in section 3.4.2.3, and it increased up to 1.36 during verification period, which is expected due to the forcing of the system with input data not used during the calibration. The increment in the average width of the uncertainty bounds during the verification period (i.e. larger *R-factors*), led to bracketing more observations than during calibration, what explains the larger P-factor during the verification step. At the other hand, subcatchment 115 is characterized by large R-factors (greater than 1 and close to 2) both in calibration and verification periods, but with P-factors still very close to one, i.e., bracketing most of the observations. In contrast to what was observed in subcatchment 090, the P-factor in subcatchment 115 was slightly smaller during verification, which was accompanied by an increase in the R-factor. The aforementioned change from calibration to verification period might be explained by the differences in streamflows from December 1981 to May 1982, where predicted streamflows are far from the corresponding observations, leading to a decrease in P-factor, along with uncertainty bounds much wider than the ones that should embrace the observations for that period, leading to an increase in the R-factor. The previous difference can only be attributed to measurement errors in precipitation, because the local water authority (CHE) confirmed that they did not experience any measurement problem on streamflows during that period.

The large R-factors obtained in subcatchment 115 during calibration and verification seems to confirm what was observed in section 3.5.1, regarding possible deficiencies in the conceptualization of subcatchment 115. If those inadequacies are enough for deciding to change the current model structure used for that catchment, will depend on the acceptance criteria adopted by the decision-makers, because notwithstanding the uncertainties are large (i.e., wide uncertainty bounds), they still embrace most of the observations; what is completely different to a situation with large uncertainties and few observations within the uncertainty bounds.

Regarding the monthly results, their behaviour is quite similar to the daily ones, as can be seen comparing their corresponding P-factors and R-factors, but with an obvious improvement in all the goodness-of-fit between observations and values simulated with the parameter sets that led

to the highest NS_{eff}, due to the smoothing effect of aggregating from daily to monthly scale.

Consequently, results involving percentage of observations embraced by the uncertainty bounds during the calibration and verification period lead to consider as "*acceptable*" the behavioural parameter sets selected for both catchments, but being wary about the wide of the uncertainty bounds in subcatchment 115. In particular, behavioural parameter sets selected during the uncertainty analysis will be used during the future scenarios, to propagate the parametric uncertainty of hydrological conceptualization into the projected impacts of climate change.

It is worth mentioning that three different approaches could be used to decrease the large R-factors obtained for subcatchment 115: (i) choosing a higher NS_{eff} at the end of the third step of the proposed methodology, in order to select parameter sets with a performance higher than the cut-off threshold currently used (NS_{eff} equal to zero), which leads to a fewer parameter sets to be used during verification; (ii) in the second step of the methodology, to select the reduced range for each parameter from narrower percentages of their likelihood-weighted cumulative distribution (90%, 85%, 70% or less, instead of the 95% currently used); and (iii) to increase the value of N in equation 3.7 in the three steps of the methodology, to reduce the relative weight associated with poor models. However, the three previously mentioned ways for decreasing the width of the uncertainty bounds, introduce an additional bias related to the expertise and judgement of the modeller, that we tried to avoid.

Finally, we want to emphasize that prediction limits obtained with GLUE are highly dependent on decisions taken by the modeller: what model structure(s) is(are) used to represent the catchment behaviour (not analysed here), what input data are used to drive the hydrological simulations (not explicitly analysed in this dissertation), which and how many parameters are selected for the uncertainty analysis, what parameter ranges are sampled for each parameter, which likelihood measure is used to assess the performance of different parameter sets, the threshold selected to discriminate between behavioural and non-behavioural simulators, and the way in which all the previous choices are combined, what is in agreement with previous studies (e.g. *Beven*, 2001; *Beven and Freer*, 2001; *Montanari*, 2005).

TABLE 3.10: Summary of the daily uncertainty analysis carried out with GLUE. Goodness-of-fit between observations and values simulated with the parameter set with the highest NS_{eff} are also presented for both the calibration (CAL, 01/Jan/1962 - 31/Dec/1980, and the verification period (VAL, 01/Jan/1981 - 31/Dec/1990.

Subb ID	Period	ME [m^3/s]	MAE [m^3/s]	RMSE [m^3/s]	PBIAS [%]	RSR [-]	P [-]	d [-]	NS_{eff} [-]	R^2 [-]	bR^2 [-]	P-factor [-]	R-factor [-]
090 (Ega)	CAL	-0.32	5.44	9.77	-2.3	0.57	-0.27	0.89	0.67	0.67	0.52	0.73	0.95
090 (Ega)	VAL	2.05	4.02	6.56	22.3	0.60	0.47	0.91	0.64	0.74	0.70	0.79	1.36
115 (Homino)	CAL	0.18	2.12	4.15	3.0	0.62	-0.37	0.86	0.61	0.62	0.48	0.94	1.43
115 (Homino)	VAL	1.45	2.19	3.96	38.7	0.87	-2.05	0.82	0.24	0.52	0.49	0.90	1.83

TABLE 3.11: Summary of the monthly uncertainty analysis carried out with GLUE. Goodness-of-fit between observations and values simulated with the parameter set with the highest NS_{eff} are also presented for both the calibration (CAL, 01/Jan/1962 - 31/Dec/1980, and the verification period (VAL, 01/Jan/1981 - 31/Dec/1990.

Subb ID	Period	ME [m^3/s]	MAE [m^3/s]	RMSE [m^3/s]	PBIAS [%]	RSR [-]	P [-]	d [-]	NS_{eff} [-]	R^2 [-]	bR^2 [-]	P-factor [-]	R-factor [-]
090 (Ega)	CAL	-0.33	3.23	4.68	-2.4	0.39	0.83	0.96	0.85	0.85	0.78	0.72	0.86
090 (Ega)	VAL	2.06	2.69	3.94	22.3	0.49	0.68	0.95	0.76	0.90	0.75	0.75	1.23
115 (Homino)	CAL	0.17	1.73	2.57	2.9	0.49	0.63	0.92	0.76	0.77	0.68	0.95	1.56
115 (Homino)	VAL	1.44	1.81	2.61	38.5	0.72	0.33	0.88	0.48	0.70	0.61	0.88	1.94

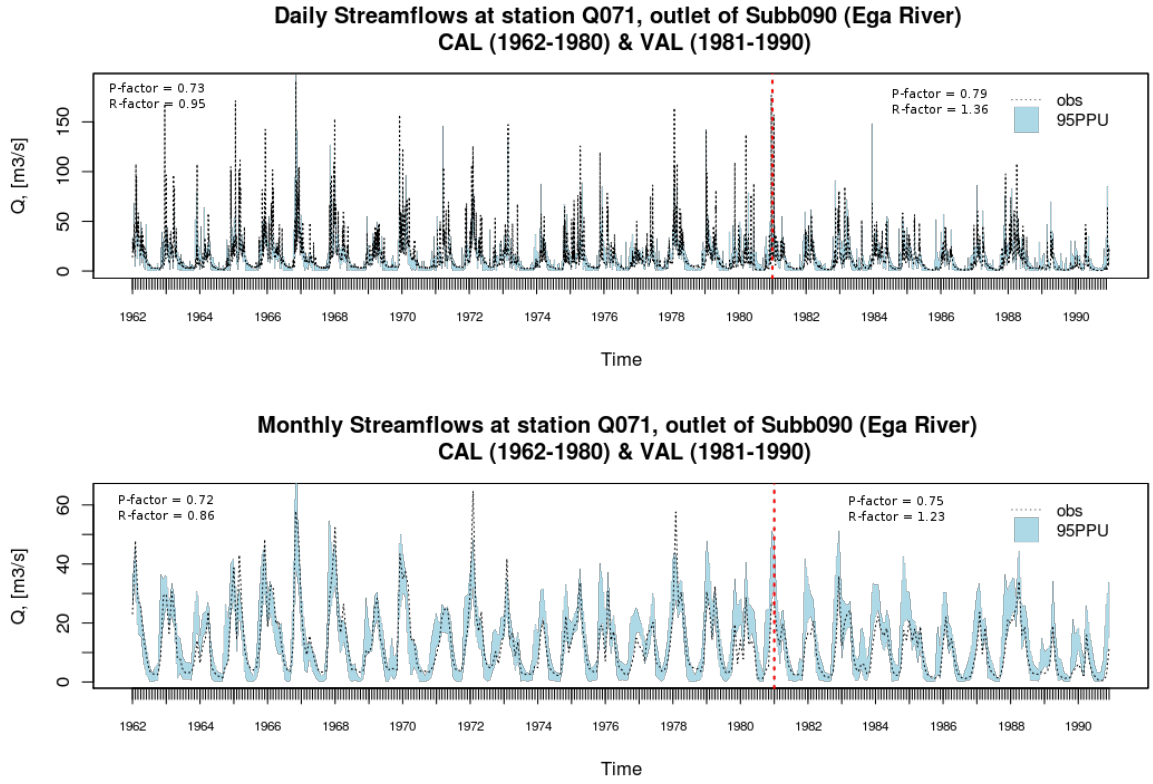

FIGURE 3.9: 95PPU (shaded area) obtained with GLUE during both the calibration (01/Jan/1962 - 31/Dec/1980) and verification period (01/Jan/1981 - 31/Dec/1990). The black dotted line correspond to the observed discharges at the basin outlet.

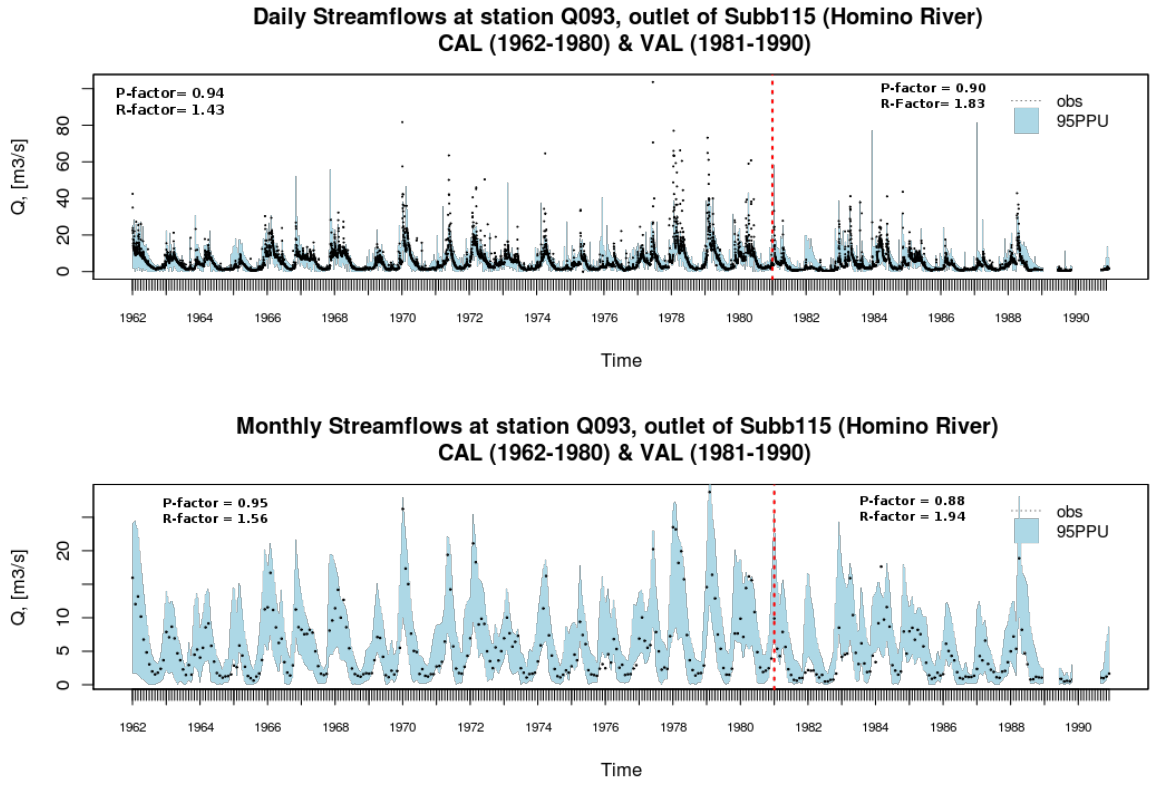

FIGURE 3.10: 95PPU (shaded area) obtained with GLUE during both the calibration (01/Jan/1962 - 31/Dec/1980) and verification period (01/Jan/1981 - 31/Dec/1990). The black dotted line correspond to the observed discharges at the basin outlet.

3.5.3 Efficiency of the Sampling Strategy

In order to assess the efficiency of the implemented sampling strategy, we also tried the classical GLUE approach -with uniform Monte Carlo sampling- for the reduced parameter ranges of subcachment 090, during the calibration period, and with different number of simulations (not shown here). We run 7000, 10000, 12000, 15000, 17000 and 20000 simulations; leading to 6777, 9670, 11605, 14521, 16464, and 19375 behavioural parameter sets; and the same P-factor equal to 0.74 and R-factor equal to 1.01 were obtained for all the experiments. The previous results confirm the efficiency of the implemented LH sampling strategy, because only a small improvement in the amount of observations bracketed by the uncertainty bounds (the R-factor changed from 0.73 to 0.74) was obtained by using a much larger number of simulations with the classical approach, but this improvement was obtained at expense of wider uncertainty bounds (R-factor changed from 0.95 to 1.01).

3.5.4 Predictive Uncertainty in Flow Duration Curves (FDCs)

Additionally to the widely used uncertainty bounds for the time series of simulated and observed values, we also present uncertainty bounds for the flow duration curves (FDC) of the two selected catchments, both during calibration and verification period. The upper and lower uncertainty bounds in the FDC space are computed as the FDC of the upper and lower uncertainty bounds obtained for the streamflow time series at the end of the GLUE analysis, respectively.

We included a comparison of observed and simulated FDCs, because FDCs are simple, yet comprehensive, graphical representations of the observed variability of streamflows in a catchment (*Vogel and Fennessey*, 1994), and because they are useful for conveying hydrological information to decision makers (*Vogel and Fennessey*, 1995). A flow duration curve summarizes the relationship between the magnitude and frequency of streamflows, allowing to identify the percentage of time that a given streamflow magnitude was equalled or exceeded during a certain observational period, but ignoring the autocorrelation structure of the corresponding time series (*Vogel and Fennessey*, 1994, 1995). To characterize the information content of a FDC we followed the criterion proposed by *Yilmaz et al.* (2008), where the curve is divided into three segments corresponding to different flow magnitudes: (i) a high-flow portion (0 - 0.2 exceedance probability), that represents the catchment response to large precipitation events; (ii) a medium-flow portion (0.2 - 0.7 exceedance probability), representing flows controlled by moderate precipitation events coupled to medium-term baseflow; and (iii) a low-flow segment (0.7 - 1.0 exceedance probability) representing a catchment response dominated by long-term baseflow during extended dry periods. *Yilmaz et al.* (2008) also proposed to use the change in the slope of the medium segment of the FDC as a signature related to soil moisture redistribution. However, due to the fact that we are not providing a single "*best*" simulation for comparison with the observed time series, we decided to use the uncertainty bounds in the FDC space to better understand if the relationship between magnitude and frequency of streamflows are captured by the behavioural parameter sets, which in turn will be used to assess the projected impacts of climate change.

Figures 3.11, 3.12, 3.13 and 3.14 show the daily and monthly FDCs and their corresponding uncertainty bounds for both, the calibration and verification period. FDCs are presented in normal and logarithmic[7] scales in order to better appreciate the uncertainty bounds in all the range of streamflow magnitudes.

Looking at the daily FDCs of subcatchment 090 (Ega River) plotted with the normal scale in Figure 3.11, it is possible to observe that almost all the observed streamflows are within the uncertainty bounds for both, the calibration and verification period, with a slight tendency to over-estimation of high and medium flows. However, when looking at the plots in logarithmic scales, we observe that the high flows (exceedance probability smaller than 0.2) fall in the middle of the uncertainty bounds during calibration, while are over-estimated during verification, but always within the

[7](Removing all the zero flows.

uncertainty bounds. During calibration, medium-flows (0.2 - 0.7 exceedance probability) are over-estimated up to exceedance probability close to 0.45 - 0.50, and from that point on they fall in the middle of the uncertainty bounds, with a similar behaviour during verification. Low flows (exceedance probability larger than 0.7) are generally underestimated during calibration, and moreover, streamflow smaller than ~ 3 m^3 s^{-1} are outside the uncertainty bounds, whereas during verification the underestimation is much less important and all the streamflows are within the uncertainty bounds. In this way, large relative uncertainties are associated to the estimation of low flows, but their absolute importance is small when compared to the magnitude of the uncertainties associated to medium and high flows. A very similar pattern to the aforementioned was observed in the monthly streamflows presented in Figure 3.12.

Observing the daily FDCs of subcatchment 115 (Homino River) plotted with the normal scale in Figure 3.13, it is possible to notice that all the observed streamflows are within the uncertainty bounds for both, the calibration and verification period, with a slight tendency to over-estimation of high and medium flows (exceedance probability smaller than 0.7) during verification. Looking at the plots in logarithmic scales, we observe that the low flows (exceedance probability higher than 0.7) are under-estimated both during calibration and verification, but they are always within the uncertainty bounds, which is due to the wide uncertainty bounds of this catchment. Again, the larger relative uncertainties correspond to the estimation of the low flows, but their absolute importance is small when compared to the magnitude of the uncertainties associated to medium and high flows. A very similar pattern to the aforementioned one can be observed in the monthly streamflows presented in Figure 3.14.

A point worthy of mention is that both subcatchments underwent a general relative under-estimation of low-flows, as shown by the logarithmic plots in Figures 3.11, 3.12, 3.13 and 3.14, which is a consequence of the use of the Nash-Sutcliffe efficiency as "*less formal*" likelihood, because this measure gives more importance to differences in high and medium flows than differences in low flows, due to the use of square differences thereof (see eq. 3.1).

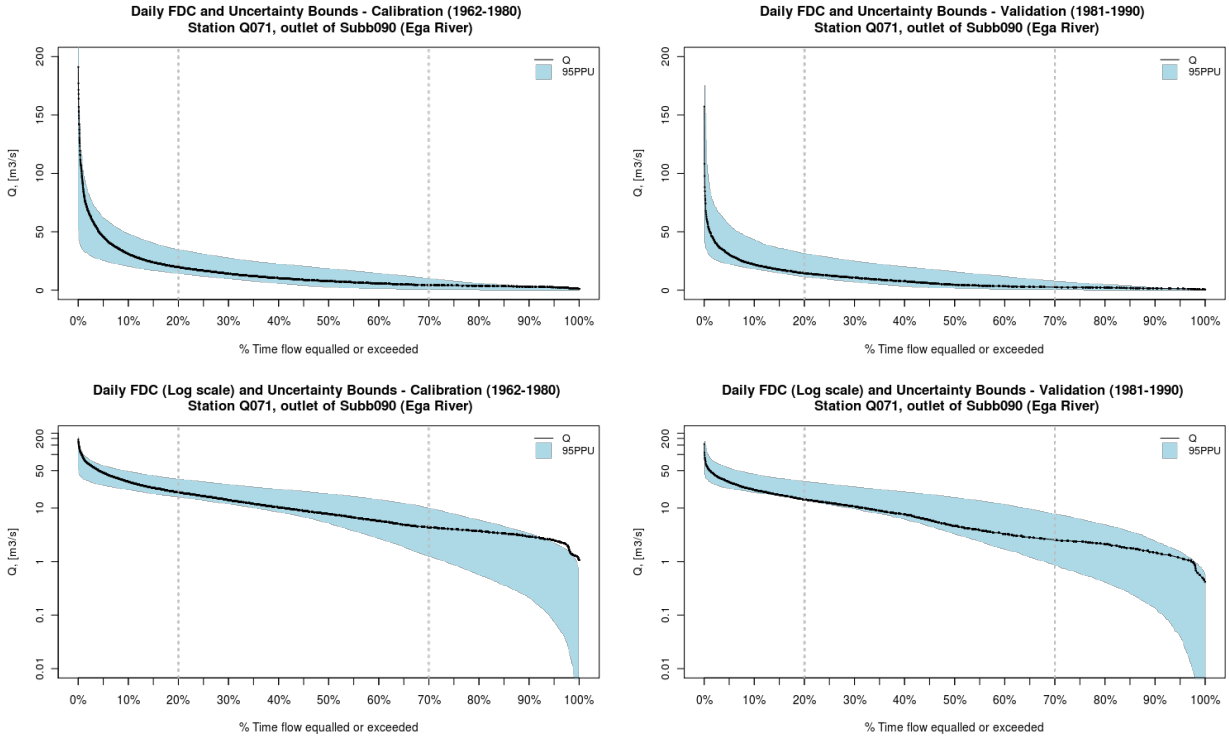

FIGURE 3.11: Daily FDCs for subcatchment 090 (Ega River) and their corresponding uncertainty bounds for both, the calibration (1962-1980) and verification (1981-1990) period. The two FDCs in the upper part are plotted with a normal scale for streamflows, whereas the two figures in the lower panel are plotted with a logarithmic scale (removing all the zero flows).

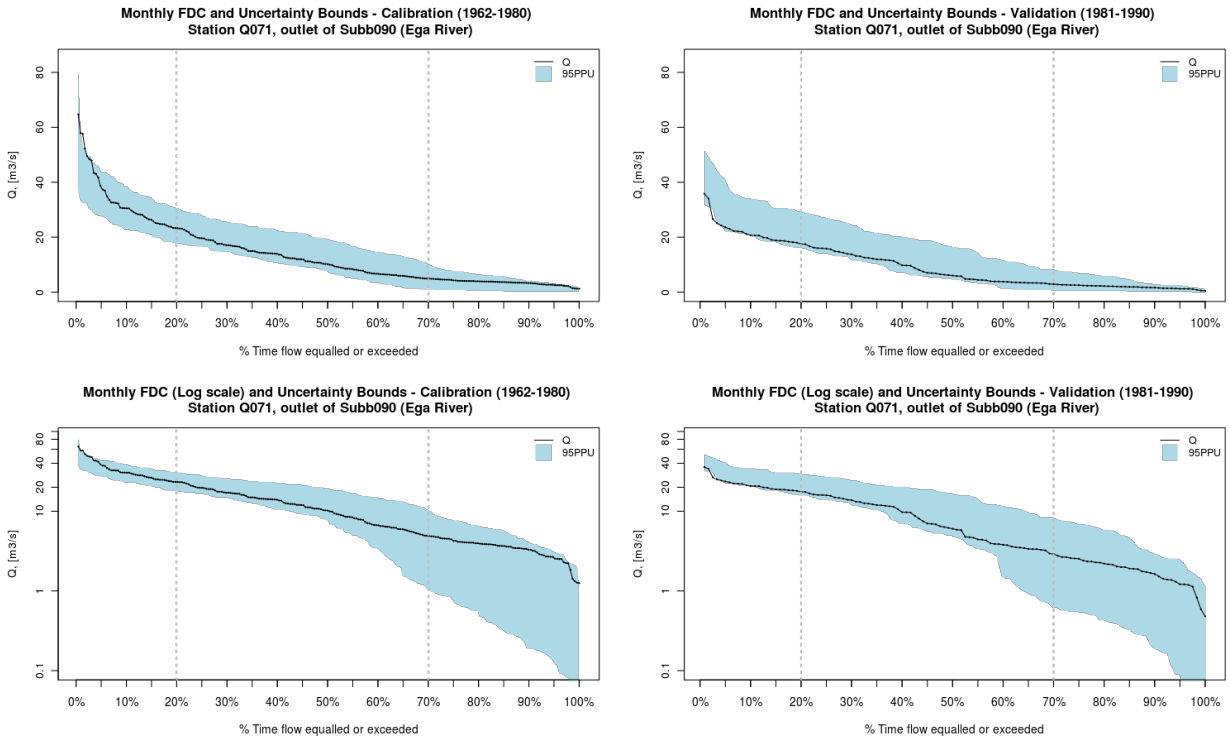

FIGURE 3.12: Monthly FDCs for subcatchment 090 (Ega River) and their corresponding uncertainty bounds for both, the calibration (1962-1980) and verification (1981-1990) period. The two FDCs in the upper part are plotted with a normal scale for streamflows, whereas the two figures in the lower panel are plotted with a logarithmic scale (removing all the zero flows).

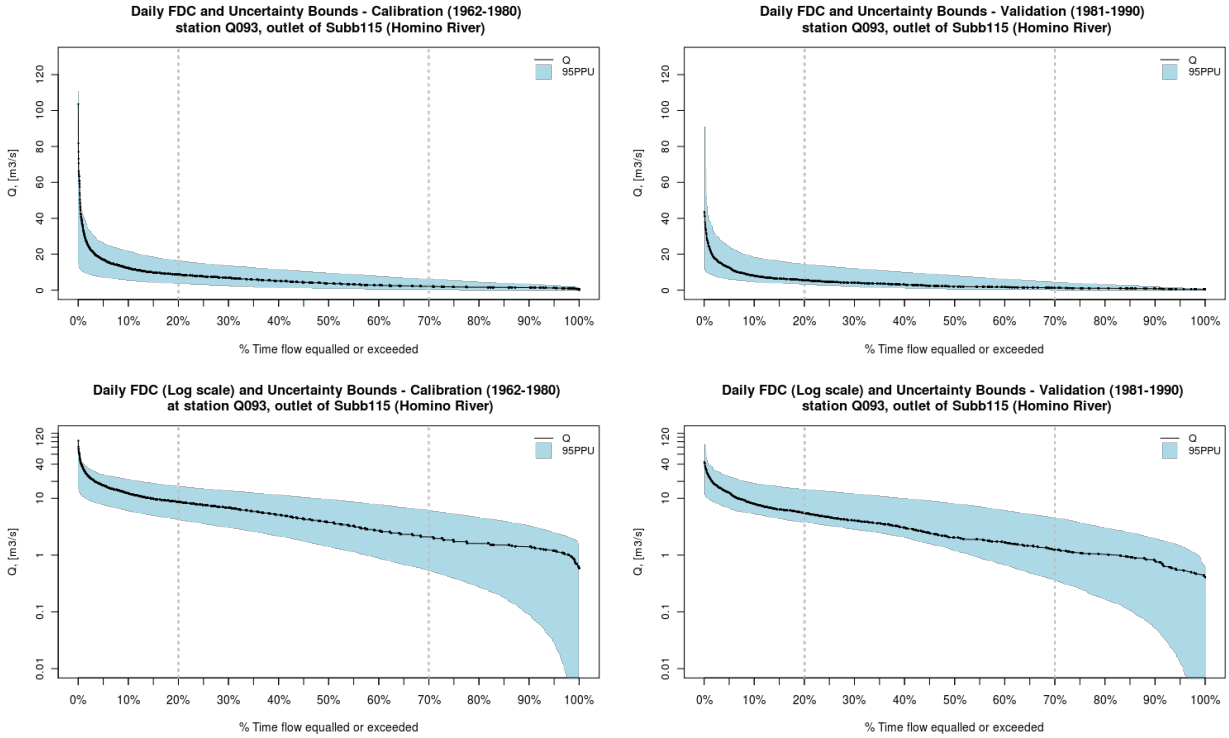

FIGURE 3.13: Daily FDCs for subcatchment 115 (Homino River) and their corresponding uncertainty bounds for both, the calibration (1962-1980) and verification (1981-1990) period. The two FDCs in the upper part are plotted with a normal scale for streamflows, whereas the two figures in the lower panel are plotted with a logarithmic scale (removing all the zero flows).

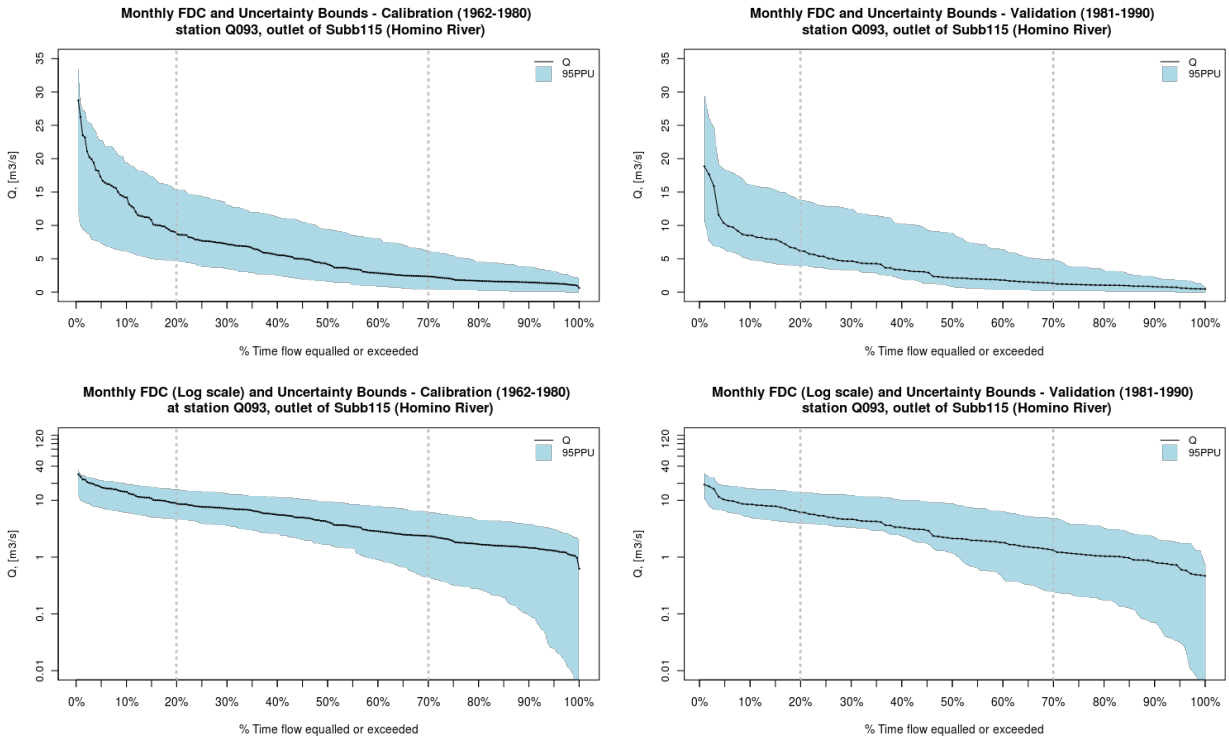

FIGURE 3.14: Monthly FDCs for subcatchment 115 (Homino River) and their corresponding uncertainty bounds for both, the calibration (1962-1980) and verification (1981-1990) period. The two FDCs in the upper part are plotted with a normal scale for streamflows, whereas the two figures in the lower panel are plotted with a logarithmic scale (removing all the zero flows).

3.6 Summary and Conclusions

The Soil and Water Assessment Tool (SWAT) hydrological model was set up for daily simulations of the western part of the Ebro River basin ($\sim$ 42000 km^2) in Spain, during the control period 01/Jan/1961 to 31/Dec/1990. Two subcatchments (090, Ega River and 115, Homino River) were selected for testing the methodology proposed to assess the effect of hydrological parameterisation on predicted streamflows. A sensitivity analysis with Latin Hypercube One-factor-At-a-Time (LH-OAT) was carried out in order to identify parameters with a high impact on simulated streamflows. Uncertainty analysis was then carried out using the Generalized Likelihood Uncertainty Estimation (GLUE) methodology, in order to select parameter sets that can be considered as acceptable simulators of the system, adopting a re-scaled NS_{eff} as "*less formal*" likelihood, and a cut-off threshold equal to zero to discriminate between behavioural and non-behavioural simulators. Afterwards, a Latin Hypercube (LH) sampling strategy was implemented within GLUE in order to reduce the number of model runs required to obtain enough parameter sets with a performance higher than the selected cut-off threshold, while keeping a good exploration of the parameter space. The NS_{eff} efficiency of the parameter sets selected as behavioural (1948 for subcatchment 090 and 1464 for subcatchment 115) were then rescaled such they sum to 1, in order to be used as "*less formal*" likelihood. The 95% of the cumulative distribution of each predicted output, weighted by the re-scaled likelihood of each behavioural parameter set, was used to compute the predictive uncertainty bounds. The main conclusions can be summarized as follow:

- The LH-OAT sensitivity analysis proved to be useful in identifying parameters that exert a significant control of the hydrological response of the catchments. However, when the simplest conceptualization of the catchment is used, i.e., a single homogeneous unit characterized by the same effective parameters all over its spatial domain, we suggest to use an absolute method for changing the parameters (instead of a relative one), because it leads to a final ranking representative of the real importance of each effective parameter.

- The three-steps methodology developed for carrying out the uncertainty analysis proved to be useful in finding a region of the parameter space where parameter sets with high likelihood values are found. Additionally, a comparison between dotty plots, with the value of each parameter against the corresponding efficiency measure, obtained after simulations with the large and reduced parameter ranges, can provide a first qualitative insight about the uncertainties involved in the representation of the catchment behaviour.

- Results of the GLUE analysis indicated that two main parameters dominate the fast response of both catchments: (i) the initial SCS curve number for moisture condition II (*CN2*), which controls the partitioning of precipitation into runoff and infiltration; and (ii) the saturated hydraulic conductivity (*SOL_K*), which takes part in the production of lateral flow and percolation to the shallow aquifer. In the case of the subcachment with more semi arid regime (115, Homino River) two additional parameters are necessary to explain the slow catchment response: (a) the deep aquifer percolation factor (*RCHRG_DP*), which controls the fraction of water that is lost from the shallow aquifer to recharge the deep aquifer (out of the catchment); and (b) the groundwater delay time (*GW_DELAY*), which represents the lag between the water exit the soil profile and enters to the shallow aquifer, affecting the slope of the recession curve. The remaining parameters present NS_{eff} greater than zero all along the reduced range used for the analysis, and their interactions contribute to partially compensate by deficiencies in the simplified representation of the catchment.

- The 95% of predictive uncertainty (95PPU) for streamflows, computed with the GLUE procedure using a LH sampling with 2000 strata within the reduced parameter ranges, led to good bracketing of observations, both during the calibration (1962-1980) and verification(1981-1990) period, as shown by P-factors larger than 0.73 for subcatchment 090 (Ega River), and larger than 0.9 for subcatchment 115 (Homino River). Consequently, those results are

deemed acceptable for assessing the projected impacts of climate change during the future scenarios.

- The relative magnitude of the uncertainty bounds for the two selected catchments were very different, as shown by their corresponding R-factors: 0.95 and 1.36 for subcatchment 090 in calibration and verification, respectively; whereas for subcatchment 115 they were 1.43 and 1.83 in both calibration and verification, respectively. If the wide uncertainty bounds for subcatchment 115 are enough for deciding to change the current model structure used to represent the catchment, will depend on the acceptance criteria adopted by the decision-makers, because notwithstanding the uncertainties are large, they embrace most of the observations; what is completely different to a situation with large uncertainties and few observations within the uncertainty bounds.

- Three different approaches could be used to decrease the large R-factors obtained for subcatchment 115: (i) choosing a higher NS_{eff} to select the parameter sets used to compute the predictive uncertainty; (ii) selecting the reduced range for each parameter from narrower percentages of their likelihood-weighted cumulative distribution (90%, 85%, 70% or less, instead of the 95% currently used); and (iii) increasing the value of the shape factor N, to reduce the relative weight associated with poor models. However, the three previously mentioned ways for decreasing the width of the uncertainty bounds, introduce an additional bias related to the expertise and judgement of the modeller, that we tried to avoid.

- The LH sampling strategy, implemented to carry out the GLUE procedure, proved to be much more efficient than the classical Monte-Carlo approach, because the uncertainty bounds obtained with the LH sampling using 2000 strata were comparable to results obtained with 5000, 10000, 12000, 17000 and 20000 runs with uniform Monte-Carlo sampling.

- Flow-duration curves (FDC) were used as a graphical representation of the magnitude and frequency of the observed streamflows in the two test catchments. Uncertainty bounds for the daily and monthly FDC of both catchments were computed as the FDC of the upper and lower uncertainty bounds obtained for the streamflow time series at the end of the GLUE analysis, respectively.

- Simulated daily and monthly FDCs, of the two analysed subcatchments, were almost completely within their respective uncertainty bounds, with a slight tendency to over-estimation of high and medium flows, and a clear under-estimation of low flows. The aforementioned over- and under-estimation are consequence of using the Nash-Sutcliffe efficiency as "*less formal*" likelihood.

- FDCs plotted with logarithmic scale were useful to visualize the relative importance of uncertainties, observing that the larger relative uncertainties correspond to the estimation of low flows, but their absolute importance is small when compared to the magnitude of the uncertainties associated to medium and high flows.

- In both catchments, the parameter set that achieved the highest NS_{eff} during calibration was not the same that achieved the highest efficiency during the verification period, emphasizing the importance of considering a *set* of acceptable simulators of the system, rather than a single "*best*" estimate. Moreover, when comparing observations to a single "*best*" simulation, the goodness-of-fit used to measure the performance of the simulations may indicate different behaviours for calibration and verification periods, making less reliable predictions with such "*best*" parameter set outside the calibration period.

- Finally, we want to emphasize that prediction limits obtained with GLUE are highly dependent on decisions taken by the modeller: what model structure(s) is(are) used to represent the catchment behaviour (not analysed here), what input data are used to drive the hydrological simulations (not explicitly dealt in this dissertation), which and how many parameters are selected for the uncertainty analysis, what parameter ranges are sampled for each

parameter, which likelihood measure is used to assess the performance of different parameter sets, the threshold selected to discriminate between behavioural and non-behavioural simulators, and the way in which all the previous choices are combined, as expressed by other authors (e.g. *Beven*, 2001; *Beven and Freer*, 2001; *Montanari*, 2005).

- The fact that many combinations of model structure and parameter sets were deemed as acceptable simulators of the two catchments under study, only means that we could not reject a larger number of them based on the available data and knowledge. Additional information (amount and/or type of data) is needed to exclude some of them under the same acceptance criteria used here. Uncertainty arising from equifinality may be though as a decision-making problem subject to imperfect knowledge and limited data, but we want to emphasize that those limitations, when made explicit to the final users, may lead to better decisions than those taken on the basis of a single "*best*" simulation during the control period, which is *expected* to perform equally well under unknown future conditions.

"To know the road ahead,
ask those coming back".
(Chinese proverb)

4

Projected Changes in Climate (2071-2100)

This chapter presents projected changes for precipitation and air temperature fields on the Ebro River basin by the end of this century (2071-2100). Firstly, section 4.1 presents a brief introduction about expected changes in climate for the Mediterranean area, climate models, future climate scenarios, and downscaling techniques, in order to set the framework for the remaining sections of this chapter. Section 4.2 describes the ensemble of six climate change scenarios, selected from the EU FP5 PRUDENCE project to sample the space of possible future climates, along with the downscaling technique adopted for passing the climate signal from the grid-scale of the RCM outputs to the point-scale of the gauging stations selected to drive the hydrological simulations in the next chapter. Section 4.3 presents the long-term averages of precipitation and temperature fields for the control period 1961-1990, whereas the anomalies expected for the future period 2071-2100 are presented in an annual, seasonal and monthly basis, including a short discussion about expected changes for different altitudes within the basin. Finally, the main results are summarized and discussed in section 4.4 at the end of this chapter.

4.1 Introduction

4.1.1 Overview

Changes in water resources are intimately linked with changes in atmospheric temperature and precipitation. Observed records of global average air and ocean temperatures, melting of snow and ice, and global sea level makes unequivocal the warming of our climate system (*Bates et al.*, 2008), which may lead to an intensification of the hydrological cycle (*Huntington*, 2006). Global mean surface temperatures have risen by $0.74°\mathrm{C} \pm 0.18°\mathrm{C}$ over the last 100 years (1906-2005) and eleven of the last twelve years (1995-2006) are among the 12 warmest years since 1850, as mentioned in the Fourth Assessment Report (AR4) of the Intergovernmental Panel on Climate Change (IPCC) (*Trenberth et al.*, 2007). This updated 100-year linear trend is larger than the $0.6°\mathrm{C} \pm 0.2$ given nine years ago in the Third Assessment Report (TAR) for 1901-2000, and the rate of warming over the last 50 years is nearly twice that for the last 100 years ($0.13°\mathrm{C} \pm 0.03°\mathrm{C}$ vs. $0.07°\mathrm{C} \pm 0.02°\mathrm{C}$ per decade). Warming is occurring in both land and ocean domains leading to changes in the overall Earth's hydrological cycle, with an increase in the number of droughts and heavy rainfall events and a decrease in the amount of ice on Earth expected for the future (*Trenberth et al.*, 2007).

According to the AR4, mean annual temperatures in Europe are likely to increase more than the global mean, with the largest warming in summer for the Mediterranean area, and in particular, the highest summer temperatures are expected to increase more than the average for central and southern Europe (*Christensen et al.*, 2007a). In the Mediterranean area, annual precipitation is very likely to decrease, whereas the annual number of precipitation days is very likely to decrease as well, leading to a likely increase in the risk of summer drought for this area (*Christensen et al.*, 2007a).

4.1.2 Future Climate Scenarios

Climate system is highly complex and non-linear, and in particular due to the intrinsic stochastic component of the future forcings (both natural and anthropogenic), and the unknown initial state of the climate system, it is nearly impossible to exactly predict how climate will evolve in the future (*Giorgi*, 2005). Notwithstanding their limitations, climate models are the best available tools for quantifying the global climate response to different future development scenarios of our society, represented by different atmospheric concentrations of carbon dioxide and other trace gases. Climate models use well-known physical principles to simulate the interactions among atmosphere, oceans, land surface and ice, through different numerical schemes and/or different parameterisations. They balance, or almost balance, incoming and outgoing energy, and any inconsistency reveals a change of the Earth's average temperature. However, since it is practically impossible for a climate model to describe all the climate processes, no matter how complex the model is, different climate models make different choices about what processes to include and how to parametrize them (*Tebaldi and Knutti*, 2007). Climate models could be grouped into Simple Climate Models (SCMs), Earth-System Models of Intermediate Complexity (EMICs) and Atmosphere-Ocean General Circulation Models (AOGCM) (*Solomon et al.*, 2007).

Up to now, the assessment of potential impacts of climate change has generally relied on data from AOGCM, which are dynamical three-dimensional representations of the atmosphere, land surface, oceans, sea ice, and simple chemistry processes, that explicitly account for the effects of anthropogenic and natural forcings (*Giorgi*, 2005). AOGCM simulations are subject to three major sources of uncertainty: model configuration, internal model variability and the stochastic nature of the future natural forcings (*Giorgi*, 2005). Spatial resolution of AOGCMs ($\sim$ few hundred kilometres) is not enough for accurately reproducing regional climate patterns. Therefore, regionalization or downscaling techniques (*Giorgi and Mearns*, 1991) are applied to the AOGCM outputs for providing fine resolution climate variables suitable for impact studies. In particular, regional climate models (RCMs) use large-scale and lateral boundary conditions from the general circulation model (GCM) to produce higher resolution outputs.

As mentioned in the AR4, there is increasing confidence that the increment in atmospheric greenhouse gas concentrations will lead to an increment of the global temperature; however, there is much less confidence about the quantification of the regional response of climate. As no method yet exists of providing confident predictions of climate change at the regional scale (*IPCC DDC*, 2010), climate scenarios are used as an alternative approach to identify the sensitivity of a system to climate change, and to help policy makers decide on appropriate policy responses. In this dissertation, a "*climate scenario*" is used as "*a plausible future climate that has been constructed for explicit use in investigating the potential consequences of anthropogenic climate change*" (*Mearns et al.*, 2001). The main objective of using scenarios is not to be considered as "*predictions*" of the future climate, but to explore some of the uncertainties arising from incomplete knowledge about the effect of increased atmospheric concentrations of greenhouse gases on global climate, in order to take informed decisions under a wide range of possible futures. Recently, *Moss et al.* (2010) describes a new parallel process for creating plausible scenarios for climate change research, aiming at improving society's understanding of plausible climate and socio-economic futures. The IPCC has proposed 40 "*plausible*" scenarios of future emissions (*Nakićenović et al.*, 2000), which are considered "*equally valid*", without an assignment of quantitative or qualitative likelihoods (see *Schneider*, 2002). These emissions scenarios are grouped into four major families, representing a different storyline of socio-economic, demographic and technological evolutions of our society. Emissions from six of these scenarios (A1T, A1F1, A1B, A2, B1, and B2) have been used to derive scenarios of future concentrations of greenhouse gases, which in turn are used to obtain projections of climate response, usually by running transient simulations of AOGCMs (*Giorgi*, 2005).

At the other hand, all the previously mentioned uncertainties involved in climate modelling have lead to a widely accepted need of probabilistic assessment of climate change at the regional scale (e.g. *Reilly et al.*, 2001; *Räisänen and Palmer*, 2001; *Webster et al.*, 2003; *Dessai*, 2003; *Giorgi*, 2005), and to the use of multi-model ensembles to better estimate of the probability of climate change, in

particular at regional scales, because no singe model provides a "*true*" representation of the future climate (*Tebaldi*, 2004). *Wilby and Harris* (2006) highlight that impact assessments based on single GCM may lead to inappropriate planning or adaptation responses.

So far, the use of multiple GCMs and emissions scenarios to drive hydrological impact studies has been adopted by researchers worldwide, but the use of multiple fine resolution RCM outputs has been limited to Europe (*Fowler et al.*, 2007). In this context, the EU Fifth Framework Programme (FP5) PRUDENCE project (Prediction of Regional scenarios and Uncertainties for Defining EuropeaN Climate change risks and Effects, *Christensen et al.*, 2007b; *Christensen and Christensen*, 2007) provided a set high resolution climate change scenarios for Europe, where eight RCMs were dynamically downscaled from four high resolution Atmospheric General Circulation Models, both during a control period (1961-1990) and a future time-slice at the end of this century (2070/71-2100), representing a stationary climate over the selected 30-years period. Most of the PRUDENCE experiments assumed the SRES (Special Report on Emissions Scenarios, *Nakićenović et al.*, 2000) A2 emissions scenario, but some also assumed the B2 scenario. A description of the experimental set-up of the PRUDENCE project is provided by *Christensen and Christensen* (2007), whereas *Jacob et al.* (2007) provides an assessment about how the systematic biases vary across the different models, and *Déqué et al.* (2007) discusses the uncertainties in model projections of the PRUDENCE experiment.

4.1.3 Downscaling Techniques

As mentioned in the previous section, AOGCMs have a spatial resolution of a few hundred kilometres ($\sim$300 km or $\sim$2.5°), which is not enough for accurately reproducing regional climate patterns, in particular, spatial patterns of precipitation (*Salathé*, 2003) and its daily variability (*Bürger and Chen*, 2005), especially in areas of complex topography and land use distribution (*Christensen et al.*, 2007b) (within the Ebro River basin, elevations range from sea-level to more than 3400 m.a.s.l.), making them unsuitable for a direct application as drivers of hydrological impacts studies (e.g. *Prudhomme et al.*, 2002; *Wilby et al.*, 1999). To overcome these limitations, in recent decades a great deal of research has been focused on the development of spatial and temporal "*downscaling*" techniques, which are carried out for limited areas and run for shorter periods, mainly oriented to better reproduce temperature and precipitation fields (e.g. *Xu*, 1999; *Wilby et al.*, 2000; *Schoof and Pryor*, 2001; *Salathé*, 2003, 2005; *Wood et al.*, 2004; *Bürger and Chen*, 2005; *Dibike and Coulibaly*, 2005; *Prudhomme*, 2006; *Burton et al.*, 2010).

Downscaling techniques can be roughly classified as (i) empirical/statistical methods, where statistical techniques are used to formulate empirical relationships between GCM climate outputs and local climate; and (ii) dynamical downscaling, where a higher resolution regional climate model (RCM) or limited-area model (LAM) is nested to a GCM, using large-scale and lateral boundary conditions from the GCM to produce higher resolution outputs (typically at $\sim$0.5 latitude and longitude). The advantages and limitations of these two approaches have been extensively discussed in literature (e.g. *Wilby and Wigley*, 1997; *Murphy*, 1999, 2000), as well as their impacts on the resulting future climate scenarios (e.g. *Hellström et al.*, 2001; *Wood et al.*, 2004; *Schmidli et al.*, 2006, 2007). *Mearns et al.* (2003) and *Giorgi* (2006) review scenarios derived from regional climate models, whereas *Fowler et al.* (2007) provides an exhaustive and updated analysis of downscaling techniques with focus in hydrological applications.

4.2 Methodology

4.2.1 Selection of Future Climate Scenarios

The use of ensembles of climate models is essential when moving towards probabilistic climate change impact, for incorporating the uncertainties derived from model parameterisation into climate change impact studies. In the present dissertation, climate change scenarios for the entire Ebro River basin were provided by a research group of the Newcastle University (*Bovolo et al.*, 2009), where an ensemble of six RCMs was selected from the red set of the EU FP5 PRUDENCE project, described in Table 4.1, which includes RCM outputs (∼50x50 km) from the Danish Meteorological Institute (DMI), the Swedish Meteorological and Hydrological Institute (SMHI), the UK's Hadley Centre, and from MétéoFrance. The six RCMs are run with boundary conditions from what may be considered as two different GCMs: the atmosphere-only HadAM3H (*Buonomo et al.*, 2007; *Gordon et al.*, 2000; *Pope et al.*, 2000) and the atmosphere-ocean ECHAM4/OPYC (*Roeckner et al.*, 1996), because the HadRM3P and ARPEGE RCM simulations derive boundary conditions from HadAM3P and the coupled AOGCM HadCM3, respectively, whereas the HadAM3H and HadAM3P GCMs are dynamically downscaled to an intermediate resolution from the HadCM3 coupled AOGCM and therefore are closely related.

The climate scenarios adopted in this dissertation only include projections using the medium-high SRES A2 emissions scenario, because: (i) recent observations seems to indicate that the increase in global mean surface temperature is in agreement with the highest projections given by the IPCC, likely because the climate system is responding faster than model projections (*Rahmstorf et al.*, 2007), and (ii) the climate change signal derived from the SRES B2 scenario is weaker than the one from A2, and can be scaled from that (*Déqué et al.*, 2005).

The selected climate scenarios have been previously described in the following Aquaterra deliverables: *Fowler et al.* (2005), *Blenkinsop and Fowler* (2005), *Bovolo et al.* (2008) and *Bovolo et al.* (2009).

TABLE 4.1: Climate change scenarios used in this dissertation, with corresponding GCM and RCM. Table also shows originating institution (**INST**, where DMI: Danish Meteorological Institute, HC: Hadley Centre for Climate Prediction and Research, SMHI: Swedish Meteorological and Hydrological Institute), model dates for the control (**CTRL**) and future (**SCEN**) scenarios, and model file names used by PRUDENCE and Aquaterra. Source: Adapted from *Bovolo et al.* (2009).

RCM	INST	GCM	Days in a Month	CTRL	SCEN	PRUDENCE Acronym CTRL	PRUDENCE Acronym A2 SCEN	Aquaterra Acronym A2 SCEN
HIRAM	DMI	HadAM3H A2	30	1961 1990	2071 2100	HC1	HS1	HIRAM_H
HIRAM	DMI	ECHAM4/OPYCA2	30	1961-1990	2071-2100	ecctrl	ecscA2	HIRAM_E
HadRM3P	HC	HadAM3P A2	30	1961-1990	2070-2100	adeha	adhfa	HAD_P_H
RCAO	SMHI	HadAM3H A2	30	1961-1990	2071-2100	HCCTL	HCA2	RCAO_H
RCAO	SMHI	ECHAM4/OPYCA2	30	1961-1990	2071-2100	MPICTL	MPIA2	RCAO_E
Arpége	Météo France	Observed SST/HadCM3 A2	normal days	1961-1990	2071-2100	DA9	DE6	ARPEGE_H

4.2.2 Downscaling RCM outputs

Notwithstanding the spatial resolution of RCM outputs is much higher than the one of the driving GCMs, further correction is usually required to overcome biased representation of observed climate (e.g., too many low-intensity rain events), mainly due to problems in conceptualization, discreatization and spatial averaging within grid cells (*Teutschbein and Seibert*, 2010). Bias in RCM outputs may lead to unreliable representation of streamflows in hydrological simulations (e.g. *Bergström et al.*, 2001). Nowadays, there are many methodologies for modifying RCM outputs, in order to be further used in hydrological simulations. *Teutschbein and Seibert* (2010) provides a brief

summary of bias-correction techniques usually applied to precipitation and temperature variables derived from RCMs.

In this dissertation, a simple **bias-correction** method was used to downscale daily precipitation and air temperature fields from the grid-cell scale of the RCM outputs to the point scale of the gauging stations. Figures 4.1 and 4.2 shows the location of the precipitation and temperature stations, respectively, used in the present dissertation, along with the RCM grid cells covering Ebro River basin. The bias-correction method applied in the present study uses monthly correction factors to modify both the **absolute magnitude** and the **seasonality** of the modelled values, based on the difference between observed values on the gauging stations and the RCM values given by the relevant grid-cell during the control period 1961-1990 (see *Fowler and Kilsby*, 2007), in order to allow the simulated monthly means to match the observed monthly averages during the control period. Under the assumption that the same model biases which apply during the control climate will apply in the future, the computed bias-correction factors are then applied to the future daily time series given by the RCM outputs, additively in the case of temperature and multiplicatively for precipitation (see *Fowler and Kilsby*, 2007), to obtain future precipitation and temperature fields, which in turn are used as input to the hydrological model. This procedure was applied to the six Regional Climate Models (RCMs), described in Table 4.1, for the 2070/71 - 2100 time-slice and the same medium-high SRES A2 emissions scenario.

In order to apply the bias-corrected method using monthly mean statistics, the observed data record must be sufficiently long to allow the derivation of representative statistics for the 30-years time period. Furthermore, the period of observations should be well represented in the control period of the models (*Bovolo et al.*, 2008). In this way, daily time series of the 349 precipitation gauging stations and the 146 temperature stations described in section 2.2.5.1, were provided to the Newcastle research group, for the period January/1961 to December/1990. Only the stations with more than 70% of valid precipitation data and 65% of temperature data during that 30-years period were considered, as described in section 2.2.5.1. All the missing values were filled in by spatial interpolation, using a modified version of the inverse distance weighted (IDW) algorithm, where the spatial distance between the station with the missing data and the one with a known value is replaced by the Pearson's product-moment coefficient of correlation between their daily time series, following the work of *Teegavarapu and Chandramouli* (2005), but using for the interpolations only the 4 closest stations (close in terms of the coefficient of correlation between the daily time series) to each target station, instead of all the available stations. A leave-one-out cross validation procedure was used for assessing the goodness-of-fit between the interpolated values and the observed ones, with good results, as shown by overall[1] mean errors of 0.011 [mm/day] and 0.30 [°C/day] for precipitation and temperature, respectively, and overall mean Nash-Sutcliffe efficiencies of 0.57 for precipitation and 0.91 for temperature.

The bias-corrected time series of daily precipitation and air temperature obtained by the aforementioned procedure are used in the present chapter to assess the projected changes in climate on the Ebro River basin by the end of this century, and will be used in the next chapter as drivers of the hydrological simulations during the future climate scenarios.

4.2.3 Computation of Anomalies

Anomalies for precipitation and temperature fields of the Ebro River basin were computed as the difference between mean projected values for the climate scenarios (Jan/2071 - Dec/2100) and the mean values observed during the control period (Jan/1961 - Dec/1990, referred as "CTRL" hereafter), and they can be viewed as expected values about which various uncertainties exist.

Long-term annual, seasonal and monthly mean values of precipitation and air temperature during the CTRL period were computed by processing daily data from the selected 349 and 146 gauging stations of precipitation and air temperature (see section 2.2.5.1), respectively, removing all the missing values from the computation. Accordingly, long-term annual, seasonal and monthly

[1] considering all the gauging stations and all the days with data during the 30-years period

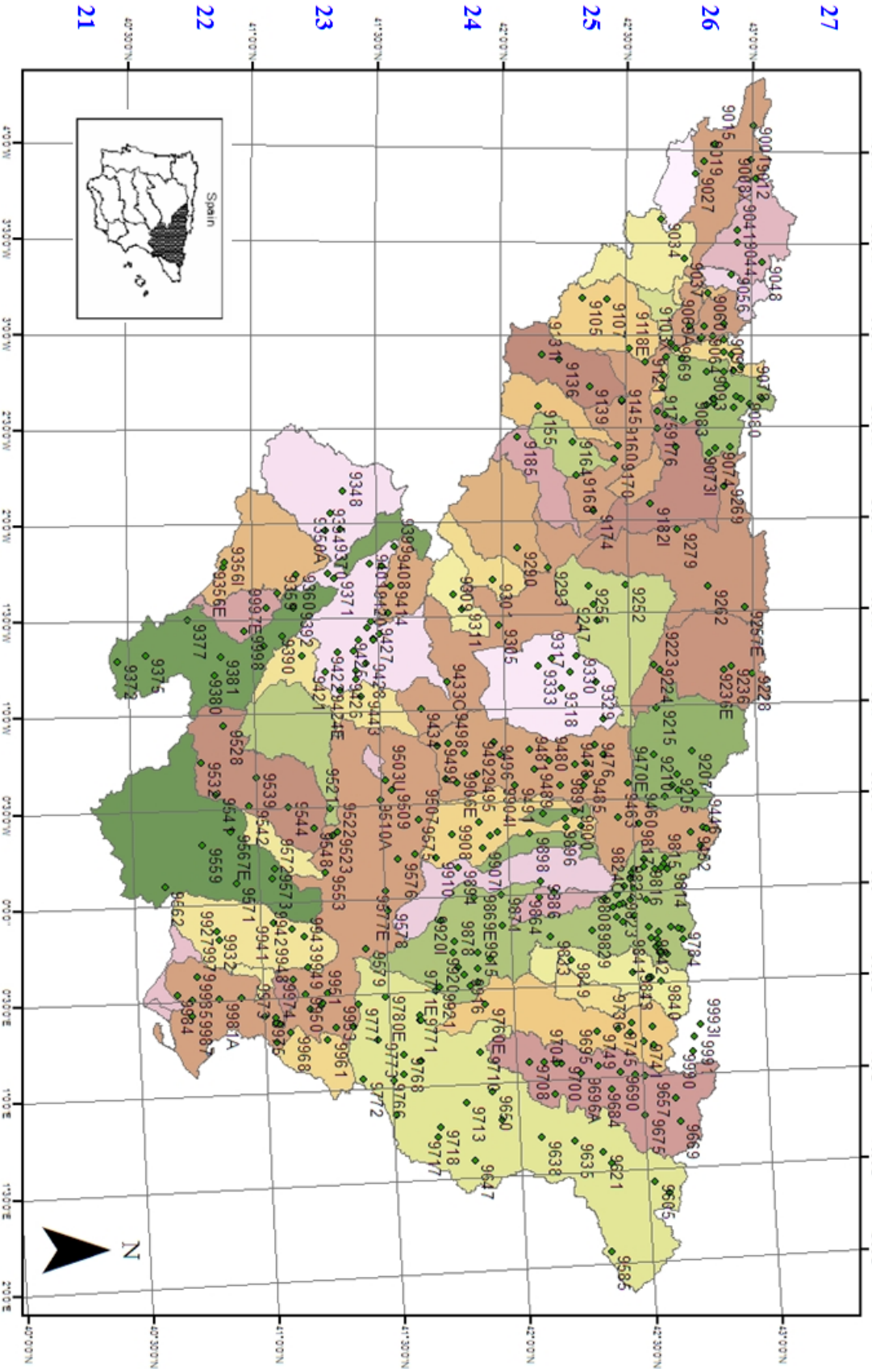

FIGURE 4.1: Precipitation gauging stations used for downscaling on the Ebro River basin. Latitude and longitude coordinates are shown (small numbers) along with the grid-cell numbering system (blue). Source: *Boyolo et al.* (2009), with permission.

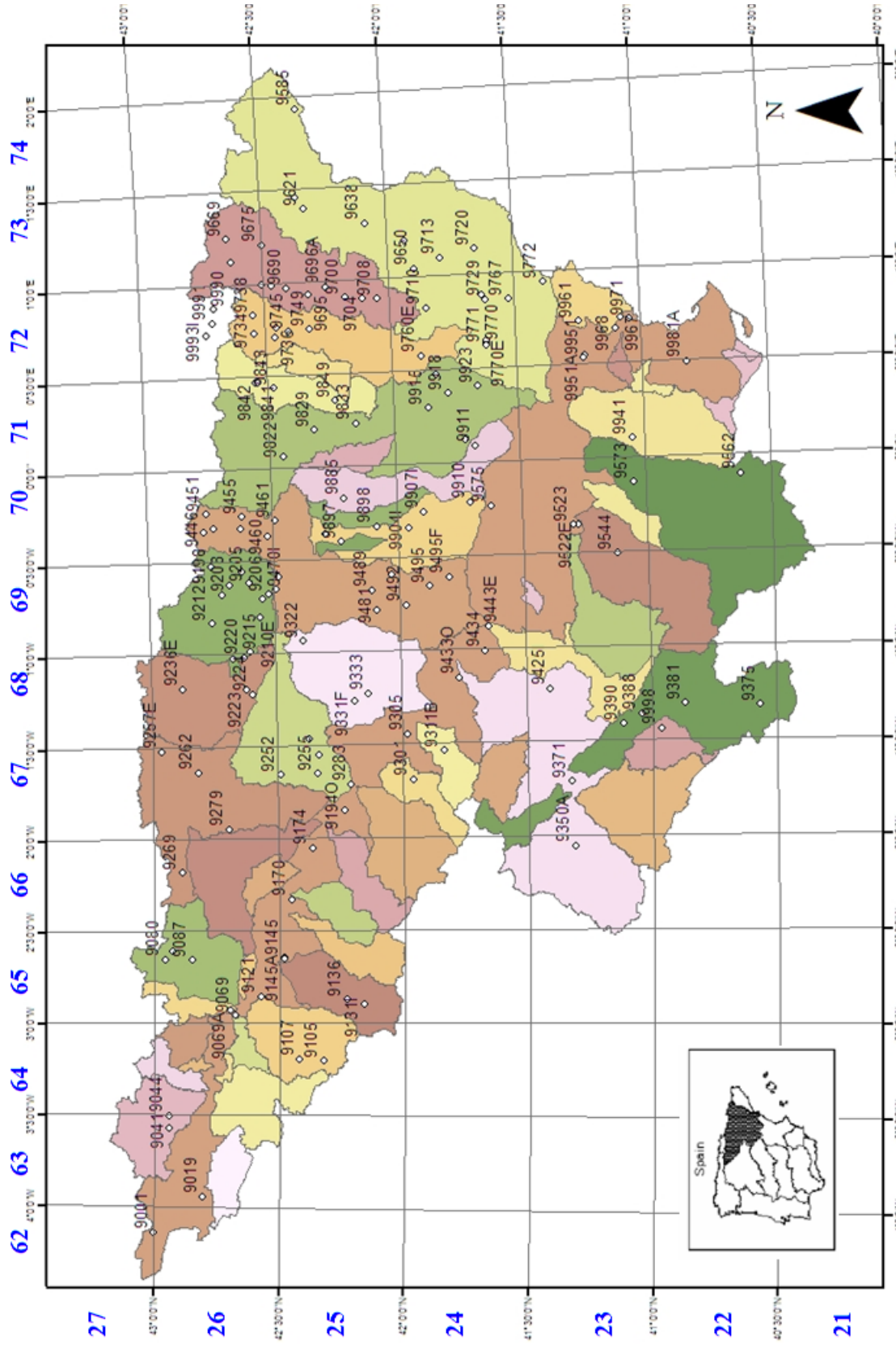

FIGURE 4.2: Temperature gauging stations used for downscaling on the Ebro River basin. Latitude and longitude coordinates are shown (small numbers) along with the grid-cell numbering system (blue). Source: *Boyolo et al.* (2009), with permission.

mean values of precipitation and air temperature for the future scenarios were computed in the same way, but using the bias-corrected daily values downscaled from the RCM outputs for each one of the gauging stations. Finally, annual, seasonal and monthly anomalies were computed by subtracting the bias-corrected values projected by each RCM to the corresponding long-term mean during the control period. For precipitation, the previous difference is further divided by the long-term mean of the CTRL period, in order to obtain the relative change, which -by multiplying by 100- is used to obtain the percentage of change discusses along this chapter. By properly adding the anomaly value to the corresponding long-term mean values of precipitation and air temperature, it is possible to obtain the projected values by each one of the RCMs described in Table 4.1.

However, values obtained by arithmetically averaging over observed values in the gauging stations does not take into account neither their spatial distribution nor the clustering effect of unevenly distributed stations. In a way of partially overcoming the previous difficulty and to avoid biased averages, in this chapter the annual, seasonal and monthly log-term mean values of precipitation and temperature were also computed by using two different methods of spatial interpolation: inverse distance weighted (**IDW**) and ordinary kriging (**OK**), over the same squared grid of 1 km^2. Anomaly maps derived from the ordinary kriging interpolations are presented along this chapter, in order to better represent the spatial variation of the projected changes in climate for the Ebro River basin. All the spatial interpolations presented in this chapter were computed in the following way:

1. Long-term averages of annual, seasonal and monthly values of precipitation/temperature during the CTRL period in each one the gauging stations are computed, and then used as input to the OK/IDW procedure.

2. A squared grid with cells of 1 km^2 is computed to sample the Ebro River basin, and then is used as spatial domain to obtain the interpolated values.

3. The *hydrokrige* function of the *R* (*R Development Core Team*, 2009) package *hydroTSM*[2] is used to compute the interpolated values in each cell of the spatial domain. This *R* package was developed by the author of this dissertation during his Ph.D, and in particular, the *hydrokrige* function is a wrapper to the *R* packages *gstat* (*Pebesma*, 2004) and *automap* (*Hiemstra et al.*, 2008), and it allows to automatically test four different variogram models (spherical, exponential, gaussian and Matern with M. Stein's parametrization) and to select the one that best fit the annual/seasonal/monthly data and its corresponding nugget, sill and range parameters.

4. Step 1 to 3 are repeated for each one of the six climate scenarios described in Table 4.1 (Jan/2071 - Dec/2100), using the corresponding bias-corrected daily values in each one of the gauging stations, to obtain the mean annual/seasonal/monthly interpolated values in each one of the cells belonging to the spatial domain defined in step 2.

5. Annual/seasonal/monthly anomalies are obtained for each cell of the spatial domain by subtracting the values obtained in step 4 from those computed in step 3. For precipitation, the previous difference is further divided by the value computed in step 3, to obtain the relative change with respect to the CTRL period, which -by multiplying by 100- is used to obtain the percentage of change.

[2] see Appendix D

4.3 Results

Projected changes in air temperature and precipitation are complex processes that exhibit significant spatial and temporal variation that can not be fully displayed in a single chart/map. Therefore, values of the annual/seasonal/monthly anomalies for the future period 2071 - 2100 are presented in tables, whereas the most relevant spatial aspects of those changes are depicted in anomaly maps specially designed to reflect those changes.

4.3.1 Control Period (1961-1990): Precipitation and Temperature

Before looking at the changes in climate, knowledge about its historical behaviour is needed for a better understanding about the significance of the ongoing changes. The amount of stations used during this preliminary analysis was selected following the criterion mentioned in the section 2.2.5.1, with gauging stations with at least 70% and 65% of precipitation and temperature data, respectively, during the control period 1961-1990, leading to the 349 and 146 selected stations of precipitation and temperature, respectively (see Appendix A, for detail of the selected stations).

The mean annual precipitation over the Ebro River basin computed by averaging the mean annual values of the 349 precipitation stations considered in the analysis is ∼609 [mm/year] (see Table 4.2). When this mean annual precipitation is computed by averaging the IDW interpolated values of all the squared cells of 1km^2 within the basin, this value decreases to 545.4 [mm/year] (see Table 4.2 and Figure 4.3). Similarly, the mean annual temperature over the Ebro River basin is 12.2°C when computed averaging the values of the 146 temperature gauging stations considered in the analysis, but this value slightly increases up to 12.7°C when computed averaging over the IDW values of all the cells belonging to the study area, as shown in Table 4.2 and Figure 4.3. It is also worth to mention that the mean values computed by the two methods of spatial interpolation did not present significant differences, which is very likely due to the smoothing effect of interpolating over such a large area.

TABLE 4.2: Mean **annual** and **seasonal** precipitation and temperature on the Ebro River basin, during the CTRL period 1961 - 1990. Values on the left are computed averaging over the corresponding annual and seasonal values at the gauging stations; values on the centre, are obtained with IDW interpolation, and values on the right are computed using OK interpolation; the latter two, computed over the same squared cells of 1km^2.

	Mean Precipitation, [mm]			Mean Temperature, [°C]		
	Stations	IDW	OK	Stations	IDW	OK
Annual	608.9	545.4	544.6	12.2	12.7	12.7
DJF	144.5	126.9	126.6	4.8	5.3	5.3
MAM	171.0	156.3	156.3	10.7	11.2	11.1
JJA	121.4	109.0	109.5	20.5	21.0	20.9
SON	170.9	152.1	151.5	13.1	13.6	13.5

TABLE 4.3: Mean **monthly temperature** on the Ebro River basin, during the CTRL period 1961 - 1990. Values on the first row are computed averaging over the corresponding gauging stations; values on the middle row are obtained with IDW interpolation, and values on the lower row are computed using OK interpolation; the latter two, computed over the same squared cells of 1km^2.

	Mean Monthly Temperature, [°C]											
	Jan	Feb	Mar	Apr	May	Jun	Jul	Aug	Sep	Oct	Nov	Dec
Stations	4.1	5.6	7.8	10.2	14.1	18.3	21.8	21.3	18.3	13.3	7.8	4.6
IDW	4.6	6.1	8.3	10.7	14.6	18.9	22.3	21.8	18.8	13.8	8.2	5.0
OK	4.6	6.1	8.2	10.7	14.5	18.7	22.2	21.7	18.6	13.7	8.2	5.1

TABLE 4.4: Average **monthly precipitation** on the Ebro River basin, during the CTRL period 1961 - 1990. Values on the first row are computed averaging over the corresponding gauging stations; values on the middle row are obtained with IDW interpolation, and values on the lower row are computed using OK interpolation; the latter two, computed over the same squared cells of 1km^2

	Monthly Precipitation, [mm]											
	Jan	Feb	Mar	Apr	May	Jun	Jul	Aug	Sep	Oct	Nov	Dec
Stations	48.6	44.3	43.8	61.0	66.2	53.0	30.2	38.3	47.6	56.6	66.6	52.9
IDW	42.7	39.3	39.8	56.0	60.5	48.4	26.9	33.7	42.8	50.5	58.9	46.0
OK	42.6	39.2	39.8	56.0	60.5	48.5	27.0	33.8	42.6	50.4	58.5	45.8

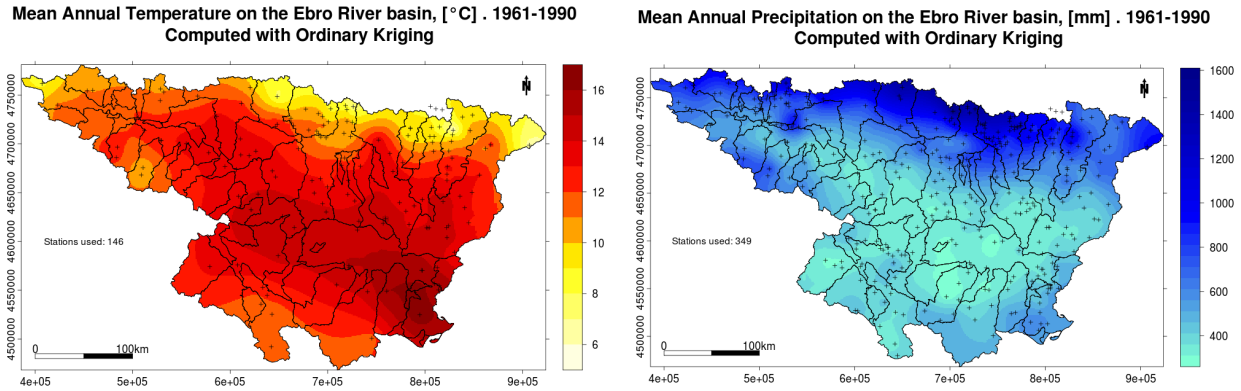

FIGURE 4.3: Spatial distribution of the mean annual temperature and precipitation during the control period 1961-1990, computed using ordinary kriging with cells of 1 km^2 and 10 nearest neighbours. Black crosses represent the location of the gauging stations.

Figure 4.3 shows that the north and north-western part of the catchment present the highest values of mean annual precipitation and the coldest mean annual temperatures, whereas the central valley is much drier and hotter.

Figure 4.4 shows that the spatial distribution of mean seasonal temperature changes significantly along the year, but for each season the highest temperatures are concentrated in the central valley, and they decrease with increasing distances to it. At the other hand, the spatial distribution of the mean seasonal precipitation looks very similar for spring (MAM) and autumn (SON), with the wettest areas in the north and north-western parts of the catchment; whereas during winter (DJF) the dry areas in the central valley occupy a much larger area than during spring and autumn; and finally, during summer (JJA) the high precipitation values are concentrated in some few places of the northern part of the catchment.

4.3.2 Future Scenarios (2071-2100): Anomalies in Precipitation and Temperature

Due to the large amount of meteorological information analysed in this dissertation, only the anomalies of bias-corrected annual/seasonal/monthly projected values of precipitation and air temperature are presented. Projected values of bias-corrected annual/ seasonal/monthly mean temperature and precipitation over the entire Ebro River basin can be found in the Appendix B for the six future climate scenarios described in Table 4.1.

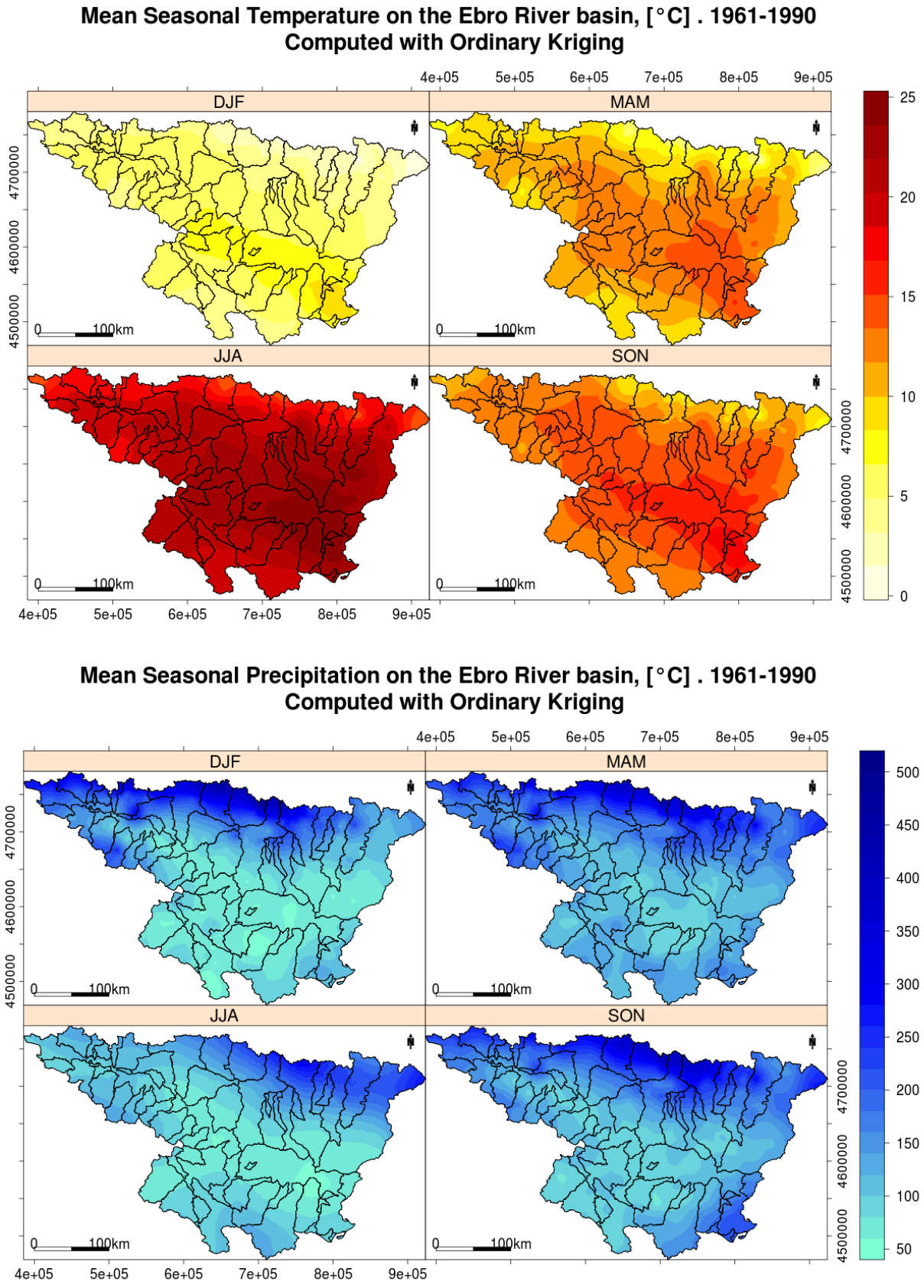

FIGURE 4.4: Spatial distribution of the **mean seasonal** temperature and precipitation during the control period 1961-1990, computed using ordinary kriging with cells of 1 km^2 and 10 nearest neighbours

4.3.2.1 Annual and Seasonal Anomalies

The anomalies of bias-corrected mean **annual** and **seasonal** precipitation and air temperature over the entire Ebro River basin during the future period 2071 - 2100 are presented in Tables 4.5, 4.6, 4.7 and Figure 4.5, for the 6 RCMs described in Table 4.1.

TABLE 4.5: Anomalies of mean **annual** and **seasonal** precipitation and temperature on the Ebro River basin, for 6 RCMs during 2071 - 2100 with respect to the the CTRL period 1961 - 1990. Values computed averaging over the corresponding **gauging stations**.

	Anomaly of Mean Precipitation, [%]					Anomaly of Mean Temperature, [°C]				
RCM	Annual	DJF	MAM	JJA	SON	Annual	DJF	MAM	JJA	SON
DMI.HS1	-3.76	21.24	-14.07	-31.63	4.01	4.20	3.28	3.26	5.56	4.41
DMI.ecscA2	-6.00	15.26	-20.10	-16.44	-3.04	5.55	4.06	5.18	7.18	5.47
HC.adhfa	-8.79	11.49	-14.81	-40.38	12.80	4.60	3.43	3.58	6.24	4.82
CNRM.DE6	-14.72	9.20	-21.62	-40.12	-9.66	4.05	2.95	3.70	5.24	3.98
SMHI.HCA2	-7.02	14.02	-12.79	-45.28	7.12	4.30	3.13	3.23	6.27	4.25
SMHI.MPIA2	-21.78	-2.75	-35.10	-35.29	-16.69	6.27	4.18	6.21	8.79	5.54
Average	-10.34	11.41	-19.75	-34.86	-0.91	4.83	3.51	4.19	6.54	4.75

TABLE 4.6: Anomalies of the mean **annual** and **seasonal** precipitation and temperature on the Ebro River basin, for the CTRL period 1961 - 1990 and for 6 RCMs during 2071 - 2100. Values computed averaging the **IDW** interpolated values in squared cells of 1km^2

	Anomaly of Mean Precipitation, [%]					Anomaly of Mean Temperature, [°C]				
RCM	Annual	DJF	MAM	JJA	SON	Annual	DJF	MAM	JJA	SON
DMI.HS1	-3.56	22.40	-14.83	-31.18	4.98	4.17	3.26	3.24	5.50	4.37
DMI.ecscA2	-4.98	17.50	-19.60	-14.75	-2.24	5.48	4.01	5.11	7.09	5.42
HC.adhfa	-7.62	13.00	-14.36	-39.54	15.52	4.56	3.37	3.53	6.21	4.78
CNRM.DE6	-14.54	10.06	-21.89	-40.27	-8.78	4.03	2.96	3.64	5.22	3.97
SMHI.HCA2	-6.56	14.53	-12.48	-45.10	8.52	4.28	3.13	3.22	6.24	4.21
SMHI.MPIA2	-20.92	-1.03	-33.39	-34.81	-16.42	6.24	4.14	6.19	8.71	5.52
Average	-9.69	12.74	-19.42	-34.28	0.26	4.80	3.48	4.16	6.50	4.71

TABLE 4.7: Anomalies of mean **annual** and **seasonal** precipitation and temperature on the Ebro River basin, for the CTRL period 1961 - 1990 and for 6 RCMs during 2071 - 2100. Values computed averaging the **OK** interpolated values in squared cells of 1km^2

	Anomaly of Mean Precipitation, [%]					Anomaly of Mean Temperature, [°C]				
RCM	Annual	DJF	MAM	JJA	SON	Annual	DJF	MAM	JJA	SON
DMI.HS1	-3.54	22.63	-14.77	-30.56	4.70	4.19	3.28	3.27	5.53	4.37
DMI.ecscA2	-4.87	18.00	-19.41	-14.22	-2.59	5.48	4.01	5.12	7.09	5.41
HC.adhfa	-7.36	13.34	-14.08	-39.18	15.65	4.56	3.39	3.55	6.22	4.77
CNRM.DE6	-14.54	10.28	-21.93	-40.01	-8.89	4.04	2.97	3.66	5.26	3.97
SMHI.HCA2	-6.63	14.77	-12.47	-45.06	8.25	4.29	3.14	3.24	6.26	4.20
SMHI.MPIA2	-20.88	-0.80	-33.43	-34.30	-16.34	6.23	4.14	6.19	8.70	5.50
Average	-9.64	13.04	-19.35	-33.89	0.13	4.80	3.49	4.17	6.51	4.70

All the RCMs predict an **increase in the mean annual temperature** and a **decrease in the mean annual precipitation** with respect to the control period (see Tables 4.5, 4.6, 4.7, and Figure 4.5). In particular, the decrease of mean annual precipitation ranges from ∼-4 to ∼-22%, with an average decrease of ∼-10% (when computed over the gauging stations); whereas the increase in mean annual temperature ranges from ∼+4 to ∼+6°C, with an average increase +4.8°C. Among all the RCMs, the RCAO_E (SMHI.MPIA2) projects the largest decrease in mean annual precipitation

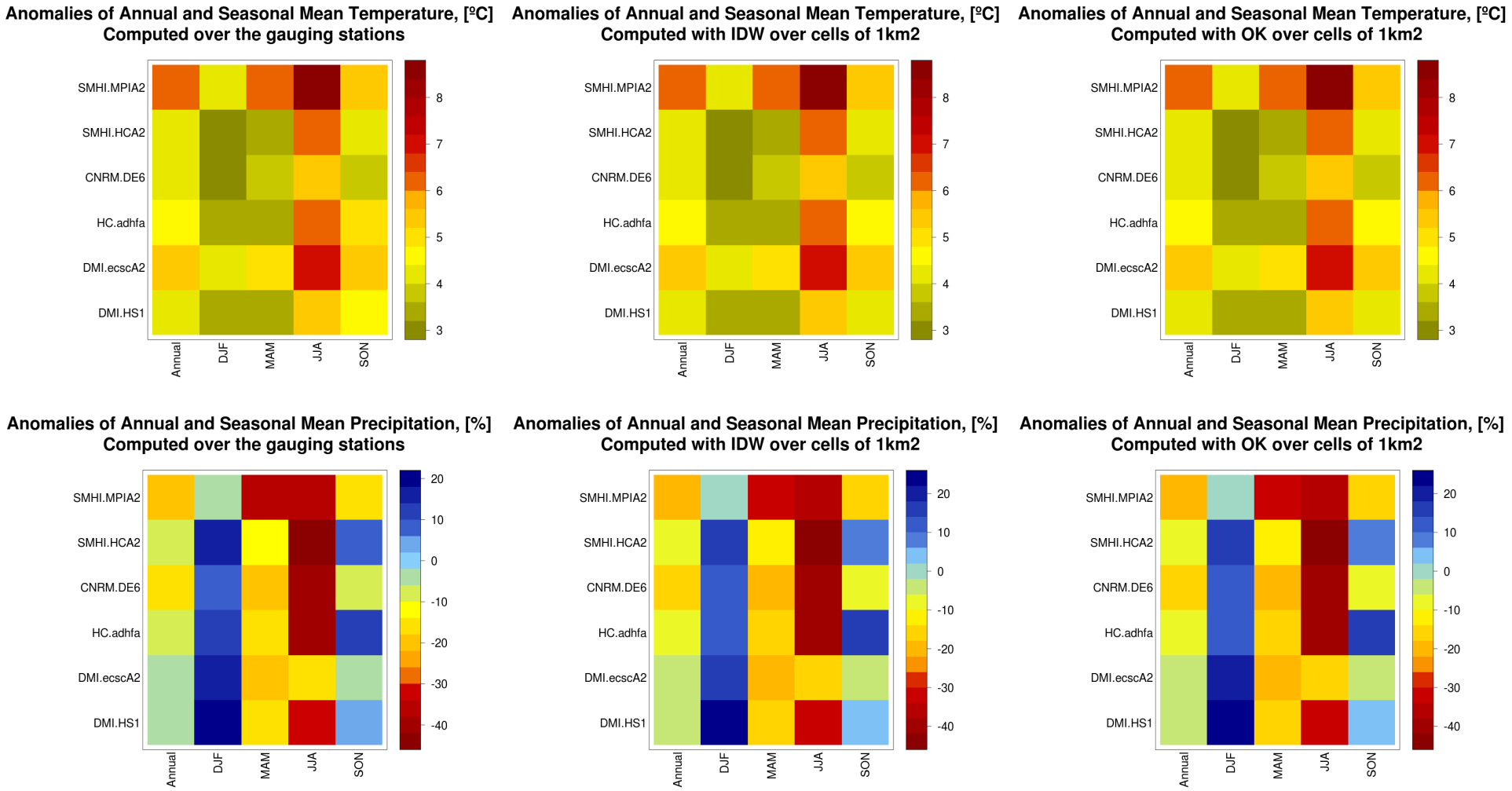

FIGURE 4.5: Anomalies of the mean **annual** and **seasonal** bias-corrected precipitation and temperature on the Ebro River basin, for 6 RCMs during 2071 - 2100 with respect to the CTRL period 1961 - 1990. Plots on the left show the values computed averaging over the corresponding gauging stations; plot on the centre, show the values obtained with IDW interpolation, and plot on the right show values obtained using OK interpolation; the latter two, computed over the same squared cells of $1km^2$

(∼-22%) and the largest increase in mean annual temperature (∼+6.3°C); whereas the HIRAM_H (DMI.HS1) projects the smallest decrease in mean annual precipitation (∼-4%) and ARPEGE_H projects the smallest increase in mean annual temperature (∼+4.1°C).

Figure 4.6 shows maps with the spatial distribution of **anomalies** of the bias-corrected **mean annual** precipitation and temperature for the 6 RCMs described in Table 4.1, computed using ordinary kriging interpolation with cells of 1km^2.

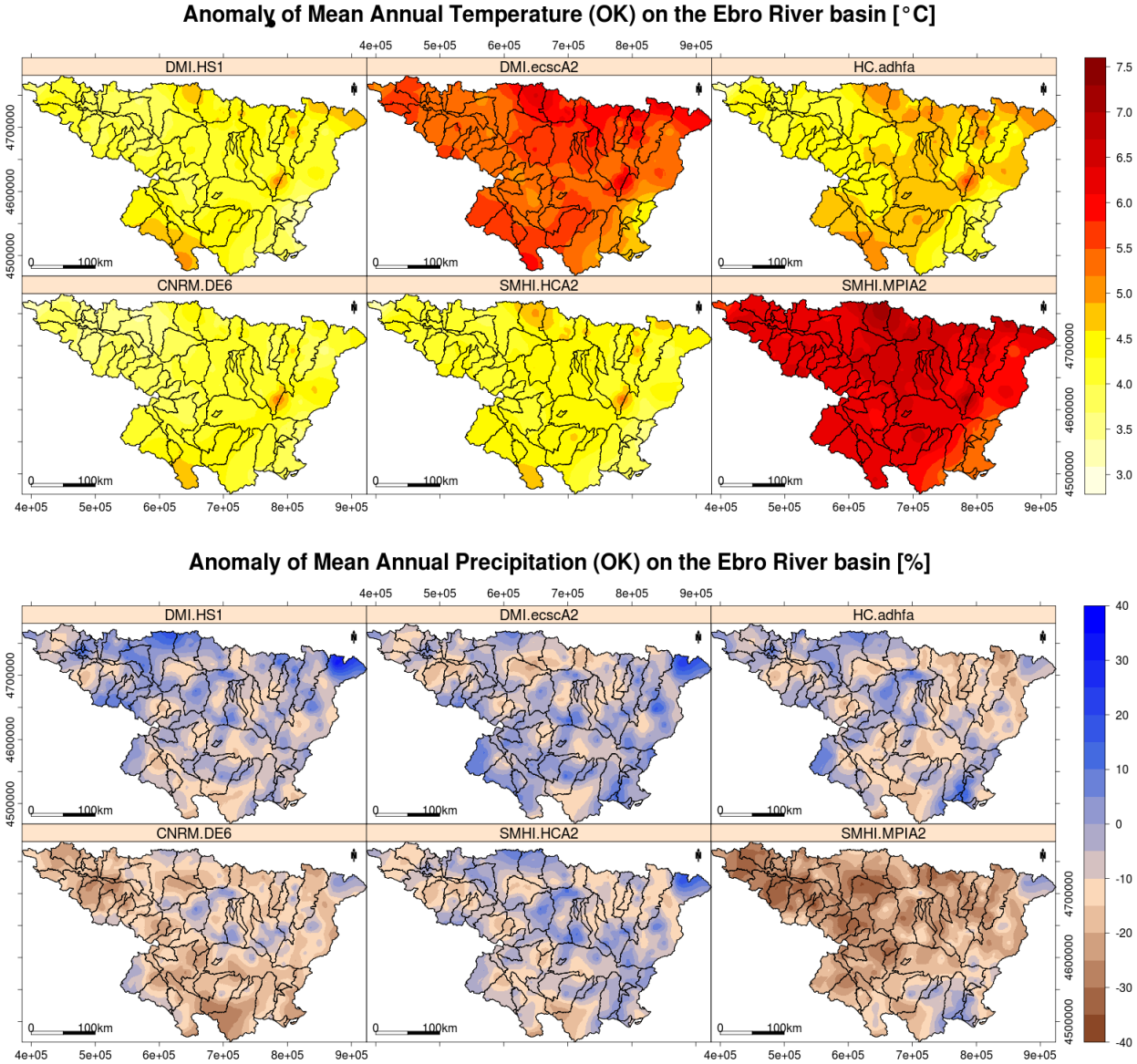

FIGURE 4.6: Spatial distribution of the anomalies of bias-corrected **mean annual** temperature and precipitation with respect to the control period 1961-1990, computed using ordinary kriging with cells of 1 km^2 and 10 nearest neighbours.

Figure 4.6 show that the RCAO_E (SMHI.MPIA2) and HIRAM_E (DMI.ecscA2) will undergo the highest increments in **mean annual temperature**, with the largest differences for the northern and south-western parts of the catchment (where the highest elevations are located), pattern shared with the other 4 RCMs. At the other hand, projected changes in **mean annual precipitation** present significant differences among the RCMs, with RCAO_E (SMHI.MPIA2) being the driest RCM (see Tables 4.5, 4.6 and 4.7), projecting larger decreases in the northern and western part of the catchment, whereas the HIRAM_H (DMI.HS1), HIRAM_E (DMI.ecscA2) and HAD_H (HC.adhfa) are the least dry, but they do not share a clear spatial pattern for the projected changes.

Looking at the seasonal distribution of the meteorological patterns, Tables 4.5, 4.6, 4.7, and Figure 4.5 show that all the RCMs project an **increase in the mean seasonal temperature** and a **decrease in the mean seasonal precipitation**, being winter (DJF) the only exception, because all the RCMs project an increase in the seasonal precipitation. In particular, for precipitation all the RCMs predicts a **decrease during the spring** (ranging from -13% to -35%, with and average value of -20%) and summer seasons (from -16% to -45%, with an average value of -35%). Regarding the temperature field, all the RCMs predicts an **increase of all the seasonal temperatures**, with the **largest increase during summer** (ranging from 5.2°C to 8.8°C, and average value of 6.5°C) and the **lowest increase during winter** (ranging from 3.0°C to 4.2°C, with an average value of 3.5°C), which seems to confirm previous results (e.g. *Bürger et al.*, 2007).

Figures 4.7, 4.8, 4.9, and 4.10 show maps with the spatial distribution of the anomalies of bias-corrected **mean seasonal** precipitation and temperature for the 6 RCMs described in Table 4.1, computed using ordinary kriging interpolation with cells of 1km^2.

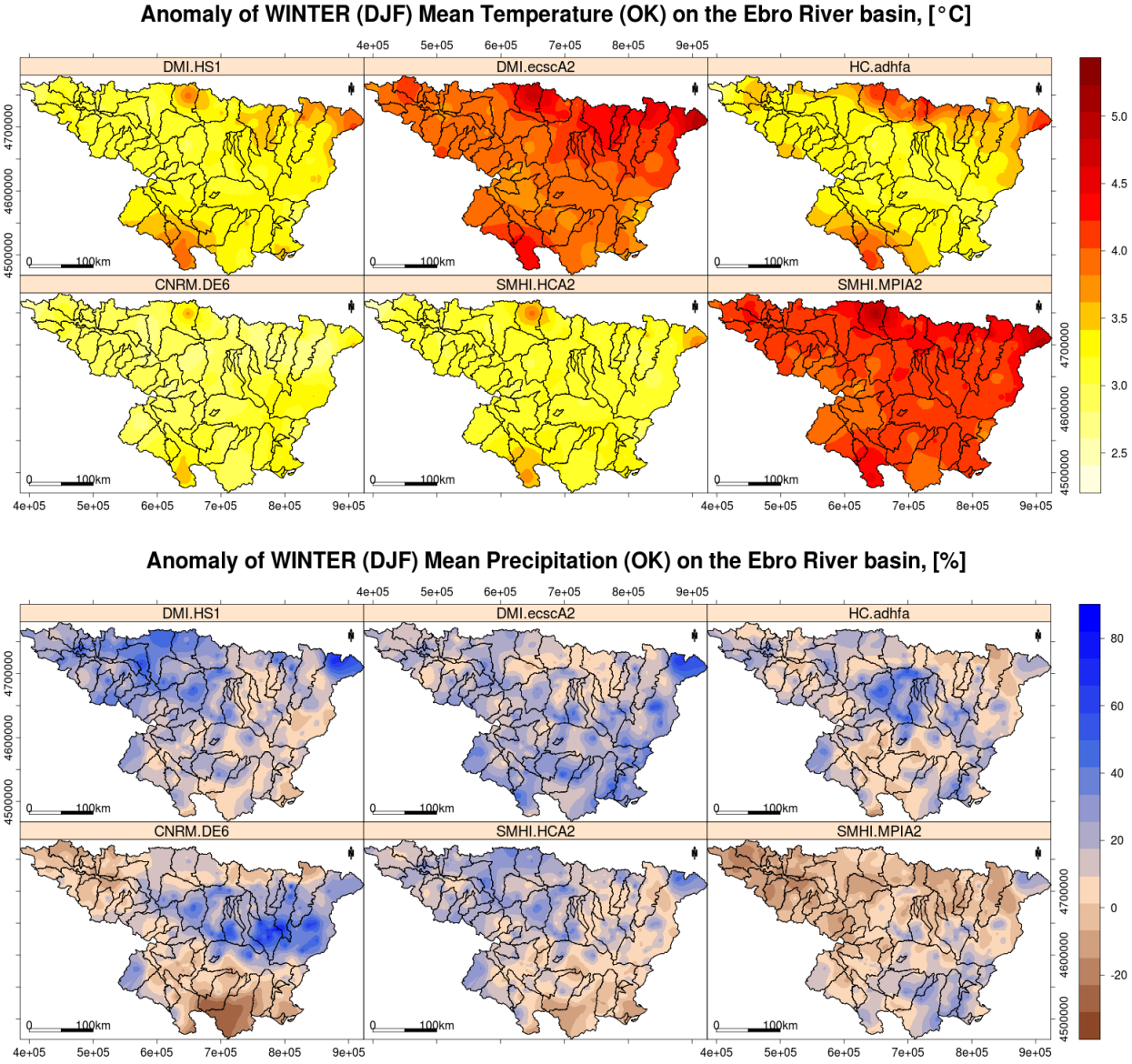

FIGURE 4.7: Spatial distribution of the anomalies of mean winter (DJF) temperature and precipitation with respect to the control period 1961-1990, computed using ordinary kriging with cells of 1 km^2.

Figure 4.7 shows that during the **winter** season (DJF) there is an average increment of the mean

seasonal temperature of +∼3.5°C and an average increment of the mean seasonal precipitation of +∼11%. The RCAO_E (SMHI.MPIA2) and HIRAM_E (DMI.ecscA2) are the warmest RCMs, but sharing similar spatial distribution of the annomalies of mean seasonal temperature with the other RCMs, with larger increases for the northern and southern regions of the catchment. At the other hand, projected changes in mean seasonal precipitation present significant differences among the RCMs, with RCAO_E (SMHI.MPIA2) being the driest (the only one with a global decrease in this season, see Tables 4.5, 4.6 and 4.7), projecting larger decreases in the northern and north-western part of the catchment, whereas HIRAM_H (DMI.HS1) is the wettest, projecting the largest increments for the same northern area. At the same time, ARPEGE_H (CNRM.DE6) projects larger decreases in mean winter precipitation for the southern part of the basin.

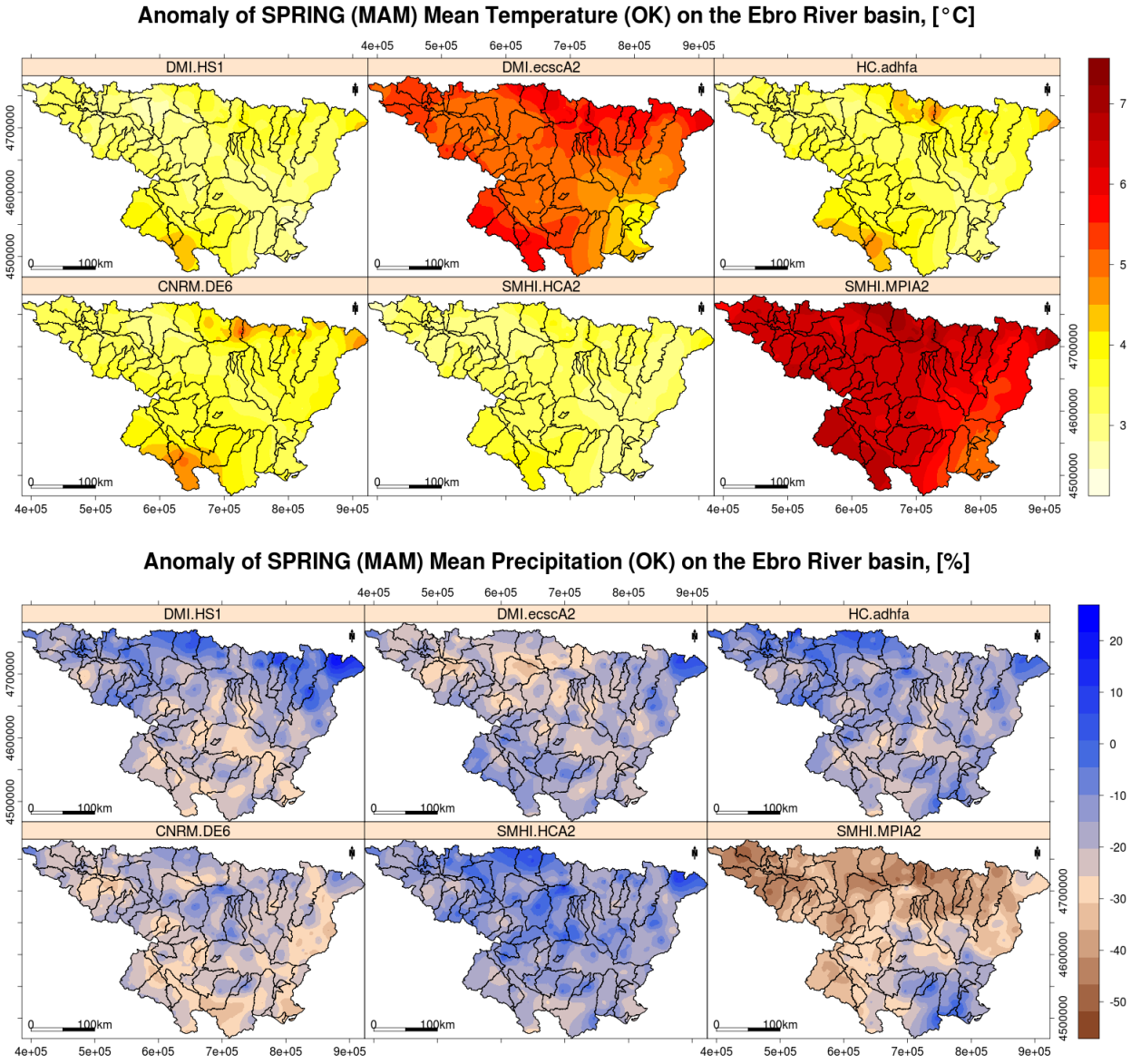

FIGURE 4.8: Spatial distribution of the anomalies of mean spring (MAM) temperature and precipitation with respect to the control period 1961-1990, computed using ordinary kriging with cells of 1 km^2.

Figure 4.8 shows that during the **spring** season (MAM) there is an average increment of the mean seasonal temperature of +∼4.2°C and an average decrease of the mean seasonal precipitation of ∼-20%. The RCAO_E (SMHI.MPIA2) and HIRAM_E (DMI.ecscA2) are, again, the warmest RCMs, but with all the RCMs projecting similar spatial distribution of the anomalies of mean sea-

sonal temperature, with larger increases for the northern and southern regions of the catchment. At the other hand, projected changes in mean seasonal precipitation present differences among the RCMS, but these differences are less evident than during the winter season. The RCAO_E (SMHI.MPIA2) is again the driest RCM (see tables 4.5, 4.6 and 4.7), projecting larger decreases in the northern and north-western part of the catchment, whereas the RCAO_H (SMHI.HCA2), HIRAM_H (DMI.HS1) and HAD_H (HC.adhfa) are the least dry RCMs, sharing similar spatial patterns, in which the largest decrease is projected for the central and southern valleys.

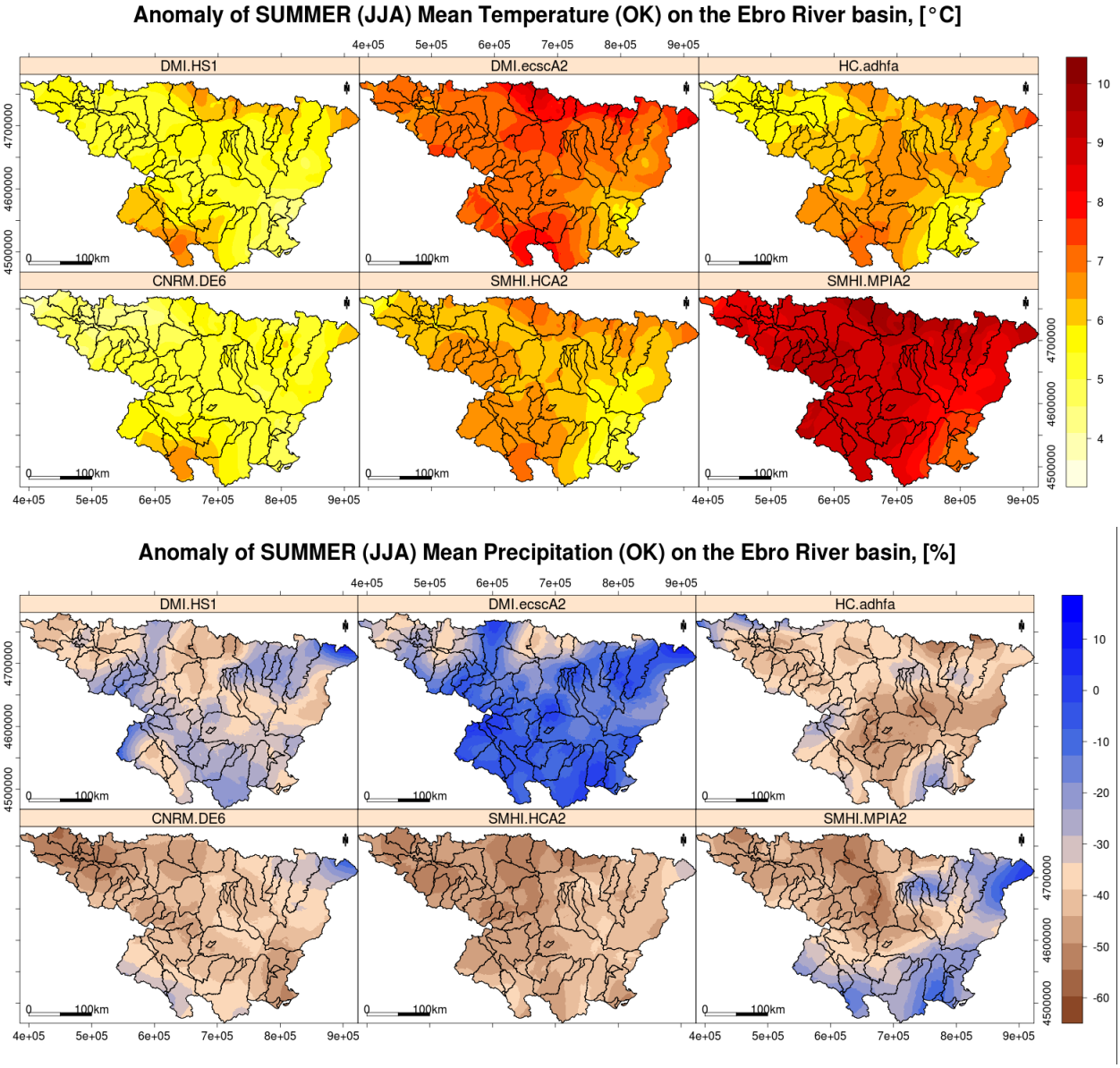

FIGURE 4.9: Spatial distribution of the anomalies of mean summer (JJA) temperature and precipitation with respect to the control period 1961-1990, computed using ordinary kriging with cells of 1 km^2.

Figure 4.9 shows that the **summer** season (JJA) is expected to undergo the most severe changes in mean seasonal precipitation and air temperature (see Figure 4.14), with an average increment of the mean seasonal temperature of +∼6.5°C and an average decrease of the mean seasonal precipitation of ∼-35%. The RCAO_E (SMHI.MPIA2) and HIRAM_E (DMI.ecscA2) are, again, the warmest RCMs, but this time RCAO_H (SMHI.HCA2) and HAD_H (HC.adhfa) are closer to the 2 previously mentioned RCMs than during winter and spring. Again, all the RCMs project larger increases in the mean seasonal temperature for the northern and southern regions of the catchment.

At the other hand, projected changes in mean seasonal precipitation present differences among the RCMs much larger than during winter and spring. This time the driest RCMs are RCAO_H (SMHI.HCA2) and ARPEGE_H (CNRM.DE6) (see Tables 4.5, 4.6 and 4.7), projecting an almost uniform decrease all over the basin; whereas the HIRAM_E (DMI.ecscA2) projects the smallest decreases for the catchment ($\sim -14\%$), and RCAO_E (SMHI.MPIA2) and HIRAM_H (DMI.HS1) presenting similar spatial patterns, with the largest decrease for the north-western part of the basin.

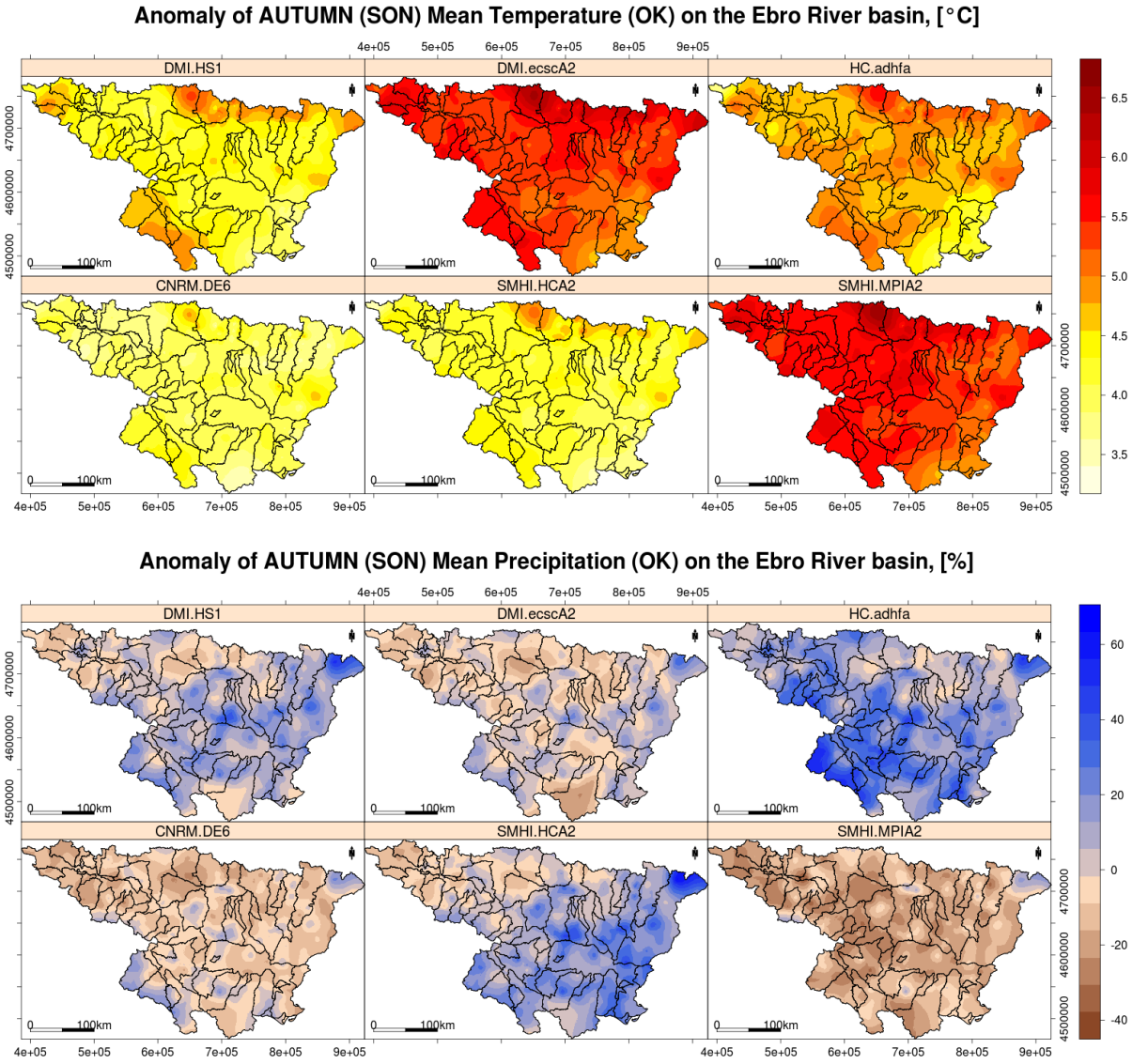

FIGURE 4.10: Spatial distribution of the anomalies of mean autumn (SON) temperature and precipitation with respect to the control period 1961-1990, computed using ordinary kriging with cells of 1 km^2.

Figure 4.10 shows that during the **autumn** season (SON) there is an expected average increment of the mean seasonal temperature of +$\sim$4.8°C and a highly uncertain decrease of the mean seasonal precipitation of -$\sim$1%. The RCAO_E (SMHI.MPIA2) and HIRAM_E (DMI.ecscA2) are, again, the warmest RCMs, but this time HAD_H (HC.adhfa) is the only RCM close to the previous 2 RCMs. Again, all the RCMs project larger increases in the mean seasonal temperature for the northern and southern regions of the catchment. At the other hand, projected changes in mean seasonal precipitation present the largest differences among the RCMs of all the seasons (see Tables 4.5, 4.6 and 4.7). ARPEGE_H (CNRM.DE6), RCAO_E (SMHI.MPIA2) and HIRAM_E (DMI.ecscA2) project a general decrease during this season (without a clear spatial pattern); whereas RCAO_H

(SMHI.HCA2), HIRAM_H (DMI.HS1) and HAD_H (HC.adhfa) project a general increase in the seasonal precipitation, with different spatial patterns, but sharing the larger projected increases for the southern part of the basin.

4.3.2.2 Monthly Anomalies

The anomalies of bias-corrected mean **monthly** precipitation over the entire Ebro River basin during the future period 2071 - 2100 are presented in Tables 4.8, 4.9 and 4.10 for the six RCMs described in Table 4.1. Projected values of monthly mean precipitation and temperature can be found in the Appendix B.

TABLE 4.8: Anomalies of mean monthly precipitation, [%], on the Ebro River basin, for 6 RCMs during 2071 - 2100 with respect to the CTRL period 1961 - 1990. Values computed averaging over the 349 **gauging stations** of precipitation.

	Anomalies of Monthly Mean Precipitation, [%]											
RCM	Jan	Feb	Mar	Apr	May	Jun	Jul	Aug	Sep	Oct	Nov	Dec
DMI.HS1	31.97	9.82	-0.25	-4.48	-32.06	-28.29	-40.67	-29.13	12.31	-1.61	2.86	24.28
DMI.ecscA2	17.58	-0.94	4.78	-30.30	-27.15	-21.38	-25.43	-2.52	3.77	-23.59	9.56	28.14
HC.adhfa	11.68	15.26	26.23	-27.48	-30.29	-37.84	-45.32	-39.99	-13.27	12.23	31.94	9.54
CNRM.DE6	20.71	17.23	-11.01	-11.32	-38.14	-42.23	-43.86	-34.27	-10.18	-5.75	-12.61	-9.66
SMHI.HCA2	18.25	8.97	3.60	4.22	-39.33	-33.00	-49.65	-58.82	30.80	-9.05	3.92	17.19
SMHI.MPIA2	11.62	-20.00	-23.99	-38.75	-39.09	-42.73	-44.44	-17.78	-9.78	-25.09	-14.50	3.74
Average	18.64	5.06	-0.11	-18.02	-34.34	-34.24	-41.56	-30.42	2.28	-8.81	3.53	12.21

TABLE 4.9: Anomalies of mean **monthly** precipitation, [%], on the Ebro River basin, for 6 RCMs during 2071 - 2100 with respect to the CTRL period 1961 - 1990. Values computed averaging the **IDW** interpolated values in squared cells of 1km^2.

	Anomalies of IDW Monthly Mean Precipitation, [%]											
RCM	Jan	Feb	Mar	Apr	May	Jun	Jul	Aug	Sep	Oct	Nov	Dec
DMI.HS1	33.05	10.08	-0.66	-5.52	-32.76	-28.36	-40.34	-27.95	14.38	-1.06	3.32	26.34
DMI.ecscA2	19.81	0.02	6.04	-30.30	-26.57	-21.32	-22.90	1.12	6.41	-23.58	9.80	31.54
HC.adhfa	11.03	15.91	28.62	-28.03	-29.96	-36.21	-44.71	-40.20	-9.75	15.85	33.63	13.44
CNRM.DE6	20.37	20.14	-11.40	-11.98	-37.97	-41.87	-44.20	-34.86	-10.64	-4.02	-11.50	-9.59
SMHI.HCA2	17.66	8.87	3.99	4.23	-38.78	-32.28	-49.74	-59.81	31.86	-9.49	7.03	19.36
SMHI.MPIA2	14.23	-18.27	-21.75	-38.26	-36.55	-41.15	-44.32	-18.15	-8.30	-23.94	-15.87	4.62
Average	19.36	6.12	0.81	-18.31	-33.77	-33.53	-41.04	-29.97	3.99	-7.71	4.40	14.28

TABLE 4.10: Anomalies of mean **monthly** precipitation, [%], on the Ebro River basin, for 6 RCMs during 2071 - 2100 with respect to the CTRL period 1961 - 1990. Values computed averaging the **OK** interpolated values in squared cells of 1km^2.

	Anomalies of OK Monthly Mean Precipitation, [%]											
RCM	Jan	Feb	Mar	Apr	May	Jun	Jul	Aug	Sep	Oct	Nov	Dec
DMI.HS1	33.36	10.34	-0.68	-5.62	-32.50	-27.77	-39.57	-27.55	14.02	-1.34	3.23	26.59
DMI.ecscA2	20.19	0.52	6.27	-30.36	-26.12	-20.90	-21.49	1.37	6.07	-23.71	9.71	32.34
HC.adhfa	11.23	16.03	28.80	-27.82	-29.45	-35.50	-44.28	-40.36	-10.04	15.98	33.82	14.18
CNRM.DE6	20.63	20.30	-11.44	-12.17	-38.01	-41.52	-43.88	-34.68	-10.84	-3.93	-11.54	-9.34
SMHI.HCA2	17.73	9.30	3.93	4.02	-38.42	-32.27	-49.47	-59.84	31.50	-9.70	7.09	19.67
SMHI.MPIA2	14.27	-18.10	-21.76	-38.40	-36.62	-40.82	-43.71	-17.32	-8.30	-23.67	-15.83	5.04
Average	19.57	6.40	0.85	-18.39	-33.52	-33.13	-40.40	-29.73	3.73	-7.73	4.41	14.74

The anomalies of bias-corrected **monthly** mean temperature over the entire Ebro River basin during the future period 2071-2100 are presented in tables 4.11, 4.12 and 4.13 for the 6 RCMs described in Table 4.1.

TABLE 4.11: Anomalies of **monthly** mean temperature, [°C], on the Ebro River basin, for 6 RCMs during 2071 - 2100 with respect to the CTRL period 1961 - 1990. Values computed averaging over the 146 **gauging stations** of temperature.

	Anomalies of Monthly Mean Temperature, [°C]											
RCM	Jan	Feb	Mar	Apr	May	Jun	Jul	Aug	Sep	Oct	Nov	Dec
DMI.HS1	3.3	3.1	2.4	3.0	4.3	5.1	5.3	6.2	5.3	4.4	3.5	3.5
DMI.ecscA2	3.9	4.5	4.0	5.3	6.2	5.9	7.8	7.8	6.6	5.3	4.5	3.8
HC.adhfa	3.4	3.4	2.7	3.6	4.4	5.7	6.4	6.7	6.4	4.1	3.9	3.6
CNRM.DE6	3.5	2.8	3.2	3.4	4.5	5.1	5.5	5.1	4.4	3.8	3.7	2.7
SMHI.HCA2	3.1	3.0	2.4	3.0	4.3	5.3	6.4	7.1	5.3	4.1	3.3	3.4
SMHI.MPIA2	4.2	4.4	5.2	6.4	7.1	7.7	9.2	9.4	7.1	5.2	4.3	4.2
Average	3.6	3.5	3.3	4.1	5.2	5.8	6.7	7.1	5.8	4.5	3.9	3.5

TABLE 4.12: Anomalies of **monthly** mean temperature, [°C], on the Ebro River basin, for the CTRL period 1961-1990 and for 6 RCMs during 2071-2100. Values computed averaging the **IDW** interpolated values in squared cells of 1km^2

	Anomalies of IDW Monthly Mean Temperature, [°C]											
RCM	Jan	Feb	Mar	Apr	May	Jun	Jul	Aug	Sep	Oct	Nov	Dec
DMI.HS1	3.2	3.1	2.4	3.0	4.3	5.1	5.2	6.1	5.3	4.3	3.4	3.5
DMI.ecscA2	3.9	4.4	4.0	5.2	6.1	5.9	7.7	7.7	6.5	5.2	4.4	3.8
HC.adhfa	3.3	3.4	2.6	3.5	4.4	5.7	6.3	6.6	6.4	4.1	3.8	3.5
CNRM.DE6	3.5	2.8	3.2	3.3	4.5	5.0	5.4	5.1	4.4	3.8	3.7	2.7
SMHI.HCA2	3.1	3.0	2.4	3.0	4.4	5.3	6.4	7.0	5.2	4.0	3.3	3.4
SMHI.MPIA2	4.2	4.3	5.1	6.4	7.1	7.7	9.1	9.3	7.1	5.1	4.3	4.1
Average	3.5	3.5	3.3	4.1	5.1	5.8	6.7	7.0	5.8	4.4	3.8	3.5

TABLE 4.13: Anomalies of **monthly** mean temperature, [°C], on the Ebro River basin, for the CTRL period 1961-1990 and for 6 RCMs during 2071-2100. Values computed averaging the **OK** interpolated values in squared cells of 1km^2

	Anomalies of OK Monthly Mean Temperature, [°C]											
RCM	Jan	Feb	Mar	Apr	May	Jun	Jul	Aug	Sep	Oct	Nov	Dec
DMI.HS1	3.2	3.2	2.5	3.0	4.3	5.1	5.2	6.2	5.3	4.4	3.4	3.5
DMI.ecscA2	3.9	4.4	4.0	5.3	6.2	5.9	7.6	7.7	6.5	5.2	4.4	3.8
HC.adhfa	3.3	3.4	2.6	3.6	4.5	5.7	6.3	6.6	6.4	4.1	3.8	3.5
CNRM.DE6	3.5	2.8	3.2	3.3	4.5	5.1	5.5	5.1	4.4	3.8	3.7	2.7
SMHI.HCA2	3.1	3.0	2.4	2.9	4.4	5.3	6.4	7.0	5.2	4.0	3.3	3.4
SMHI.MPIA2	4.2	4.4	5.1	6.4	7.1	7.7	9.1	9.3	7.1	5.1	4.3	4.1
Average	3.5	3.5	3.3	4.1	5.2	5.8	6.7	7.0	5.8	4.4	3.8	3.5

Figure 4.11, show a visual summary of the anomalies of the bias-corrected **monthly** mean precipitation and air temperature presented in Tables 4.8, 4.9 and 4.10. This figure shows that almost all the RCMs project an increase in the **monthly mean precipitation** during December and January, with the *largest average increase during January* (from +12% to +32%, with an average value of +19%) and a decrease from April to August, with the *largest decrease in July* (from -25% to -50%, with an average value of -42%) and almost no change during March (average value of +1%). For

the **monthly mean temperature**, all the RCMs projects an *increase in the monthly mean temperature all along the year*, with the largest increase for August (ranging from +5.1°C to +9.4°C, with an average value of +7.1°C) and the *lowest increase for March* (ranging from +2.4°C to +5.2°C, and average value of +3.3°C).

4.3.3 Changes with Elevation

Due to the high spatial heterogeneity showed by the spatial distribution of the projected changes in annual/seasonal/monthly mean precipitation and air temperature discussed in the previous section 4.3.2, here we analyse how those changes are distributed along four different elevation bands, representing the first, second and third quartiles of elevation provided by a DEM of 1 km^2 resolution, in a way of providing practical guidelines about the spatial location in which those changes are likely to happen.

4.3.3.1 Control Period

TABLE 4.14: Elevation bands used for analysing the projected changes in temperature and precipitation on the Ebro River basin. Elevation values of 421, 694, 1019 and 3312 [m.a.s.l.] represent the minimum, first quartile, median, third quartile and maximum values of the elevations provided by a DEM of 1km^2 resolution.

Elevation Range, [m.a.s.l.]	ID	Precipitation Stations	Temperature Stations
0-421	Low	103	57
422-694	Med.Low	117	38
695-1019	Med.High	81	36
1020-3312	High	48	15

TABLE 4.15: Mean annual and seasonal precipitation and air temperature on the Ebro River basin, during the CTRL period 1961 - 1990. Values on are computed averaging over the corresponding gauging stations.

Elev. Band	Mean Precipitation, [mm]					Mean Temperature, [°C]				
	Annual	DJF	MAM	JJA	SON	Annual	DJF	MAM	JJA	SON
Low	388.0	78.6	113.3	76.2	119.5	14.0	6.1	12.8	22.8	14.8
Med.Low	571.6	142.8	164.4	107.3	155.7	12.4	5.1	10.9	20.4	13.3
Med.High	743.3	182.5	205.0	150.3	204.0	10.7	3.6	8.9	18.6	11.7
High	947.3	225.9	253.4	204.1	262.3	8.4	2.0	6.4	15.9	9.4

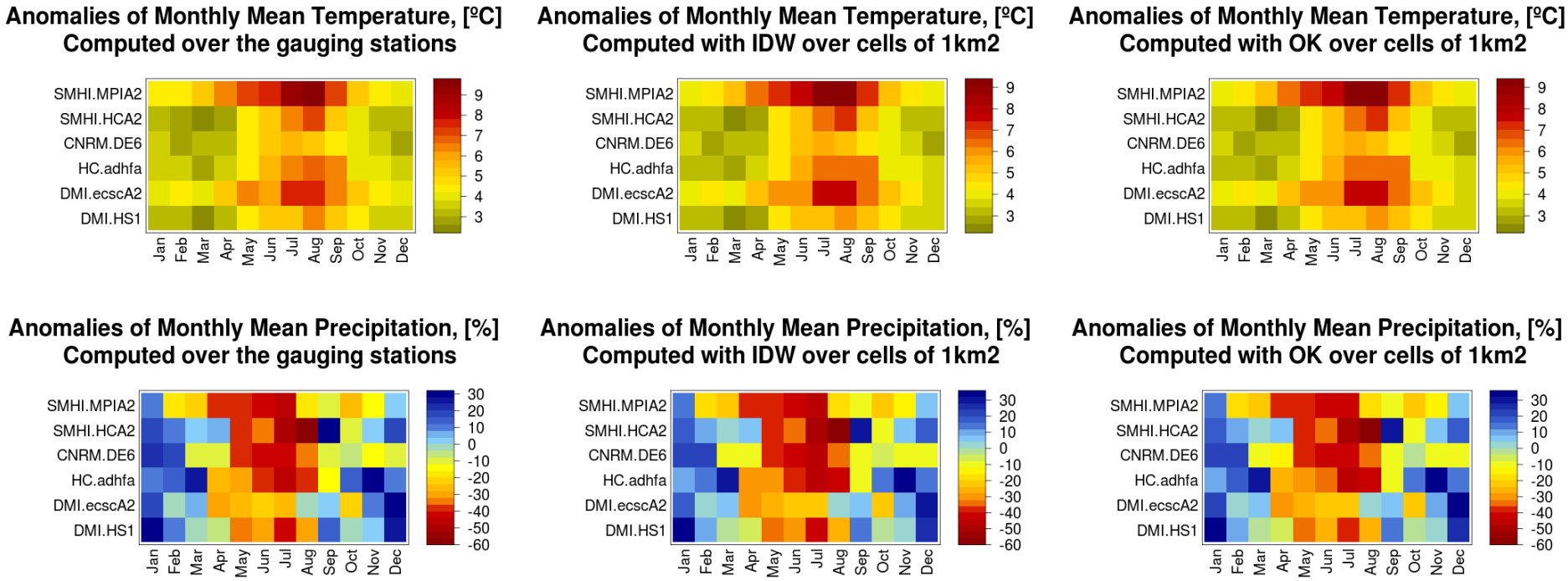

FIGURE 4.11: Anomalies of the bias-corrected **monthly** mean temperature and precipitation on the Ebro River basin, for 6 RCMs during 2071-2100 with respect to the CTRL period 1961-1990. Plots on the left show the values computed averaging over the corresponding gauging stations; plot on the centre, show the values obtained with IDW interpolation, and plot on the right show values obtained using OK interpolation; the latter two, computed over the same squared cells of 1km^2

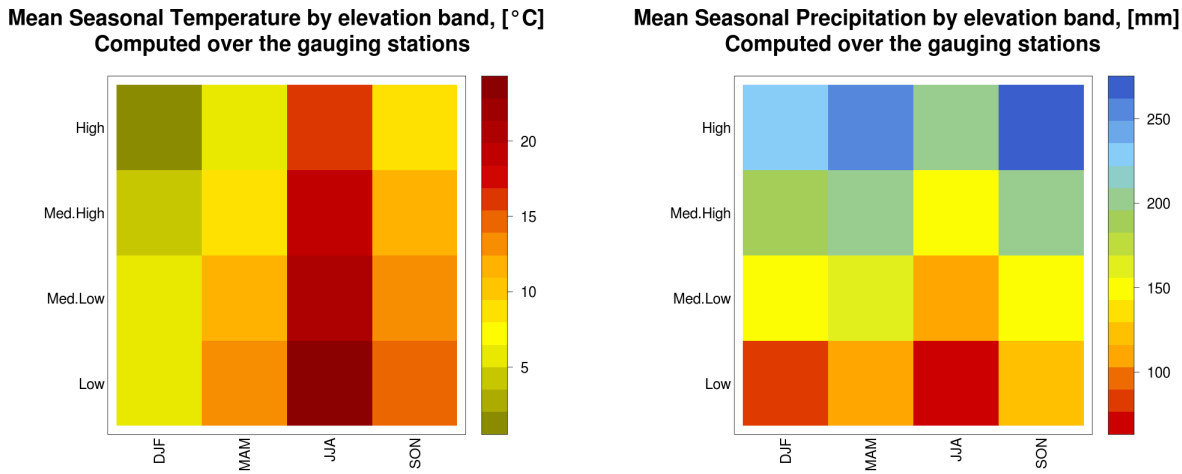

FIGURE 4.12: Mean **seasonal** temperature and precipitation for different elevation bands on the Ebro River basin, during the CTRL period 1961-1990. Values computed averaging over the 146 and 349 gauging stations of temperature and precipitation, respectively.

Table 4.15 and Figure 4.12 confirm the well known fact that **annual and mean seasonal precipitation increase with increasing elevation values**, whereas **annual and seasonal values of air temperature decreases with higher elevations**.

4.3.3.2 Anomalies

The anomalies of bias-corrected **mean annual** precipitation and air temperature over each one of the four elevation bands described in Table 4.14 for the entire Ebro River basin during the future period 2071 - 2100 are presented in Table 4.16 for the 6 RCMs described in Table 4.1. Projected values of annual/seasonal/monthly bias-corrected mean air temperature and precipitation for each band can be found in Appendix B.2, for the 6 RCMs described in Table 4.1.

TABLE 4.16: Anomalies of bias-corrected mean annual precipitation and air temperature for different elevation bands on the Ebro River basin, for the 6 RCMs during 2071 - 2100. Values computed averaging over the 349 and 146 gauging stations of precipitation and temperature, respectively.

	Anomalies of Mean Precipitation, [%]				Anomalies of Mean Temperature, [°C]			
Scenario	Low	Med.Low	Med.High	High	Low	Med.Low	Med.High	High
DMI.HS1	-4.27	-3.29	-3.89	-3.83	4.08	4.07	4.37	4.60
DMI.ecscA2	-1.54	-6.40	-6.62	-8.49	5.35	5.47	5.73	6.05
HC.adhfa	-6.14	-6.96	-8.97	-13.56	4.52	4.44	4.71	5.02
CNRM.DE6	-11.75	-16.14	-14.28	-15.82	4.09	3.82	4.12	4.32
SMHI.HCA2	-3.17	-7.00	-7.82	-9.40	4.23	4.18	4.39	4.62
SMHI.MPIA2	-15.95	-22.55	-22.63	-24.64	6.13	6.21	6.39	6.67
Average	-7.13	-10.39	-10.70	-12.62	4.73	4.70	4.95	5.21

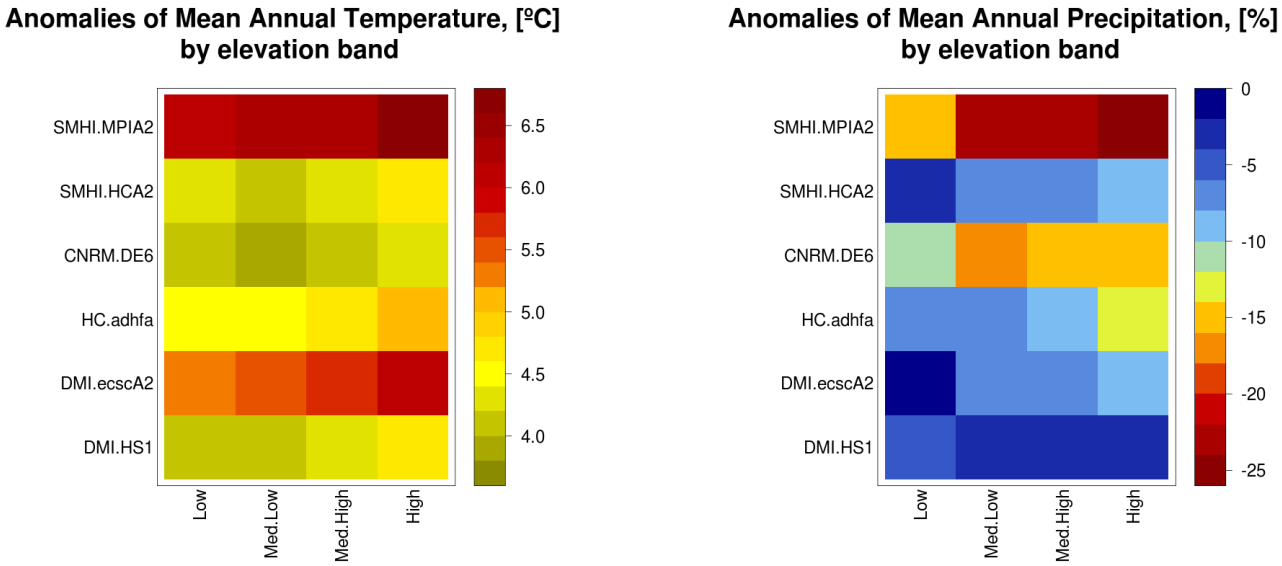

FIGURE 4.13: Anomalies of bias-corrected **mean annual** precipitation and temperature for different elevation bands on the Ebro River basin, for the RCMs during 2071-2100. Values computed averaging over the 349 and 146 gauging stations of precipitation and temperature, respectively.

Table 4.16 and Figure 4.13 show that the mean **annual temperature** expect larger increments for higher elevations, whereas mean **annual precipitation** expect larger decreases with higher elevation values.

Tables 4.17, 4.18, 4.19, 4.20 present the anomalies of bias-corrected **mean seasonal** precipitation and air temperature over each one of the four elevation bands described in Table 4.14 for the entire Ebro River basin during the future period 2071 - 2100 and for the 6 RCMs described in Table 4.1. Projected seasonal bias-corrected mean air temperature and precipitation for each band can be found on tables B.11, B.12, B.13, B.14 (Appendix B.2), for the 6 RCMs described in Table 4.1.

TABLE 4.17: Anomalies of bias-corrected mean **winter** (DJF) precipitation and air temperature for different elevation bands on the Ebro River basin, for the 6 RCMs during 2071 - 2100. Values computed averaging over the 349 and 146 gauging stations of precipitation and temperature, respectively.

	Anomalies of Mean Precipitation, [%]				Anomalies of Mean Temperature, [°C]			
Scenario	Low	Med.Low	Med.High	High	Low	Med.Low	Med.High	High
DMI.HS1	16.16	24.90	20.18	20.85	3.20	3.19	3.38	3.53
DMI.ecscA2	24.15	16.23	12.69	10.65	3.93	4.01	4.19	4.40
HC.adhfa	17.95	12.08	12.37	4.58	3.23	3.38	3.60	3.92
CNRM.DE6	22.43	5.97	9.18	4.33	3.03	2.81	2.95	3.03
SMHI.HCA2	11.16	15.49	13.78	14.24	3.09	3.05	3.19	3.30
SMHI.MPIA2	9.74	-4.70	-5.24	-5.68	4.09	4.13	4.26	4.45
Average	16.93	11.66	10.49	8.16	3.43	3.43	3.60	3.77

TABLE 4.18: Anomalies of bias-corrected mean **spring** (MAM) precipitation and air temperature for different elevation bands on the Ebro River basin, for the 6 RCMs during 2071 - 2100. Values computed averaging over the 349 and 146 gauging stations of precipitation and temperature, respectively.

	Anomalies of Mean Precipitation, [%]				Anomalies of Mean Temperature, [°C]			
Scenario	Low	Med.Low	Med.High	High	Low	Med.Low	Med.High	High
DMI.HS1	-19.44	-14.59	-12.86	-9.75	3.06	3.17	3.55	3.57
DMI.ecscA2	-19.47	-20.93	-19.62	-20.04	4.82	5.18	5.54	5.68
HC.adhfa	-16.09	-13.16	-14.68	-16.36	3.32	3.47	3.90	4.09
CNRM.DE6	-22.05	-22.55	-20.38	-21.42	3.54	3.44	4.01	4.25
SMHI.HCA2	-12.93	-12.18	-12.76	-13.66	3.10	3.13	3.45	3.46
SMHI.MPIA2	-23.93	-35.50	-38.21	-40.94	5.92	6.24	6.50	6.56
Average	-18.98	-19.82	-19.75	-20.36	3.96	4.10	4.49	4.60

TABLE 4.19: Bias-corrected anomalies of mean **summer** (JJA) precipitation and air temperature for different elevation bands on the Ebro River basin, for the 6 RCMs during 2071 - 2100. Values computed averaging over the 349 and 146 gauging stations of precipitation and temperature, respectively.

	Anomalies of Mean Precipitation, [%]				Anomalies of Mean Temperature, [°C]			
Scenario	Low	Med.Low	Med.High	High	Low	Med.Low	Med.High	High
DMI.HS1	-31.14	-33.38	-30.28	-31.48	5.26	5.45	5.91	6.10
DMI.ecscA2	-9.80	-19.43	-15.25	-19.40	6.83	7.12	7.52	7.83
HC.adhfa	-42.41	-38.38	-38.24	-43.97	6.22	6.03	6.36	6.51
CNRM.DE6	-40.46	-44.08	-39.02	-36.15	5.20	5.02	5.43	5.44
SMHI.HCA2	-42.52	-46.25	-44.60	-47.09	6.03	6.23	6.50	6.72
SMHI.MPIA2	-33.23	-37.40	-33.15	-36.87	8.46	8.78	9.06	9.43
Average	-33.26	-36.49	-33.42	-35.83	6.33	6.44	6.80	7.01

TABLE 4.20: Bias-corrected anomalies of mean **autumn** (SON) precipitation and air temperature for different elevation bands on the Ebro River basin, for the 6 RCMs during 2071 - 2100. Values computed averaging over the 349 and 146 gauging stations of precipitation and temperature, respectively.

	Anomalies of Mean Precipitation, [%]				Anomalies of Mean Temperature, [°C]			
Scenario	Low	Med.Low	Med.High	High	Low	Med.Low	Med.High	High
DMI.HS1	12.22	2.58	1.88	0.86	4.25	4.34	4.56	4.87
DMI.ecscA2	3.18	-3.30	-5.11	-6.01	5.29	5.45	5.60	5.94
HC.adhfa	20.50	14.81	9.55	6.67	4.72	4.76	4.89	5.21
CNRM.DE6	-6.17	-9.93	-10.53	-11.54	4.01	3.86	3.99	4.18
SMHI.HCA2	20.61	4.11	3.88	2.52	4.15	4.19	4.31	4.64
SMHI.MPIA2	-15.63	-16.73	-16.76	-17.58	5.44	5.51	5.60	5.84
Average	5.78	-1.41	-2.85	-4.18	4.64	4.69	4.82	5.11

Figure 4.14, shows a visual summary of the anomalies of the bias-corrected mean **seasonal** precipitation and air temperature presented in Tables 4.17, 4.18, 4.19, 4.20 for the 6 RCMs described in Table 4.1, during the future period 2071-2100.

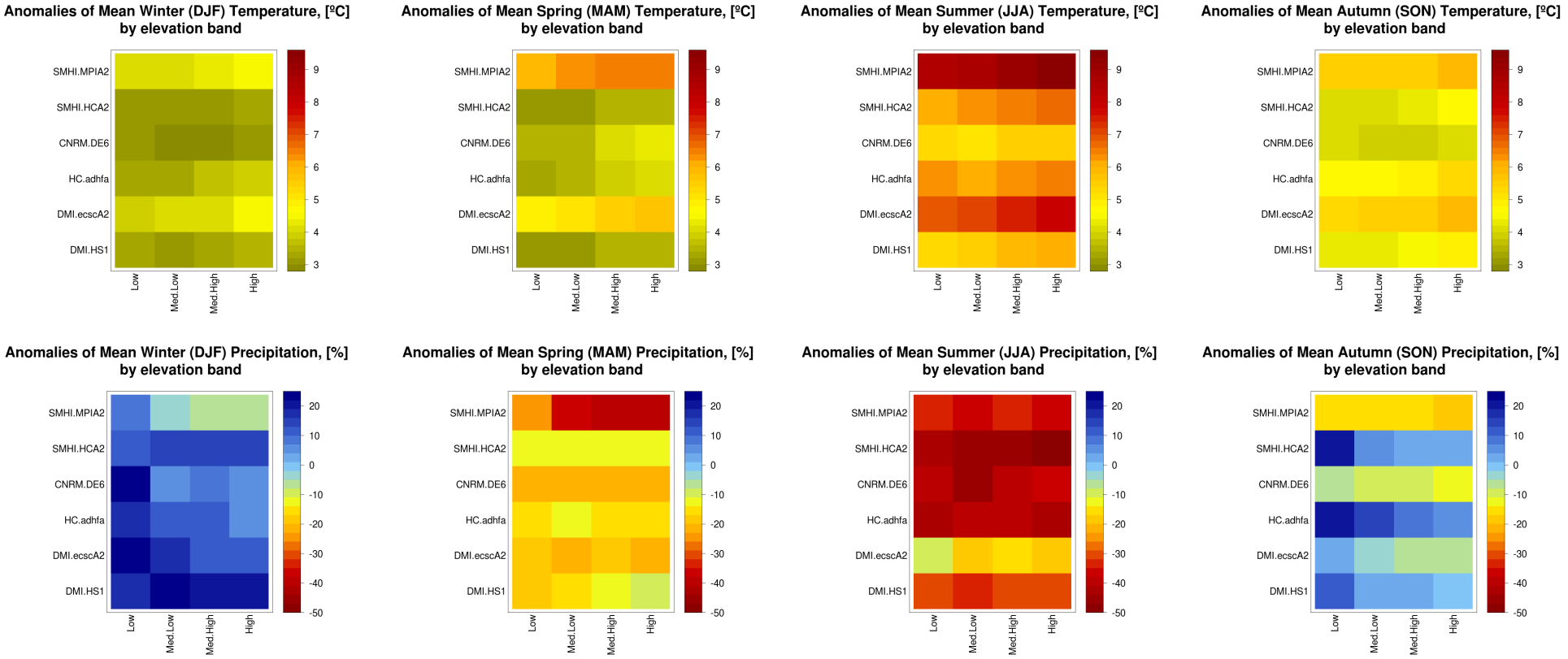

FIGURE 4.14: Anomalies of bias-corrected mean **seasonal** precipitation and temperature for different elevation bands on the Ebro River basin, for the 6 RCMs during 2071-2100. Values computed averaging over the 349 and 146 gauging stations of precipitation and temperature, respectively.

During **winter** (DJF), there is almost no difference in the mean seasonal temperature between Low and Med.Low elevations, but there is *an increase thereof from Med.Low to High elevations*; whereas for mean seasonal precipitation, almost all the RCMs project *larger increments with lower elevations*, with the exception of RCAO_E, (SMHI.MPIA2) which projects a uniform decrease from Med.Low to High elevations.

For **spring** (MAM), the *mean seasonal temperature increases with increasing elevation values*; whereas almost *all the RCMs do not present significant differences in projected changes in precipitation among different elevation ranges*, with the exception of RCAO_E (SMHI.MPIA2) and HIRAM_H (DMI.HS1) which project larger and smaller changes with increasing elevation values, respectively.

The **summer** season presents *larger increments in mean seasonal temperature with increasing elevations*, with the exception of the HAD_H (HC.adhfa) and ARPEGE_H (CNRM.DE6), which project larger increases in Low elevations than in Med.Low ones; whereas the *mean seasonal precipitation does not present a clear dependence on elevation values*, but with the *highest drops for Med.Low and High elevations* (see Table 4.19).

Finally, during **autumn** (SON) all the RCMs project *larger increments in mean seasonal temperatures with increasing elevations*. At the other hand, this is the season with *the most contradictory projections for mean seasonal precipitation*, because RCAO_H (SMHI.HCA2), HIRAM_H (DMI.HS1) and HAD_H (HC.adhfa) project an increase in this seasonal value; whereas RCAO_E (SMHI.MPIA2), HIRAM_E (DMI.ecscA) and ARPEGE_H (CNRM.DE6) project a decrease thereof, with larger drops for higher elevations. When looking an explanation on the monthly projected anomalies (see Tables 4.29, 4.30, 4.31), it can be seen that during September the monthly precipitation is expected to increase for Low and Med.Low elevations and to decrease for Med.High and High elevations; during October the monthly precipitation is expected to decrease, with larger decreases for higher elevations; and during November, this monthly value is expected to increase, with the larger increases for lower elevations.

The anomalies of bias-corrected **mean monthly** precipitation and air temperature over each one of the four elevation bands described in Table 4.14 for the entire Ebro River basin during the future period 2071 - 2100 are presented in tables 4.21 to 4.32, for the 6 RCMs described in Table 4.1. Monthly projections for each elevation band can be found in in tables B.15, to B.26 (Appendix B.2).

TABLE 4.21: Bias-corrected anomalies of mean **January** (JAN) precipitation and temperature for different elevation bands on the Ebro River basin, for the 6 RCMs during 2071-2100. Values computed averaging over the 349 and 146 gauging stations of precipitation and temperature, respectively.

	Mean Precipitation, [%]				Mean Temperature, [°C]			
Scenario	Low	Med.Low	Med.High	High	Low	Med.Low	Med.High	High
DMI.HS1	23.16	36.62	32.13	31.04	3.22	3.17	3.38	3.44
DMI.ecscA2	33.14	16.87	14.80	10.97	3.82	3.91	4.09	4.16
HC.adhfa	2.45	13.70	14.77	11.19	3.19	3.38	3.60	3.88
CNRM.DE6	51.79	9.18	24.27	10.91	3.54	3.32	3.47	3.39
SMHI.HCA2	11.39	17.77	19.88	21.87	3.07	3.02	3.16	3.16
SMHI.MPIA2	31.94	9.50	8.13	4.64	4.12	4.19	4.32	4.39
Average	25.65	17.27	19.00	15.10	3.50	3.50	3.67	3.74

TABLE 4.22: Bias-corrected anomalies of mean **February** (FEB) precipitation and temperature for different elevation bands on the Ebro River basin, for the 6 RCMs during 2071-2100. Values computed averaging over the 349 and 146 gauging stations of precipitation and temperature, respectively.

	Mean Precipitation, [%]				Mean Temperature, [°C]			
Scenario	Low	Med.Low	Med.High	High	Low	Med.Low	Med.High	High
DMI.HS1	-2.22	14.96	9.32	11.44	3.04	3.03	3.31	3.43
DMI.ecscA2	-0.32	-1.04	-1.91	0.09	4.24	4.43	4.69	4.94
HC.adhfa	6.04	20.77	18.23	9.37	3.22	3.32	3.61	3.79
CNRM.DE6	35.59	17.61	11.77	10.59	2.85	2.63	2.92	3.03
SMHI.HCA2	-0.36	12.55	8.74	10.66	2.98	2.88	3.08	3.11
SMHI.MPIA2	-3.29	-23.75	-23.37	-21.87	4.21	4.36	4.57	4.77
Average	5.91	6.85	3.80	3.38	3.42	3.44	3.70	3.84

TABLE 4.23: Bias-corrected anomalies of mean **march** (MAR) precipitation and temperature for different elevation bands on the Ebro River basin, for the 6 RCMs during 2071-2100. Values computed averaging over the 349 and 146 gauging stations of precipitation and temperature, respectively.

	Mean Precipitation, [%]				Mean Temperature, [°C]			
Scenario	Low	Med.Low	Med.High	High	Low	Med.Low	Med.High	High
DMI.HS1	-7.78	1.76	-0.30	3.43	2.36	2.33	2.62	2.66
DMI.ecscA2	11.64	5.60	1.91	1.06	3.73	4.04	4.26	4.45
HC.adhfa	33.97	30.69	23.03	16.02	2.42	2.66	2.96	3.24
CNRM.DE6	-11.00	-12.54	-9.76	-10.18	3.02	3.01	3.48	3.75
SMHI.HCA2	3.59	6.36	1.84	1.42	2.35	2.21	2.50	2.51
SMHI.MPIA2	-16.98	-22.30	-27.09	-28.96	4.90	5.25	5.40	5.58
Average	2.24	1.60	-1.73	-2.87	3.13	3.25	3.54	3.70

TABLE 4.24: Bias-corrected anomalies of mean **April** (APR) precipitation and temperature for different elevation bands on the Ebro River basin, for the 6 RCMs during 2071-2100. Values computed averaging over the 349 and 146 gauging stations of precipitation and temperature, respectively.

	Mean Precipitation, [%]				Mean Temperature, [°C]			
Scenario	Low	Med.Low	Med.High	High	Low	Med.Low	Med.High	High
DMI.HS1	-8.39	-5.31	-3.42	-0.86	2.77	2.99	3.30	3.34
DMI.ecscA2	-33.78	-31.18	-28.63	-27.86	4.94	5.35	5.69	5.82
HC.adhfa	-31.03	-26.14	-28.70	-24.57	3.28	3.54	3.98	4.20
CNRM.DE6	-9.49	-13.75	-10.02	-10.87	3.18	3.13	3.64	4.00
SMHI.HCA2	7.24	2.23	3.96	4.96	2.78	2.97	3.20	3.27
SMHI.MPIA2	-32.24	-39.76	-40.35	-41.05	6.10	6.43	6.65	6.68
Average	-17.95	-18.99	-17.86	-16.71	3.84	4.07	4.41	4.55

TABLE 4.25: Bias-corrected anomalies of mean **may** (MAY) precipitation and temperature for different elevation bands on the Ebro River basin, for the 6 RCMs during 2071-2100. Values computed averaging over the 349 and 146 gauging stations of precipitation and temperature, respectively.

	Mean Precipitation, [%]				Mean Temperature, [°C]			
Scenario	Low	Med.Low	Med.High	High	Low	Med.Low	Med.High	High
DMI.HS1	-35.71	-35.61	-30.29	-25.64	4.03	4.28	4.70	4.69
DMI.ecscA2	-25.60	-29.97	-25.84	-26.27	5.77	6.26	6.63	6.73
HC.adhfa	-32.82	-32.05	-27.23	-29.22	4.25	4.31	4.73	4.79
CNRM.DE6	-39.26	-38.50	-37.34	-37.58	4.42	4.28	4.86	4.99
SMHI.HCA2	-39.83	-39.89	-38.40	-39.23	4.15	4.29	4.61	4.57
SMHI.MPIA2	-20.94	-40.84	-43.79	-48.24	6.76	7.14	7.41	7.40
Average	-32.36	-36.14	-33.81	-34.36	4.90	5.09	5.49	5.53

TABLE 4.26: Bias-corrected anomalies of mean **June** (JUN) precipitation and temperature for different elevation bands on the Ebro River basin, for the 6 RCMs during 2071-2100. Values computed averaging over the 349 and 146 gauging stations of precipitation and temperature, respectively.

	Mean Precipitation, [%]				Mean Temperature, [°C]			
Scenario	Low	Med.Low	Med.High	High	Low	Med.Low	Med.High	High
DMI.HS1	-31.61	-29.83	-26.22	-25.82	4.82	5.05	5.48	5.54
DMI.ecscA2	-19.88	-25.77	-19.95	-18.50	5.66	5.87	6.25	6.37
HC.adhfa	-37.55	-36.93	-37.03	-40.47	5.62	5.48	5.81	5.85
CNRM.DE6	-44.12	-44.83	-41.32	-38.06	5.16	4.74	5.22	5.09
SMHI.HCA2	-26.54	-34.04	-33.68	-36.59	5.07	5.27	5.49	5.51
SMHI.MPIA2	-39.70	-41.47	-42.29	-47.84	7.46	7.68	7.99	8.14
Average	-33.23	-35.48	-33.41	-34.54	5.63	5.68	6.04	6.08

TABLE 4.27: Bias-corrected anomalies of mean **July** (JUL) precipitation and temperature for different elevation bands on the Ebro River basin, for the 6 RCMs during 2071-2100. Values computed averaging over the 349 and 146 gauging stations of precipitation and temperature, respectively.

	Mean Precipitation, [%]				Mean Temperature, [°C]			
Scenario	Low	Med.Low	Med.High	High	Low	Med.Low	Med.High	High
DMI.HS1	-40.73	-42.41	-39.65	-39.86	5.02	5.13	5.61	5.72
DMI.ecscA2	-23.69	-27.36	-23.12	-27.00	7.41	7.71	8.14	8.46
HC.adhfa	-47.08	-44.17	-43.05	-48.17	6.39	6.15	6.48	6.56
CNRM.DE6	-41.14	-49.51	-43.31	-39.82	5.41	5.28	5.73	5.72
SMHI.HCA2	-50.67	-51.14	-48.32	-48.89	6.15	6.33	6.62	6.77
SMHI.MPIA2	-46.77	-46.31	-41.42	-44.42	8.78	9.19	9.53	9.96
Average	-41.68	-43.48	-39.81	-41.36	6.53	6.63	7.02	7.20

TABLE 4.28: Bias-corrected anomalies of mean **August** (AUG) precipitation and temperature for different elevation bands on the Ebro River basin, for the 6 RCMs during 2071-2100. Values computed averaging over the 349 and 146 gauging stations of precipitation and temperature, respectively.

	Mean Precipitation, [%]				Mean Temperature, [°C]			
Scenario	Low	Med.Low	Med.High	High	Low	Med.Low	Med.High	High
DMI.HS1	-24.15	-31.46	-28.13	-31.45	5.89	6.12	6.62	7.05
DMI.ecscA2	13.97	-4.37	-2.16	-13.97	7.38	7.71	8.15	8.66
HC.adhfa	-46.41	-35.98	-35.91	-44.81	6.62	6.40	6.78	7.10
CNRM.DE6	-34.70	-38.87	-32.26	-30.52	4.99	4.99	5.31	5.52
SMHI.HCA2	-60.36	-59.74	-56.71	-58.96	6.81	7.02	7.39	7.89
SMHI.MPIA2	-14.95	-24.80	-13.54	-16.30	9.10	9.40	9.64	10.19
Average	-27.76	-32.54	-28.12	-32.67	6.80	6.94	7.32	7.73

TABLE 4.29: Bias-corrected anomalies of mean **September** (SEP) precipitation and temperature for different elevation bands on the Ebro River basin, for the 6 RCMs during 2071-2100. Values computed averaging over the 349 and 146 gauging stations of precipitation and temperature, respectively.

	Mean Precipitation, [%]				Mean Temperature, [°C]			
Scenario	Low	Med.Low	Med.High	High	Low	Med.Low	Med.High	High
DMI.HS1	27.78	11.27	7.88	2.28	4.98	5.27	5.65	5.96
DMI.ecscA2	27.21	0.09	-3.10	-8.33	6.26	6.60	6.86	7.24
HC.adhfa	-7.07	-9.94	-15.74	-21.46	6.29	6.38	6.54	6.85
CNRM.DE6	-9.19	-11.74	-9.93	-9.49	4.32	4.26	4.49	4.57
SMHI.HCA2	41.67	29.49	27.72	24.53	5.07	5.23	5.45	5.80
SMHI.MPIA2	0.88	-11.94	-11.42	-16.52	6.89	7.07	7.22	7.42
Average	13.55	1.20	-0.77	-4.83	5.64	5.80	6.03	6.31

TABLE 4.30: Bias-corrected anomalies of mean **October** (OCT) precipitation and temperature for different elevation bands on the Ebro River basin, for the 6 RCMs during 2071-2100. Values computed averaging over the 349 and 146 gauging stations of precipitation and temperature, respectively.

	Mean Precipitation, [%]				Mean Temperature, [°C]			
Scenario	Low	Med.Low	Med.High	High	Low	Med.Low	Med.High	High
DMI.HS1	-2.65	-1.31	-2.06	-0.33	4.25	4.28	4.57	4.72
DMI.ecscA2	-19.13	-25.27	-25.96	-22.66	5.05	5.30	5.51	5.69
HC.adhfa	26.64	13.71	3.52	6.49	3.96	4.08	4.27	4.39
CNRM.DE6	-1.94	-5.90	-7.12	-7.72	3.81	3.70	3.89	3.97
SMHI.HCA2	-6.35	-11.56	-9.73	-7.30	4.01	3.96	4.17	4.32
SMHI.MPIA2	-22.03	-23.37	-27.82	-27.22	5.01	5.14	5.30	5.42
Average	-4.24	-8.95	-11.53	-9.79	4.35	4.41	4.62	4.75

TABLE 4.31: Bias-corrected anomalies of mean **November** (NOV) precipitation and temperature for different elevation bands on the Ebro River basin, for the 6 RCMs during 2071-2100. Values computed averaging over the 349 and 146 gauging stations of precipitation and temperature, respectively.

	Mean Precipitation, [%]				Mean Temperature, [°C]			
Scenario	Low	Med.Low	Med.High	High	Low	Med.Low	Med.High	High
DMI.HS1	13.00	0.18	1.04	0.82	3.39	3.39	3.59	3.72
DMI.ecscA2	3.73	12.26	10.50	9.16	4.42	4.39	4.55	4.66
HC.adhfa	39.89	31.48	31.55	26.53	3.79	3.75	3.97	4.16
CNRM.DE6	-7.72	-12.02	-13.72	-16.08	3.77	3.54	3.70	3.79
SMHI.HCA2	28.71	0.56	-1.17	-4.93	3.25	3.31	3.45	3.60
SMHI.MPIA2	-24.46	-14.43	-11.37	-10.50	4.29	4.24	4.39	4.47
Average	8.86	3.01	2.81	0.83	3.82	3.77	3.94	4.07

TABLE 4.32: Bias-corrected anomalies of mean **December** (DEC) precipitation and temperature for different elevation bands on the Ebro River basin, for the 6 RCMs during 2071-2100. Values computed averaging over the 349 and 146 gauging stations of precipitation and temperature, respectively.

	Mean Precipitation, [%]				Mean Temperature, [°C]			
Scenario	Low	Med.Low	Med.High	High	Low	Med.Low	Med.High	High
DMI.HS1	31.07	24.28	21.57	22.82	3.47	3.42	3.57	3.73
DMI.ecscA2	38.22	30.91	24.79	20.83	3.82	3.74	3.88	4.11
HC.adhfa	42.17	3.80	7.00	-2.85	3.44	3.55	3.76	4.17
CNRM.DE6	-15.07	-8.83	-8.44	-8.51	2.84	2.59	2.64	2.76
SMHI.HCA2	24.79	17.55	15.30	13.48	3.33	3.31	3.44	3.65
SMHI.MPIA2	5.71	2.78	3.70	3.76	4.21	4.07	4.17	4.38
Average	21.15	11.75	10.65	8.26	3.52	3.45	3.58	3.80

4.4 Summary and Conclusions

Bias-corrected daily time series of precipitation and air temperature were derived from an ensemble of six climate change scenarios, selected from the EU FP5 PRUDENCE project. Long-term averages of precipitation and air temperature fields were computed for the control period 1961 - 1990, and projected anomalies for the future period 2071 - 2100 were computed as well, in an annual, seasonal and monthly basis, including expected changes for different elevation bands within the basin. The main findings of this chapter can be summarized as follow:

- All the RCMs predict an **increase in the mean annual temperature** (Average[3] value of 4.8°C) and a **decrease in the mean annual precipitation** (average value of -∼10%) with respect to the control period (e.g. Table 4.5 and Figure 4.5), and those changes are **stronger at increasing elevation** values (see Table 4.16 and Figure 4.13).

- Among all the RCMs, the RCAO_E (SMHI.MPIA2) is the most severe in terms of annual values, because it projects the largest decrease in mean annual precipitation (average value of -∼22%) and the largest increase in **mean annual temperature** (average value of ∼+6.3°C); whereas ARPEGE_H (CNRM.DE6) projects the smallest increase in mean annual temperature (∼+4.0°C) and HIRAM_H (DMI.HS1), is the least dry (∼-4%). In this way, climate sce-

[3]average computed with the values of the 6 RCMs presented in Table 4.1

narios derived from the two different GCMs used in this dissertation provided the extreme expected changes in annual precipitation and temperature by the end of this century.

- About the spatial distribution of the annual changes, all the RCMs present a similar pattern for the mean annual temperature, projecting the largest increments for higher elevation values (northern and south-western parts of the basin). At the other hand, projected changes in **mean annual precipitation** present significant differences in their spatial distribution among the RCMs, but the RCAO_E (SMHI.MPIA2) is the single RCM projecting a general decrease almost all over the basin, with larger decreases for higher elevations.

- Regarding seasonal projections, all the RCMs predicts an **increase of all the seasonal temperatures**, with the **largest increase during summer** (average value of $\sim$+6.5°C) and the **lowest increase during winter** (average value of $\sim$+3.5°C), which seems to confirm previous results (e.g. *Bürger et al.*, 2007). Regarding projected changes in seasonal precipitation, all the RCMs predicts a **decrease of the mean precipitation during spring** (average value of $\sim$-20%) and **summer** (average value of $\sim$-35%) seasons; almost all the models predict an increase during winter (average value of $\sim$+10%) and contradictory projections are projected for the autumn season.

- During the **winter** (DJF), there is an expected average increment of the mean seasonal temperature of +$\sim$3.5°C and an average increment of the mean seasonal precipitation of +$\sim$11%. The RCAO_E (SMHI.MPIA2) and HIRAM_E (DMI.ecscA2) are the warmest RCMs, sharing similar spatial distribution of the anomalies of bias-corrected **mean seasonal temperature** (see Figure 4.7), with almost no difference between low and medium-low elevations, but with an increase from medium-low to high elevations (larger increments are projected for the northern and southern regions of the basin). At the other hand, projected changes in **mean seasonal precipitation** present significant differences among the RCMs, with almost all the RCMs projecting *larger increments with lower elevations* (see Table 4.17), with the exception of RCAO_E, (SMHI.MPIA2), which projects a uniform decrease from Med.Low to High elevations ($\sim$-5%) .

- For the **spring** season (MAM) there is an average increment of the mean seasonal temperature of +$\sim$4.2°C and an average decrease of the mean seasonal precipitation of $\sim$-20%. The RCAO_E (SMHI.MPIA2) and HIRAM_E (DMI.ecscA2) are, again, the warmest RCMs, projecting larger increments for increasing elevation values (northern and southern regions of the catchment). At the other hand, the RCAO_E (SMHI.MPIA2) is again the driest RCM (e.g. Table 4.5 and Figure 4.8), projecting larger decreases with increasing elevations (see Table 4.18), whereas the other RCMs present significant differences in the spatial distribution of projected changes of **mean seasonal precipitation**, but these differences are less evident than during the winter season, and with the elevation value exerting only a small influence on this change.

- The **summer** season is expected to undergo the most severe changes in the mean seasonal precipitation and air temperature (see Figure 4.14), with an average increment of the mean seasonal temperature of +$\sim$6.5°C and an average decrease of the mean seasonal precipitation of $\sim$-35%, with almost all the RCMs projecting larger increments in **mean seasonal temperature** for increasing elevation values; whereas differences in RCMs indicate that the **mean seasonal precipitation** does not present a clear dependence on the elevation values (see Table 4.19). The RCAO_E (SMHI.MPIA2) and HIRAM_E (DMI.ecscA2) are, again, the warmest RCMs (see Table 4.5 and Figure 4.9), but this time RCAO_H (SMHI.HCA2) and HAD_H (HC.adhfa) are closer to the 2 previously mentioned RCMs than during winter and spring. The driest RCMs are RCAO_H (SMHI.HCA2) and ARPEGE_H (CNRM.DE6) (see Figure 4.9 and Table 4.5), projecting an almost uniform decrease all over the basin ($\sim$-45% and $\sim$-40%, respectively); whereas the HIRAM_E (DMI.ecscA2) projects the smallest decreases in mean seasonal precipitation for the catchment ($\sim$-14%), without a clear dependence on elevation.

- Finally, during **autumn** (SON) there is an expected average increment of the mean seasonal temperature of +∼4.8°C and a highly uncertain decrease of the mean seasonal precipitation of -∼1%. All the RCMs project larger increments in **mean seasonal temperature** with increasing elevations (northern and southern regions of the basin). At the other hand, there are contradictory projections for **mean seasonal precipitation**, because RCAO_H (SMHI.HCA2), HIRAM_H (DMI.HS1) and HAD_H (HC.adhfa) project an increase in this seasonal value, but with smaller increments with increasing elevations; whereas RCAO_E (SMHI.MPIA2), HIRAM_E (DMI.ecscA) and ARPEGE_H (CNRM.DE6) project a decrease thereof, with larger drops for higher elevations. When looking a possible explanation on the corresponding monthly anomalies (see Tables 4.29, 4.30, 4.31), it can be seen that during September the average monthly precipitation is expected to increase for Low and Med.Low elevations, and to decrease for Med.High and High elevations; during October the average monthly precipitation is expected to decrease, with larger decreases for higher elevations (excluding the High elevations); and during November, this monthly average value is expected to increase, with the larger increases for lower elevations.

- Looking at the projected changes on monthly values, almost all the RCMs project an increase in the **monthly mean precipitation** during December and January (see 4.11), with the *largest average increase during January* (+∼19%) and a decrease from April to August, with the *largest average decrease in July* (-∼42%) and almost no change during March (average value of +1%). For the **monthly mean temperature**, all the RCMs projects an *increase in the monthly mean temperature all along the year*, with the largest average increase during August (+∼7.1°C) and the *lowest average increase for March* (+∼3.3°C).

- Areas located in higher elevation are expected to suffer large increments in the annual and seasonal air temperature, and the larger decreases in annual and mean seasonal precipitation when compared to lower elevation zones, situation that may have a strong impact on the future climatological regime of the Ebro River basin, due to its likely effects on glaciers and snow-pack located in the northern part of the basin.

- An advice to any further study regarding impacts of climate change on this area is to look carefully to the expected changes for the autumn (SON), because this is the season with the most contradictory projections for the expected changes in seasonal precipitation.

- The seasonal changes on the meteorological driving forces, mentioned in section 4.4, may have important effects on the water availability of the Ebro River basin, because the projected increments in mean temperature and decreases in mean precipitation are concentrated in seasons characterized by intense irrigation activities, and a hydrological modelling work that incorporates the impacts of these meteorological drivers on agriculture and energy should prove be very useful for decision makers aiming at avoiding a future crisis in those strategic sectors.

- This chapter showed that the chosen future climate scenarios provided very different projections of bias-corrected annual/seasonal/monthly temperature and precipitation fields, even under the same emissions scenario (the medium-high SRES A2 in this dissertation). RCAO_E (SMHI.MPIA2) is the most severe RCM in terms of projected annual anomalies. However, when moving into seasonal and monthly projections, considering different elevation bands within the catchment, it is possible to observe that different combinations of projected changes in temperature and precipitation fields can lead to choose a different RCM as the most severe for the particular objective of a specific project. Moreover, extreme projected changes were given by climate scenarios that used boundary conditions from the two different GCMs used in the present dissertation. This proves that the use of ensembles of RCMs, driven by different GCMs, should be a mandatory step in any hydrological study aiming at having a better assessment of the full range of likely changes in climate.

- By no means it should be thought that the future changes in climate expected for the Ebro River basin will certainly lie between the ranges given in this dissertation. Additional uncertainties (reliability of SRES scenarios, skill of the GCM/RCM to provide a realistic response to a emission forcing that have been never observed before, downscaling technique, small number of driving GCMs considered in this dissertation as boundary conditions of the future scenarios, unforeseen natural phenomena, etc.) sum additional degrees of freedom to an already complex issue. It can only be claimed that we explored some possible scenarios of future climate, with the best information we had at this moment, and that the results provided here correspond to the best projections we could make based on our imperfect knowledge about a very complex, heterogeneous and non-linear problem.

*"Doubt is not a pleasant condition,
but certainty is absurd one."*
(Voltaire)

5 Hydrological Impacts of Climate Change (2071-2100)

This chapter presents projected changes on water resources for two selected subcatchments of the Ebro River basin by the end of this century (2071-2100), considering an ensemble of high-resolution future climate scenarios, the effects of hydrological parameterisation, and the bias of the hydrological model in representing different streamflow magnitudes. Section 5.1 gives a brief introduction about expected changes in water resources for the Mediterranean area, methodologies for assessment of hydrological impacts of climate change, and the *cascade of uncertainty* involved in the quantification of the hydrological impacts of climate change, in order to set the background for the remaining sections of this chapter. Section 5.2 describes the methodology developed to assess the hydrological impacts of climate change subject to hydrological parametric uncertainty, including: (i) the six climate change scenarios used to sample the space of possible future climates; (ii) the downscaling technique adopted for passing the climate signal from the grid-scale of the RCM outputs to the point-scale of the gauging stations used in the hydrological simulations, (iii) the parameter sets used to obtain ensembles of projected streamflows for each climate scenario; (iv) the use of flow duration curves (FDCs) to qualitatively assess the relative importance of the uncertainties coming from hydrological parameterisation and from the driving climate scenario; and (v) the use of three percentiles (Q5, Q50 and Q95) to quantitatively assess projected changes in streamflows, taking into account possible bias of the hydrological model in representing some streamflow magnitudes. Section 5.3 presents projected changes in the overall and seasonal streamflows by the end of this century. Finally, a summary with the main results is included in section 5.4, at the end of this chapter.

5.1 Introduction

5.1.1 Overview

Changes in regional water availability and frequency/intensity of extreme events will be among the most significant impacts of climate change on our society. Such hydrological changes will have implications on important aspects of our every-day life, from agricultural productivity and energy production to flood control, highlighting the necessity of a better understanding about how those changes in global climate will affect local water resources (*Xu*, 1999). According to Fourth Assessment Report (AR4) of the Intergovernmental Panel on Climate Change (IPCC) almost all Europe is deemed to be negatively affected by future impacts of climate change, including a higher risk of floods, droughts and erosion (*Alcamo et al.*, 2007). In particular, southern Europe is likely to suffer a decrease in annual runoff, by 0 to 23% up to 2020s and by 6 to 36% up to 2070s (A2 and B2 scenarios and two different climate models), accompanied with a decrease by up to 80% of low summer flows, making the risk of drought particularly important. Moreover, projected increase of water withdrawals in southern Europe would amplify the risks associated to climate change, being the Mediterranean (Spain and Portugal) the region more exposed to drought risk (*Alcamo et al.*, 2007).

5.1.2 Methodologies for Assessing the Hydrological Impacts of Climate Change

Quantification of climate changes impacts on water resources is important to evaluate its effects on the balance between demand and availability of all the socially valued water uses (*Kundzewicz et al.*, 2007), and it is necessary to design and implement long-term adaptation and mitigation policies. A traditional way to conceptualise and investigate how the allocation of water resources will evolve under changes in water availability and water uses has been through the use of hydrological and/or hydrogeological models. Hydrological models represent basins behaviour through a mathematical formulation of the most relevant and well-known physical process. The characteristics and data requirements of each model will depend on the particular modelling task, thus they could be grouped in different ways: deterministic/stochastic, surface runoff/groundwater; water-quantity/water-quality; metric (black/box)/parametric (conceptual)/mechanistic (physically-based) (*Wagener et al.*, 2004; *Wheater*, 2008); lumped/distributed/semi-distributed, or many combinations among them. However, passing the signal of climate change from climate models to hydrological models is not an easy task, as meteorological variables from climate models are often affected by systematic errors (*Graham et al.*, 2007a).

Nowadays, climate models are the only available tools for quantifying the global climate response to different future development scenarios of our society, represented by different atmospheric concentrations of carbon dioxide and other trace gases. Climate models use well-known physical principles to simulate the interactions among atmosphere, oceans, land surface and ice. Up to now, the assessment of potential impacts of climate change has generally relied on data from Atmosphere-Ocean General Circulation Models (AOGCM), with a spatial resolution of a few hundred kilometres ($\sim$300 km or $\sim$2.5°), which is not enough for reproducing spatial patterns of precipitation (*Salathé*, 2003) and its daily variability (*Bürger and Chen*, 2005), especially in areas of complex topography and land use distribution (*Christensen et al.*, 2007b), making them unsuitable for a direct application as drivers of hydrological impacts studies (*Prudhomme et al.*, 2002). To overcome these limitations, spatial and temporal downscaling techniques are carried out for limited areas and run for shorter periods, mainly oriented to better reproduce temperature and precipitation fields (e.g. *Fowler et al.*, 2007; *Prudhomme*, 2006; *Dibike and Coulibaly*, 2005; *Salathé*, 2005, 2003; *Wood et al.*, 2004; *Prudhomme et al.*, 2002; *Wilby et al.*, 2000, 1999; *Xu*, 1999).

Once the climatological fields have been downscaled, conceptual rainfall-runoff models, whether lumped (e.g. *Mimikou et al.*, 2000; *Pilling and Jones*, 2002; *Arnell*, 2003a; *Thodsen*, 2007; *Chiew et al.*, 2009) or semi-distributed (e.g. *Andréasson et al.*, 2004; *Thomson et al.*, 2005; *Arheimer et al.*, 2005; *Booij*, 2005; *Gosain et al.*, 2006; *Graham et al.*, 2007b; *Steele-Dunne et al.*, 2008; *Abbaspour et al.*, 2009) have been -to date- the preferred tools of many climate-change researchers worldwide to assess the likely impacts of climate change, in spite of their known limitations, related to parameter identifiability, equifinality and predictive uncertainty (see section 3.1.2). The main reasons for this preference are: (i) relative low data-requirements, (ii) computation time suited for long-term hydrological simulations, and (iii) a large amount of models are available, already calibrated and verified during years of application to water management and related problems.

An early review of techniques used for assessing the effects of climate change on water resources is provided by *Leavesley* (1994), whereas an updated review can be found in *Praskievicz and Chang* (2009), with focus on the hydrological impacts of climate change and urban development. Following *Xu* (1999), the assessment of the hydrological impacts of climate change can be carried out with four different approaches, which are briefly summarised next.

Using hypothetical scenarios as input to hydrological models

Different climate models may give different values of climate variables for the same period, therefore they do not provide a single estimate that could be used as a reliable projection for hydrological planning. Consequently, many hydrologists have used hypothetical climate change scenarios for hydrological impact assessments, based on "*double* CO_2" conditions. In the simplest form,

average annual changes in precipitation and temperature using either GCM outputs, projected historical trends, or personal estimates (typically $\triangle$T = +1°C, +2°C and +4°C and $\triangle$P = $\pm$10%, $\pm$20%) are used to define the hypothetical scenarios.

Direct use of GCM-derived hydrological output

Notwithstanding General Circulation Models (GCMs) were developed to predict the average synoptic-scale, and general circulation patterns of the atmosphere, not to be directly used in the assessment of the hydrological response to climate change, some studies have used GCM-derived outputs to predict the impact of future climate change on macroscale watersheds. However, the very simple representation of the complex hydrologic cycle within a GCM (most of them do not include any water routing within the land phase) leads to very low predictive capabilities thereof.

Coupling GCMs and macroscale hydrological models

Some studies have coupled meteorological fields given as output of GCMs (e.g., precipitation and temperature) to directly drive a hydrological model for a large river basin (e.g. *Arnell*, 1999), leading to a better representation of the observed flow regime than using the GCM runoff. However, due to the coarse spatial resolution of GCMs, they are not able to solve process occurring at smaller scales.

Downscaling GCM climate outputs to drive a hydrological model

As mentioned in section 4.2.2, since there is a gap between the coarse spatial resolution of GCM outputs and the smallest spatial resolution needed for hydrological impact studies, in recent decades a great deal of research has been focused on the development of "*downscaling*" techniques (e.g. *Xu*, 1999; *Wilby et al.*, 1999; *Murphy*, 1999; *Prudhomme et al.*, 2002; *Wood et al.*, 2004; *Salathé*, 2005; *Kay et al.*, 2006; *Graham et al.*, 2007b,a; *Burton et al.*, 2010), aiming at producing climate information with a spatial resolution finer than the large-scale GCM outputs. Downscaling techniques can be roughly classified as (i) empirical/statistical methods, where statistical techniques are used to formulate empirical relationships between GCM climate outputs and local climate; and (ii) dynamical downscaling, where a higher resolution regional climate model (RCM) or limited-area model (LAM) is nested to a GCM, and it uses large-scale and lateral boundary conditions from the GCM to produce higher resolution outputs. An exhaustive and updated review of downscaling techniques with focus in hydrological applications is provided by *Fowler et al.* (2007). This is the approach used in the present dissertation for assessing the likely impacts of climate change on water resources of the Ebro River basin.

Teutschbein and Seibert (2010) provides a review of hydrological impact studies based on RCM outputs, pointing out that inter-model variability and bias in the representation of observed climate may have important consequences in the final impacts, emphasizing that multi-model approaches along with appropriate bias-correction procedures should be preferred to impact studies based on a single RCM. They also confirmed previous results (e.g. *Giorgi et al.*, 1994; *Hagemann et al.*, 2004) regarding that raw RCM-simulated runoff are often error-prone.

5.1.3 Uncertainty in Impacts of Climate Change

Since the TAR (IPCC, 2001) there has been a significant progress in better understanding the physical process involved in the climate change, in model climate simulation, and methods of analysis and evaluation of climate feedbacks (*Randall et al.*, 2007). However, the Working Group II in the AR4 of the IPCC mentioned that there are still major uncertainties in how much the hydrological characteristics of a basin will change (*Kundzewicz et al.*, 2007), what implies that planners usually have to take decisions based on a wide range of predicted changes, from different models of unknown relative quality. A clear representation of all the uncertainties involved in the assessment

process is fundamental to provide useful and technically-based advice to policy makers, in order to devise suitable strategies of mitigation and risk reduction (*Reilly et al.*, 2001), for then selecting the best possible choice based on the current knowledge.

Projected impacts of climate change will depend on the combination of emissions scenarios, climate forcings, and impact model used to assess the local impacts (*Viner*, 2003; *Olesen et al.*, 2007). The assessment process begins with the selection of one or more emissions scenarios, normally adopted from the Special Report on Emissions Scenarios (SRES, *Nakićenović et al.*, 2000), which are derived from four main storylines (A1, A2, B1, B2) describing different socio-economic, demographic and technological evolutions of our society, which have to be treated as being equally plausible (*Schneider*, 2002; *Viner*, 2003). Emissions are then converted to concentrations of greenhouse gases by gas-cycle models, and scenarios of future concentrations are then used to derive projections of climate response, usually through complex coupled atmosphere-ocean General Circulation Models (AOGCM). To overcome limitations related to spatial resolution of AOGCM, spatial and/or temporal downscaling techniques are carried out for limited areas and run for shorter periods, with the purpose of better reproducing temperature and precipitation fields. Finally, downscaled climate fields are used to drive impact models, and to obtain projected impacts and their corresponding predictive uncertainties. In particular, hydrological impact studies involve important decisions which effects are reflected into the final impacts. Firstly, the modeller select one or more model structure(s) to represent the main physical process undergoing in the catchment; secondly, one or many parameter sets are used to describe some effective properties of the catchment within the adopted model structure(s); then, parameter values are obtained by using one or more goodness-of-fit measure selected by the modeller, for comparing observed and simulated values during a user-defined calibration period, with or without explicit consideration of errors in the input data used to drive the simulations. As a result, quantification of impacts of climate change have to be seen as a "*cascade of uncertainty*" (*New and Hulme*, 2000; *Mearns et al.*, 2001; *Schneider*, 2002; *Viner*, 2003; *Giorgi*, 2005; *Wilby*, 2005), as shown in Figure 5.1, in which decisions taken in every step of the assessment process, going from emissions scenario to projected impacts, convey uncertainties that are unavoidably propagated to subsequent levels.

In the last decades, a great deal of research has been focused on uncertainty in climate-change scenarios (e.g. *New and Hulme*, 2000; *Allen et al.*, 2001; *Lambert and Boer*, 2001; *Wigley and Raper*, 2001; *Webster et al.*, 2003; *Arnell*, 2003b; *Arnell et al.*, 2003, 2004; *Zierl and Bugmann*, 2005; *Rowell*, 2006; *Prudhomme and Davies*, 2007; *Lenderink et al.*, 2007; *Maurer*, 2007; *Moss et al.*, 2010), the use of ensembles in impact assessment (e.g. *Giorgi and Mearns*, 2003; *Murphy et al.*, 2004; *Tebaldi et al.*, 2005; *Hewitt*, 2005; *Christensen et al.*, 2007b; *Collins*, 2007; *Meehl et al.*, 2007; *Tebaldi and Knutti*, 2007; *Maurer*, 2007; *Groves et al.*, 2008; *Bormann et al.*, 2009; *Manning et al.*, 2009; *Halenka et al.*, 2009; *Sankarasubramanian et al.*, 2009; *Fowler and Ekström*, 2009), downscaling from global climate changes to regional scales (e.g. *Xu*, 1999; *Murphy*, 1999; *Wilby et al.*, 2000; *Prudhomme et al.*, 2002; *Wood et al.*, 2004; *Salathé*, 2005; *Kay et al.*, 2006; *Graham et al.*, 2007b,a; *Burton et al.*, 2010), as well as in hydrological impacts of climate change (e.g. *Christensen et al.*, 2004; *Payne et al.*, 2004; *Arnell*, 2005; *Booij*, 2005; *Dibike and Coulibaly*, 2005; *Bürger et al.*, 2007; *Graham et al.*, 2007b; *Steele-Dunne et al.*, 2008; *Chiew et al.*, 2009; *Peng and Xu*, 2009; *Abbaspour et al.*, 2009). However, most of the studies providing an assessment of the impacts of climate change on water resources have used one single hydrological model, i.e, a unique combination of model structure and parameter set, to quantify the future streamflows, overlooking the relative importance of hydrological uncertainties into the final impacts. Comparatively, only few quantitative studies have looked at the propagation of the aforementioned uncertainties into the final hydrological impacts (e.g. *Jakeman et al.*, 1993; *Wilby*, 2005; *Dibike and Coulibaly*, 2005; *Zierl and Bugmann*, 2005; *Horton et al.*, 2006; *Cameron*, 2006; *Wilby and Harris*, 2006; *Graham et al.*, 2007b,a; *Prudhomme and Davies*, 2009a,b), being the work of *Kay et al.* (2009) the one that compared the largest number of uncertainty sources of which the author of this dissertation is aware.

Most of the studies comparing uncertainties coming from different future climate scenarios with those coming from hydrological parameterisation indicate that the greatest source in the cascade of uncertainty is the GCM chosen to drive the simulations (e.g. *Wilby and Harris*, 2006; *Prudhomme*

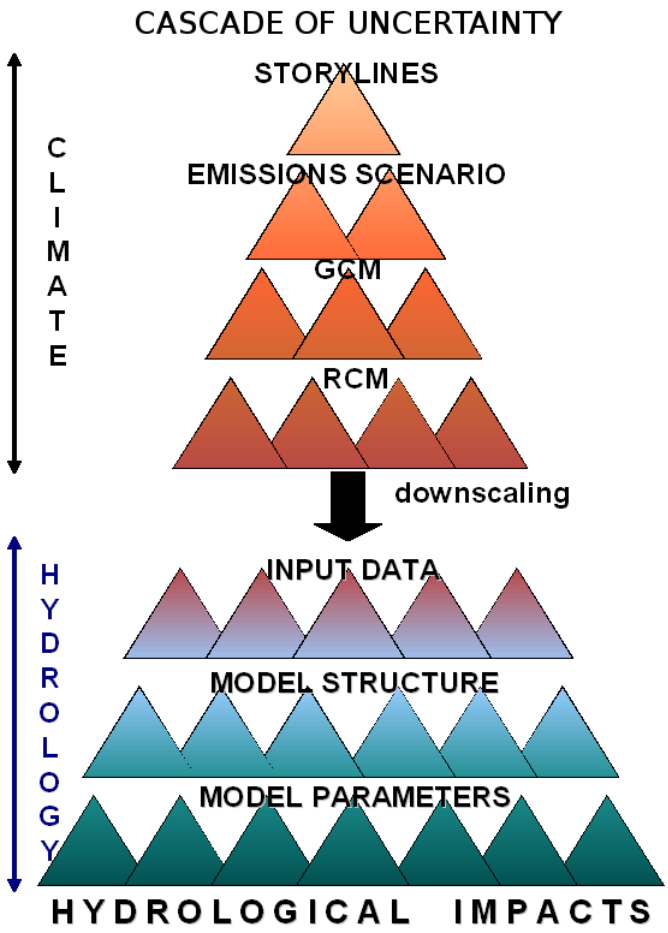

FIGURE 5.1: Schematic representation of the *"cascade of uncertainty"* involved in the quantification of hydrological impacts of climate change. Modified after *Viner* (2003).

and Davies, 2009a,b; *Kay et al.*, 2009). *Caballero et al.* (2007) ordered the sources of uncertainty, related to hydrological impacts of climate change, in decreasing order as follow: emissions scenarios, climate model parameterization, downscaling, and hydrological model parameterisation, without giving an explicit reason for that, whereas *Wilby and Harris* (2006) suggested the following decreasing order: GCM, downscaling, hydrological model structure, hydrological parameterisation, and emission scenario. *Prudhomme and Davies* (2009b) claim that the largest source of uncertainty in future streamflows is the driving GCM, with uncertainties coming from downscaling and emissions scenario being similar in magnitude, but generally smaller than the uncertainty coming from the driving GCM. *Prudhomme and Davies* (2009b) also claim that hydrological modelling uncertainty can be neglected when it is smaller than GCM variability for baseline flows, but it may be significant otherwise. *Kay et al.* (2009) suggest that uncertainties related to the representation of future climate are generally larger than those related to hydrological modelling or emissions, however, they also mention that the effect of hydrological parameterisation may be under-represented in their study, because the uncertainty coming from equifinality was not considered. As far as the author of this dissertation is aware, *Abbaspour et al.* (2009) were the first in arguing that the relative importance of the uncertainty may be dependent on the scale of the study, with hydrological model uncertainty being larger and uncertainties due to emissions scenarios becoming smaller as the scale of the study increases. This dissertation attempt to provide new insights about the relative magnitudes of uncertainties derived from the driving climate model and hydrological parameterisation, and its implications for hydrological impact assessment.

5.2 Methodology

This chapter focuses in two steps of the "*cascade of uncertainty*" involved in the quantifications of the hydrological impacts of climate change: (i) the hydrological parameterisation used to represent the catchment response to a given climatological forcing, and (ii) its interaction with different climate change scenarios, used to sample the space of future climates expected by the end of this century. The Generalised Likelihood Uncertainty Estimation (GLUE) methodology is used to select parameters sets that can be considered as acceptable simulators of the system, based on a user-defined percentage of observations bracketed by the predictive uncertainty bounds derived from using those parameters sets during independent calibration and verification stages within the control period 1961-1990. Afterwards, the same parameter sets selected during the uncertainty analysis of the control period are used to represent the catchment response to different scenarios of future climate. Finally, the bias-corrected daily time series derived from each climate scenario are run with the behavioural parameter sets selected for each catchment, and then they are used to produce probabilistic projections of future streamflows, taking into account bias of the hydrological modelling in the representation of river flows of different magnitudes and for different seasons.

The approach developed in this dissertation differs from previous studies related to propagation of hydrological parametric uncertainty into projections of hydrological impacts of climate change, as (a) it allows to select parameter sets to be used in hydrological simulations of future scenarios based on an objective criterion, i.e, a user-defined minimum percentage of observations embraced by the uncertainty bounds; (b) it presents an assessment of the streamflow magnitudes that are better/worse represented by the hydrological model; and (c) it provides probabilistic information about projected seasonal changes in low, medium and high streamflows, taking into account the bias of the hydrological model in representing the catchment response.

The developed framework to obtain probabilistic projections of future river flows involved four steps, described in the following sections: (i) selection of an ensemble of six future climate-change scenarios for the Ebro River basin, which is used to sample the space of possible future climate in the basin; (ii) downscaling the future climate scenarios from the RCM grid scale to the point scale, in order to be used by the hydrological model; (iii) selection of the parameters sets to be considered as acceptable simulators of the system during the control period, by using the Generalised Likelihood Uncertainty Estimation (GLUE) methodology; and (iv) computation of probabilistic projections of future streamflows, by using flow values derived from running each climate scenario with all the behavioural parameter sets selected for each one of the selected catchments.

5.2.1 Selection of Climate Scenarios and Downscaling of RCM Outputs

It is widely accepted that the assessment of projected impacts of climate change on water resources requires the use of multi-model ensembles to better estimate the likely changes in climate, in particular at regional scales, because no singe model provides a "*true*" representation of the future climate (*Tebaldi*, 2004). The climate scenarios used in this dissertation to sample the space of future possible climates on the Ebro River basin were already described in section 4.2.1, along with the downscaling technique used to pass from the grid-scale of the RCM outputs to the point scale of the gauging stations used to drive the hydrological simulations on the two selected catchments, described in section 3.3.1. Therefore, a brief summary is presented here just for completeness.

An ensemble of six climate scenarios were selected from the red set of the EU FP5 PRUDENCE project, described in Table 4.1, corresponding to six different RCMs run with boundary conditions taken from what can be considered two different GCMs: the atmosphere-only HadAM3H (*Buonomo et al.*, 2007; *Gordon et al.*, 2000; *Pope et al.*, 2000) and the atmosphere-ocean ECHAM4/OPYC (*Roeckner et al.*, 1996), under the same medium-high SRES A2 emissions scenario.

Section 4.2.2 describes the simple **bias-correction** method used to downscale daily precipitation and air temperature fields from the grid-cell scale of the RCM outputs to the point scale of the

gauging stations selected in section 2.2.5.1, in order to allow the simulated monthly means to match the observed monthly averages during the control period. The bias-corrected daily time series of precipitation and temperature where then used to drive the hydrological simulations on two selected catchments (see section 3.3.1), during the future period 2071-2100, in order to assess the likely impacts of climate change on the water resources of both catchments.

5.2.2 Hydrological Parameterisation

Chapter 3 described the set up of the hydrological model, and the uncertainty analysis carried out in order to select the parameter sets that are used in this chapter to describe the catchment response to different climate forcings. Therefore, they are briefly summarized next just for completeness.

In section 3.3, the Soil and Water Assessment Tool (SWAT) hydrological model was set up on the western part of the Ebro River basin (NE Spain, $\sim$ 42000 km^2), in order to carry out daily simulations of river flows during the control period 01/Jan/1961 - 31/Dec/1990. Afterwards, two subcatchments (090, Ega River and 115, Homino River) were selected in section 3.3.1 to test the proposed methodology, aiming at assessing the impact of hydrological parameterisation on the predicted streamflows. A sensitivity analysis with Latin Hypercube One-factor-At-a-Time (LH-OAT) was carried out in section 3.4.1, in order to identify parameters with a high impact on simulated streamflows. In section 3.4.2, the Generalized Likelihood Uncertainty Estimation (GLUE) methodology, was applied to select parameter sets that can be considered as acceptable simulators of the catchment response, using a re-scaled Nash-Sutcliffe efficiency (*Nash and Sutcliffe*, 1970) as "*less formal*" likelihood, and a cut-off threshold equal to zero to discriminate between behavioural and non-behavioural simulators. A Latin Hypercube (LH) sampling strategy was implemented within GLUE in order to efficiently sample the parameter space. Parameter sets that led to predictive uncertainty bounds that encompass a number of observations close to or larger than 75% during independent calibration and verification stages were selected as acceptable simulators of the two test catchments, and are used in this chapter to derive the uncertainties coming from hydrological parameterisation for each one the six climate scenarios briefly described in the previous section 5.2.1. An important assumption that may modify the results presented in this chapter is that both the land use and soil properties will remain constant on the two selected catchments during the future scenarios. The consequences of no fulfilment of that assumption were not explored due to time constrains, and because it is not the main focus of the present dissertation, but it should be explored when significant changes in land cover and/or soil types can be expected for the study catchments.

For each one of the climate scenarios defined in section 5.2.1, an ensemble of projected streamflows for the future period was obtained, by running the hydrological model with all the behavioural parameter sets obtained in section 3.5.1 for each subcatchment, while driven by the bias-corrected daily climatological forcings derived from each scenario.

5.2.3 Flow Duration Curves (FDCs) for Assessing Relative Uncertainties

The relative importance of the uncertainty coming from the driving RCM and from hydrological parameterisation is strongly related to the methodology used to carry out this comparison. Most of the studies that have compared the relative importance of these two uncertainty sources have been based on an arbitrary number of "*near-optimal*" parameter sets (e.g. *Wilby and Harris*, 2006; *Prudhomme and Davies*, 2009b). Those parameter sets are usually selected because they provide values of some efficiency measure (e.g., Nash-Sutcliffe efficiency) higher than a pre-defined threshold for some calibration period, and because they are "*stable*" under different (dry/wet) evaluation periods. However, there is no explicit attempt to look at how well the ensemble of predicted streamflows represents different streamflow magnitudes or different seasons (e.g., the percentage of observations that are within the predictive uncertainty bounds derived from the selected parameter sets), i.e., overlooking -in advance- the importance of hydrological parametric uncertainty.

Flow duration curves (FDCs) were described in section 3.5.4, and they were selected to assess the relative importance of these two uncertainty sources because they are simple, yet comprehensive, graphical representations of the streamflow variability of a catchment (*Vogel and Fennessey*, 1994), and because they are useful for conveying hydrological information to decision makers (*Vogel and Fennessey*, 1995). To characterize the information content of a FDC we applied the same criteria described in section 3.5.4, where the curve is divided into three segments corresponding to different flow magnitudes: (i) a high-flow portion (0 - 0.2 exceedance probability), that represents the catchment response to large precipitation events; (ii) a medium-flow portion (0.2 - 0.7 exceedance probability), representing flows controlled by moderate precipitation events coupled to medium-term baseflow; and (iii) a low-flow segment (0.7 - 1.0 exceedance probability) representing a catchment response dominated by long-term baseflow during extended dry periods.

To compare the relative importance of the uncertainty derived from hydrological parameterisation with the one derived from the driving RCM, we plotted 29-years daily FDCs for each one of the climate scenarios defined in section 5.2.1, along with their corresponding uncertainty bounds derived from hydrological parameterisation. The last twenty nine years of the control period 1961-1990 and of the future scenarios 2071-2100 were used to compute the FDCs, because the first year was used as spin-up for all the hydrological simulations, and it was decided to use the same 29-years base for all the FDCs, including the one corresponding to the observed values.

For each future climate scenario, a single FDC was considered as representative of the ensemble of projected streamflows obtained by running the hydrological model with all the behavioural parameter sets of each subcatchment (see Section 3.5.1). This representative FDC was obtained by computing the 29-years daily FDC corresponding to the median of the streamflows projected for each scenario. Following what described in section 3.4.2.3, uncertainty coming from hydrological parameterisation in the FDC space was represented by the 95% of predictive uncertainty (95PPU) of each scenario, which was computed as the 29-years daily FDC of the streamflows corresponding to the 2.5% and 97.5% of the cumulative distribution of every simulated streamflow. In this way, one figure is obtained for each future scenario, with the 29-years daily FDC representing the stremaflows derived from each scenario, and the uncertainty bounds corresponding to hydrological parameterisation. This figures only allow to visualise the magnitude of the hydrological uncertainty for different streamflows magnitudes projected for each scenario. Finally, in order to facilitate the comparison of the uncertainties coming from the driving climate scenario and from hydrological parameterisation for different streamflow magnitudes, a single figure was prepared for each subcatchment, which is described in Section 5.3.1.1.

5.2.4 Computation of ECDF for Q5, Q50, Q95

The FDCs with the corresponding uncertainty bounds, derived from hydrological parameterisation, allow to have a qualitative idea about the relative importance of uncertainties coming from hydrological parameterisation and from the choice of driving RCM. However, in order to provide a quantitative assessment of the projected changes in streamflows by different climate change scenarios, we computed empirical cumulative density functions (ECDF) for 3 different percentiles[1], that represent different stramflow magnitudes: (i) Q5, representing low flows; (ii) Q50, representing medium flows, and (iii) Q95, standing for high flows.

The procedure used for computing the ECDF for Q5, Q50 and Q95 for the six climate scenarios described in Table 4.1 is as follow:

1. Run the same climate scenario with all the behavioural parameter sets obtained in section 3.5.1 (1948 for subcatchment 090, and 1464 for subcatchment 115);
2. Compute the Q5, Q50, and Q95 percentile corresponding to each behavioural parameter set, from the daily streamflow values obtained for the period 2072-2100 with each RCM, and

[1]Here we adopted the definition used by most of the statistical softwares, in particular *R* (*R Development Core Team*, 2009), knowing that other authors use a different meaning.

3. Compute the ECDF of the Q5, Q50 and Q95 percentiles, by weighting the analysed percentile by the re-scaled likelihood of the corresponding behavioural parameter set obtained in section 3.5.1.

5.3 Results

5.3.1 Relative Uncertainties: Hydrological Parameterisation vs Driving RCM

5.3.1.1 Overall Impacts

Appendix C presents, for the two selected catchments, 29-years daily flow duration curves (FDCs) for the control period and each one of the six future climate scenarios described in Table 4.1, along with the corresponding 95% of predictive uncertainty (95PPU) derived from hydrological parameterisation. In order to facilitate the comparison of the uncertainties coming from the driving climate scenario and from hydrological parameterisation for different streamflow magnitudes, a single figure was prepared for each subcatchment. This figure contains six FDCs representing the median streamflows derived from each future scenario, and the vertical distance between the outermost FDCs represent the magnitude of the uncertainty coming from the driving RCM for a given streamflow value. The same figure contains an overall uncertainty bound, obtained by overlapping the 95PPU of the six future climate scenarios, and the vertical distance between the upper and lower uncertainty bounds represents the magnitude of the uncertainty coming from hydrological parameterisation for a given streamflow value.

Figures 5.2 and 5.3 show 29-years flow duration curves (FDCs) and the overall uncertainty bounds corresponding to hydrological parameterisation, for subcatchments 090 (Ega River) and 115 (Homino River), respectively. They show that for both catchments the hydrological parametric uncertainty is larger than the uncertainty coming from the driving RCM, because the overall hydrological uncertainty bounds (shaded area in the figures of this chapter), obtained from running the climatological fields derived from each one of the six RCMs with the behavioural parameter sets obtained for each subcatchment in section 3.4.2, encompass the median of the streamflow projections of the six considered RCMs, all along the range of streamflow magnitudes. However, this result can not be generalised, because it is conditional to decisions taken during the uncertainty analysis and to the ensemble of RCMs considered. In particular, the wide uncertainty bounds obtained for both catchments result from running the hydrological model with a single model structure (described in section 3.3.1), with the behavioural parameter sets selected during he GLUE analysis (1948 and 1464 for subcatchments 090 and 115, respectively), using the Nash-Sutcliffe efficiency as "*less formal*" likelihood with a shape factor N equal to one, and a cut-off threshold equal to zero to separate behavioural from non-behavioural parameter sets. The choice the cut-off threshold equal to zero (the minimum acceptable value) can be criticized as the main factor affecting the width of the uncertainty bounds; however, it was defined at the beginning of the uncertainty analysis (see section 3.4.2) to be used in combination with the criterion of considering as acceptable simulators of the systems under study all the parameter sets that lead to uncertainty bounds that embrace a percentage observations close to or greater than 75% during the control period. Choosing a higher cut-off threshold obviously will decrease the width of the uncertainty bounds corresponding to hydrological parameterisation, but it will do it so at expense of a smaller number of observations embraced by the uncertainty bounds, at least within the same model structure and criterion adopted for exploring the parameter space (see section 3.4.2.2) in the present dissertation. Therefore, we claim that decisions about the efficiency measure to be used as "*less formal*" likelihood and the cut-off threshold used to separate behavioural from non-behavioural parameter sets, have to be taken during the uncertainty analysis of the control period, in a dialogue between the modeller and the decision-maker, taking into account the objectives of the study along with data and model availability.

The previous finding is opposed to what has been previously claimed by *Prudhomme and Davies*

(2009b) and *Wilby and Harris* (2006), both of whom put uncertainties due to hydrological model parameters as less important than those derived from the choice of the driving GCM, even if *Prudhomme and Davies* (2009b) warned that their results are site-specific and that this statement cannot be generalised. However, both of the aforementioned studies rely in hydrological simulations carried out with a subset of the "*best*" and more stable parameter sets obtained during calibration and evaluation periods, without making any explicit analysis about neither how wide (or narrow) the uncertainty bounds provided by the selected parameter sets are, nor the skill of the hydrological model to represent different flow magnitudes, data both very informative to decision makers. Additionally, parameter sets in previous studies were selected based on their Nash-Sutcliffe efficiency index (*Nash and Sutcliffe*, 1970), which is know to be biased towards high flows, what would be observed if an uncertainty analysis were provided for those simulations. Consequently, it is not surprising that hydrological parametric uncertainty obtained with parameter sets with similar high Nash-Sutcliffe efficiencies be smaller than the one related to the choice of driving GCM, because those parameter sets are expected to produce a similar catchment response.

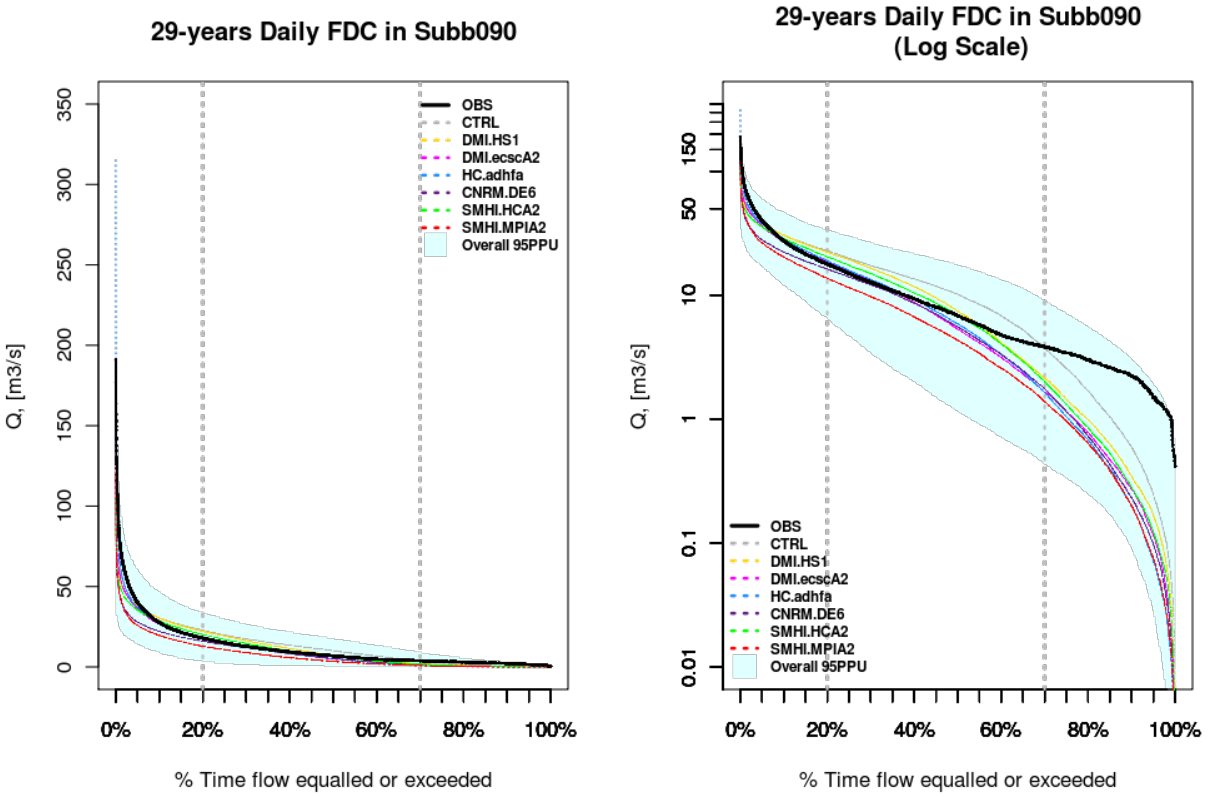

FIGURE 5.2: 29-years flow duration curve (FDC) for subcatchment 090 (Ega River). Left side shows the FDC with a normal vertical scale, and figure on the right show the FDC with logarithmic vertical scale (removing zero values). Black continuous line is the observed FDC during the period 1962-1990, grey dotted line represent the median of the GLUE simulations for the same control period, and coloured dotted lines show the median of the simulations corresponding to different climate scenarios during the period 2072-2100. Shaded area represent the overall uncertainty due to the hydrological parameterisation adopted for GLUE simulations.

FDCs plotted with normal scale in Figures 5.2 and 5.3 also show that the absolute hydrological parametric uncertainty is larger for high flows than for low ones, whereas the corresponding FDCs plotted with logarithmic scales show that the relative uncertainties are larger for low flows than for high ones.

Comparison of the FDCs corresponding to observed discharges during the control period 1962-1990 (labelled as "OBS" with black continuous line) with the FDCs corresponding to the median of the simulated streamflows (labelled as "CTRL" with grey dotted line) obtained for the same con-

trol period with the behavioural parameter sets (1948 for subcatchment 090 and 1464 for subcatchment 115) selected during the uncertainty analysis described in section 3.4.2, show that the median of the hydrological simulations, for the two selected catchments, provides a good representation of high flows, a slight over-estimation of medium flows, and a relative large under-estimation of low flows, which is not surprising due to the use of the Nash-Sutcliffe efficiency as *"less formal"* likelihood to select the behavioural parameter sets. The previously mentioned systematic bias are expected to remain during the future scenarios, and it is integrated into interpretations of projected impacts of climate change hereafter.

Projected changes in the overall hydrological regime of the two selected catchments depend on the magnitude of river flows under consideration. For subcatchment 090 (Ega River), the one with more humid regime, the highest flows (exceedance probability lower than 0.1) are expected to decrease; medium-high and medium flows (exceedance probability between 01 - 0.5) present contradictory projections depending on the driving RCM; and medium-low and low flows (exceedance probability higher than 0.5) are expected to decrease, with the largest relative decrease for the lower river flows. At the other hand, subcatchment 115, the one with more semi-arid regime, expect a general decrease of streamflows in the full range of magnitudes, and again the larger relative decreases are expected for the lower river flows. If the relative under-estimation of the low flows during the control period is taken into account, the large decrease is less dramatic, but still important. A probabilistic quantification of the projected changes in seasonal streamflows is given in the next section 5.3.1.2.

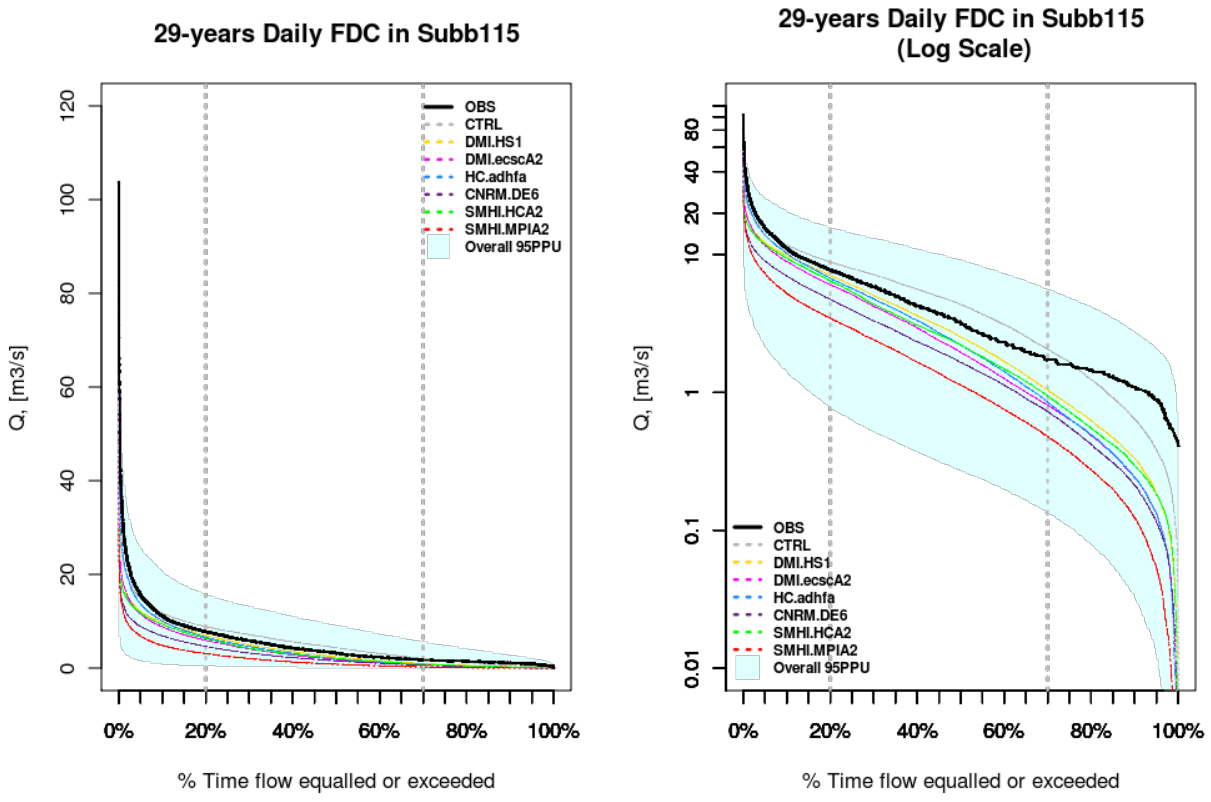

FIGURE 5.3: 29-years flow duration curve (FDC) for subcatchment 115 (Homino River). Left side shows the FDC with a normal vertical scale, and figure on the right show the FDC with logarithmic vertical scale (removing zero values). Black continuous line is the observed FDC during the period 1962-1990, grey dotted line represent the median of the GLUE simulations for the same control period, and coloured dotted lines show the median of the simulations corresponding to different climate scenarios during the period 2072-2100. Shaded area represent the overall uncertainty due to the hydrological parameterisation adopted for GLUE simulations.

Regarding the differences due to the driving RCM, the smallest decreases in the overall stream-

flows are projected for simulations driven by the DMI.HS1 RCM, whereas the largest decreases are expected for simulations driven by SMHI.MPIA2, which correspond to simulations driven by the two different GCMs used to provide boundary conditions to all the selected RCMs (see section 4.2.1). The previous projected changes are in full agreement with projections for annual precipitation and temperature, as can be seen in Table 4.6 in Chapter 4, where SMHI.MPIA2 projected the largest decrease in annual precipitation (-21%) and the largest increase in mean annual temperature (+ 6.24 °C), whereas DMI.HS1 RCM projected the lower decrease in annual precipitation (-4%) and one of the lower increases in mean annual temperature (+4.19 °C).

5.3.1.2 Seasonal Impacts

Figures 5.4 and 5.5 show, for subcatchment 090 (Ega River) and 115 (Homino River), respectively, 29-years seasonal FDCs and their overall uncertainty bounds corresponding to hydrological parameterisation. They show that for both catchments the hydrological parametric uncertainty in all the seasons is larger than the uncertainty coming from the driving RCM, because the overall hydrological uncertainty bounds encompass the median of the seasonal streamflow projections of the six RCMs considered, all along the range of streamflow magnitudes. Again, this result can not be generalised, because it is conditional to decisions taken during the uncertainty analysis and to the ensemble of RCMs considered.

A probabilistic quantification of the projected changes in streamflows is given -when deemed suitable- in the next paragraphs, considering the fifth percentile (Q5, value which marks off the lowest 5 per cent of the observations) as representative of low flows, the 50th percentile (Q50, the value below which the 50% percent of observations fall) as representative of medium flows, and the 95th percentile (Q95) as representative of high flows.

a) **Winter (DJF)**

During winter, FDCs plotted with normal scale in Figures 5.4 and 5.5 show that the absolute hydrological parametric uncertainty is larger for high flows than for low ones, whereas the corresponding FDCs plotted with logarithmic scales show that the relative uncertainties are important for all streamflow magnitudes, but the lower the river flow magnitude the higher the relative importance.

Comparison of the FDCs corresponding to observed winter discharges during the control period (labelled as "OBS" with black continuous line) with the FDCs corresponding to the median of the simulated streamflows (labelled as "CTRL" with grey dotted line), show (Figures C.3 and C.4 in Appendix C present a clearer view) that the median of the hydrological simulations provides a good representation of high flows in subcatchment 115, whereas they are slightly underestimated in subcatchment 090. Medium flows are over-estimated for both catchments, and low flows are consistently over-estimated in subcatchment 090, whereas in subcatchment 115 they are over-estimated up to an exceedance probability equal to 0.95, and under-estimated for larger exceedances.

Projected changes in the winter regime of the two selected catchments depend on the magnitude of river flows under consideration. The two analysed catchments expect a general decrease of high flows. Medium flows are expected to increase for subcatchment 090 (Ega River) and present contradictory projections for subcatchment 115 (Homino River). Low flows are expected to increase in subcatchment 090, whereas they present contradictory projections for subcachment 115 up to an exceedance probability equal to 0.95, and a general projected decrease of the lowest flows (exceedance probability higher than 0.95).

Regarding differences due to the driving RCM, the smallest drops in seasonal high flows and the larger increments of medium and low flows are projected for simulations driven by the DMI.HS1 RCM, whereas the larger drops in high flows and the lower increments in medium and low flows correspond to simulations driven by SMHI.MPIA2, with the only exception of the lowest flows (exceedance probability larger than 0.97) which present the largest drops for simulations driven

by HC.adhfa. The previous projected changes present a general agreement with projections for winter precipitation and temperature, as can be seen in Table 4.6 in Chapter 4, where SMHI.MPIA2 was the only RCM projecting a decrease of the winter precipitation (-1 %), and it projected the largest increase in mean winter temperature (+4.14 °C), whereas DMI.HS1 RCM projected the largest increase in winter precipitation (+22%) and one of the lowest increases in mean winter temperature (+3.26 °C).

b) **Spring (MAM)**

During spring, FDCs plotted with normal scale in Figures 5.4 and 5.5 show that the absolute hydrological parametric uncertainty is larger for high flows than for low ones in both catchments, whereas the corresponding FDCs plotted with logarithmic scales show that the relative uncertainties are important for all streamflow magnitudes, but the lower the river flow magnitude the higher the relative importance.

Comparison of the FDCs corresponding to observed spring discharges during the control period (labelled as "OBS" with black continuous line) with the FDCs corresponding to the median of the simulated streamflows (labelled as "CTRL" with grey dotted line), show (Figures C.5 and C.6 in Appendix C present a clearer view) that the median of the hydrological simulations, provides a fairly good representation of all the streamflow magnitudes in both catchments, because both lines are practically indistinguishable.

A general decrease in spring flows is expected for the two selected catchments, which do not depend on the magnitude of river flows under consideration, but with larger projected relative decreases for subcatchment 115.

Regarding differences due to the driving RCM, the smallest drops in spring streamflows are projected for simulations driven by the DMI.HS1 RCM, whereas the larger drops correspond to simulations driven by SMHI.MPIA2. The previous projected changes present a general agreement with projections for seasonal precipitation and temperature, as can be seen in Table 4.6 in Chapter 4, where SMHI.MPIA2 projected the largest decrease of spring precipitation (-33 %), and projected the largest increase in mean spring temperature (+6.2 °C), whereas DMI.HS1 RCM projected one of the lowest drops in seasonal precipitation (-15%) and one of the lowest increases in mean spring temperature (+3.24 °C).

c) **Summer (JJA)**

During summer, FDCs plotted with normal scale in Figures 5.4 and 5.5 show that the absolute hydrological parametric uncertainty is only important for high flows in both catchments, because there is a general agreement among the projections of the six future scenarios that medium and low flows will be less than 1 m^3/s in both catchments. The FDCs plotted with logarithmic scales show that the relative uncertainties are equally large for all the streamflow magnitudes.

Comparison of the FDCs corresponding to observed summer discharges during the control period (labelled as "OBS" with black continuous line) with the FDCs corresponding to the median of the simulated streamflows (labelled as "CTRL" with grey dotted line), show (Figures C.7 and C.8 in Appendix C present a clearer view) different behaviours in each catchment. Ega River (subcatchment 090) shows a good representation of the highest flows (exceedance probability lower than 0.05), whereas medium-high flows present a slight over-estimation, and medium and low flows are generally under-estimated. At the other hand, the subcatchment with more semi-arid regime (115, Homino River), shows a good representation of high and medium flows, and a slight under-estimation of low flows.

Projected changes for the summer season in the two selected catchments do not depend on the magnitude of river flows under consideration, because both catchments expect a general large decrease of summer flows.

Regarding differences due to the driving RCM, the smallest drops in summer streamflows are projected for simulations driven by the SMHI.HCA2 and DMI.HS1 RCMs, whereas the larger drops are -in general- derived from simulations driven by SMHI.MPIA2. The previous changes projected by different climate scenarios do not present a clear relationship with projections for the

corresponding seasonal precipitation and temperature, what can be due to spatial variations of the climatological fields. Table 4.6 in Chapter 4, shows that SMHI.MPIA2 projects the largest increase in summer mean temperature (+8.72 °C), and one of the largest decreases in mean summer precipitation (-35 %), but the latter is 10% lower than the highest decrease projected by SMHI.HCA2 (-45%). At he the other hand, DMI.HS1 projects one of the lowest increases in mean summer temperature (+5.5°C) and one of the lowest projected decreases in mean summer temperature (-35 %), whereas SMHI.MPIA2 projects one of the highest increases in mean summer temperature (+6.25 °C).

d) **Autumn (SON)**

During autumn, FDCs plotted with normal scale in Figures 5.4 and 5.5 show that the absolute hydrological parametric uncertainty is larger for high flows than for low ones, whereas the corresponding FDCs plotted with logarithmic scales show that the relative uncertainties are important for all streamflow magnitudes.

Comparison of the FDCs corresponding to observed autumn discharges during the control period (labelled as "OBS" with black continuous line) with the FDCs corresponding to the median of the simulated streamflows (labelled as "CTRL" with grey dotted line), show (Figures C.9 and C.10 in Appendix C present a clearer view) that the median of the hydrological simulations, only provides a good representation of the highest flows in both catchments, whereas high and medium flows (exceedance probability between 0.05 and 0.5) are over-estimated, and medium-low and low flows (exceedance probability larger than 0.5) are under-estimated for both catchments.

Projected changes in the autumn regime of the two selected catchments depend on the magnitude of river flows and the catchment under consideration. In the Ega River (sucatchment 090), the seasonal high and medium-high flows (exceedance probability lower than 0.1) present contradictory projections, the medium-high and medium flows (exceedance probability between 0.10 and 0.4) expect a general increase, whereas medium-low to low flows (exceedance probability larger than 0.4) expect a general decrease. At the other hand, the Homino River (subcatchment 115) present contradictory projections for high and medium-high flows (exceedance probability lower than 0.3), whereas the medium-low and low flows (exceedance probability higher than 0.3) expect a general decrease.

Regarding differences due to the driving RCM, there is not a clear patter during autumn, what may be due the contradictory projections for autumn precipitation given by the six RCMs presented in Table 4.6. In general, lower values of seasonal streamflows are given by simulations driven by SMHI.MPIA2, whereas the higher values of streamflows are given by simulations driven by HC.adhfa (high and medium-high flows) and DMI.HS1 (medium and low flows), what is in partial agreement with the largest increase in mean seasonal temperature (+5.52 °C) and the largest decrease in mean seasonal precipitation (-16%) given by SMHI.MPIA2.

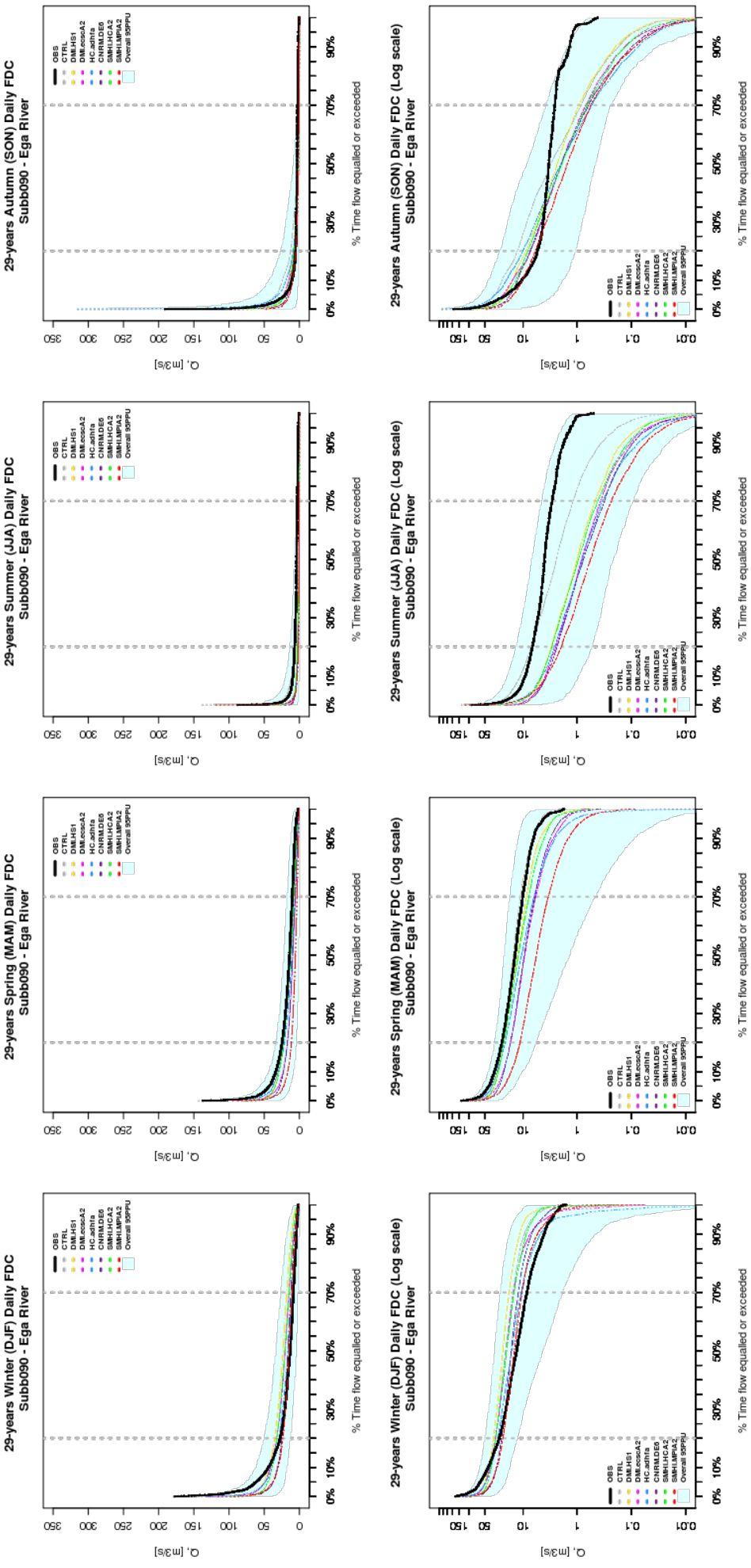

FIGURE 5.4: 29-years seasonal flow duration curves (FDCs) for subcatchment 090 (Ega River). From left to right, figures in the upper panel represent summer, spring, summer and autumn FDCs with a normal vertical scale, whereas figures on the bottom represent the same FDCs but with logarithmic vertical scale (removing zero values). Black continuous line is the observed seasonal FDC during the period 1962-1990, grey dotted line represent the median of the GLUE seasonal simulations for the same control period, and coloured dotted lines show the median of the seasonal simulations corresponding to different climate scenarios during the period 2072-2100. Shaded area represent the overall uncertainty due to the hydrological parameterisation adopted for GLUE simulations.

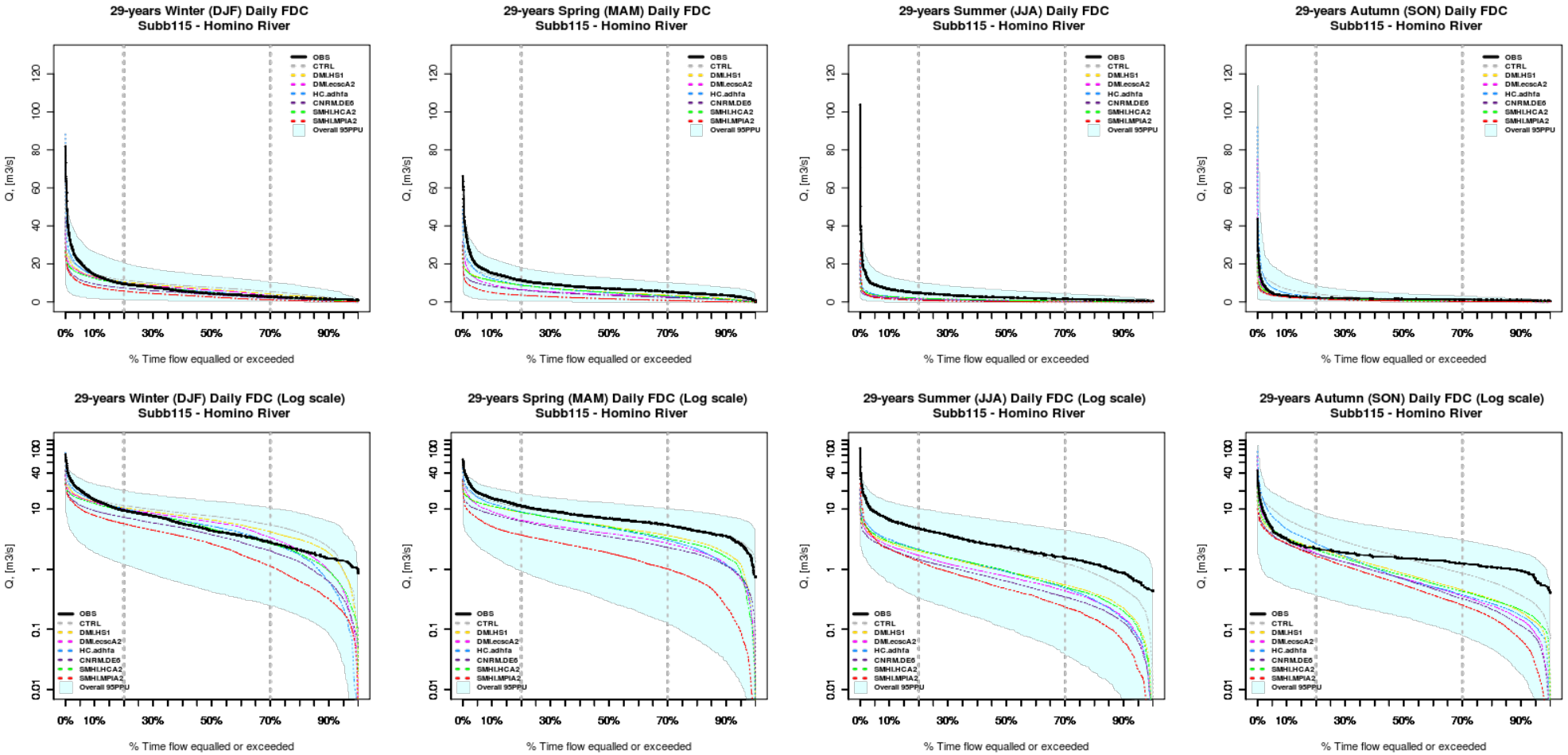

FIGURE 5.5: 29-years seasonal flow duration curves (FDCs) for subcatchment 115 (Homino River). From left to right, figures in the upper panel represent summer, spring, summer and autumn FDCs with a normal vertical scale, whereas figures on the bottom represent the same FDCs but with logarithmic vertical scale (removing zero values). Black continuous line is the observed seasonal FDC during the period 1962-1990, grey dotted line represent the median of the GLUE seasonal simulations for the same control period, and coloured dotted lines show the median of the seasonal simulations corresponding to different climate scenarios during the period 2072-2100. Shaded area represent the overall uncertainty due to the hydrological parameterisation adopted for GLUE simulations.

5.3.2 Projected Changes in Q5, Q50 and Q95

5.3.2.1 Overall Impacts

Figures 5.6 and 5.7 provide information about projected changes for different flow magnitudes in the two selected catchments: Q5, representing low flows, in the left hand side; Q50, representing medium flows, in the centre; and Q95, standing for high flows, at the right hand side of the figures. Vertical black dotted lines represent the observed value of the three analysed percentiles during the 29-years control period 1962-1990 (the first year 1961 was excluded from the analysis because it was used as spin-up period for the hydrological simulations, and we decided to use the same 29-years basis for all the analysis). Coloured continuous lines represent the weighted ECDF of the Q5, Q50 and Q95 percentiles for the six climate scenarios described in Table 4.1, computed according to the procedure described in section 5.2.4. In addition, the grey continuous line represent the weighted ECDF corresponding to simulations during the 29-years of the control period, which is presented in order to provide an estimation of the bias associated to the computation of streamflows of different magnitudes when using the hydrological model with the behavioural parameter sets selected for each one of the two selected catchments. A grey horizontal line is drawn for a value of the ECDF equal to 0.5, in order to easily visualize the value of Q50 for the weighted ECDF of each one of the analysed scenarios, which corresponds to the median of the hydrological simulations carried out for each scenario, using the behavioural parameter sets selected for each catchment in the uncertainty analysis described in section 3.4.2.

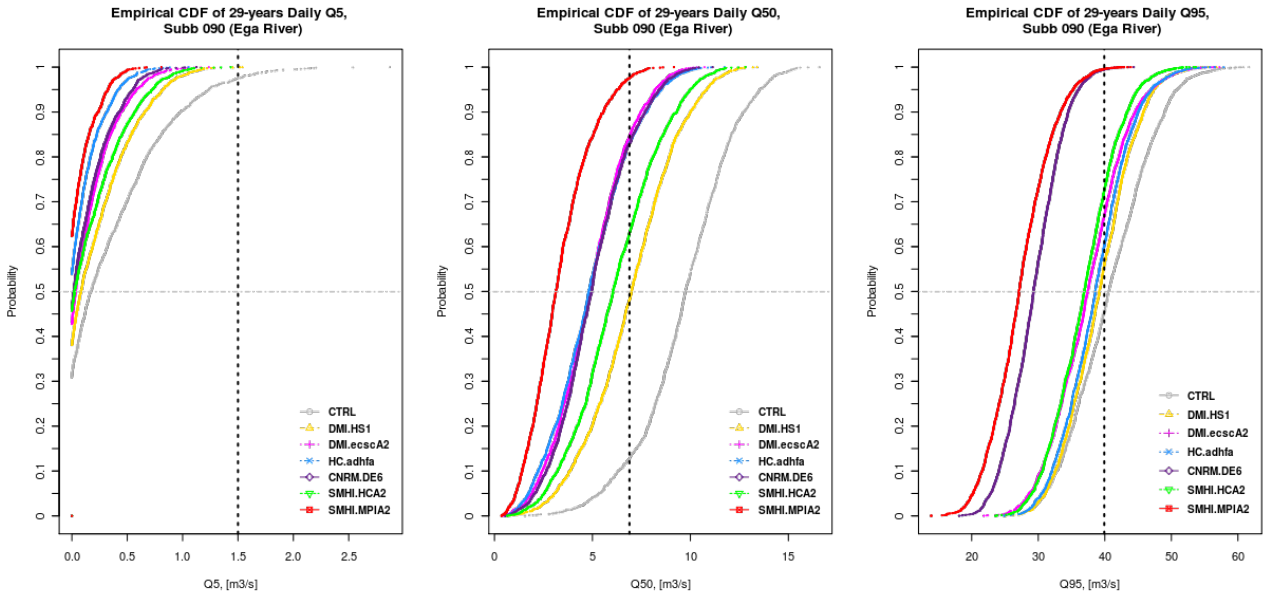

FIGURE 5.6: Empirical cumulative density function (ECDF) of streamflows in subcatchment 090 (Ega River). From left to right, figures represent the ECDF of low (Q5 percentile), medium (Q50 percentile), and high flows (Q95 percentile).

Looking at the left hand side of Figures 5.6 and 5.7, we can see that for both catchments the hydrological model introduced a large bias towards under-estimation of low flows (Q5) during the control period (depicted by a grey ECDF), because the observed Q5 is larger than ∼97% of the simulated Q5 for subcatchment 090, and larger than ∼75% of the simulated Q5 for subcatchment 115. However, still considering the under-estimation of Q5 by the hydrological simulations, it is possible to observe a slight projected reduction for low flows, because the medians of the Q5 for the six RCMs are lower than the median of the Q5 of the hydrological simulations during the control period, with the smallest reductions projected by simulations driven by DMI.HS1, and the largest reductions associated to simulations driven by SMHI.SMPIA2 in both catchments, representing conditions from the two different GCMs used to drive the selected RCMs. Larger relative

decreases are projected for the subcatchment with more semi-arid regime (115, Homino River), as depicted by the horizontal distance between the median Q5 during the control period and the median Q5 corresponding to each one of the future scenarios, along the horizontal line representing an accumulated probability of 0.5. Consequently, we are only able to make a qualitative assessment about *"small"* projected decreases in low flows (Q5) for both catchments, an any quantitative assessment must be interpreted taking into account the bias due to the hydrological modelling.

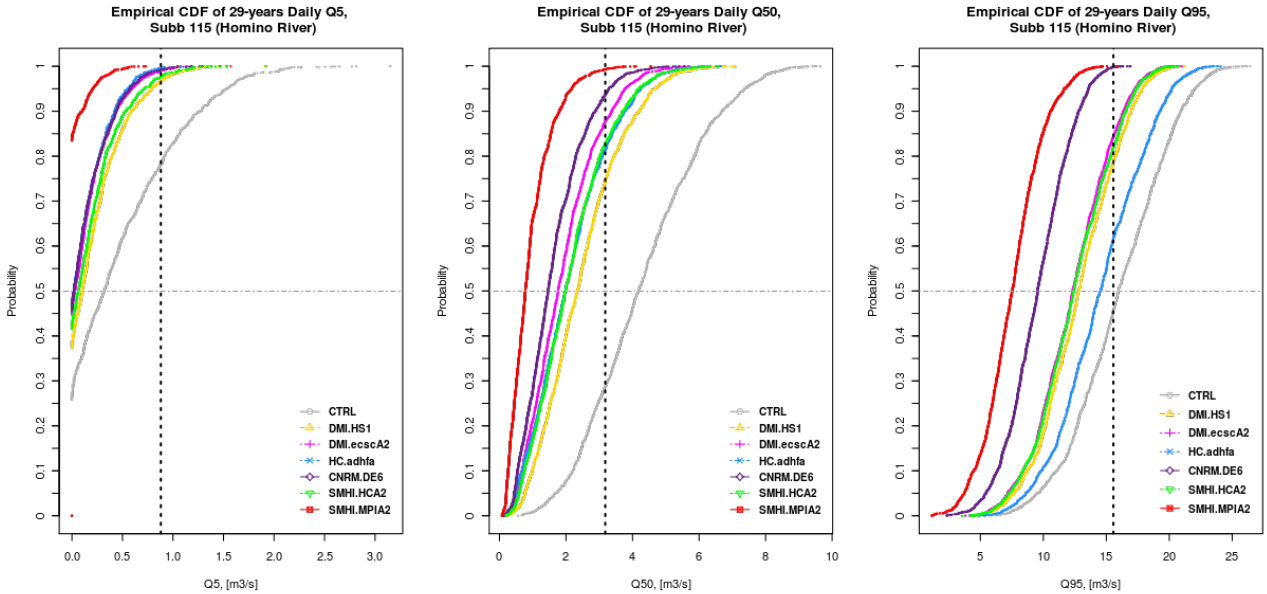

FIGURE 5.7: Empirical cumulative density function (ECDF) of streamflows in subcatchment 115 (Homino River). From left to right, figures represent the ECDF of low (Q5 percentile), medium (Q50 percentile), and high flows (Q95 percentile).

Regarding medium flows (Q50), it is observed that for both catchments the hydrological model introduced a bias towards over-estimation of medium flows (Q50) during the control period (depicted by the grey ECDF), because the observed Q50 is smaller than∼87% of the simulated Q50 for subcatchment 090, and smaller than ∼70% of the simulated Q5 for subcatchment 115. However, still considering the over-estimation of Q50 by the hydrological simulations, it is possible to observe a clear reduction projected for medium flows, because the medians of the Q50 for the six RCMs are lower than the median of the Q50 corresponding to the hydrological simulations during the control period, with the smallest reductions projected by simulations driven by DMI.HS1, and the largest reductions associated to simulations driven by SMHI.SMPIA2 in both catchments, representing conditions from the two different GCMs used to drive the selected RCMs. Relative projected decreases are similar for both subcatchments, as depicted by the horizontal distance between the median Q50 during the control period and the median Q50 corresponding to each one of the future scenarios, along the horizontal line representing an accumulated probability of 0.5. Again, we are only able to make a qualitative assessment about a projected decrease in medium flows (Q50) for both catchments, an any quantitative assessment must be interpreted under the umbrella of the bias due to the hydrological modelling.

Finally, looking at the right hand side of Figures 5.6 and 5.7, we can see that for both catchments the hydrological model reproduced almost perfectly the high flows (Q95) during the control period (depicted by a grey ECDF), because the observed Q95 is practically equal to the simulated Q95. It is possible to observe a general projected reduction of high flows, because the medians of the Q95 for the six RCMs are lower than the median of the Q95 corresponding to the simulations during the control period, with the smallest reductions projected by simulations driven by HC.adhfa and DMI.HS1 in subcatchment 090, and by simulations driven by HC.adhfa in subcatchment 115, whereas the largest reductions are associated to simulations driven by SMHI.SMPIA2 in both catchments, representing conditions from the two different GCMs used to drive the selected

RCMs. Projected decreases of high flows range from 0 to 40 % for subcatchment 090, and from 10 to 60% for subcatchment 115.

It is worth to mention that it is not surprising than low flows (Q5) have been under-estimated, the medium flows (Q50) have been slightly over-estimated, and the high flows of the overall time series have been perfectly reproduced by the hydrological simulations. The previous bias are a consequence of using the Nash-Sutcliffe efficiency as "*less formal*" likelihood for selecting the behavioural parameter sets in the GLUE procedure, because it is well know that this goodness-of-fit measure is biased towards high flows, due to the use of the squared of the residuals. The previously mentioned point makes very clear the importance of the criteria used to select the "*less formal*" likelihood in the GLUE procedure. We emphasize that **the goodness-of-fit measure used during the uncertainty analysis have to reflect the objective of the modelling study**, i.e., the use of a Nash-Sutcliffe efficiency may be very well suited to flood impact studies, whereas other goodness-of-fit not based on the use of the squared residuals (e.g. the modified index of agreement proposed by *Legates and McCabe Jr.*, 1999, or the modified Nash-Sutcliffe efficiency proposed by *Krause et al.*, 2005) may be better suited to low-flow impact studies, what is a well know fact in hydrology but hardly ever applied to studies regarding hydrological impacts of climate change.

5.3.2.2 Seasonal Impacts

Figures 5.8, 5.10, 5.12, and 5.14 show projected seasonal changes for low (Q5), medium (Q50) and high flows (Q95) in subcatchment 090 (Ega River), whereas Figures 5.9, 5.11, 5.13, and 5.15 depict the same changes for subcatchment 115 (Homino River). Again, vertical black dotted lines represent the observed value of the three analysed percentiles during the 29-years control period 1962-1990 (excluding the year 1961 from the analysis). Coloured continuous lines represent the weighted ECDFs of the Q5, Q50 and Q95 percentiles for the six climate scenarios described in Table 4.1, computed according to the procedure described in section 5.2.4. In addition, the grey continuous line represent the weighted ECDF corresponding to simulations during the 29-years of the control period, which is presented in order to provide an estimation of the bias associated to the computed streamflows of different magnitudes when using the hydrological model with the behavioural parameter sets selected for each one of the two selected catchments. A grey horizontal line is drawn for a value of the ECDF equal to 0.5, in order to easily visualize the value of Q50 for the weighted ECDF of each one of the analysed scenarios, which corresponds to the median of the hydrological simulations carried out for each scenario. This analysis is identical to the one carried out for the overall values in the previous section 5.3.2.1, and only the projected seasonal changes for Q50 will be discussed, as representative of the expected changes for each season, and similar analysis can be made for the seasonal Q5 and Q95.

a) **Winter (DJF)**

The two analysed catchments presents a large bias in the estimation of the winter Q50, in particular, practically all the simulated values of winter Q50 for subcatchment 090 are larger than the observed Q50 during the control period, and almost 95% of the simulated Q50 for subcatchment 115 are larger than its corresponding observed Q50. When considering as simulated winter Q50 the value obtained by the median of the Q50 computed with the behavioural parameter sets during the control period, the over-estimation in the seasonal Q50 correspond to $\sim$70% and $\sim$60% for subcatchments 090 and 115, respectively. Consequently, projected changes for these winter medium with respect to the observed winter Q50 must be interpreted with care. The increase in Q50 for subcatchment 090 ranges from $\sim$7% (DMI.HS1) to $\sim$85% (SMHI.MPIA2), but this is very likely due to the 70% of over-estimation intrinsic to the hydrological simulations rather than to climate change. At the other hand, projected changes in Q50 for subcatchment 115 range from $\sim$-60% (SMHI.MPIA2) to $\sim$+60% (DMI.HS1), so when the 60% of overestimation due to hydrological modelling is taken into account, the more likely projected change for winter flows in this catchment is a decrease, that may range from 0 to 120%, but this can only be confirmed by further simulations tailored to better represent winter flows. The only clear pattern is that the simulations driven by DMI.HS1 and SMHI.MPIA2 encompass the simulation driven by the other climate sce-

narios.

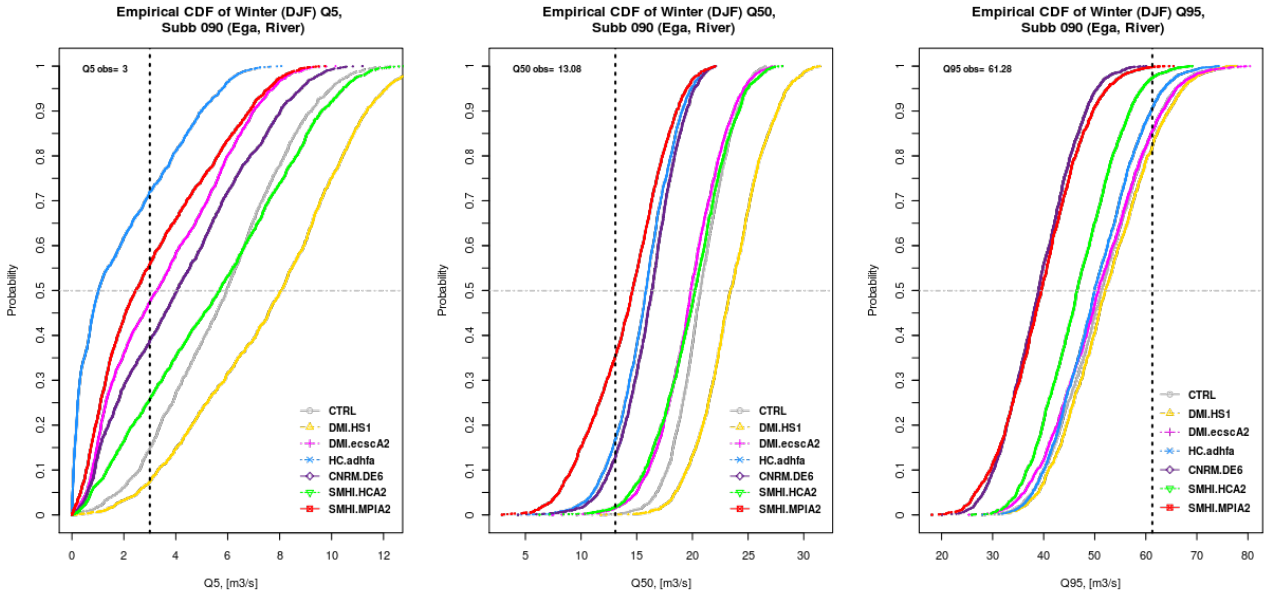

FIGURE 5.8: Empirical cumulative density function (ECDF) of winter (DJF) flows in subcatchment 090 (Ega River). From left to right, figures represent the ECDF of low (Q5 percentile), medium (Q50 percentile), and high winter flows (Q95 percentile).

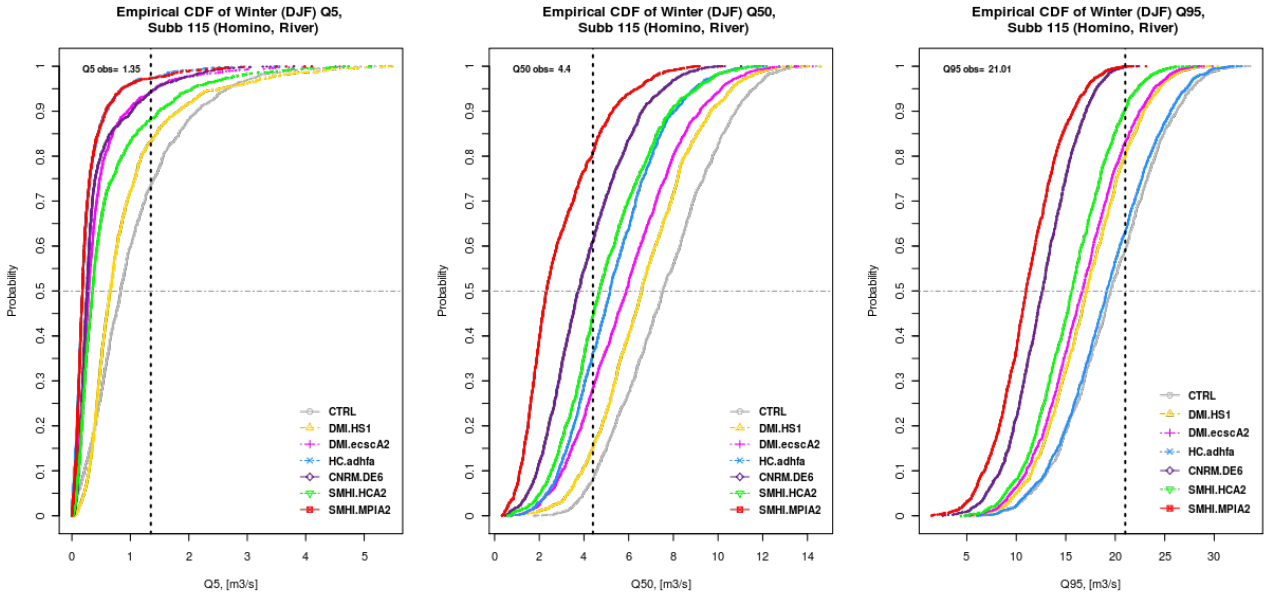

FIGURE 5.9: Empirical cumulative density function (ECDF) of winter (DJF) flows in subcatchment 115 (Homino River). From left to right, figures represent the ECDF of low (Q5 percentile), medium (Q50 percentile), and high winter flows (Q95 percentile).

b) **Spring (MAM)**

For the two analysed catchments the hydrological model provides a fairly good representation of the spring Q50, in particular for subcatchment 115, where the median of the simulated values of spring Q50 is practically equal to the observed Q50 during the control period, whereas subcatchment 090 presents a slight bias towards over-estimation, because 65% of the simulated Q50 for this catchment are larger than its corresponding observed Q50. When considering as simulated spring Q50 the value obtained by the median of the Q50 computed with the behavioural parameter sets during the control period, the over-estimation in the seasonal Q50 is ∼7% for subcatchments 090

and may be neglected for subcatchment 115. Consequently, projected changes for these spring medium flows with respect to the observed spring Q50 can be considered reliable (within the set of assumptions adopted in this dissertation). There is a general projected decrease in spring Q50 for both subcatchments, ranging from ∼-14% (DMI.HS1) to ∼-64% (SMHI.MPIA2) for subcatchment 090, and from ∼-28% (DMI.HS1) to ∼-80% (SMHI.MPIA2). Again, simulations driven by DMI.HS1 and SMHI.MPIA2 encompass the simulation driven by the other climate scenarios.

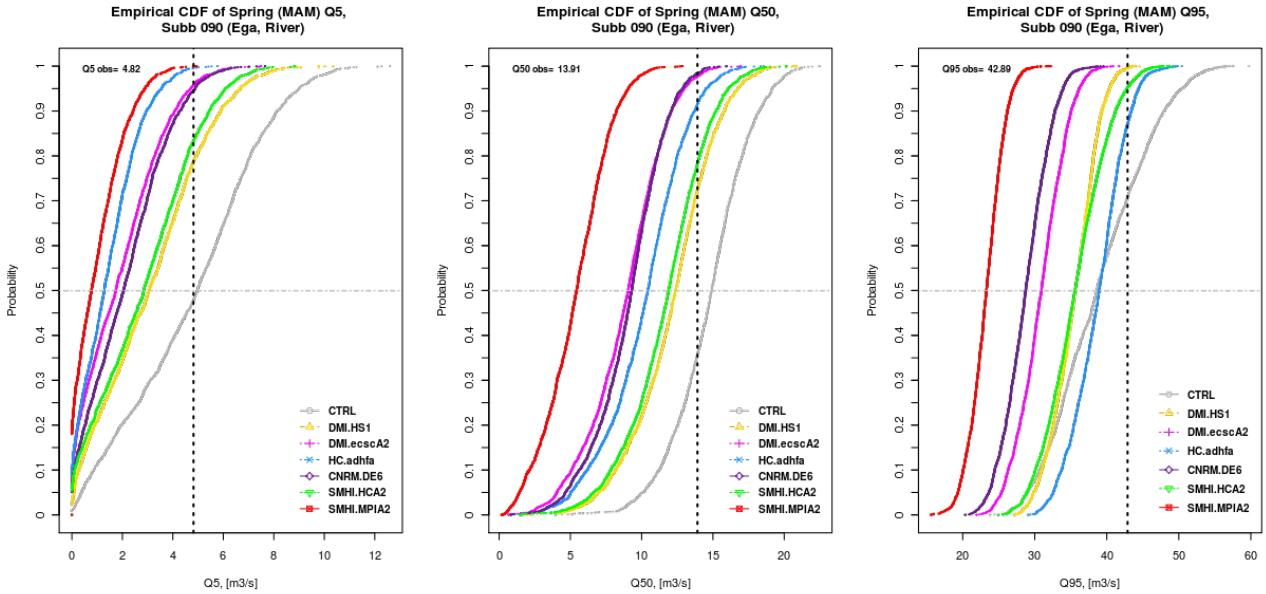

FIGURE 5.10: Empirical cumulative density function (ECDF) of spring (MAM) flows in subcatchment 090 (Ega River). From left to right, figures represent the ECDF of low spring flows (Q5 percentile), medium spring flows (Q50 percentile), and high spring flows (Q95 percentile).

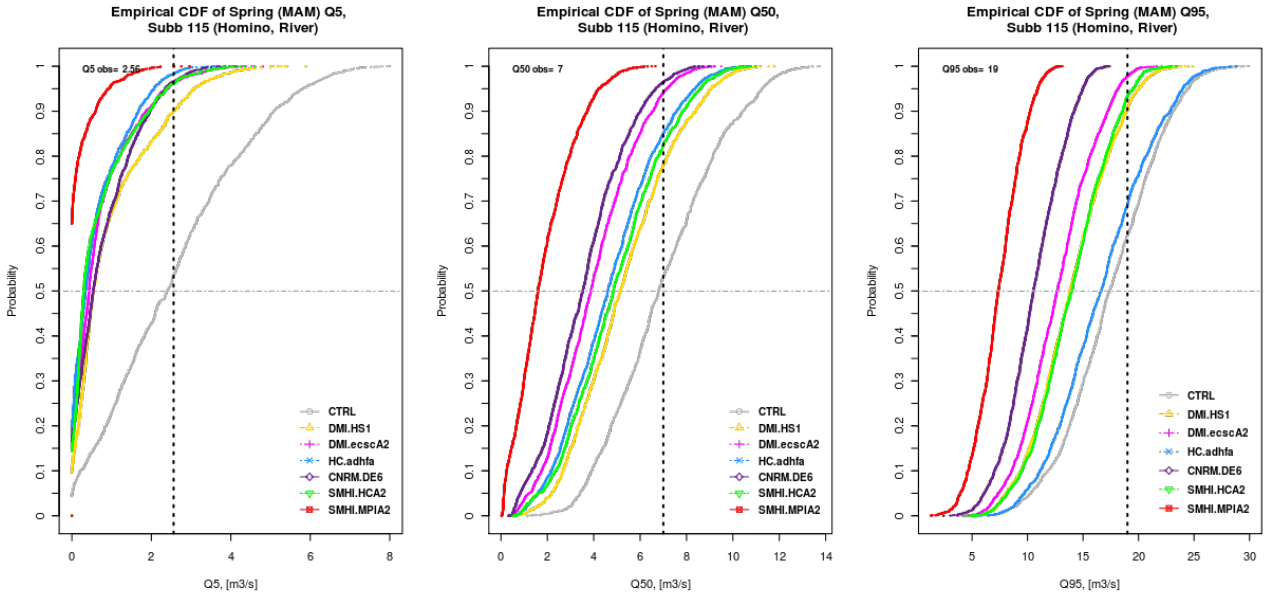

FIGURE 5.11: Empirical cumulative density function (ECDF) of spring (MAM) flows in subcatchment 115 (Homino River). From left to right, figures represent the ECDF of low (Q5 percentile), medium (Q50 percentile), and high spring flows (Q95 percentile).

c) **Summer (JJA)**

The two analysed catchments expect a general decrease of summer Q50 flows, but with different skill of the hydrological model. In particular, hydrological simulations in subcatchment 115 provide a fairly good representation of the summer Q50, because the median of the simulated values is very close to the observed Q50 during the control period, whereas subcatchment 090 presents a bias towards under-estimation, because almost 80% of the simulated Q50 for this catchment are lower than its corresponding observed Q50. When considering as simulated summer Q50 the value obtained by the median of the Q50 computed with the behavioural parameter sets during the control period, the under-estimation in the seasonal Q50 correspond to ∼45% and ∼10% for subcatchments 090 and 115, respectively. Consequently, projected changes for summer medium flows with respect to the observed Q50 must be interpreted with care for subcatchment 090, and can be considered as reliable for subcatchment 115 (within the set of assumptions adopted in this dissertation). The projected decrease in the seasonal Q50 for subcatchment 090, with respect to the Q50 observed during the control period, ranges from ∼-75% (DMI.HS1/SMHI.HCA2) to ∼-95% (SMHI.MPIA2), but an important part of this projected decrease is due to the 45% of under-estimation intrinsic to the hydrological simulations rather than to climate change. At the other hand, projected changes in Q50 for subcatchment 115 (Homino River, with a more arid regime) range from ∼-60% (DMI.HS1/SMHI.HCA2) to ∼-90% (SMHI.MPIA2), so still considering the 10% of under-estimation due to hydrological modelling, the more likely change for summer flows in this catchment is a general decrease. This time, simulations of the climate scenarios are encompassed by simulations driven by DMI.HS1/SMHI.HCA2 and SMHI.MPIA2.

d) **Autumn (SON)**

The two analysed catchments expect a general decrease of autumn Q50 flows, but with different skill of the hydrological model. In particular, hydrological simulations in subcatchment 115 provide a fairly good representation of the autumn Q50, where the median of the simulated values of summer Q50 is practically equal to the observed Q50 during the control period, whereas subcatchment 090 presents a slight bias towards under-estimation, because almost 65% of the simulated Q50 for this catchment are lower than its corresponding observed Q50. When considering as simulated autumn Q50 the value obtained by the median of the Q50 computed with the behavioural parameter sets during the control period, the under-estimation in the seasonal Q50 correspond to ∼15% for subcatchments 090 and can be neglected for subcatchment 115. Consequently, projected changes for autumn medium flows with respect to the observed Q50 must be interpreted with some care for subcatchment 090, and can be considered as reliable for subcatchment 115 (within the set of assumptions adopted in this dissertation). The projected decrease in the seasonal Q50 for subcatchment 090, with respect to the Q50 observed during the control period, ranges from ∼-40% (DMI.HS1) to ∼-60% (SMHI.MPIA2/HC.adhfa), so still considering the 15% of under-estimation due to hydrological modelling, the more likely change for autumn flows in this catchment is a general decrease. At the other hand, projected changes in seasonal Q50 for subcatchment 115 (Homino River) range from ∼-40% (DMI.HS1) to ∼-73% (SMHI.MPIA2). Climate scenarios are encompassed by simulations driven by DMI.HS1 and SMHI.MPIA2.

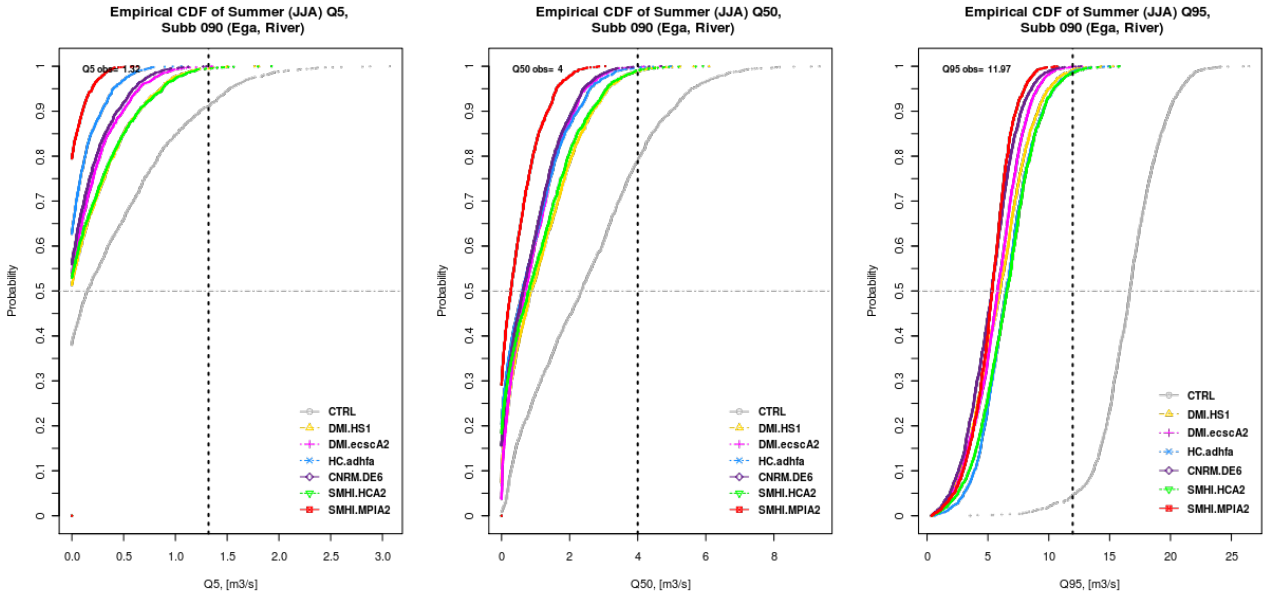

FIGURE 5.12: Empirical cumulative density function (ECDF) of summer (JJA) flows in subcatchment 090 (Ega River). From left to right, figures represent the ECDF of low (Q5 percentile), medium (Q50 percentile), and high winter flows (Q95 percentile).

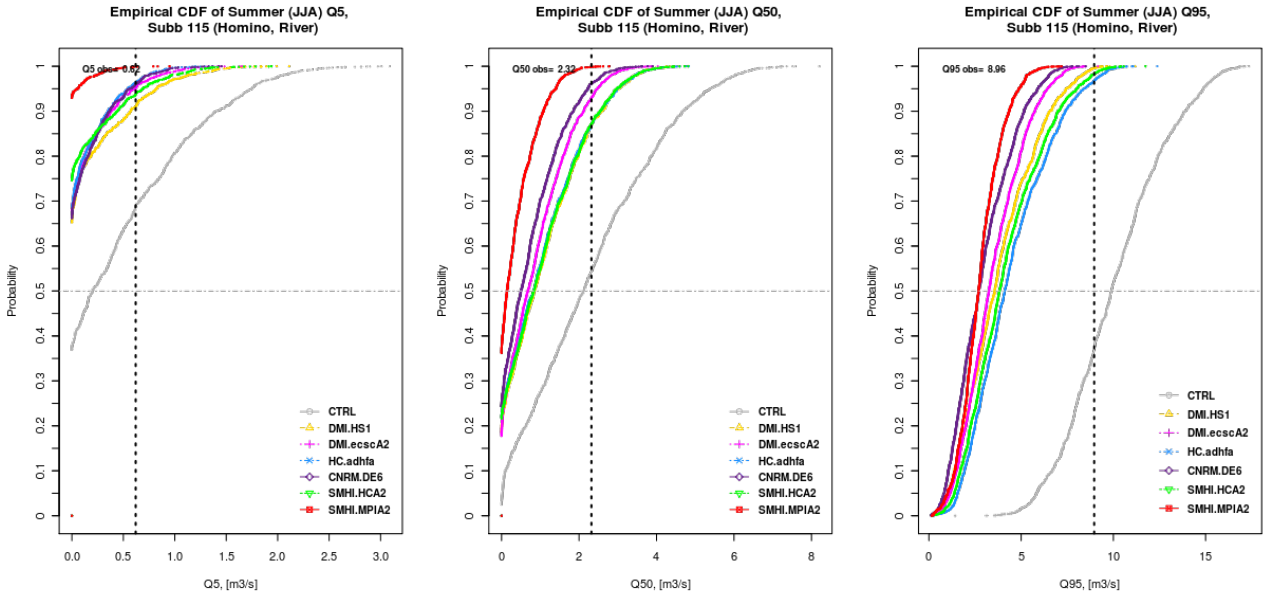

FIGURE 5.13: Empirical cumulative density function (ECDF) of summer (JJA) flows in subcatchment 115 (Homino River). From left to right, figures represent the ECDF of low (Q5 percentile), medium (Q50 percentile), and high summer flows (Q95 percentile).

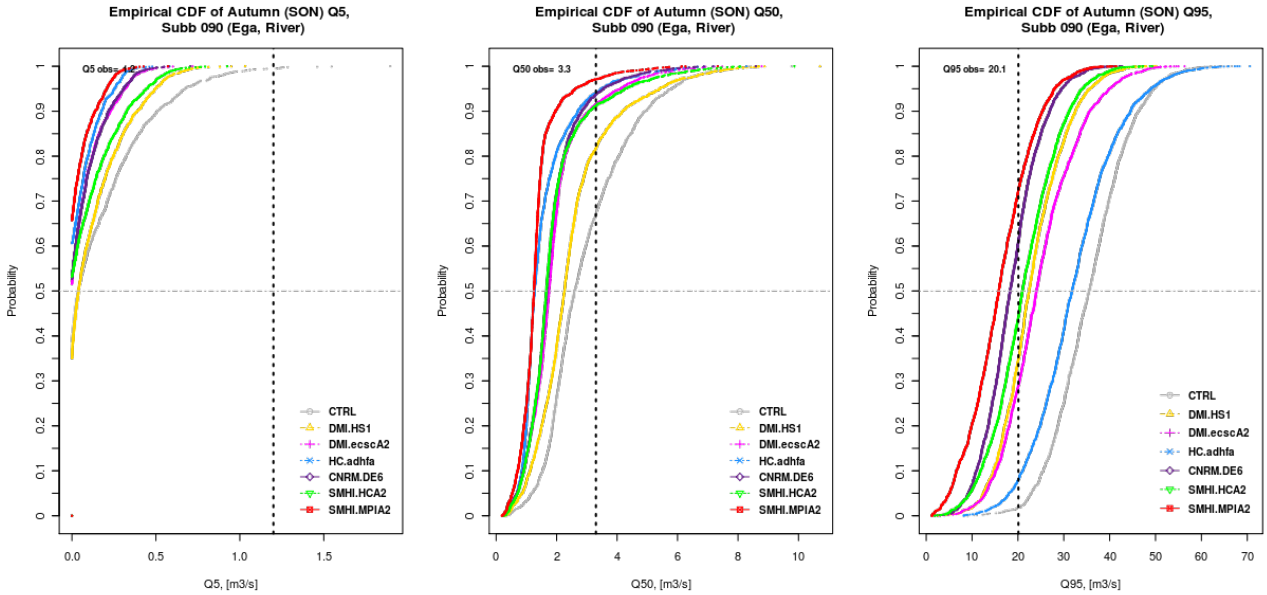

FIGURE 5.14: Empirical cumulative density function (ECDF) of autumn (SON) flows in subcatchment 115 (Homino River). From left to right, figures represent the ECDF of low autumn flows (Q5 percentile), medium autumn flows (Q50 percentile), and high autumn flows (Q95 percentile).

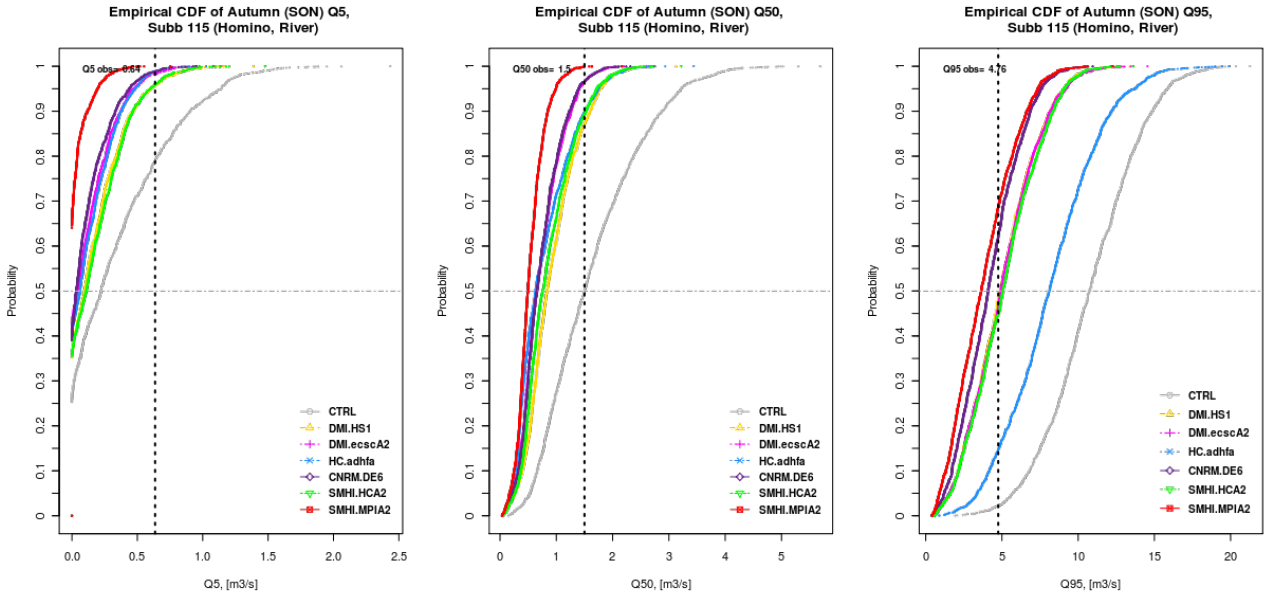

FIGURE 5.15: Empirical cumulative density function (ECDF) of autumn (SON) flows in subcatchment 115 (Homino River). From left to right, figures represent the ECDF of low (Q5 percentile), medium (Q50 percentile), and high autumn flows (Q95 percentile).

It is worth to mention that the bias observed for the estimation of low and medium flows by the hydrological model, discussed during the analysis of the overall time series in section 5.3.2.1, was not observed during the seasonal analysis. The reason for not observing a clear pattern for the bias in the estimation of seasonal values rely in the fact that the goodness-of-fit used during the uncertainty analysis considered the time series during the control period as a whole, without making any distinction for seasonal values.

5.4 Summary and Conclusions

Bias-corrected daily time series of precipitation and air temperature were derived from an ensemble of six climate change scenarios, selected from the EU FP5 PRUDENCE project, and were then used to drive daily hydrological simulations for the period 2071-2100 on two selected subcatchments of the Ebro River basin (090, Ega River and 115, Homino River). For each climate scenario, a number of simulations equal to the number of behavioural parameter sets obtained during the uncertainty analysis (see Chapter 3) was carried out. Resulting streamflows were used to compute 29-years daily flow duration curves (FDCs) to provide a qualitative assessment of the relative importance of uncertainties coming from the choice of the driving RCM and from hydrological parameterisation. Also, streamflows derived from each climate scenario were used to compute empirical cumulative density functions (ECDFs) of three selected percentiles, representing different flow magnitudes: Q5 (low flows), Q50 (medium flows) and Q95 (high flows), in order to provide a quantitative assessment of the projected changes in streamflows. The main findings of this chapter can be summarized as follow:

- In the two analysed catchments the hydrological parametric uncertainty was larger than the uncertainty coming from the driving RCM, both during the complete future period and for each one of the four seasons. However, this result can not be generalised, because it is conditional to decisions taken during the uncertainty analysis and to the ensemble of RCMs considered. We argue that the decision about the efficiency measure to be used as "*less formal*" likelihood and the cut-off threshold used to separate behavioural from non-behavioural parameter sets must be taken during the uncertainty analysis of the control period, in a dialogue between the modeller and the decision-maker, taking into account the objectives of the study along with data and model availability.

- FDCs in normal and logarithmic scales were used to assess the relative importance of the uncertainties for different streamflow magnitudes. In general, the absolute hydrological parametric uncertainty is larger for high flows than for low ones, whereas the relative uncertainties are larger for low flows than for high ones.

- Comparison of the observed and simulated FDCs during the control period 1962-1990 show that the median of the hydrological simulations, for the two selected catchments, provides a good representation of high flows, a slight over-estimation of medium flows, and a relative large under-estimation of low flows, what is not surprising due to the use of the Nash-Sutcliffe efficiency as "*less formal*" likelihood to select the behavioural parameter sets. These bias remained during the future scenarios, and were considered in the interpretation of projected impacts of climate change.

- Projected changes in the overall hydrological regime of the two selected catchments may depend on the magnitude of river flows under consideration. For subcatchment 090 (Ega River), the one with more humid regime, the highest flows are expected to decrease; medium-high and medium flows present contradictory projections depending on the driving RCM; and medium-low and low flows are expected to decrease, with the largest relative decrease for the lower river flows. At the other hand, subcatchment 115, the one with more semi-arid regime, expect a general decrease of streamflows in the full range of magnitudes, and again the larger relative decreases are expected for the lower river flows. If the relative under-estimation of the low flows during the control period is taken into account, the large decrease is less dramatic, but still important.

- Regarding the differences due to the driving RCM, the smallest decreases in the overall streamflows are projected for simulations driven by the DMI.HS1 RCM, whereas the largest decreases are expected for simulations driven by SMHI.MPIA2. The previous projected changes are in full agreement with projections for annual precipitation and temperature, where SMHI.MPIA2 projected the largest decrease in annual precipitation (-21%) and the

largest increase in mean annual temperature (+ 6.24 °C), whereas DMI.HS1 RCM projected the lower decrease in annual precipitation (-4%) and one of the lower increases in mean annual temperature (+4.19 °C). The two aforementioned RCMs represent conditions from the two different GCMs considered is the future climate scenarios. In this way, climate scenarios derived from the two different GCMs used in this dissertation provided the extreme expected changes in streamflows by the end of this century.

- For both catchments the hydrological model introduced a large bias towards under-estimation of low flows (Q5) during the control period. Consequently, we are only able to make a qualitative assessment about "*small*" projected decreases in low flows (Q5) for both catchments, with the smallest reductions projected by simulations driven by DMI.HS1, and the largest reductions associated to simulations driven by SMHI.SMPIA2 in both catchments.

- Regarding medium flows (Q50), for both catchments the hydrological model introduced a bias towards over-estimation of medium flows (Q50) during the control period. Again, we are only able to make a qualitative assessment about a projected decrease of medium flows (Q50) for both catchments, with the smallest reductions projected by simulations driven by DMI.HS1, and the largest reductions associated to simulations driven by SMHI.SMPIA2 in both catchments

- The hydrological model reproduced almost perfectly the high flows (Q95) of both catchments during the control period. A general projected reduction of high flows is expected for both catchments, with the smallest reductions projected by simulations driven by HC.adhfa and DMI.HS1 in subcatchment 090, and by simulations driven by HC.adhfa in subcatchment 115; whereas the largest reductions are associated to simulations driven by SMHI.SMPIA2 in both catchments. Projected decreases range from 0 to 40 % for subcatchment 090, and from 10 to 60% for subcatchment 115.

- It is not surprising the under-estimation of low flows, the slight over-estimation of medium flows, and the fairly good representation of high flows of the overall time series by the hydrological model. The previous bias are a consequence of using the Nash-Sutcliffe efficiency as "*less formal*" likelihood for selecting the behavioural parameter sets in the GLUE procedure. We emphasize that **the goodness-of-fit measure used during the uncertainty analysis have to reflect the objective of the modelling study**, i.e., the use of a Nash-Sutcliffe efficiency may be very well suited to flood impact studies, whereas other goodness-of-fit may be better suited to low-flow impact studies, what is a well know fact in hydrological modelling but hardly ever applied to studies regarding hydrological impacts of climate change.

- The aforementioned pattern for the bias in the estimation of different streamflow magnitudes was not observed during the seasonal analysis, because the goodness-of-fit used during the uncertainty analysis considered the time series as a whole, without taking into account seasonal differences.

- During winter (DJF), in both catchments the absolute hydrological parametric uncertainty is larger for high flows than for low ones, whereas the relative uncertainties are important for all streamflow magnitudes. Comparison of the observed and simulated FDCs during the control period 1962-1990 shows that the median of the hydrological simulations, provides a general good representation of the high seasonal flows in both catchments, whereas medium an low flows are generally over-estimated for both catchments. Projected changes in the winter regime of the two selected catchments depend on the magnitude of river flows under consideration. The two analysed catchments expect a general decrease of high flows. Medium flows are expected to increase for subcatchment 090 and present contradictory projections for subcatchment 115. Low flows are expected to increase in subcatchment 090, whereas they present contradictory projections for subcachment 115. The smallest drops in high flows and the larger increments in medium and low flows are projected for simulations

driven by the DMI.HS1 RCM, whereas the larger drops in high flows and the lower increments in medium and low flow correspond to simulations driven by SMHI.MPIA2. The previous projected changes present a general agreement with projections for winter precipitation and temperature.

- During winter (DJF) there is a large bias in the estimation of Q50 for both catchments. The increase in Q50 for subcatchment 090 ranges from ∼7% (DMI.HS1) to ∼85% (SMHI.MPIA2), but this is very likely due to the 70% of over-estimation intrinsic to the hydrological simulations rather than to climate change. At the other hand, projected changes in Q50 for subcatchment 115 ranges from ∼-60% (SMHI.MPIA2) to ∼+60% (DMI.HS1), so when the 60% of overestimation due to hydrological modelling is taken into account, the more likely projected change for winter flows in this catchment is a decrease, that may range from 0 to 120%, but this can only be confirmed by further simulations tailored to better represent winter flows. The only clear pattern is that the simulations driven by DMI.HS1 and SMHI.MPIA2 encompass the simulations driven by the other climate scenarios.

- During spring (MAM) the absolute hydrological parametric uncertainty is larger for high flows than for low ones in both catchments, whereas the relative uncertainties are important for all streamflow magnitudes in both catchments. Comparison of the observed and simulated FDCs during the control period 1962-1990 shows that the median of the hydrological simulations provides a fairly good representation of all the streamflow magnitudes in both catchments. A general decrease is expected for spring flows of the two selected catchments, which do not depend on the magnitude of river flows under consideration. The smallest drops in spring streamflows are projected for simulations driven by the DMI.HS1 RCM, whereas the larger drops correspond to simulations driven by SMHI.MPIA2, what is in general agreement with projections for seasonal precipitation and temperature.

- During spring (MAM), for the two analysed catchments the hydrological model provides a fairly good representation of Q50. There is a general projected decrease in spring Q50 for both subcatchments, ranging from ∼-14% (DMI.HS1) to ∼-64% (SMHI.MPIA2) for subcatchment 090, and from ∼-28% (DMI.HS1) to ∼-80% (SMHI.MPIA2) for subcatchment 115. Again, simulations driven by DMI.HS1 and SMHI.MPIA2 encompass the simulations driven by the other climate scenarios.

- During summer (JJA), the absolute hydrological parametric uncertainty is only important for high flows in both catchments, because there is a general agreement among the projections of the six scenarios that medium and low flows will be less than 1 m^3/s in both catchments, whereas the relative uncertainties are equally large for all the streamflow magnitudes. Comparison of the observed and simulated FDCs during the control period 1962-1990 shows different behaviours for each catchment. Subcatchment 090 shows a general good representation of high flows, whereas medium and low flows are generally under-estimated. At the other hand, subcatchment 115 shows a good representation of high and medium flows and a slight under-estimation of low flows. A general decrease is expected for summer flows of the two selected catchments, which do not depend on the magnitude of river flows under consideration. The smallest drops in summer streamflows are projected for simulations driven by the SMHI.HCA2 and DMI.HS1 RCMs, whereas the larger drops are -in general- derived from simulations driven by SMHI.MPIA2. The previous changes projected by different climate scenarios do not present a clear relationship with projections for the corresponding seasonal precipitation and temperature, what may be due to spatial variations of the climatological fields.

- During summer (JJA), the two analysed catchments expect a general decrease of summer Q50 flows, but with different skill of the hydrological model. The projected decrease in the seasonal Q50 for subcatchment 090, with respect to the Q50 observed during the control period, ranges from ∼-75% (DMI.HS1/SMHI.HCA2) to ∼-95% (SMHI.MPIA2), but an

important part of this projected decrease is due to the 45% of under-estimation intrinsic to the hydrological simulations rather than to climate change. At the other hand, projected changes in Q50 for subcatchment 115 range from ∼-60% (DMI.HS1/SMHI.HCA2) to ∼-90% (SMHI.MPIA2), so still considering the 10% of under-estimation due to hydrological modelling, the more likely change for summer flows in this catchment is a general decrease. The simulations of the six climate scenarios are encompassed by simulations driven by DMI.HS1/SMHI.HCA2 and SMHI.MPIA2.

- During autumn (SON), the absolute hydrological parametric uncertainty is larger for high flows than for low ones, whereas the relative uncertainties are important for all streamflow magnitudes. Comparison of the observed and simulated FDCs during the control period 1962-1990 shows that the median of the hydrological simulations only provides a good representation of the highest flows in both catchments, whereas high and medium flows are over-estimated, and medium-low and low flows are under-estimated for both catchments. Projected changes in the autumn regime of the two selected catchments depend on the magnitude of river flows and the catchment under consideration. In sucatchment 090, the seasonal highest flows present contradictory projections, the medium-high flows expect a general increase, whereas medium-low to low flows expect a general decrease. At the other hand, subcatchment 115 present contradictory projections for high and medium-high flows, whereas the medium-low and low flows expect a general decrease. There is not a clear pattern related to differences due to the driving RCM, what may be due the contradictory projections for autumn precipitation given by the six RCMs.

- The two analysed catchments expect a general decrease of autumn (SON) Q50 flows, but with different skill of the hydrological model. The projected decrease in the seasonal Q50 for subcatchment 090 ranges from ∼-40% (DMI.HS1) to ∼-60% (SMHI.MPIA2/HC.adhfa), so still considering the 15% of under-estimation due to hydrological modelling, the more likely change for autumn flows in this catchment is a general decrease. At the other hand, projected changes in seasonal Q50 for subcatchment 115 (Homino River) range from ∼-40% (DMI.HS1) to ∼-73% (SMHI.MPIA2). Climate scenarios are encompassed by simulations driven by DMI.HS1 and SMHI.MPIA2.

- The bias of the hydrological model in representing some seasonal river flows or flows with a certain magnitude may be comparable to the projected changes in those flows (e.g., the observed Q5 in subcatchment 090, Ega River, is larger than 97% of the corresponding simulated values during the control period), hampering a correct interpretation of projected changes in future streamflows.

- Following what mentioned at the end of the previous chapter, by no means it should be thought that the hydrological impacts of climate change expected for the two selected catchments will certainly lie between the specific ranges given in this chapter. Additional uncertainties (reliability of SRES scenarios, skill of the GCM/RCM to provide a realistic response to a emission forcing that have been never observed before, small number of driving GCMs considered in this dissertation as boundary conditions of the future scenarios, downscaling technique, unforeseen natural phenomena, unconsidered changes in land use and/or soil properties, consideration of different hydrological model structures, errors in input data, etc.) add additional complexity to the *cascade of uncertainty* involved in the impact assessment. However, it can be claimed that we explored some possible scenarios of future climate, with the best information available at this moment, and that the projected hydrological impacts provided in this chapter correspond to the best projections we can make based on our imperfect knowledge of this challenging topic.

"Live as if you were to die tomorrow.
Learn as if you were to live forever."
(Mahatma Gandhi)

6 Discussion

Projected changes in water resources due to climate change are often used to design mitigation plans, to determine if a new infrastructure should or should not be constructed, and to decide the destination of important amount of funds that could be spent in dealing with other important problem. Therefore, quantification of the reliability of hydrological predictions has a societal importance, and the correct understanding, treatment and communication of the uncertainties involved in the assessment of the likely impacts of climate change, not only must not be underestimated, but it has to be undertaken with a major responsibility.

This dissertation developed a framework to provide probabilistic projections of future river flows, taking into account uncertainties coming from the hydrological parameterisation used to represent the catchment response to a given climatological forcing, and its interactions with different climate change scenarios used to sample the space of future climates expected by the end of this century. The approach developed in this dissertation differs from previous studies related to propagation of hydrological parametric uncertainty into projections of hydrological impacts of climate change, as (a) it allows to select parameter sets to be used in hydrological simulations of future scenarios based on an objective criteria, i.e, a user-defined minimum percentage of observations embraced by the uncertainty bounds; (b) it presents an assessment of the streamflow magnitudes that are better/worse represented by the hydrological model; and (c) it provides probabilistic information about projected seasonal changes in low, medium and high streamflows, taking into account the bias of the hydrological model in representing the catchment response.

This chapter provides a discussion of the main findings already presented in previous chapters, and some advice for further research in this area.

6.1 Uncertainty analysis during control period (1961-1990)

- Results of the GLUE analysis indicated that two main parameters dominate the fast response of the two selected catchments (*CN2*, *SOL_K*), and two additional parameters are necessary to explain the slow catchment response (*RCHRG_DP*, *GW_DELAY*). However, experimental simulations carried out with only five parameters did not provide uncertainty bounds able to encompass more than 75% of the observations during the control period, making evident that the other parameters -notwithstanding are not well identified- help to partially compensate by equifinallity problems derived from the simple structure adopted to represent the catchment behaviour.

- A clear definition of what is considered as an "*unacceptable high*" value of predictive uncertainty have to be made at the beginning of the modelling study, between the final user and the modeller. That definition may be used latter to assess the predictive capabilities of the hydrological model, and it may be considered as an objective criterion for rejecting the conceptual model structure adopted, to review the quality of the input data, or to decide changing the goodness-of-fit used to measure how close simulated values are from observations. We propose to use *a priori* overall/annual/seasonal values of P-factor and R-factor for this purpose.

- FDCs plotted with logarithmic scale proved to be useful to visualize the relative importance of uncertainties for different streamflow magnitudes. In particular, the use of the Nash-Sutcliffe efficiency to measure the goodness-of-fit between simulations and observed values led to obtain larger relative uncertainties for the estimation of low flows, but with an small absolute importance when compared to the magnitude of the uncertainties associated to medium and high flows. This could be deemed acceptable for a flood impact study, but it may not be well suited for making projections regarding hydrological droughts.

- In the two selected catchments, the parameter set that achieved the highest NS_{eff} during calibration was not the same that achieved the highest efficiency during the verification period, emphasizing the importance of not considering one single "*best*" simulation, but considering several acceptable simulators of the system.

- The fact that many combinations of model structure and parameter sets may be deemed as acceptable simulators of the two catchments under study, only means that we could not reject a larger number of them based on the available data, criteria of acceptance, and knowledge. Additional data are needed to discard some of them. Uncertainty arising from equifinallity may be though as a decision-making problem subject to imperfect knowledge and limited data, but we claim that those limitations, when made explicit to the final users, may lead to better decisions than those taken on the basis of a single "*best*" simulation during the control period, which is *expected* to perform equally well under unknown future conditions.

- The previous point put in evidence the importance of collecting data, and to look for its quality, because even a hypothetical *perfect* model, without data is nothing more than numbers and beautiful plots.

- We want to emphasize that prediction limits obtained with GLUE are highly dependent on decisions taken by the modeller, mainly: what model structure(s) is(are) used to represent the catchment behaviour (not analysed here), what input data are used to drive the hydrological simulations (not explicitly dealt in this dissertation), which and how many parameters are selected for the uncertainty analysis, what parameter ranges are sampled for each parameter, which likelihood measure is used to assess the performance of different parameter sets, the threshold selected to discriminate between behavioural and non-behavioural simulators, and the way in which all the previous choices are combined, as expressed by other authors (e.g. *Beven and Freer*, 2001; *Montanari*, 2005).

6.2 Projected changes in climate (2071-2100)

- The seasonal changes on the meteorological driving forces may have important effects on the water availability of the Ebro River basin, because the predicted increments in mean temperature and decreases in mean precipitation are concentrated during seasons characterized by intense irrigation activities, and a hydrological modelling work that incorporates the impacts of these meteorological drivers on agriculture and energy should prove be very useful for decision makers aiming at avoiding a future crisis in those strategic sectors.

- The use of a multi-model ensemble of six RCMs allowed to take into account uncertainties coming from numerical schemes and parameterisation used by different climate models. However, the small number of RCMs considered in this dissertation, and in particular the use of only two GCMs to provide boundary conditions for the future climate scenarios, should not be considered as a representative sample of the complete range of expected future climates on the basin. However, the use of such ensemble of high resolution RCMs is an advance over studies based on GCM outputs, and it includes the best available data we had at the moment.

- The chosen future climate scenarios provided very different projections of bias-corrected annual, seasonal and monthly temperature and precipitation fields, even under the same emissions scenario (the medium-high SRES A2 in this dissertation). However, extreme projected changes were given by climate scenarios that used boundary conditions from the two different GCMs used in this dissertation. This proves that the use of ensemble of future climate scenarios, driven by different GCMs, should be a mandatory step in any hydrological study aiming at providing a better assessment of the full range of likely changes in climate.

- By no means it should be thought that the future changes in climate expected for the Ebro River basin will certainly lie between the ranges given in this dissertation. Additional uncertainties (reliability of SRES scenarios, skill of the GCM/RCM to provide a realistic response to a emission forcing that have been never observed before, small number of driving GCMs considered in this dissertation as boundary conditions of the future scenarios, unforeseen natural phenomena, etc.) sum additional degrees of freedom to an already complex issue. It can only be claimed that we explored some possible scenarios of future climate, with the best information we had at this moment, and that the results provided here correspond to the best projections we could make based on our imperfect knowledge about a very complex, heterogeneous and non-linear problem.

6.3 Hydrological impacts of climate change (2071-2100)

Bias-corrected daily time series of precipitation and temperature were derived from an ensemble of six climate change scenarios, selected from the EU FP5 PRUDENCE project, and were then used to drive daily hydrological simulations for the period 2071-2100 on two selected subcatchments of the Ebro River basin (090, Ega River and 115, Homino River). For each climate scenario, a number of simulations equal to the number of behavioural parameter sets obtained during the uncertainty analysis of the control period was carried out. Resulting streamflows were used to compute 29-years daily flow duration curves (FDCs) to provide a qualitative assessment of the relative importance of uncertainties coming from the choice of the driving RCM and from hydrological parameterisation. Also, streamflows derived from running each climate scenario with its corresponding behavioural parameter sets, were used to compute empirical cumulative density functions (ECDFs) of three selected percentiles, representing different flow magnitudes: Q5 (low flows), Q50 (medium flows) and Q95 (high flows), in order to provide a quantitative assessment of the projected changes in streamflows.

- The proposed framework allowed to explore the relative importance of hydrological parameterisation and the choice of driving climate model into the final impacts. We observed that the hydrological parametric uncertainty was larger than the uncertainty coming from the driving RCM during the complete future period and for each one of the four seasons, for the two selected catchments. However, this result can not be generalised, because it is conditional to decisions taken during the uncertainty analysis and to the ensemble of future climate scenarios considered.

- The proposed framework allowed to provide meaningful estimates of future hydrological impacts of climate change, taking into account the likely bias existing in the hydrological model for representing the catchment response, bias that might be even comparable in magnitude to the projected changes for some months/seasons/streamflow magnitudes.

- We claim that the decision about which parameter sets have to be included in an uncertainty analysis, carried out to explore the relative importance of the different sources of uncertainty, should not be taken in an arbitrary way, i.e., selecting a fix amount of parameter sets or a pre-defined cut-off value of some efficiency measure, without providing an assessment of the predictive capabilities of those parameter sets during the control period, and without providing an assessment of the range of streamflows best represented by those parameter

sets. Monthly and/or seasonal projections of hydrological impacts of climate change are usually interpreted as being equally skilful during all the months/seasons, and this dissertation showed that a large bias may be found in projections for some months/seasons, and those bias have to be made explicit to the decision-maker.

- The larger decreases in the overall streamflows are expected for simulations driven by SMHI.MPIA2 (RCAO_E), whereas the smallest decreases are projected for simulations driven by the DMI.HS1 (HIRAM_H) RCM, changes that are in full agreement with projections for annual values of precipitation and air temperature. In this way, extreme projections for the overall streamflows are derived from climate change scenarios driven by the two different GCMs considered in this dissertation.

- ECDFs computed for projected values of low (Q5), medium (Q50) and high (Q95) flows show that, for the two selected catchments, there is a general projected decrease in all the streamflow magnitudes, but bias in the representation of the streamflows during the control period 1961-1990 hamper the assessment of reliable quantitative projections for low and medium flow, whereas projected decreases for high flow range from 0 to 60%, depending on the catchment and the climate scenario considered.

- ECDFs computed for projected seasonal medium flow values (Q50) show that for the two selected catchments there is a general projected decrease for all the seasons, with seasonal projections limited by bias of different magnitudes for each season. In particular, projections for summer flows are really severe, still considering the bias in the representation of medium-low and low flows, with projected decreases ranging from 60% to 90% for the catchment better represented by the hydrological model (115, Homino River), leading to projected seasonal river flows smaller than 1 m^3/s. Projected decreases in summer flows may lead to several problems related to water availability, in particular, they may have strong implications for drinking water, irrigation and hydro-electrical supply.

- By no means it should be thought that the hydrological impacts of climate change expected for the two selected catchments will certainly lie between the specific ranges given in this dissertation. Additional uncertainties (reliability of SRES scenarios, skill of the GCM/RCM to provide a realistic response to a emission forcing that have been never observed before, small number of driving GCMs considered in this dissertation as boundary conditions of the future scenarios, performance of the downscaling technique, unforeseen natural phenomena, unconsidered changes in land use and/or soil properties, consideration of different hydrological model structures, errors in input data, etc.) add additional complexity to the *cascade of uncertainty* involved in the impact assessment. However, it can be claimed that we explored some possible scenarios of future climate, with the best information available at this moment, and that the projected hydrological impacts provided in this chapter correspond to the best projections we can make based on our imperfect knowledge about this challenging topic.

6.4 Further Research

- Although the simple bias-correction method, used in this dissertation to downscale from the grid-scale of the RCM outputs to the point-scale of the gauging stations used as input to the hydrological simulations, is able to reproduce the observed monthly climate statistics, it fails to rectify some differences between simulated and observed climate, in particular observed variability and interdependencies between precipitation and temperature (e.g., frequency of wet-warm and wet-cold winters) (*Fowler et al.*, 2007). Therefore, more robust methods may be explored to force simulated climate to match the observed one, e.g., the quantile-based approach (*Wood et al.*, 2004) may be used to force the probability distribution of the output precipitation and temperature fields during the control period to match the corresponding observed distributions.

- The use of ensemble of climate models is essential when trying to provide a probabilistic assessment of the likely impacts of climate change. Notwithstanding the ensemble of future climate scenarios used in the present dissertation allowed to take into account uncertainties derived from model parameterisation and numerical schemes used by different climate models, the reduced number (two) of GCMs used as boundary conditions of the selected climate scenarios, only provides a small sample of the likely scenarios of future climate. Therefore, projects as ENSEMBLES (*Hewitt*, 2005), that aim at providing a larger number of high resolution future climate scenarios represent a step forward towards better sampling the space of likely future climates.

- This dissertation only dealt with expected changes on water availability for the Ebro River basin by the end of this century. However, changes in the evolution of water demand, which is expected to increase, may intensify the foreseen problems associated to summer droughts. Thus, integrated studies that take into account both, projections in water availability and water demand may prove be very useful for assessing the final real effect of alternative mitigation policies.

- Within the complex cascade of uncertainty involved in the assessment of hydrological impacts of climate change, this dissertation only explored uncertainties coming from hydrological paramterisation and driving climate scenario, due to time constrains. However, the analysis developed here can be embedded into a general quantitative framework for assessing the likely impacts of climate change, as the one proposed by *Wilby and Harris* (2006).

- Streamflows projected by different climate scenarios were considered as equally likely in the computation of the ECDFs of future streamflows. However, it widely accepted that different climate models represent the observed climate with different levels of accuracy, and it seems logical to use the skill of the climate model in representing the observed climate to weight the future streamflows derived from each climate model. Therefore, it may be worthy to explore an adaptation to the framework proposed by *Rojas et al.* (2008), in which streamflows computed with the GLUE methodology are combined by using Bayesian Model Averaging, using the skill of each climate model in reproducing the observed climate during the control period as the weight to be applied to streamflows derived from each climate scenario.

Bibliography

Abbaspour, K. C. (2008), *SWAT-CUP2: SWAT calibration and uncertainty analysis programs - A User Manual, 95pp*, Eawag: Swiss Fed. Inst. of Aquat. Sci. and Technol. Dübendorf, Switzerland, Available at http://www.eawag.ch/organisation/abteilungen/siam/software/swat/index_EN. 36, 37

Abbaspour, K. C., J. Yang, I. Maximov, R. Siber, K. Bogner, J. Mieleitner, J. Zobrist, and R. Srinivasan (2007), Modelling hydrology and water quality in the pre-alpine/alpine Thur watershed using SWAT, *Journal of Hydrology*, *333*(2-4), 413–430, doi:10.1016/j.jhydrol.2006.09.014. 22, 23, 32, 37

Abbaspour, K. C., J. Yang, M. Vejdani, and S. Haghighat (2008), SWAT-CUP: calibration and uncertainty programs for SWAT, in *4th Int. SWAT Conf. Proc.*, in press. 36

Abbaspour, K. C., M. Faramarzi, S. S. Ghasemi, and H. Yang (2009), Assessing the impact of climate change on water resources in Iran, *Water Resour. Res.*, *45*(10), W10,434, doi:10.1029/2008WR007615. 2, 3, 22, 37, 86, 88, 89

Ajami, N. K., Q. Duan, and S. Sorooshian (2007), An integrated hydrologic Bayesian multimodel combination framework: Confronting input, parameter, and model structural uncertainty in hydrologic prediction, *Water Resources Research*, *43*, W01,403, doi:10.1029/2005WR004745. 19

Alcamo, J., et al. (2007), Europe, in *Climate change 2007: impacts, adaptation and vulnerability. Contribution of working group II to the fourth assessment report of the intergovernmental panel on climate change*, edited by M. L. Parry, O. F. Canziani, J. P. Palutikof, P. J. van der Linden, and C. E. Hanson, pp. 541–580, Cambridge University Press, UK, Cambridge. 1, 85

Allen, M., S. Raper, and J. Mitchell (2001), Climate change. Uncertainty in the IPCC's third assessment report, *Science*, *293*(5529), 430–433, doi:10.1126/science.1062823. 88

Andréasson, J., S. Bergström, B. Carlsson, L. P. Graham, and G. Lindström (2004), Hydrological change climate change impact simulations for Sweeden, *Ambio*, *33*(4-5), 228–234. 86

Arabi, M., R. S. Govindaraju, M. M. Hantush, and B. A. Engel (2006), Role of watershed subdivision on modeling the effectiveness of best management practices with SWAT, *Journal of The American Water Resources Association*, *42*(2), 513–528. 25

Arheimer, B., J. Andréasson, S. Fogelberg, H. Johnsson, C. B. Pers, and K. Persson (2005), Climate change impact on water quality: Model results from southern Sweden, *Ambio*, *34*(7), 559–566. 86

Arnell, N., M. Livermore, S. Kovats, P. Levy, R. Nicholls, M. Parry, and S. Gaffin (2004), Climate and socio-economic scenarios for global-scale climate change impacts assessments: characterising the SRES storylines, *Global Environmental Change*, *14*(1), 3–20, doi:10.1016/j.gloenvcha.2003.10.004. 88

Arnell, N. W. (1999), The effect of climate change on hydrological regimes in Europe: a continental perspective, *Global Environmental Change*, *9*(1), 5–23, doi:10.1016/S0959-3780(98)00015-6. 87

Arnell, N. W. (2003a), Relative effects of multi-decadal climatic variability and changes in the mean and variability of climate due to global warming: future streamflows in Britain, *Journal of Hydrology*, *270*(3-4), 195–213, doi:S0022-1694(02)00288-3. 2, 86

Arnell, N. W. (2003b), Effects of IPCC SRES emissions scenarios on river runoff: a global perspective, *Hydrology and Earth System Sciences*, *7*(5), 619–641. 88

Arnell, N. W. (2005), Implications of climate change for freshwater inflows to the Arctic Ocean, *Journal ff Geophysical Research-Atmospheres*, *110*, D07,105, doi:10.1029/2004JD005348. 88

Arnell, N. W., D. A. Hudson, and R. G. Jones (2003), Climate change scenarios from a regional climate model: Estimating change in runoff in southern Africa, *Journal of Geophysical Research*, *108*(D16), 4519, doi:10.1029/2002JD002782. 88

Arnold, J. G., and N. Fohrer (2005), SWAT2000: current capabilities and research opportunities in applied watershed modelling, *Hydrological Processes*, *19*(3), 563–572, doi:10.1002/hyp.5611. 22

Arnold, J. G., P. M. Allen, and G. Bernhardt (1993), A comprehensive surface-groundwater flow model, *Journal of Hydrology*, *142*(1-4), 47–69, doi:10.1016/0022-1694(93)90004-S. 24

Arnold, J. G., R. Srinivasan, R. S. Muttiah, and J. R. Williams (1998), Large area hydrologic modeling and assessment part I: Model development, *Journal of the American Water Resources Association*, *34*(1), 73–89. 22, 24

Arnold, J. G., R. Srinivasan, R. S. Muttiah, and P. M. Allen (1999), Continental scale simulation of the hydrologic balance, *Journal of the American Water Resources Association*, *35*(5), 1037–1051. 22

Arnold, J. G., K. N. Potter, K. W. King, and P. M. Allen (2005), Estimation of soil cracking and the effect on surface runoff in a texas blackland prairie watershed, *Hydrological Processes*, *19*(3), 589, doi:10.1002/hyp.5609. 22

Bates, B. C., Z. W. Kundzewicz, S. Wu, and J. P. Palutikof (Eds.) (2008), *Climate Change and Water*, Technical Paper of the Intergovernmental Panel on Climate Change, IPCC Secretariat, Geneva, 210pp. 1, 51

Beck, M. B. (1987), Water quality modeling: A review of the analysis of uncertainty, *Water Resour. Res.*, *23*(8), 1393–1442. 20

Bekele, E. G., and J. W. Nicklow (2007), Multi-objective automatic calibration of SWAT using NSGA-II, *Journal of Hydrology*, *341*, 165–176, doi:10.1016/j.jhydrol.2007.05.014. 18

Bergström, S., B. Carlsson, M. Gardelin, G. Lindström, A. Pettersson, and M. Rummukainen (2001), Climate change impacts on runoff in Sweeden - assessments by global climate models, dynamical downscaling and hydrological modelling, *Climate Research*, *16*, 101–112. 54

Beven, K. J. (2001), How far can we go in distributed hydrological modelling?, *Hydrology and Earth System Sciences*, *5*(1), 1–12. 21, 42, 50

Beven, K. J. (2006), A manifesto for the equifinality thesis, *Journal of Hydrology*, *320*(1-2), 18–36, doi:10.1016/j.jhydrol.2005.07.007. 2, 16, 20, 37

Beven, K. J. (2009), Comment on "Equifinality of formal (DREAM) and informal (GLUE) Bayesian approaches in hydrologic modeling?" by Jasper A. Vrugt, Cajo J. F. ter Braak, Hoshin V. Gupta and Bruce A. Robinson, *Stochastic Environmental Research and Risk Assessment*, *23*(7), 1059–1060, doi:10.1007/s00477-008-0283-x. 22

Beven, K. J., and A. Binley (1992), The future of distributed models - model calibration and uncertainty prediction, *Hydrological Processes*, *6*(3), 279–298. 2, 16, 19, 20, 21

Beven, K. J., and J. Freer (2001), Equifinality, data assimilation, and uncertainty estimation in mechanistic modelling of complex environmental systems using the GLUE methodology, *Journal of Hydrology*, *249*(1-4), 11–29, doi:10.1016/S0022-1694(01)00421-8. 2, 20, 21, 36, 42, 50, 114

Beven, K. J., J. Freer, B. Hankin, and K. Schulz (2000), The use of generalized likelihood measures for uncertainty estimation in higher-order models of environmental systems, in *Nonlinear and Nonstationary Signal Processing*, edited by W. J. Fitzgerald, R. L. Smith, A. Walden, and P. Young, pp. 115–151, Cambridge University Press, UK. 20, 21, 35

Beven, K. J., P. Smith, and J. Freer (2007), Comment on "hydrological forecasting uncertainty assessment: Incoherence of the GLUE methodology" by Pietro Mantovan and Ezio Todini, *Journal of Hydrology*, *338*(3-4), 315, doi:10.1016/j.jhydrol.2007.02.023. 20, 21

Beven, K. J., P. J. Smith, and J. E. Freer (2008), So just why would a modeller choose to be incoherent ?, *Journal of Hydrology*, *354*(1-4), 15, doi:10.1016/j.jhydrol.2008.02.007. 19, 20, 21

Binger, R. L., J. Garbrecht, J. G. Arnold, and R. Srinivasan (1997), Effect of watershed subdivision on simulation runoff and fine sediment yield, *Transactions of the ASAE*, *40*(5), 1329–1335. 25

Blasone, R.-S., H. Madsen, and D. Rosbjerg (2008a), Uncertainty assessment of integrated distributed hydrological models using GLUE with Markov Chain Monte Carlo sampling, *Journal of Hydrology*, *353*(1-2), 18–32, doi:10.1016/j.jhydrol.2007.12.026. 20

Blasone, R.-S., J. A. Vrugt, H. Madsen, D. Rosbjerg, B. A. Robinson, and G. A. Zyvoloski (2008b), Generalized likelihood uncertainty estimation (GLUE) using adaptive Markov Chain Monte Carlo sampling, *Advances in Water Resources*, *31*(4), 630, doi:10.1016/j.advwatres.2007.12.003. 36

Blenkinsop, S., and H. J. Fowler (2005), Assessment of climatology in climate model, *Aquaterra deliverable H1.4*, Newcastle University, School of Civil Engineering and Geosciences, Newcastle upon Tyne, NE1 7RU, UK. 54

Booij, M. (2005), Impact of climate change on river flooding assessed with different spatial model resolutions, *Journal of Hydrology*, *303*(1-4), 176–198, doi:10.1016/j.jhydrol.2004.07.013. 2, 86, 88

Borah, D. K., and M. Bera (2004), Watershed-scale hydrologic and nonpoint-source pollution models: Review of applications, *Transactions of the ASAE*, *47*(3), 789–803. 22

Bormann, H., L. Breuer, T. Gräff, J. Huisman, and B. Croke (2009), Assessing the impact of land use change on hydrology by ensemble modelling (LUCHEM) IV: Model sensitivity to data aggregation and spatial (re-)distribution, *Advances in Water Resources*, *32*(2), 171–192, doi:10.1016/j.advwatres.2008.01.002. 88

Bosch, D. D., J. M. Sheridan, H. L. Batten, and J. G. Arnold (2004), Evaluation of the SWAT model on a coastal plain agricultural watershed, *Transactions of The ASAE*, *47*, 1493–1506. 7

Bovolo, C. I., S. Blenkinsop, H. J. Fowler, C. Bürger, and B. Majone (2008), Application of climate change scenarios in AT case study catchments, *Aquaterra deliverable H1.12*, University of Newcastle, School of Civil Engineering and Geosciences and University of Tübingen and University of Trento, Dep. of Civil and Environmental Engineering. 54, 55

Bovolo, C. I., S. Blenkinsop, H. J. Fowler, M. Zambrano-Bigiarini, and A. Bellin (2009), Production of climate change scenarios for large catchments, *Aquaterra deliverable H1.13*, Newcastle University, School of Civil Engineering and Geosciences and University of Trento, Dep. of Civil and Environmental Engineering. 54, 56, 57

Boyle, D. P., H. V. Gupta, and S. Sorooshian (2000), Toward improved calibration of hydrologic models: Combining the strengths of manual and automatic methods, *Water Resources Research*, *36*(12), 3663–3674. 18

Buonomo, E., R. Jones, C. Huntingford, and J. Hannaford (2007), On the robustness of changes in extreme precipitation over europe from two high resolution climate change simulations, *Quarterly Journal of the Royal Meteorological Society*, *133*(622), 65–81, doi:10.1002/qj.13. 54, 90

Bürger, C. M., O. Kolditz, H. J. Fowler, and S. Blenkinsop (2007), Future climate scenarios and rainfall-runoff modelling in the Upper Gallego catchment (spain), *Environmental Pollution*, *148*(3), 842–854, doi:10.1016/j.envpol.2007.02.002, aquaTerra: Pollutant behavior in the soil, sediment, ground, and surface water system. 65, 82, 88

Bürger, G., and Y. Chen (2005), Regression-based downscaling of spatial variability for hydrologic applications, *Journal of Hydrology*, *311*(1-4), 299–317, doi:10.1016/j.jhydrol.2005.01.025. 53, 86

Burton, A., H. J. Fowler, S. Blenkinsop, and C. G. Kilsby (2010), Downscaling transient climate change using a Neyman-Scott Rectangular Pulses stochastic rainfall model, *Journal of Hydrology*, *381*(1-2), 18–32, doi:10.1016/j.jhydrol.2009.10.031. 53, 87, 88

Butts, M. B., J. T. Payne, M. Kristensen, and H. Madsen (2004), An evaluation of the impact of model structure on hydrological modelling uncertainty for streamflow simulation, *Journal Of Hydrology*, *298*(1-4), 242–266, doi:10.1016/j.hydrol.2004.03.042. 19

Caballero, Y., S. Voirin-Morel, F. Habets, J. Noilhan, P. LeMoigne, A. Lehenaff, and A. Boone (2007), Hydrological sensitivity of the Adour-Garonne river basin to climate change, *Water Resour. Res.*, *43*(7), W07,448, doi:10.1029/2005WR004192. 89

Cameron, D. (2006), An application of the UKCIP02 climate change scenarios to flood estimation by continuous simulation for a gauged catchment in the northeast of Scotland, UK (with uncertainty), *Journal of Hydrology*, *328*(1-2), 212–226, doi:10.1016/j.jhydrol.2005.12.024. 3, 88

Campolongo, F., S. Tarantola, and A. Saltelli (2000), Sensitivity anaysis as an ingredient of modeling, *Statistical Science*, *15*(4), 377, doi:10.1214/ss/1009213004. 16

Cao, W. Z., W. B. Bowden, T. Davie, and A. Fenemor (2006), Multi-variable and multi-site calibration and validation of swat in a large mountainous catchment with high spatial variability, *Hydrological Processes*, *20*(5), 1057–1073, doi:10.1002/hyp.5933. 18, 22

Chaplot, V., A. Saleh, and D. Jaynes (2005), Effect of the accuracy of spatial rainfall information on the modeling of water, sediment, and NO3-N loads at the watershed level, *Journal of Hydrology*, *312*(1-4), 223–234, doi:10.1016/j.jhydrol.2005.02.019. 7

Chaubey, I., A. S. Cotter, T. A. Costello, and T. S. Soerens (2005), Effect of DEM data resolution on SWAT output uncertainty, *Hydrological Processes*, *19*(3), 621, doi:10.1002/hyp.5607. 7

CHE (2008), Caracterización de las alteraciones del régimen hidrológico sufridas en las estaciones de aforos de la cuenca del Ebro [Characterization of the disturbances to the hydrological regime on the streamflow stations of the Ebro basin], *Tech. rep.*, available on http://oph.chebro.es/documentacion/TablaResumenCaudalEA/AlteracionesEA.htm. [last accessed June-2008]. 27

Chiew, F. H. S., J. Teng, J. Vaze, D. A. Post, J. M. Perraud, D. G. C. Kirono, and N. R. Viney (2009), Estimating climate change impact on runoff across southeast Australia: Method, results, and implications of the modeling method, *Water Resour. Res.*, *45*(10), W10,414, doi:10.1029/2008WR007338. 2, 86, 88

Christensen, J., et al. (2007a), Regional climate projections, in *Climate Change 2007: The Physical Science Basis. Contribution of Working Group I to the Fourth Assessment Report of the Intergovernmental Panel on Climate Change*, edited by S. Solomon, D. Qin, M. Manning, Z. Chen, M. Marquis, K. B. Averyt, M. Tignor, and H. L. Miller, Cambridge University Press, Cambridge, United Kingdom and New York, NY, USA. 1, 51

Christensen, J., T. R. Carter, M. Rummukainen, and G. Amanatidis (2007b), Evaluating the performance and utility of climate models: the PRUDENCE project, *Climatic Change*, *81*(1), 1–6, doi:10.1007/s10584-006-9211-6. 1, 25, 53, 86, 88

Christensen, J. H., and O. B. Christensen (2007), A summary of the PRUDENCE model projections of changes in European climate by the end of this century, *Climatic Change*, *81*, 7–30, doi:10.1007/s10584-006-9210-7. 53

Christensen, N. S., A. W. Wood, N. Voisin, D. P. Lettenmaier, and R. N. Palmer (2004), The effects of climate change on the hydrology and water resources of the Colorado River basin, *Climatic Change*, *62*(1-3), 337–363, doi:10.1023/B:CLIM.0000013684.13621.1f. 88

Cochrane, T. A., and D. C. Flanagan (2005), Effect of DEM resolutions in the runoff and soil loss predictions of the WEPP watershed model, *Transactions of The ASAE*, *48*, 109–120. 7

Collins, M. (2007), Ensembles and probabilities: a new era in the prediction of climate change, *Philos Transact A Math Phys Eng Sci*, *365*(1857), 1957–1970, doi:10.1098/rsta.2007.2068. 88

Confederación Hidrográfica del Ebro & Ministerio de Medio Ambiente y Medio Rural y Marino (2009), Coberturas del "GIS-Ebro". 8, 9, 10

Cooper, V. A., V. T. V. Nguyen, and J. A. Nicell (1997), Evaluation of global optimization methods for conceptual rainfall-runoff model calibration, *Water Science and Technology*, *36*(5), 53–60. 17

Cotter, A. S., I. Chaubey, T. A. Costello, T. S. Soerens, and M. A. Nelson (2003), Water quality model output uncertainty as affected by spatial resolution of input data, *Journal of The American Water Resources Association*, *39*, 977–986. 7

Defourny, P., G. Hecquet, and T. Philippart (1999), Digital terrain modeling: Accuracy assessment and hydrological simulation sensitivity, in *Spatial Accuracy Assessment: Land information Uncertainty in Natural Resources*, edited by K. Lowell and A. Jaton, p. 323, Ann Arbor Press, Chelsea, Michigan. 7

Déqué, M., et al. (2005), Global high resolution versus Limited Area Model climate change projections over europe: quantifying confidence level from PRUDENCE results, *Climate Dynamics*, *25*(6), 653–670, doi:10.1007/s00382-005-0052-1. 54

Déqué, M., et al. (2007), An intercomparison of regional climate simulations for Europe: assessing uncertainties in model projections, *Climatic Change*, *81*(S1), 53–70, doi:10.1007/s10584-006-9228-x. 53

Dessai, M., S.and Hulme (2003), Does climate policy need probabilities?, *Working paper*, Tyndall Centre Working Papers. 52

Di Luzio, M., R. Srinivasan, and J. G. Arnold (2002a), Integration of watershed tools and SWAT model into BASINS, *Journal of The American Water Resources Association*, *38*(4), 1127–1141, doi:10.1111/j.1752-1688.2002.tb05551.x. 7, 24, 25, 32

Di Luzio, M., R. Srinivasan, J. G. Arnold, and S. L. Neitsch (2002b), *Soil and Water Assessment Tool. ArcView GIS Interface Manual: Version 2000*, GSWRL Report 02-03, BRC Report 02-07. Published by Texas Water Resources Institute TR-193, College Station, TX. 346p. 24, 25, 32

Di Luzio, M., R. Srinivasan, and J. G. Arnold (2004), A GIS-coupled hydrological model system for the watershed assessment of agricultural nonpoint and point sources of pollution, *Transactions in GIS*, *8*(1), 113–136, doi:10.1111/j.1467-9671.2004.00170.x. 7, 24, 25, 32

Di Luzio, M., J. G. Arnold, and R. Srinivasan (2005), Effect of GIS data quality on small watershed stream flow and sediment simulations, *Hydrological Processes*, *19*(3), 629, doi:10.1002/hyp.5612. 7

Dibike, Y., and P. Coulibaly (2005), Hydrologic impact of climate change in the Saguenay watershed: comparison of downscaling methods and hydrologic models, *Journal of Hydrology*, *307*(1-4), 145–163, doi:10.1016/j.jhydrol.2004.10.012. 3, 53, 86, 88

Duan, Q., S. Sorooshian, and V. Gupta (1992), Effective and efficient global optimization for conceptual rainfall-runoff models, *Water Resources Research*, *28*, 1015–1031. 2, 16, 17, 36

Duan, Q., S. Sorooshian, and V. K. Gupta (1994), Optimal use of the SCE-UA global optimization method for calibrating watershed models, *Journal Of Hydrology*, *158*, 265–284, gives recommended values for the use of the SCE-UA algorithm:. 36

Eckhardt, K., and J. G. Arnold (2001), Automatic calibration of a distributed catchment model, *Journal of Hydrology*, *251*(1-2), 103–109, doi:10.1016/S0022-1694(01)00429-2. 32

Eckhardt, K., S. Haverkamp, N. Fohrer, and H. Frede (2002), SWAT-G, a version of SWAT99.2 modified for application to low mountain range catchments, *Physics and Chemistry of ohe Earth*, *27*(9-10), 641–644, doi:S1474-7065(02)00048-7. 22

Engeland, K., I. Braud, L. Gottschalk, and E. Leblois (2006), Multi-objective regional modelling, *Journal of Hydrology*, *327*(3-4), 339–351, doi:10.1016/j.jhydrol.2005.11.022. 18

Feyen, L., J. A. Vrugt, B. Ó. Nualláin, J. van der Knijff, and A. De Roo (2007), Parameter optimisation and uncertainty assessment for large-scale streamflow simulation with the LISFLOOD model, *Journal of Hydrology*, *332*(3-4), 276, doi:10.1016/j.jhydrol.2006.07.004. 16

Fitzhugh, T. W., and D. S. Mackay (2000), Impacts of input parameter spatial aggregation on an agricultural nonpoint source pollution model, *Journal of Hydrology*, *236*(1-2), 35–53, doi:doi:10.1016/S0022-1694(00)00276-6. 22, 25

Fontaine, T. A., T. S. Cruickshank, J. G. Arnold, and R. H. Hotchkiss (2002), Development of a snowfall-snowmelt routine for montainous terrain for the soil water assessment tool (SWAT), *Journal of Hydrology*, *262*(1-4), 209–223, doi:10.1016/S0022-1694(02)00029-X. 22, 23

Fowler, H. J., and M. Ekström (2009), Multi-model ensemble estimates of climate change impacts on UK seasonal precipitation extremes, *International Journal of Climatology*, *29*(3), 385–416, doi:10.1002/joc.1827. 88

Fowler, H. J., and C. G. Kilsby (2007), Using regional climate model data to simulate historical and future river flows in northwest England, *Climatic Change*, *80*(3-4), 337–367, doi:10.1007/s10584-006-9117-3. 55

Fowler, H. J., N. Baran, C. Mouvet, and A. Gutierrez (2005), Report detailing selection of GCM outputs and pre-processed observed rainfall and PE data for calibration of catchment models, *Aquaterra deliverable H1.1*, University of Newcastle, School of Civil Engineering and Geosciences, Newcastle upon Tyne, NE1 7RU, UK. 54

Fowler, H. J., S. Blenkinsop, and C. Tebaldi (2007), Linking climate change modelling to impacts studies: recent advances in downscaling techniques for hydrological modelling, *International Journal of Climatology*, *27*(12), 1547–1578, doi:10.1002/joc.1556. 53, 86, 87, 116

Franchini, M., G. Galeati, and S. Berra (1998), Global optimization techniques for the calibration of conceptual rainfall-runoff models, *Hydrological Sciences Journal-Journal Des Sciences Hydrologiques*, *43*(3), 443–458. 17

Francos, A., F. J. Elorza, F. Bouraoui, G. Bidoglio, and L. Galbiati (2003), Sensitivity analysis of distributed environmental simulation models: understanding the model behaviour in hydrological studies at the catchment scale, *Reliability Engineering & System Safety*, *79*(2), 205–218, doi:10.1016/S0951-8320(02)00231-4. 16, 32

Freer, J., B. Ambroise, and K. J. Beven (1996), Bayesian estimation of uncertainty in runoff prediction and the value of data: an application of the GLUE approach, *Wat. Resour. Res.*, *32*(7), 2161–2173. 2, 16, 17, 19, 20, 21

Gassman, P. W., M. R. Reyes, C. H. Green, and J. G. Arnold (2007), The soil and water assessment tool: Historical development, applications, and future research directions, *Transactions of the ASABE*, *50*(4), 1211–1250, doi:10.1007/s00477-0060057-2ASABE, complete document in: http://ideas.repec.org/p/isu/genres/12744.html. 22

George, C., and L. F. Leon (2007), WaterBase: SWAT in an open source GIS, *The Open Hydrology Journal*, *1*, 19–24. 24

Geza, M., and J. E. Mccray (2008), Effects of soil data resolution on SWAT model stream flow and water quality predictions, *Journal of Environmental Management*, *88*(3), 393–406, doi:10.1016/j.jenvman.2007.03.016. 7

Giorgi, F. (2005), Climate change prediction, *Climatic Change*, *73*(3), 239–265, doi:10.1007/s10584-005-6857-4. 3, 52, 88

Giorgi, F. (2006), Regional climate modeling: Status and perspectives, *Journal de Physique IV France*, *139*, 101–118, doi:10.1051/jp4:2006139008. 53

Giorgi, F., and L. O. Mearns (1991), Approaches to regional climate change simulation: A review, *Rev. Geo.*, *29*, 191–216. 52

Giorgi, F., and L. O. Mearns (2003), Probability of regional climate change based on the Reliability Ensemble Averaging (REA) method, *Geophys. Res. Lett.*, *30*(12), 1629, doi:10.1029/2003GL017130. 25, 88

Giorgi, F., S. W. Hostetler, and C. S. Brodeur (1994), Analysis of the surface hydrology in a regional climate model, *Quarterly Journal of the Royal Meteorological Society*, *120*(515), 161–183, doi:10.1002/qj.49712051510. 87

Gordon, C., C. Cooper, C. A. Senior, H. Banks, J. M. Gregory, T. C. Johns, J. F. B. Mitchell, and R. A. Wood (2000), The simulation of SST, sea ice extents and ocean heat transports in a version of the Hadley Centre coupled model without flux adjustments, *Climate Dynamics*, *16*(2-3), 147–168, doi:10.1007/s003820050010. 54, 90

Gosain, A. K., S. Rao, R. Srinivasan, and N. G. Reddy (2005), Return-flow assessment for irrigation command in the palleru river basin using swat model, *Hydrological Processes*, *19*(3), 673–682, doi:10.1002/hyp.5622. 22

Gosain, A. K., S. Rao, and D. Basuray (2006), Climate change impact assessment on hydrology of Indian river basin, *Current Science*, *90*(3), 346–353. 2, 86

Graham, L. P., S. Hagemann, S. Jaun, and M. Beniston (2007a), On interpreting hydrological change from regional climate models, *Climatic Change*, *81*, 97–122, doi:10.1007/s10584-006-9217-0. 2, 86, 87, 88

Graham, L. P., J. Andreasson, and B. Carlsson (2007b), Assessing climate change impacts on hydrology from an ensemble of regional climate models, model scales and linking methods - a case study on the Lule River basin, *Climatic Change*, *81*(1), 293–307, doi:10.1007/s10584-006-9215-2. 3, 86, 87, 88

Groves, D. G., D. Yates, and C. Tebaldi (2008), Developing and applying uncertain global climate change projections for regional water management planning, *Water Resources Research*, *44*, W12,413, doi:10.1029/2008WR006964. 88

Hagemann, S., B. Machenhauer, R. Jones, O. B. Christensen, M. Déqué, D. Jacob, and P. L. Vidale (2004), Evaluation of of water and energy budgets in regional climate models applied over Europe, *Climate Dynamics*, *23*(5), 547–567, doi:10.1007/s00382-004-0444-7. 87

Halenka, T., J. Miksovsky, M. Belda, and P. Huszar (2009), High resolution regional climate change modelling in CECILIA Project - climate change signal in central and Eastern Europe, *IOP Conference Series: Earth and Environmental Science*, *6*(2), 022,006, doi:10.1088/1755-1307/6/2/022006. 88

Hargreaves, G. L., G. H. Hargreaves, and J. P. Riley (1985), Agricultural benefits for Senegal River Basin, *J. Irrig. and Drain. Engr.*, *111*(2), 113–124. 23

Haverkamp, S., N. Fohrer, and H.-G. Frede (2005), Assessment of the effect of land use patterns on hydrologic landscape functions: a comprehensive GIS-based tool to minimize model uncertainty resulting from spatial aggregation, *Hydrological Processes*, *19*(3), 715–727, doi:10.1002/hyp.5626. 22

Hellström, C., D. Chen, C. Achberger, and J. Räisänen (2001), Comparison of climate change scenarios for Sweden based on statistical and dynamical downscaling of monthly precipitation, *Climate Research*, *19*(1), 44–55, doi:10.3354/cr019045. 53

Hewitt, C. (2005), ENSEMBLES - providing ensemble-based predictions of climate changes and their impacts, Parliament Magazine, 11 July 2005, p. 57. Available online at http://ensembles-eu.metoffice.com/docs/ParlMag_11Jul05.pdf. 88, 117

Hiemstra, P. H., E. J. Pebesma, C. J. W. Twenh"ofel, and G. B. M. Heuvelink (2008), Real-time automatic interpolation of ambient gamma dose rates from the Dutch Radioactivity Monitoring Network, *Computers & Geosciences*, doi:http://dx.doi.org/10.1016/j.cageo.2008.10.011. 30, 58

Holvoet, K., A. van Griensven, P. Seuntjens, and P. Vanrolleghem (2005), Sensitivity analysis for hydrology and pesticide supply towards the river in SWAT, *Physics and Chemistry of The Earth*, *30*(8-10), 518–526, doi:10.1016/j.pce.2005.07.006. 16, 32

Holvoet, K., A. van Griensven, V. Gevaert, P. Seuntjens, and P. A. Vanrolleghem (2008), Modifications to the SWAT code for modelling direct pesticide losses, *Environmental Modelling & Software*, *23*(1), 72, doi:10.1016/j.envsoft.2007.05.002. 22

Hornberger, G. M., and R. C. Spear (1981), An approach to the preliminary-analysis of environmental systems, *J. of Environ. Manage.*, *12*(1), 7–18. 20

Hornberger, G. M., K. J. Beven, B. J. Cosby, and D. E. Sappington (1985), Shenandoah watershed study: Calibration of a topography-based, variable contributing area hydrological model to a small forested catchment, *Water Resour. Res.*, *21*(12), 1841–1850, doi:10.1029/WR021i012p01841. 2, 16

Horton, P., B. Schaefli, A. Mezghani, H. Benoît, and A. Musy (2006), Assessment of climate-change impacts on alpine discharge regimes with climate model uncertainty, *Hydrological Processes*, *20*, 2091–2109, doi:10.1002/hyp.6197. 88

Huntington, T. G. (2006), Evidence for intensification of the global water cycle: Review and synthesis, *Journal of Hydrology*, *319*(1-4), 83–95, doi:10.1016/j.jhydrol.2005.07.003. 51

IPCC DDC (2010), Climate model output: period-averages, http://www.ipcc-data.org/ddc_climscen.html, [Online; last accessed Feb-2010]. 52

Jacob, D., et al. (2007), An inter-comparison of regional climate models for Europe: model performance in present-day climate, *Climatic Change*, *81*(S1), 31–52, doi:10.1007/s10584-006-9213-4. 53

Jakeman, A. J., and G. M. Hornberger (1993), How much complexity is warranted in a rainfall-runoff model, *Wat. Resour. Res.*, *29*(8), 2637–2649. 16, 33

Jakeman, A. J., T. H. Chen, D. A. Post, G. M. Hornberger, and I. G. Littlewood (1993), Assessing uncertainties in hydrological response to climate at large scales, in *Macroscale modelling of the hydrosphere*, edited by W. B. Wilkinson, pp. 37–47, IAHS Press, Wallingford, UK. 3, 88

Janssen, P. H. M., and P. S. C. Heuberger (1995), Calibration of process-oriented models, *Ecological Modelling*, *83*(1-2), 55–66, doi:10.1016/0304-3800(95)00084-9, modelling Water, Carbon and Nutrient Cycles in Forests. 17

Jha, M., P. W. Gassman, S. Secchi, R. Gu, and J. Arnold (2004), Effect of watershed subdivision on swat flow, sediment, and nutrient predictions, *Journal Of The American Water Resources Association*, *40*(3), 811–825. 25

Johnston, P. R., and D. H. Pilgrim (1976), Parameter optimization for watershed models, *Water Resour. Res.*, *12*(3), 477–486. 2, 16

Kannan, N., S. White, F. Worrall, and M. Whelan (2007), Sensitivity analysis and identification of the best evapotranspiration and runoff options for hydrological modelling in SWAT-2000, *Journal of Hydrology*, *332*(3-4), 456–466, doi:10.1016/j.jhydrol.2006.08.001. 32

Kay, A. L., R. G. Jones, and N. S. Reynard (2006), RCM rainfall for uk flood frequency estimation. ii. climate change results, *Journal Of Hydrology*, *318*, 163–172, doi:10.1016/j.jhydrol.2005.06.013. 87, 88

Kay, A. L., H. N. Davies, V. A. Bell, and R. G. Jones (2009), Comparison of uncertainty sources for climate change impacts: flood frequency in England, *Climatic Change*, *92*(1-2), 41–63, doi: 10.1007/s10584-008-9471-4. 88, 89

Kitanidis, P. K., and R. L. Bras (1980), Real-time forecasting with a conceptual hydrologic model 2. applications and results, *Water Resources Research*, *16*(6), 1034–1044. 17, 29, 37

Krause, P., D. P. Boyle, and B. F. (2005), Comparison of different efficiency criteria for hydrological model assessment, *Advances in Geosciences*, *5*, 89–97. 17, 18, 36, 37, 103

Krysanova, V., D.-I. Müller-Wohlfeil, and A. Becker (1998), Development and test of a spatially distributed hydrological water quality model for mesoscale watersheds, *Ecological Modelling*, *106*(2-3), 261–289. 22

Krysanova, V., F. Hattermann, and F. Wechsung (2007), Implications of complexity and uncertainty for integrated modelling and impact assessment in river basins, *Environmental Modelling & Software*, *22*(5), 701–709, doi:10.1016/j.envsoft.2005.12.029. 22

Kuczera, G. (1983), Improved parameter inference in catchment models 2. combining different kinds of hydrologic data and testing their compatibility, *Water Resour. Res.*, *19*(5), 1163–1172. 2, 16

Kuczera, G., and B. J. Williams (1992), Effect of rainfall errors on accuracy of design flood estimates, *Water Resour. Res.*, *28*(4), 1145–1153. 30

Kuczera, G., D. Kavetski, S. Franks, and M. Thyer (2006), Towards a bayesian total error analysis of conceptual rainfall-runoff models: Characterising model error using storm-dependent parameters, *Journal of Hydrology*, *331*(1-2), 161, doi:10.1016/j.jhydrol.2006.05.010. 17, 19

Kumar, S., and V. Merwade (2009), Impact of watershed subdivision and soil data resolution on SWAT model calibration and parameter uncertainty, *JAWRA Journal of the American Water Resources Association*, *45*(5), 1179, doi:10.1111/j.1752-1688.2009.00353.x, effect of input data resolution on SWAT simulations. 7

Kundzewicz, Z. W., et al. (2007), Freshwater resources and their management, in *Climate Change 2007: Impacts, Adaptation and Vulnerability. Contribution of Working Group II to the Fourth Assessment Report of the Intergovernmental Panel on Climate Change*, edited by M. L. Parry, O. F. Canziani, J. P. Palutikof, P. J. van der Linden, and C. Hanson, Cambridge University Press, Cambridge, UK, 173-210. 86, 87

Lambert, S. J., and G. J. Boer (2001), CMIP1 evaluation and intercomparison of coupled climate models, *Climate Dynamics*, *17*(2-3), 83–106, doi:10.1007/PL00013736. 88

Le Coz, M., F. Delclaux, P. Genthon, and G. Favreau (2009), Assessment of digital elevation model (DEM) aggregation methods for hydrological modeling: Lake chad basin, africa, *Computers & Geosciences*, *35*(8), 1661, doi:10.1016/j.cageo.2008.07.009. 7

Leavesley, G. H. (1994), Modeling the effects of climate change on water resources - a review, *Climatic Change*, *28*(1-2), 159–177, doi:10.1007/BF01094105. 86

Legates, D. R., and G. J. McCabe Jr. (1999), Evaluating the Use of "Goodness-of-Fit" Measures in Hydrologic and Hydroclimatic Model Validation, *Water Resources Research*, *35*(1), 233–241, doi:10.1029/1998WR900018. 17, 18, 36, 103

Lenderink, G., A. Buishand, and W. Van Deursen (2007), Estimates of future discharges of the river Rhine using two scenario methodologies: direct versus delta approach, *Hydrology and Earth System Sciences*, *11*(3), 1143–1159, doi:10.1029/2002GL016433. 88

Lenhart, T., K. Eckhardt, N. Fohrer, and H. Frede (2002), Comparison of two different approaches of sensitivity analysis, *Physics and Chemistry of the Earth*, *27*, 645–654, doi:S1474-7065(02)00049-9. 32

Lin, Z., and D. Radcliffe (2006), Automatic calibration and predictive uncertainty analysis of a semidistributed watershed model, *Vadose Zone Journal*, *5*, 248–260, doi:10.2136/vzj2005.0025. 17

Linkov, I., and D. Burmistrov (2003), Model uncertainty and choices made by modelers: Lessons learned from the international atomic energy agency model intercomparisons, *Risk. Anal.*, *23*(6), 1297–1308, doi:10.1111/j.0272-4332.2003.00402. 20

Madsen, H., G. Wilson, and H. C. Ammentrop (2002), Comparison of different automated strategies for calibration of rainfall-runoff models, *Journal of Hydrology*, *261*(1-4), 48–59, doi:10.1016/S0022-1694(01)00619-9. 17

Manning, L. J., J. W. Hall, H. J. Fowler, C. G. Kilsby, and C. Tebaldi (2009), Using probabilistic climate change information from a multimodel ensemble for water resources assessment, *Water Resources Research*, *45*(11), W11,411, doi:10.1029/2007WR006674. 88

Mantovan, P., and E. Todini (2006), Hydrological forecasting uncertainty assessment: Incoherence of the GLUE methodology, *Journal of Hydrology*, *330*(1-2), 368, doi:10.1016/j.jhydrol.2006.04.046. 21

Mantovan, P., E. Todini, and M. L. V. Martina (2007), Reply to comment by keith beven, paul smith and jim freer on "hydrological forecasting uncertainty assessment: Incoherence of the glue methodology", *Journal of Hydrology*, *338*(3-4), 319, doi:10.1016/j.jhydrol.2007.02.029. 21

Mapfumo, E., D. S. Chanasyk, and W. D. Willms (2004), Simulating daily soil water under foothills fescue grazing with the soil and water assessment tool model (Alberta, Canada), *Hydrological Processes*, *18*(15), 2787–2800, doi:10.1002/hyp.1493. 22

Matott, L., J. Babendreier, and S. Purucker (2009), Evaluating uncertainty in integrated environmental models: A review of concepts and tools, *Water Resources Research*, *45*(6), W06,421, doi:10.1029/2008WR007301. 19, 20

Maurer, E. P. (2007), Uncertainty in hydrologic impacts of climate change in the Sierra Nevada, California, under two emissions scenarios, *Climatic Change*, *82*(3-4), 309, doi:10.1007/s10584-006-9180-9. 88

McKay, M. D., R. J. Beckman, and W. J. Conover (1979), A comparison of three methods for selecting values of input variables in the analysis of output from a computer code, *Technometrics*, *42*(1), 55–61. 17

Mearns, L. O., M. Hulme, T. R. Carter, and P. Whetton (2001), Climate scenario development, in *Climate Change 2001: The Scientific Basis, Chapter 13, Contribution of Working Group I to the Third Assessment Report of the Intergovernmental Pannel on Climate Change (IPCC)*, edited by J. T. Houghton, K. Maskell, X. Dai, P. J. van der Linden, C. A. Johnson, Y. Ding, D. J. Griggs, and M. Noguer, pp. 739–768, Cambridge University Press, Cambridge, UK. 3, 52, 88

Mearns, L. O., F. Giorgi, P. Whetton, D. Pabon, M. Hulme, and M. Lal (2003), Guidelines for use of climate scenarios developed from regional climate model experiments, http://www.ipcc-data.org/guidelines/dgm_no1_v1_10-2003.pdf, [Online; last accessed December-2009]. 53

Meehl, G. A., et al. (2007), Global climate projections, in *Climate Change 2007: The Physical Science Basis. Contribution of Working Group I to the Fourth Assessment Report of the Intergovernmental Panel on Climate Change*, edited by S. Solomon, D. Qin, M. Manning, Z. Chen, M. Marquis, K. Averyt, M. Tignor, and H. Miller, Cambridge University Press, Cambridge, United Kingdom and New York, NY, USA. 25, 88

Mimikou, M. A., E. Baltas, E. Varanou, and K. Pantazis (2000), Regional impacts of climate change on water resources quantity and quality indicators, *Journal of Hydrology*, *234*(1-2), 95–109, doi:10.1016/S0022-1694(00)00244-4. 86

Ministerio del Medio Ambiente y Confederación Hidrográfica del Ebro (2007), Plan especial de actuación en situaciones de alerta y eventual sequía en la cuenca hidrográfica del ebro [special plan of action in situations of alert and possible droughts on the ebro river basin], *Tech. rep.* 5

Montanari, A. (2005), Large sample behaviors of the generalized likelihood uncertainty estimation (GLUE) in assessing the uncertainty of rainfall-runoff simulations, *Water Resour. Res.*, *41*(8), W08,406, doi:10.1029/2004WR003826. 21, 42, 50, 114

Monteith, J. L. (1965), Evaporation and the environment, in *The State and movement of water in living organisms. 19th Symposia of the Society for Experimental Biology*, pp. 205–234, Cambridge Univ. Press, London, UK. 23

Moriasi, D. N., J. G. Arnold, M. W. V. Liew, R. L. Binger, R. D. Harmel, and T. Veith (2007), Model evaluation guidelines for systematic quantification of accuracy in watershed simulations, *Transactions of the ASABE*, *50*(3), 885–900. 17, 18, 29, 36, 37

Morris, M. D. (1991), Factorial sampling plans for preliminary computational experiments, *Technometrics*, *33*(2), 161–174. 16

Moss, R. H., et al. (2010), The next generation of scenarios for climate change research and assessment, *Nature*, *463*(7282), 747–756, doi:10.1038/nature08823. 52, 88

Moulin, L., E. Gaume, and C. Obled (2009), Uncertainties on mean areal precipitation: assessment and impact on streamflow simulations, *Hydrology And Earth System Sciences*, *13*, 99–114, doi:10.1029/2005WR00459. 30

MRC (2006), Link rainfall run off to DSF through SWAT model, *Powerpoint presentation*, Modelling Team. Technical Support Division, MRC Secretariat, Available online at http://www.mrcmekong.org. [Last accessed: January 2010]. 34

Mroczkowski, M., G. P. Raper, and G. Kuczera (1997), The quest for more powerful validation of conceptual catchment models, *Wat. Resour. Res.*, *33*(10), 2325–2335. 19

Muleta, M. K., and J. W. Nicklow (2005), Sensitivity and uncertainty analysis coupled with automatic calibration for a distributed watershed model, *Journal of Hydrology*, *306*(1-4), 127–145, doi:10.1016/j.jhydrol.2004.09.005. 32

Muleta, M. K., J. W. Nicklow, and E. G. Bekele (2007), Sensitivity of a distributed watershed simulation model to spatial scale, *Journal of Hydrologic Engineering*, *12*(2), 163–172, doi:10.1061/(ASCE)1084-0699(2007)12:2(163). 25

Murphy, J. (1999), An evaluation of statistical and dynamical techniques for downscaling local climate, *Journal of Climate*, *12*, 2256–2284. 53, 87, 88

Murphy, J. (2000), Predictions of climate change over Europe using statistical and dynamical downscaling techniques, *Jornal of Climatology*, *20*(5), 489–501, doi:10.1002/(SICI)1097-0088(200004)20:5⟨489::AID-JOC484⟩3.0.CO;2-6. 53

Murphy, J. M., D. M. H. Sexton, D. N. Barnett, G. S. Jones, M. J. Webb, and M. Collins (2004), Quantification of modelling uncertainties in a large ensemble of climate change simulations, *Nature*, *430*, 768–772, doi:10.1038/nature02771. 88

Nakićenović, N., et al. (2000), *Special Report on Emissions Scenarios: a Special Report of Working Group III of the Intergovernmental Panel on Climate Change*, Cambridge University Press, Cambridge, UK. 52, 53, 88

Nash, J. E., and J. V. Sutcliffe (1970), River flow forecasting through conceptual models part I - a discussion of principles, *Journal of Hydrology*, *10*(3), 282–290, doi:10.1016/0022-1694(70)90255-6. 17, 21, 29, 37, 38, 91, 94

Ndomba, P., F. Mtalo, and A. Killingtveit (2008), SWAT model application in a data scarce tropical complex catchment in Tanzania, *Physics and Chemistry of The Earth*, *33*(8-13), 626–632, doi:10.1016/j.pce.2008.06.013. 22

Neitsch, S. L., J. G. Arnold, J. R. Kiniry, and J. R. Williams (2005a), *Soil and Water Assessment Tool Theoretical Documentation Version 2005*, Grassland, Soil and Water Research Laboratory; Agricultural Research Service 808 East Blackland Road; Temple, Texas 76502; Blackland Research & Extension Center; Texas Agricultural Experiment Station 720 East Blackland Road Temple, Texas 76502, USA. 22, 23, 24, 25, 33, 34

Neitsch, S. L., J. G. Arnold, J. R. Kiniry, R. Srinivasan, and J. R. Williams (2005b), *Soil and Water Assessment Tool Input/Output file documentation, Version 2005*, Grassland, Soil and Water Research Laboratory; Agricultural Research Service 808 East Blackland Road; Temple, Texas 76502; Blackland Research & Extension Center; Texas Agricultural Experiment Station 720 East Blackland Road Temple, Texas 76502, USA. 22, 33

New, M., and M. Hulme (2000), Representing uncertainties in climate change scenarios: a Monte Carlo approach, *Integrated Assessment*, *1*(3), 203–213. 3, 88

Olesen, J. E., et al. (2007), Uncertainties in projected impacts of climate change on European agriculture and terrestrial ecosystems based on scenarios from regional climate models, *Climatic Change*, *81*(1), 123–143, doi:10.1007/s10584-006-9216-1. 3, 88

Olivera, F., M. Valenzuela, R. Srinivasan, J. Choi, H. Cho, S. Koka, and A. Agrawal (2006), ArcGIS-SWAT: A geodata model and GIS interface for SWAT, *Journal of the American Water Resources Association*, *42*(2), 295, doi:10.1111/j.1752-1688.2006.tb03839.x. 24

Payne, J. T., A. Wood, A. Hamlet, R. N. Palmer, and D. P. Lettenmaier (2004), Mitigating the effects of climate change on the water resources of the Columbia River basin, *Climatic Change*, *62*(1-3), 233–256, doi:10.1023/B:CLIM.0000013694.18154.d6. 88

Pebesma, E. J. (2004), Multivariable geostatistics in S: the gstat package, *Computers & Geosciences*, *30*, 683–691, doi:10.1016/j.cargo.2004.03.012. 30, 58

Peng, D. Z., and Z. X. Xu (2009), Simulating the impact of climate change on streamflow in the Tarim River basin by using a modified semi-distributed monthly water balance model, *Hydrological Processes*, *24*(2), 209–216, doi:10.1002/hyp.7485. 88

Peschel, J. M., P. K. Haan, and R. E. Lacey (2006), Influences of soil dataset resolution on hydrologic modeling, *Journal of The American Water Resources Association*, *42*, 1371–1389. 7

Pilling, C. G., and J. A. A. Jones (2002), The impact of future climate change on seasonal discharge, hydrological processes and extreme flows in the Upper Wye experimental catchment, Mid-Wales, *Hydrological Processes*, *16*(6), 1201–1213, doi:10.1002/hyp.1057. 86

Pokhrel, P., K. K. Yilmaz, and H. V. Gupta (2008), Multiple-criteria calibration of a distributed watershed model using spatial regularization and response signatures, *Journal of Hydrology*, doi:10.1016/j.jhydrol.2008.12.004, in press. 18

Pope, V. D., M. L. Gallani, P. R. Rowntree, and R. A. Stratton (2000), The impact of new physical parametrizations in the Hadley Centre climate model: HadAM3, *Climate Dynamics*, *16*(2-3), 123–146, doi:10.1007/s003820050009. 54, 90

Praskievicz, S., and H. Chang (2009), A review of hydrological modelling of basin-scale climate change and urban development impacts, *Progress in Physical Geography*, *33*(5), 650–671, doi:10.1177/0309133309348098. 86

Priestey, C. H. B., and T. R. J. (1972), On the assessment of surface heat flux and evaporation using large-scale parameters, *Mon. Weather Rev.*, *100*, 81–92. 23

Prudhomme, C. (2006), GCM and downscaling uncertainty in modelling of current river flow: why is it important for future impacts?, in *5th FRIEND World Conf.*, pp. 375–381, Havana. IAHS Publication 308. 53, 86

Prudhomme, C., and H. Davies (2007), Comparison of different sources of uncertainty in climate change impact studies in Great Britain, in *Climatic and anthropogenic impacts on the variability of water resources*, pp. 183–190, FRIEND, Paris. Paris, UNESCO. 88

Prudhomme, C., and H. Davies (2009a), Assessing uncertainties in climate change impact analyses on the river flow regimes in the UK. Part 1: baseline climate, *Climatic Change*, *93*(1-2), 177–195, doi:10.1007/s10584-008-9464-3. 3, 88

Prudhomme, C., and H. Davies (2009b), Assessing uncertainties in climate change impact analyses on the river flow regimes in the UK. Part 2: future climate, *Climatic Change*, *93*(1-2), 197–222, doi:10.1007/s10584-008-9461-6. 3, 88, 89, 91, 93, 94

Prudhomme, C., N. Reynard, and S. Crooks (2002), Downscaling of global climate models for flood frequency analysis: where are we now?, *Hydrol. Process*, *16*(6), 1137–1150, doi:10.1002/hyp.1054. 53, 86, 87, 88

R Development Core Team (2009), *R: A Language and Environment for Statistical Computing*, Vienna, Austria, ISBN 3-900051-07-0. 30, 58, 92

Rahmstorf, S., A. Cazenave, J. A. Church, J. E. Hansen, R. F. Keeling, D. E. Parker, and R. C. J. Somerville (2007), Recent climate observations compared to projections, *Science*, *316*(5825), 709, doi:10.1126/science.1136843. 54

Räisänen, J., and T. N. Palmer (2001), A probability and decision-model analysis of a multimodel ensemble of climate change simulations, *Journal of Climate*, *14*, 3212–3226. 52

Randall, D. A., et al. (2007), Climate models and their evaluation, in *Climate Change 2007: The Physical Science Basis. Contribution of Working Group I to the Fourth Assessment Report of the Intergovernmental Panel on Climate Change*, edited by S. Solomon, D. Qin, M. Manning, Z. Chen,

M. Marquis, K. B. Averyt, M. Tignor, and H. L. Miller, Cambridge University Press, Cambridge, United Kingdom and New York, NY, USA. 87

Refsgaard, J. C., J. P. van der Sluijs, J. Brown, and P. van der Keur (2006), A framework for dealing with uncertainty due to model structure error, *Advances in Water Resources*, *29*(11), 1586, doi:10.1016/j.advwatres.2005.11.013. 19

Refsgaard, J. C., J. P. van der Sluijs, A. L. Højberg, and P. A. Vanrolleghem (2007), Uncertainty in the environmental modelling process - a framework and guidance, *Environmental Modelling & Software*, *22*(11), 1543–1556, doi:10.1016/j.envsoft.2007.02.004. 2, 19, 20

Reilly, J., P. H. Stone, C. E. Forest, M. D. Webster, H. D. Jacoby, and R. G. Prinn (2001), Climate change. Uncertainty and climate change assessments, *Science*, *293*(5529), 430–433, doi:10.1126/science.1062001. 52, 88

Roeckner, E., et al. (1996), The atmospheric general circulation model ECHAM-4: Model description and simulation of present-day climate, *Report no. 218*, Max Planck Institute for Meteorology, Hamburg, Germany, ISSN 0937-1060. 54, 90

Rojas, R., L. Feyen, and A. Dassargues (2008), Conceptual model uncertainty in groundwater modeling: Combining generalized likelihood uncertainty estimation and bayesian model averaging, *Water Resources Research*, *44*(12), W12,418, doi:10.1029/2008WR006908. 117

Rowell, D. P. (2006), A demonstration of the uncertainty in projections of UK climate change resulting from regional model formulation, *Climate Change*, *79*, 243–257, doi:10.1007/s10584-006-9100-z. 88

Salathé, E. P. (2003), Comparison of various precipitation downscaling methods for the simulation of streamflow in a rainshadow river basin, *International Journal of Climatology*, *23*(8), 887–901, doi:10.1002/joc.922. 53, 86

Salathé, E. P. (2005), Downscaling simulations of future global climate with application to hydrologic modelling, *International Journal of Climatology*, *25*(4), 419–436, doi:10.1002/joc.1125. 53, 86, 87, 88

Saltelli, A., K. Cahn, and E. M. Scott (Eds.) (2000), *Sensitivity Analysis*, Wiley Series in Probability and Statistics, New York: John Wiley and Sons. 16

Sankarasubramanian, A., U. Lall, F. A. Souza Filho, and A. Sharma (2009), Improved water allocation utilizing probabilistic climate forecasts: Short-term water contracts in a risk management framework, *Water Resour. Res.*, *45*(11), W11,409, doi:10.1029/2009WR007821. 88

Schmidli, J., C. Frei, and P. L. Vidale (2006), Downscaling from GCM precipitation: a benchmark for dynamical and statistical downscaling methods, *International Journal of Climatology*, *26*(5), 679–689, doi:10.1002/joc.1287. 53

Schmidli, J., C. M. Goodess, C. Frei, M. R. Haylock, Y. Hundecha, J. Ribalaygua, and T. Schmith (2007), Statistical and dynamical downscaling of precipitation: An evaluation and comparison of scenarios for the European Alps, *Journal of Geophysical Research*, *112*(D4), D04,105, doi:10.1029/2005JD007026. 53

Schneider, S. H. (2002), Can we estimate the likelihood of climatic changes at 2100?, *Climatic Change*, *52*(4), 441–451, doi:10.1023/A:1014276210717. 3, 52, 88

Schoof, J. T., and S. Pryor (2001), Downscaling temperature and precipitation: a comparison of regression-based methods and artificial neural networks, *International Journal of Climatology*, *21*(7), 773–790, doi:10.1002/joc.655. 53

Schuol, J., K. C. Abbaspour, H. Yang, R. Srinivasan, and A. J. B. Zehnder (2008a), Modeling blue and green water availability in Africa, *Water Resour. Res.*, *44*(7), W07,406, doi:10.1029/2007WR006609. 22, 37

Schuol, J., K. Abbaspour, R. Srinivasan, and H. Yang (2008b), Estimation of freshwater availability in the West African sub-continent using the SWAT hydrologic model, *Journal of Hydrology*, *352*(1-2), 30, doi:10.1016/j.jhydrol.2007.12.025. 22

Seibert, J. (1997), Estimation of parameter uncertainty in the HBV model, *Nordic Hydrol.*, *28*(4/5), 247–262. 2, 16

Seibert, J., and J. J. McDonnell (2002), On the dialog between experimentalist and modeler in catchment hydrology: Use of soft data for multicriteria model calibration, *Water Resources Research*, *38*(11), 1241, doi:10.1029/2001WR000978. 18

Setegn, S. G., R. Srinivasan, A. M. Melesse, and B. Dargahi (2009), SWAT model application and prediction uncertainty analysis in the Lake Tana Basin, Ethiopia, *Hydrological Processes*, *4*(3), 357–367, doi:10.1002/hyp.7457. 22

Sieber, A., and S. Uhlenbrook (2005), Sensitivity analyses of a distributed catchment model to verify the model structure, *Journal of Hydrology*, *310*(1-4), 216–235, doi:10.1016/j.jhydrol.2005.01.004. 16

Singh, V. P. (Ed.) (1995), *Computer Models of Watershed Hydrology*, Water Resources Publications. 22

Singh, V. P., and D. K. Frevert (Eds.) (2001), *Mathematical Models of Large Watershed Hydrology*, Water Resources Publication. 22

Singh, V. P., and D. K. Frevert (Eds.) (2006), *Watershed Models*, CRC Press, 6000 Broken Sound Parkway NW, Suite 300. Boca Raton, FL 33487-2742. 22

Sloan, P. G., and I. D. Morre (1984), Modeling subsurface stormflow on steeply sloping forested watersheds, *Water Resources Research*, *20*(12), 1815–1822. 24

Sloan, P. G., I. D. Morre, G. B. Coltharp, and J. D. Eigel (1983), Modeling surface and subsurface stormflow on steeply-sloped forested watersheds, Water Resources Inst. Report 142, Univ. Kentucky, Lexington. 24

Smith, P. J., K. J. Beven, and J. A. Tawn (2008a), Detection of structural inadequacy in process-based hydrological models: A particle-filtering approach, *Water Resour. Res.*, *44*(1), W01,410, doi:10.1029/2006WR005205. 19

Smith, P. J., K. J. Beven, and J. A. Tawn (2008b), Informal likelihood measures in model assessment: Theoretic development and investigation, *Advances in Water Resources*, *31*(8), 1087, doi:10.1016/j.advwatres.2008.04.012. 21

Solomon, S., et al. (2007), Technical summary, in *Climate Change 2007: The Physical Science Basis. Contribution of Working Group I to the Fourth Assessment Report of the Intergovernmental Panel on Climate Change*, edited by S. Solomon, D. Qin, M. Manning, Z. Chen, M. Marquis, K. B. Averyt, M. Tignor, and H. Miller, Cambridge University Press, Cambridge, United Kingdom and New York, NY, USA. 52

Sophocleous, M., J. Koelliker, R. Govindaraju, T. Birdie, S. Ramireddygari, and S. Perkins (1999), Integrated numerical modelling for basin-wide water management: the case of the rattlesnake creek basin in south-central kansas, *Journal of Hydrology*, pp. 179–196. 22

Sorooshian, S., and J. A. Dracup (1980), Stochastic parameter estimation procedures for hydrologic rainfall-runoff models: Correlated and heteroscedastic error cases, *Water Resour. Res.*, *16*(2), 430–442. 2, 16

Sorooshian, S., and V. K. Gupta (1983), Automatic calibration of conceptual rainfall-runoff models : The question of parameter observability and uniqueness, *Water Resour. Res.*, *19*(1), 260–268. 2, 16

Sorooshian, S., and V. K. Gupta (1985), The analysis of structural identifiability: Theory and application to conceptual rainfall-runoff models, *Water Resour. Res.*, *21*(4), 487–495. 19

Sorooshian, S., V. K. Gupta, and J. L. Fulton (1983), Evaluation of maximum likelihood parameter estimation techniques for conceptual rainfall-runoff models : Influence of calibration data variability and length on model credibility, *Water Resour. Res.*, *19*(1), 251–259. 2, 16

Stedinger, J. R., R. M. Vogel, S. U. Lee, and R. Batchelder (2008), Appraisal of the generalized likelihood uncertainty estimation (GLUE) method, *Water Resour. Res.*, *44*, W00B06, doi:10.1029/2008WR006822. 21

Steele-Dunne, S., P. Lynch, R. McGrath, T. Semmler, S. Wang, J. Hanafin, and P. Nolan (2008), The impacts of climate change on hydrology in Ireland, *Journal of Hydrology*, *356*(1-2), 28–45, doi:10.1016/j.jhydrol.2008.03.025. 2, 86, 88

Tebaldi, C. (2004), Regional probabilities of precipitation change: A Bayesian analysis of multimodel simulations, *Geophysical Research Letters*, *31*(24), L24,213, doi:10.1029/2004GL021276. 53, 90

Tebaldi, C., and R. Knutti (2007), The use of the multi-model ensemble in probabilistic climate projections., *Philos Transact A Math Phys Eng Sci*, *365*(1857), 2053–2075, doi:10.1098/rsta.2007.2076. 25, 52, 88

Tebaldi, C., R. L. Smith, D. Nychka, and L. O. Mearns (2005), Quantifying uncertainty in projections of regional climate change: A Bayesian approach to the analysis of multi-model ensembles, *Journal of Climate*, *18*, 1524–1540. 88

Teegavarapu, R. S., and V. Chandramouli (2005), Improved weighting methods, deterministic and stochastic data-driven models for estimation of missing precipitation records, *Journal of Hydrology*, *312*(1-4), 191, doi:10.1016/j.jhydrol.2005.02.015. 55

Teutschbein, C., and J. Seibert (2010), Regional climate models for hydrological impact studies at the catchment scale: a review of recent model strategies, *Geography Compass*, in press. 54, 87

Thodsen, H. (2007), The influence of climate change on stream flow in Danish rivers, *Journal of Hydrology*, *333*(2-4), 226–238, doi:10.1016/j.jhydrol.2006.08.012. 2, 86

Thomson, A. M., R. A. Brown, N. J. Rosenberg, R. Srinivasan, and R. C. Izaurralde (2005), Climate change impacts for the conterminous USA: An integrated assessment: Part4. Water resources, *Climatic Change*, *69*(1), 67–88, doi:10.1007/s10584-005-3610-y. 22, 86

Trenberth, K., et al. (2007), Observations: Surface and atmospheric climate change, in *Climate Change 2007: The Physical Science Basis. Contribution of Working Group I to the Fourth Assessment Report of the Intergovernmental Panel on Climate Change*, edited by S. Solomon, D. Qin, M. Manning, Z. Chen, M. Marquis, K. Averyt, M. Tignor, and H. Miller, Cambridge University Press, Cambridge, United Kingdom and New York, NY, USA. 1, 51

Tripathi, M. P., N. S. Raghuwanshi, and G. P. Rao (2006), Effect of watershed subdivision on simulation of water balance components, *Hydrological Processes*, *20*(5), 1137, doi:10.1002/hyp.5927. 25

Uhlenbrook, S., and A. Sieber (2005), On the value of experimental data to reduce the prediction uncertainty of a process-oriented catchment model, *Environmental Modelling & Software*, *20*(1), 19–32, doi:10.1016/j.envsoft.2003.12.006. 19

Uhlenbrook, S., J. Seibert, C. Leibundgut, and A. Rohde (1999), Prediction uncertainty of conceptual rainfall-runoff models caused by problems to identify model parameters and structure, *Hydrological Sciences Journal*, *44*(5), 779–797. 16, 19

van Griensven, A., and W. Bauwens (2003), Multiobjective autocalibration for semidistributed water quality models, *Wat. Resour.Res.*, *39*(12), 1348, doi:10.1029/2003WR002284. 17, 18

van Griensven, A., and T. Meixner (2003), Sensitivity, optimization and uncertainty analysis for the model parameters of SWAT, in *SWAT2003: 2nd International SWAT Conference*, Bary, Italy, 1-4 July. 32

van Griensven, A., T. Meixner, S. Grunwald, T. Bishop, M. Di Luzio, and R. Srinivasan (2006), A global sensitivity analysis tool for the parameters of multi-variable catchment models, *Journal of Hydrology*, *324*(1-4), 10–23, doi:10.1016/j.jhydrol.2005.09.008. 17, 32

Van Liew, M. W., and J. Garbrecht (2003), Hydrologic simulation of the Little Washita River experimental watershed using SWAT, *Journal of the American Water Resources Association*, *39*(2), 413–426, doi:10.1111/j.1752-1688.2003.tb04395.x. 22

Viner, D. (2003), A qualitative assessment of the sources of uncertainty in climate change impacts assessment studies, in *Climatic Change: Implications for the Hydrological Cycle and for Water Management*, *Advances in Global Change Research*, vol. 10, pp. 139–149, Springer Netherlands, doi:10.1007/0-306-47983-4_8. 3, 88, 89

Vogel, R., and N. Fennessey (1995), Flow duration curves II: A review of applications in water resources planning, *Water Resources Bulletin*, *31*(6), 1029–1039, doi:10.1111/j.1752-1688.1995.tb03419.x. 44, 92

Vogel, R., and N. M. Fennessey (1994), Flow duration curves I: A new interpretation and confidence intervals, *ASCE, Journal of Water Resources Planning and Management*, *120*(4). 44, 92

Vrugt, J. A., H. V. Gupta, W. Bouten, and S. Sorooshian (2003a), A Shuffled Complex Evolution Metropolis algorithm for optimization and uncertainty assessment of hydrological model parameters, *Water Resources Research*, *39*(8), 1201, doi:10.1029/2002WR001642. 17

Vrugt, J. A., H. V. Gupta, L. Bastidas, W. Bouten, and S. Sorooshian (2003b), Effective and efficient algorithm for multiobjective optimization of hydrologic models, *Water Resources Research*, *39*, 1214, doi:10.1029/2002WR001746. 18, 19

Vrugt, J. A., B. O. Nuallain, B. A. Robinson, W. Bouten, S. Dekker, and P. Sloot (2006), Application of parallel computing to stochastic parameter estimation in environmental models, *Computers & Geosciences*, *32*(8), 1139–1155, doi:10.1016/j.cageo.2005.10.015. 17

Vrugt, J. A., C. J. F. ter Braak, M. P. Clark, J. M. Hyman, and B. A. Robinson (2008), Treatment of input uncertainty in hydrologic modeling: Doing hydrology backward with Markov Chain Monte Carlo simulation, *Water Resources Research*, *44*, W00B09, doi:10.1029/2007WR006720. 19

Vrugt, J. A., C. J. F. Braak, H. V. Gupta, and B. A. Robinson (2009a), Equifinality of formal (DREAM) and informal (GLUE) Bayesian approaches in hydrologic modeling?, *Stochastic Environmental Research and Risk Assessment*, *23*(7), 1011–1026, doi:10.1007/s00477-008-0274-y. 21

Vrugt, J. A., C. J. F. ter Braak, H. V. Gupta, and B. A. Robinson (2009b), Response to comment by Keith Beven on "Equifinality of formal (DREAM) and informal (GLUE) Bayesian approaches in hydrologic modeling?", *Stochastic Environmental Research and Risk Assessment*, *23*(7), 1061–1062, doi:10.1007/s00477-008-0284-9. 22

Wagener, T., D. P. Boyle, M. J. Lees, H. S. Wheater, H. V. Gupta, and S. Sorooshian (2001), A framework for development and application of hydrological models, *Hydrology and Earth System Sciences*, *5*(1), 13–26. 18

Wagener, T., N. McIntyre, M. J. Lees, H. S. Wheater, and H. V. Gupta (2003), Towards reduced uncertainty in conceptual rainfall-runoff modelling: dynamic identifiability analysis, *Hydrol Process*, *17*(2), 455–476, doi:10.1002/hyp.1135. 19

Wagener, T., H. S. Wheather, and H. V. Gupta (2004), *Rainfall-Runoff Modelling in Gauged and Ungauged Catchments*, 300 pp., Imperial College Press, London UK. 15, 16, 22, 86

Walker, W. E., P. Harremoës, J. Rotmans, J. P. van der Sluijs, M. van Asselt, P. Janssen, and M. K. von Krauss (2003), Defining uncertainty: A conceptual basis for uncertainty management in model-based decision support, *Integrated Assessment, Vol 4, No 1 (2003)*, *4*(1), 5–17, doi:10.1076/iaij.4.1.5.16466. 2, 19, 20

Wang, M. H., A. T. Hjelmfelt, and J. Garbrecht (2000), DEM aggregation for watershed modeling, *Journal of The American Water Resources Association*, *36*(3), 579–584. 7

Wang, X., and A. M. Melesse (2006), Effects of STATSGO and SSURGO as inputs on SWAT model's snowmelt simulation, *Journal of The American Water Resources Association*, *42*, 1217–1236. 7

Webster, M., et al. (2003), Uncertainty analysis of climate change and policy response, *Climatic Change*, *61*(3), 295–320, doi:10.1023/B:CLIM.0000004564.09961.9f. 52, 88

Wheater, H. S. (2008), Modelling hydrological process in arid and semi-arid areas: an introduction to the workshop, in *Hydrological Modelling in Arid and Semi-Arid Areas*, edited by H. Wheater, S. Sorooshian, and K. D. Sharma, Cambridge University Press. 15, 16, 86

Wheater, H. S., N. McIntire, and T. Wagener (2008), Calibration, uncertainty, and regional analysis of conceptual rainfall-runoff models, in *Hydrological Modelling in Arid and Semi-Arid Areas*, edited by H. Wheater, S. Sorooshian, and K. D. Sharma, Cambridge University Press. 19

White, K. L., and I. Chaubey (2005), Sensitivity analysis, calibrations, and validations for a multisite and multivariable SWAT model, *Journal of the American Water Resources Association*, *41*(5), 1077–1089, doi:10.1111/j.1752-1688.2005.tb03786.x. 32

Whitehead, P., and P. Young (1979), Water quality in river systems: Monte-Carlo analysis, *Water Resources Research*, *15*, 451–459. 20

Wigley, T. M., and S. C. Raper (2001), Interpretation of high projections for global-mean warming, *Science*, *293*(5529), 451–454, doi:10.1126/science.1061604. 88

Wilby, R. L. (2005), Uncertainty in water resource model parameters used for climate change impact assessment, *Hydrological Processes*, *19*(16), 3201–3219, doi:10.1002/hyp.5819. 3, 88

Wilby, R. L., and I. Harris (2006), A framework for assessing uncertainties in climate change impacts: Low-flow scenarios for the River Thames, UK, *Water Resour. Res.*, *42*(2), W02,419, doi:10.1029/2005WR004065. 3, 53, 88, 89, 91, 94, 117

Wilby, R. L., and T. M. L. Wigley (1997), Downscaling general circulation model output: a review of methods and limitations, *Progress in Physical Geography*, *21*(4), 530–548, doi:10.1177/030913339702100403. 53

Wilby, R. L., L. E. Hay, and G. H. Leavesley (1999), A comparison of downscaled and raw GCM output: implications for climate change scenarios in the San Juan River basin, Colorado, *Journal ff Hydrology*, *225*(1-2), 67–91, doi:10.1016/S0022-1694(99)00136-5. 53, 86, 87

Wilby, R. L., L. E. Hay, W. J. Gutowski Jr., R. W. Arritt, E. S. Takle, Z. Pan, G. H. Leavesley, and M. P. Clark (2000), Hydrological responses to dynamically and statistically downscaled climate model output, *Geophysical Research Letters*, *27*(8), 1199–1202. 53, 86, 88

Willmott, C. J. (1981), On the validation of models, *Physical Geography*, *2*, 184–194. 17, 29, 37

Willmott, C. J. (1984), On the evaluation of model performance in physical geography, in *Spatial Statistics and Models*, edited by G. L. Gaile and C. J. Willmott, pp. 443–460, Dordrecht, Holland: D. Reidel. 17, 18, 29, 37

Willmott, C. J., S. G. Ackleson, R. E. Davis, J. J. Feddema, K. M. Klink, D. R. Legates, J. O'Donnell, and C. M. Rowe (1985), Statistics for the Evaluation and Comparison of Models, *Journal of Geophysical Research*, *90*(C5), 8995–9005, doi:10.1029/JC090iC05p08995. 18, 37

Winchell, M., R. Srinivasan, M. Di Luzio, and J. G. Arnold (2007), *ArcSWAT interface for SWAT2005 - User's guide*, Blackland Research Center, Texas Agricultural Experiment Station and Grassland, Soil and Water Research Laboratory, USDA Agricultural Research Service, Temple, Tex. 24

Wood, A. W., L. R. Leung, V. Sridhar, and D. P. Lettenmaier (2004), Hydrologic implications of dynamical and statistical approaches to downscaling climate model outputs, *Climatic Change*, *62*(1-3), 189–216, doi:10.1023/B:CLIM.0000013685.99609.9e. 53, 86, 87, 88, 116

Wu, K., and C. A. Johnston (2007), Hydrologic response to climatic variability in a great lakes watershed: A case study with the SWAT model, *Journal of Hydrology*, *337*(1-2), 187, doi:10.1016/j.jhydrol.2007.01.030. 22

Xu, C.-y. (1999), From GCMs to river flow: a review of downscaling methods and hydrologic modelling approaches, *Progress in Physical Geography*, *23*(2), 229–249, doi:10.1177/030913339902300204. 1, 2, 53, 85, 86, 87, 88

Yang, J., P. Reichert, K. C. Abbaspour, and H. Yang (2007), Hydrological modelling of the chaohe basin in china: Statistical model formulation and bayesian inference, *Journal of Hydrology*, *340*(3-4), 167, doi:10.1016/j.jhydrol.2007.04.006. 22

Yang, J., P. Reichert, K. C. Abbaspour, J. Xia, and H. Yang (2008), Comparing uncertainty analysis techniques for a SWAT application to the Chaohe Basin in China, *Journal of Hydrology*, *358*(1-2), 1–23, doi:10.1016/j.jhydrol.2008.05.012. 20

Yapo, P. O., H. V. Gupta, and S. Sorooshian (1996), Automatic calibration of conceptual rainfall-runoff models: Sensitivity to calibration data, *Journal of Hydrology*, *181*(1-4), 23–48. 16, 17, 29, 36, 37

Yapo, P. O., H. V. Gupta, and S. Sorooshian (1998), Multi-objective global optimization for hydrologic models, *Journal of Hydrology*, *204*(1-4), 83–97, doi:10.1016/S0022-1694(97)00107-8. 17, 18

Yilmaz, K. K., H. V. Gupta, and T. Wagener (2008), A process-based diagnostic approach to model evaluation: Application to the NWS distributed hydrologic model, *Water Resources Research*, *44*(9), W09,417, doi:10.1029/2007WR006716. 19, 37, 44

Young, P. C. (1983), The validity and credibility of models for badly-defined systems, in *Uncertainty and Forecasting of Water Quality*, edited by M. B. Beck and G. van Straten, pp. 69–98, Springer-Verlag:Berlin. 20

Zambrano-Bigiarini, M., B. Majone, A. Bellin, G. Botter, L. Nicotina, S. Zanetti, E. Alessi Celegon, M. Marani, and A. Rinaldo (2007), Intermediate data collection for the entire Ebro River Basin, *Aquaterra deliverable C3.4*, University of Trento and University of Padova. 6, 11

Zambrano-Bigiarini, M., A. Bellin, G. Botter, L. Nicotina, S. Zanetti, E. Alessi Celegon, M. Marani, and A. Rinaldo (2008), GEOTRANSF applications to the Ebro River Basin (analysis of data consistency and conceptual model), *Aquaterra deliverable C3.5*, University of Trento and University of Padova. 10

Zhang, X., R. Srinivasan, and M. Van Liew (2008), Multi-site calibration of the SWAT model for hydrologic modeling, *Transactions of The Asabe*, *51*(6), 2039–2049, doi:10.1029/2004WR003695. 18

Zhang, X., R. Srinivasan, K. Zhao, and M. Van Liew (2009a), Evaluation of global optimization algorithms for parameter calibration of a computationally intensive hydrologic model, *Hydrological Processes*, *23*(3), 430–441, doi:10.1002/hyp.7152. 17

Zhang, X., R. Srinivasan, and D. Bosch (2009b), Calibration and uncertainty analysis of the SWAT model using Genetic Algorithms and Bayesian Model Averaging, *Journal of Hydrology*, *374*(3-4), 307, doi:10.1016/j.jhydrol.2009.06.023. 22, 32

Zierl, B., and H. Bugmann (2005), Global change impacts on hydrological processes in Alpine catchments, *Water Resources Research*, *41*, W02,028, doi:10.1029/2004WR003447. 88

Appendices

A

Selected Gauging Stations

This Appendix present the gauging stations used in the present dissertation.

A.1 Precipitation

TABLE A.1: Precipitation gauging stations selected for the analysis, with more than 70% of days with information within the control period 01/Jan/1661-31/Dec/1990

N°	ID	Data N° in CTRL	% Data in CTRL	Easting, [m] (ED_50, Z30N)	Northing, [m] (ED_50, Z30N)	Elevation [m.a.s.l.]	CHE_BASIN_NAMEs
1	P9001	9281	0.85	407235.94	4761652.30	855	EBRO
2	P9008X	10926	1.00	430755.90	4763101.71	858	EBRO
3	P9012	10041	0.92	422553.49	4760474.64	850	EBRO
4	P9015	10045	0.92	415115.36	4745044.05	740	EBRO
5	P9019	10014	0.91	423070.09	4739829.28	716	EBRO
6	P9027	10864	0.99	428594.66	4735882.73	1025	RUDRON
7	P9034	9478	0.86	448757.76	4721019.98	990	HOMINO
8	P9037	9710	0.89	466184.21	4731061.70	598	HOMINO
9	P9041	10776	0.98	453311.97	4754458.00	595	NELA
10	P9044	9741	0.89	459162.26	4754914.26	595	NELA
11	P9048	10712	0.98	467937.31	4765541.18	693	NELA
12	P9056	10397	0.95	473042.49	4751822.60	645	JEREA
13	P9060	8005	0.73	481221.38	4741338.15	697	PURON
14	P9063O	10541	0.96	494737.71	4748779.53	575	OMECILLO
15	P9063U	8128	0.74	500522.07	4743780.32	674	OMECILLO
16	P9064A	10773	0.98	501340.27	4738443.95	620	OMECILLO
17	P9064	10957	1.00	500976.74	4738906.59	566	OMECILLO
18	P9064I	9039	0.82	496002.65	4739709.69	500	OMECILLO
19	P9065I	10314	0.94	496135.25	4733139.31	473	EBRO
20	P9069A	8766	0.80	505779.39	4727156.48	475	BAYAS
21	P9069	10926	1.00	503641.60	4725180.88	520	EBRO
22	P9072	9099	0.83	513957.42	4756102.52	618	BAYAS
23	P9072D	8828	0.81	515709.45	4752898.16	652	BAYAS
24	P9072H	9192	0.84	508524.71	4751867.52	606	BAYAS
25	P9072I	9131	0.83	507394.59	4748627.25	604	BAYAS
26	P9072J	9195	0.84	502041.52	4748407.65	710	BAYAS
27	P9073I	9039	0.82	552382.11	4741881.86	674	ZADORRA
28	P9074C	9161	0.84	549566.42	4751331.58	638	ZADORRA
29	P9074	8077	0.74	550248.86	4744827.43	605	ZADORRA
30	P9076	10915	1.00	531848.61	4753170.00	570	ZADORRA
31	P9077E	9679	0.88	528012.67	4765461.70	559	ZADORRA
32	P9078	8919	0.81	530185.80	4760134.17	600	ZADORRA
33	P9080C	8919	0.81	527197.62	4754167.98	546	ZADORRA
34	P9080	10926	1.00	528480.54	4756332.54	540	ZADORRA
35	P9083	10896	0.99	528147.75	4743529.37	547	ZADORRA
36	P9085I	9045	0.82	531179.12	4740827.85	575	ZADORRA
37	P9086	9635	0.88	530662.90	4744558.08	515	ZADORRA
38	P9087	7829	0.71	528212.31	4744393.36	521	ZADORRA
39	P9091I	8765	0.80	522520.69	4749678.13	517	ZADORRA
40	P9092	9172	0.84	516036.31	4748827.06	550	ZADORRA
41	P9093	8462	0.77	516326.85	4741085.13	495	ZADORRA
42	P9094U	10520	0.96	510416.60	4730153.98	467	ZADORRA
43	P9095	10926	1.00	535451.71	4722463.61	785	EGA
44	P9095E	8857	0.81	537365.55	4730678.96	774	ZADORRA
45	P9103	10957	1.00	523432.98	4721394.63	744	INGLARES

Continued on next page...

Table A.1 – Continued

N°	ID	Data N° in CTRL	% Data in CTRL	Easting, [m] (ED_50, Z30N)	Northing, [m] (ED_50, Z30N)	Elevation [m.a.s.l.]	CHE_BASIN_NAMEs
46	P9103I	8910	0.81	517761.10	4721963.86	578	INGLARES
47	P9103X	9050	0.83	509857.80	4723274.49	459	EBRO
48	P9105	10791	0.98	483360.05	4685964.84	960	TIRON
49	P9107	10776	0.98	484276.55	4696573.22	770	TIRON
50	P9118E	8646	0.79	505728.00	4706674.98	540	TIRON
51	P9121	10804	0.99	512151.16	4713715.95	479	TIRON
52	P9131I	8676	0.79	508811.46	4668153.84	900	NAJERILLA
53	P9136	10896	0.99	510567.23	4675558.67	1020	NAJERILLA
54	P9139	7949	0.72	522787.24	4688974.03	690	NAJERILLA
55	P9145A	10926	1.00	529384.08	4703464.97	430	EBRO
56	P9145	10835	0.99	529041.86	4703401.84	437	EBRO
57	P9155	8126	0.74	531584.24	4666029.17	1103	IREGUA
58	P9160	8430	0.77	548849.26	4701754.22	370	EBRO
59	P9164	10927	1.00	547362.87	4681755.85	717	LEZA
60	P9168	8369	0.76	562215.61	4683136.47	898	LEZA
61	P9170	10946	1.00	555027.80	4700227.03	352	EBRO
62	P9174	9071	0.83	578022.20	4690944.77	310	EBRO
63	P9175	10957	1.00	533986.97	4719340.77	756	EGA
64	P9176	10929	1.00	541207.53	4719472.44	740	EGA
65	P9177U	8208	0.75	549331.01	4727144.79	600	EGA
66	P9182I	8160	0.74	574801.98	4715989.67	572	EGA
67	P9185	8943	0.82	545254.62	4656912.02	1223	CIDACOS
68	P9198	10741	0.98	703136.38	4735971.44	1160	ARAGON (TRAMO SUPERIOR)
69	P9199A	8247	0.75	701851.89	4728523.82	950	ARAGON (TRAMO SUPERIOR)
70	P9199	9987	0.91	699742.53	4725838.34	1000	ARAGON (TRAMO SUPERIOR)
71	P9200	10897	0.99	704628.75	4722430.34	920	ARAGON (TRAMO SUPERIOR)
72	P9205	8004	0.73	694779.50	4728105.05	1040	ARAGON (TRAMO SUPERIOR)
73	P9207	9678	0.88	684127.01	4734666.59	860	ARAGON (TRAMO SUPERIOR)
74	P9210	10866	0.99	685835.65	4717610.32	690	ARAGON (TRAMO SUPERIOR)
75	P9215	9990	0.91	665056.82	4718597.70	510	ARAGON (TRAMO SUPERIOR)
76	P9223	10774	0.98	648334.28	4720133.60	515	IRATI
77	P9224	10376	0.95	646380.79	4717654.12	455	IRATI
78	P9228	8125	0.74	649926.62	4761029.71	820	IRATI
79	P9236	10342	0.94	646633.25	4751853.94	1047	IRATI
80	P9236E	7915	0.72	648292.59	4748556.40	1060	IRATI
81	P9246	8766	0.80	626316.19	4692544.43	340	ARAGON (AGUAS ABAJO YESA)
82	P9247	8549	0.78	619302.81	4690600.95	348	ARAGON (AGUAS ABAJO YESA)
83	P9252	10806	0.99	610583.18	4705113.03	395	ARAGON (AGUAS ABAJO YESA)
84	P9255	9009	0.82	611004.81	4688613.33	304	ARAGON (AGUAS ABAJO YESA)
85	P9257E	8280	0.76	620598.39	4757827.62	615	ARGA
86	P9262	9526	0.87	611480.01	4741535.65	442	ARGA
87	P9269	10255	0.94	566824.30	4748886.38	525	ARGA
88	P9279	9256	0.84	586298.70	4728154.89	475	ARGA
89	P9290	10806	0.99	594537.23	4656997.81	438	ALHAMA
90	P9293	9188	0.84	603208.30	4670878.18	300	ALHAMA
91	P9301	10684	0.97	608518.94	4646246.52	410	QUEILES
92	P9305	10805	0.99	628741.72	4648559.02	242	EBRO
93	P9309	9831	0.90	614928.93	4628577.41	594	HUECHA
94	P9311A	8254	0.75	621393.53	4632602.51	448	HUECHA
95	P9311	8979	0.82	621789.34	4632393.29	448	HUECHA
96	P9317	9622	0.88	649619.49	4680258.91	484	ARBA
97	P9318	7760	0.71	656647.47	4676585.40	463	ARBA
98	P9322	9466	0.86	669963.73	4695011.72	760	ARBA
99	P9329	10074	0.92	653679.61	4691641.43	601	ARBA
100	P9330	10926	1.00	642292.20	4683254.18	442	ARBA
101	P9331F	8675	0.79	643318.72	4672227.99	360	ARBA
102	P9333	9100	0.83	646773.26	4666127.53	321	ARBA
103	P9348	8212	0.75	569421.83	4579627.73	783	JALON
104	P9350A	8890	0.81	579125.03	4574113.71	700	JALON
105	P9353	10198	0.93	586237.86	4578296.88	730	JALON
106	P9354	10773	0.98	586710.22	4571825.34	680	JALON
107	P9356E	8094	0.74	603280.14	4526731.36	1180	PIEDRA
108	P9356I	8248	0.75	600698.53	4527219.99	1147	PIEDRA
109	P9359	8160	0.74	614381.27	4550430.34	1108	PIEDRA
110	P9360	10898	0.99	606255.04	4558851.96	820	PIEDRA
111	P9370	8523	0.78	606050.08	4572914.61	678	JALON
112	P9371	10713	0.98	607751.35	4575839.19	570	JALON
113	P9372	10957	1.00	644929.82	4479801.61	1023	JILOCA
114	P9375	8825	0.81	642199.75	4491995.71	983	JILOCA
115	P9377	7973	0.73	626569.77	4510529.80	1196	JILOCA
116	P9380	9284	0.85	651128.96	4522497.22	1141	JILOCA
117	P9381	8854	0.81	642874.90	4525263.63	932	JILOCA

Continued on next page...

Table A.1 – Continued

N°	ID	Data N° in CTRL	% Data in CTRL	Easting, [m] (ED_50, Z30N)	Northing, [m] (ED_50, Z30N)	Elevation [m.a.s.l.]	CHE_BASIN_NAMEs
118	P9388	8798	0.80	637989.77	4544698.24	793	JILOCA
119	P9390	10957	1.00	633427.76	4552788.84	779	JILOCA
120	P9392	9773	0.89	621263.44	4557574.33	842	JILOCA
121	P9399	10807	0.99	593734.78	4602356.65	1050	JALON
122	P9400	7729	0.70	602289.09	4597044.06	950	JALON
123	P9401	7910	0.72	601604.01	4591358.62	752	JALON
124	P9405E	8126	0.74	626904.76	4592221.50	460	JALON
125	P9408	9160	0.84	611204.35	4600754.40	631	ARANDA
126	P9414	9163	0.84	623065.94	4599620.74	482	ARANDA
127	P9416A	10107	0.92	632727.50	4596090.03	377	JALON
128	P9420	10529	0.96	629883.44	4590454.26	460	JALON
129	P9421	10501	0.96	649697.79	4571738.94	681	JALON
130	P9422	10835	0.99	640959.70	4577086.76	830	JALON
131	P9424E	8065	0.74	657463.77	4578536.87	660	JALON
132	P9425	10440	0.95	635133.07	4586508.96	510	JALON
133	P9425F	8068	0.74	639985.81	4584163.88	598	JALON
134	P9425I	8461	0.77	649140.04	4585272.25	496	JALON
135	P9426	10836	0.99	652928.26	4585197.01	531	JALON
136	P9427A	8221	0.75	634456.53	4592913.46	380	JALON
137	P9427	8612	0.79	635381.44	4593085.00	370	JALON
138	P9428	10807	0.99	645444.08	4590010.18	435	JALON
139	P9433O	9496	0.87	653781.12	4625605.65	235	EBRO
140	P9434	10957	1.00	665849.88	4614241.49	247	EBRO
141	P9440E	8139	0.74	642286.18	4561563.31	866	HUERVA
142	P9443	10656	0.97	660633.51	4587647.26	460	HUERVA
143	P9446	10772	0.98	718417.16	4739248.04	1285	GALLEGO
144	P9446E	9526	0.87	718562.05	4741136.32	1460	GALLEGO
145	P9451	10772	0.98	726344.97	4738237.47	1660	GALLEGO
146	P9452	10745	0.98	720535.23	4734189.27	1091	GALLEGO
147	P9460	10926	1.00	716824.35	4710851.11	790	GALLEGO
148	P9463	7946	0.72	713861.05	4701712.53	780	GALLEGO
149	P9470E	7822	0.71	698504.41	4706136.70	920	GALLEGO
150	P9474	8857	0.81	686090.82	4695206.22	589	GALLEGO
151	P9476	8945	0.82	681538.24	4691629.43	696	GALLEGO
152	P9477	10651	0.97	689844.36	4687589.81	745	GALLEGO
153	P9478	8553	0.78	690578.63	4682485.47	582	GALLEGO
154	P9480	9156	0.84	688778.61	4670953.91	475	GALLEGO
155	P9481	10795	0.98	684090.64	4662279.91	400	GALLEGO
156	P9484	10957	1.00	699658.48	4686504.12	760	GALLEGO
157	P9485	9617	0.88	695842.41	4687754.82	790	GALLEGO
158	P9487	10569	0.96	699659.57	4675977.05	469	GALLEGO
159	P9489	10803	0.99	692654.20	4664422.05	413	GALLEGO
160	P9491	9709	0.89	699581.87	4655970.85	390	GALLEGO
161	P9492	10772	0.98	686242.09	4649526.78	335	GALLEGO
162	P9495	10379	0.95	694761.53	4638704.86	298	GALLEGO
163	P9495F	7945	0.72	698549.50	4630258.97	415	GALLEGO
164	P9496	8705	0.79	680460.91	4646815.63	387	GALLEGO
165	P9497	8401	0.77	696726.05	4625177.09	473	GALLEGO
166	P9497E	7950	0.73	685301.49	4633452.22	280	GALLEGO
167	P9498	9638	0.88	681138.22	4626493.54	243	GALLEGO
168	P9499	10957	1.00	682093.53	4621641.38	225	GALLEGO
169	P9503U	8187	0.75	697479.94	4598559.86	195	GINEL
170	P9507	10619	0.97	715179.53	4613421.59	432	EBRO
171	P9509	9228	0.84	701910.85	4601059.37	172	EBRO
172	P9510A	10807	0.99	706293.08	4596244.57	161	EBRO
173	P9521	10136	0.93	709877.51	4574245.98	273	AGUAS VIVAS
174	P9522	10807	0.99	720360.94	4577118.68	153	EBRO
175	P9523	10866	0.99	721889.09	4575096.83	143	EBRO
176	P9528	10682	0.97	673532.21	4526445.59	970	MARTIN
177	P9532	10898	0.99	689781.51	4516723.79	1206	MARTIN
178	P9539	7797	0.71	696253.48	4541458.65	541	MARTIN
179	P9541	10348	0.94	703884.91	4523395.12	1019	MARTIN
180	P9542	9070	0.83	708976.12	4538105.89	668	MARTIN
181	P9544	9345	0.85	709274.58	4555492.12	342	MARTIN
182	P9548	10622	0.97	718951.01	4566734.40	209	MARTIN
183	P9553	10193	0.93	738176.91	4571907.45	187	EBRO
184	P9559	10864	0.99	726300.38	4517195.06	583	GUADALOPE
185	P9562	8460	0.77	745224.09	4500662.51	990	GUADALOPE
186	P9567E	8674	0.79	720151.67	4529788.93	632	GUADALOPE
187	P9571	10186	0.93	743404.63	4532311.13	611	GUADALOPE
188	P9572	8430	0.77	736769.07	4549199.04	360	GUADALOPE
189	P9573	8617	0.79	740952.01	4548501.81	325	GUADALOPE

Continued on next page...

Table A.1 – Continued

N°	ID	Data N° in CTRL	% Data in CTRL	Easting, [m] (ED_50, Z30N)	Northing, [m] (ED_50, Z30N)	Elevation [m.a.s.l.]	CHE_BASIN_NAMEs
190	P9575	9547	0.87	730453.90	4611611.00	466	EBRO
191	P9576	9254	0.84	732526.61	4604113.03	491	EBRO
192	P9577E	8065	0.74	746883.86	4598723.77	263	EBRO
193	P9578	10866	0.99	755162.45	4599660.53	292	EBRO
194	P9579	10774	0.98	772251.04	4589814.16	321	EBRO
195	P9585	9498	0.87	906833.31	4698752.80	1704	SEGRE
196	P9601U	7760	0.71	880457.73	4724593.35	1720	SEGRE
197	P9605	7760	0.71	875431.08	4718161.57	1500	SEGRE
198	P9619	9435	0.86	867279.56	4699100.82	692	SEGRE
199	P9621	10957	1.00	862114.88	4695150.07	642	SEGRE
200	P9635	10957	1.00	857411.84	4682473.53	540	SEGRE
201	P9638	10836	0.99	855931.20	4668077.50	480	SEGRE
202	P9647	10864	0.99	866204.38	4638194.86	448	SEGRE
203	P9649	8156	0.74	848072.44	4650305.40	360	SEGRE
204	P9650	8065	0.74	835842.48	4646222.35	320	SEGRE
205	P9657	10347	0.94	838326.77	4727420.40	940	NOGUERA PALLARESA
206	P9669	10434	0.95	848642.09	4729416.62	1100	NOGUERA PALLARESA
207	P9675	10834	0.99	846137.95	4713671.70	850	NOGUERA PALLARESA
208	P9684	9861	0.90	834517.13	4699249.94	790	NOGUERA PALLARESA
209	P9688	9131	0.83	828730.88	4714002.49	2120	NOGUERA PALLARESA
210	P9689	10957	1.00	828154.38	4709244.50	1270	NOGUERA PALLARESA
211	P9690	10714	0.98	826886.13	4702599.10	1020	NOGUERA PALLARESA
212	P9695	10898	0.99	824387.22	4692743.55	660	NOGUERA PALLARESA
213	P9696A	10319	0.94	827672.43	4685290.61	550	NOGUERA PALLARESA
214	P9700	10865	0.99	822814.39	4676532.82	425	NOGUERA PALLARESA
215	P9701E	7918	0.72	823105.86	4674691.27	415	NOGUERA PALLARESA
216	P9703E	7822	0.71	836866.01	4674161.06	797	NOGUERA PALLARESA
217	P9704	10866	0.99	822360.99	4668845.17	380	NOGUERA PALLARESA
218	P9708	10867	0.99	822458.79	4662666.77	399	NOGUERA PALLARESA
219	P9710	10926	1.00	818369.28	4640812.39	245	SEGRE
220	P9713	10684	0.97	840588.09	4634420.03	349	SEGRE
221	P9717	9986	0.91	855920.58	4622117.38	540	SEGRE
222	P9718	8230	0.75	851406.21	4622914.95	478	SEGRE
223	P9726	10410	0.95	846129.97	4603455.74	660	SEGRE
224	P9729	10743	0.98	821966.29	4614266.65	268	SEGRE
225	P9734	9713	0.89	806480.62	4717005.05	1093	NOGUERA RIBAGORZANA
226	P9736	10835	0.99	805020.74	4707544.19	960	NOGUERA RIBAGORZANA
227	P9738	9911	0.91	814808.87	4717346.48	1280	NOGUERA RIBAGORZANA
228	P9741	8521	0.78	812988.72	4713090.92	1096	NOGUERA RIBAGORZANA
229	P9744A	7822	0.71	809282.06	4707453.79	1000	NOGUERA RIBAGORZANA
230	P9745	10926	1.00	807571.64	4701597.83	845	NOGUERA RIBAGORZANA
231	P9749	8610	0.79	808690.08	4692343.13	717	NOGUERA RIBAGORZANA
232	P9760E	8280	0.76	797094.96	4642890.21	315	NOGUERA RIBAGORZANA
233	P9766	10957	1.00	830551.61	4602105.82	386	SEGRE
234	P9766E	8035	0.73	827839.02	4606556.95	321	SEGRE
235	P9768	10073	0.92	818956.94	4606806.86	264	SEGRE
236	P9770E	10926	1.00	804070.80	4614042.57	150	SEGRE
237	P9771	8093	0.74	801497.48	4614026.73	199	SEGRE
238	P9771E	9257	0.84	803707.91	4614398.05	150	SEGRE
239	P9772	8553	0.78	830089.20	4588823.00	665	SEGRE
240	P9773	10408	0.95	812443.42	4595302.32	377	SEGRE
241	P9777	8185	0.75	796946.14	4586552.99	397	SEGRE
242	P9780E	8738	0.80	793515.64	4598802.95	170	SEGRE
243	P9782	10957	1.00	762454.77	4725397.91	1150	CINCA
244	P9783	9473	0.86	767804.95	4730391.55	1920	CINCA
245	P9784	10957	1.00	763356.34	4729880.93	1200	CINCA
246	P9784E	9831	0.90	762849.33	4728224.25	1050	CINCA
247	P9787	10166	0.93	774394.49	4720576.87	1124	CINCA
248	P9789A	10101	0.92	773471.70	4720818.53	1422	CINCA
249	P9789	9934	0.91	774237.88	4723382.42	1000	CINCA
250	P9790	10641	0.97	770933.31	4718587.07	1100	CINCA
251	P9791	10623	0.97	770318.81	4719706.30	1306	CINCA
252	P9792	10531	0.96	767448.61	4716567.37	1000	CINCA
253	P9793	10049	0.92	767772.52	4719422.23	1218	CINCA
254	P9794	10499	0.96	764380.65	4719755.64	760	CINCA
255	P9796	8094	0.74	762535.34	4715422.29	700	CINCA
256	P9804	10726	0.98	750385.25	4714109.11	1143	CINCA
257	P9805E	9892	0.90	757357.17	4709050.37	963	CINCA
258	P9807	9679	0.88	760049.45	4703682.51	699	CINCA
259	P9808	10440	0.95	758182.51	4700956.54	589	CINCA
260	P9813	10624	0.97	732125.39	4722616.98	1333	CINCA
261	P9814	10803	0.99	736904.26	4723612.50	1053	CINCA

Continued on next page...

Table A.1 – Continued

N°	ID	Data N° in CTRL	% Data in CTRL	Easting, [m] (ED_50, Z30N)	Northing, [m] (ED_50, Z30N)	Elevation [m.a.s.l.]	CHE_BASIN_NAMEs
262	P9814E	9162	0.84	734506.51	4721677.93	1113	CINCA
263	P9815	10957	1.00	736105.06	4720960.04	1005	CINCA
264	P9815E	8890	0.81	732488.83	4713117.13	1033	CINCA
265	P9815I	10471	0.96	736795.45	4718111.29	863	CINCA
266	P9816	10198	0.93	735962.96	4713048.83	1103	CINCA
267	P9817	10772	0.98	736556.59	4709023.17	770	CINCA
268	P9817I	10259	0.94	738435.69	4707543.03	767	CINCA
269	P9818E	10834	0.99	740800.37	4707253.73	738	CINCA
270	P9818I	10167	0.93	741263.48	4707084.44	740	CINCA
271	P9819E	9831	0.90	745690.33	4708629.03	870	CINCA
272	P9820E	10561	0.96	744369.70	4704567.33	812	CINCA
273	P9821E	10376	0.95	748082.38	4701146.35	1040	CINCA
274	P9821I	9319	0.85	750513.10	4707379.95	915	CINCA
275	P9822	10927	1.00	752215.98	4703920.02	643	CINCA
276	P9823	9824	0.90	752462.38	4702168.26	716	CINCA
277	P9824I	10044	0.92	753893.29	4699316.56	666	CINCA
278	P9824O	10135	0.93	750126.90	4695813.91	775	CINCA
279	P9829	9838	0.90	763900.85	4690141.65	504	CINCA
280	P9833	10804	0.99	767032.47	4671662.78	425	CINCA
281	P9840	8879	0.81	786477.84	4721034.29	1100	ESERA
282	P9841	9437	0.86	784803.30	4716206.43	930	ESERA
283	P9842	8521	0.78	784918.57	4715624.02	928	ESERA
284	P9843	10835	0.99	782486.58	4708541.19	816	ESERA
285	P9849	10804	0.99	777108.98	4680826.39	498	ESERA
286	P9862	10906	0.99	747411.13	4673417.49	625	VERO
287	P9864	10772	0.98	749226.62	4666902.81	465	VERO
288	P9869E	8646	0.79	761890.35	4650341.21	382	CINCA
289	P9874	10956	1.00	748009.27	4649780.64	480	CINCA
290	P9875	10957	1.00	749582.45	4637790.88	400	CINCA
291	P9878	10469	0.95	768960.51	4629167.35	340	CINCA
292	P9878E	7913	0.72	759534.30	4623197.23	186	CINCA
293	P9886	9771	0.89	742104.10	4667396.08	539	ALCANADRE
294	P9894	9709	0.89	736220.25	4630634.36	281	ALCANADRE
295	P9895	10227	0.93	717471.40	4685613.61	990	FLUMEN
296	P9896	10547	0.96	718310.21	4678538.03	720	FLUMEN
297	P9897	8249	0.75	714191.98	4678133.48	680	FLUMEN
298	P9898	10915	1.00	721151.39	4662570.85	541	FLUMEN
299	P9900	9651	0.88	711352.02	4682524.35	726	ISUELA
300	P9901B	9434	0.86	712184.43	4668594.19	475	ISUELA
301	P9904I	8035	0.73	720632.68	4648197.38	335	FLUMEN
302	P9906E	7884	0.72	716084.34	4640122.89	350	FLUMEN
303	P9907E	10562	0.96	722158.64	4645095.64	340	FLUMEN
304	P9907I	10222	0.93	727763.58	4641444.32	365	FLUMEN
305	P9908	8217	0.75	721648.26	4628129.31	369	FLUMEN
306	P9910	10957	1.00	732032.00	4620832.30	356	FLUMEN
307	P9913	10803	0.99	776498.66	4644685.77	471	CINCA
308	P9914	8583	0.78	788741.13	4636490.07	282	CINCA
309	P9914E	8189	0.75	781046.65	4639395.61	318	CINCA
310	P9914I	7825	0.71	786928.79	4639599.34	361	CINCA
311	P9915	8796	0.80	773874.84	4639703.09	285	CINCA
312	P9916	10499	0.96	783768.22	4633695.04	262	CINCA
313	P9918	9434	0.86	780362.89	4630934.32	218	CINCA
314	P9920	9889	0.90	789109.20	4622817.17	250	CINCA
315	P9920E	8916	0.81	773776.34	4628423.56	234	CINCA
316	P9920I	8669	0.79	773868.73	4628427.10	225	CINCA
317	P9921	10526	0.96	790689.46	4620965.49	320	SEGRE
318	P9927	7976	0.73	768513.78	4524814.40	560	MATARRANA
319	P9932	10957	1.00	764447.04	4523741.13	620	MATARRANA
320	P9941	10286	0.94	760544.98	4549079.80	359	MATARRANA
321	P9942	9391	0.86	763685.94	4557283.74	304	MATARRANA
322	P9943	9744	0.89	766815.24	4562400.76	242	MATARRANA
323	P9947	10045	0.92	780675.59	4564341.88	363	MATARRANA
324	P9948	10957	1.00	786139.51	4557727.04	442	EBRO
325	P9949	8998	0.82	792252.09	4563190.22	486	EBRO
326	P9950	10590	0.97	791943.41	4572631.77	76	EBRO
327	P9951A	10839	0.99	797262.57	4570282.77	42	EBRO
328	P9951	10865	0.99	796229.13	4570456.91	56	EBRO
329	P9952	10896	0.99	806787.66	4584460.25	520	EBRO
330	P9953	9734	0.89	807391.89	4576791.22	336	EBRO
331	P9953E	8766	0.80	799199.92	4565140.40	69	EBRO
332	P9961	10866	0.99	812467.31	4573144.82	357	MONTSANT
333	P9968	8615	0.79	809648.06	4556584.33	110	EBRO

Continued on next page…

Table A.1 – Continued

N°	ID	Data N° in CTRL	% Data in CTRL	Easting, [m] (ED_50, Z30N)	Northing, [m] (ED_50, Z30N)	Elevation [m.a.s.l.]	CHE_BASIN_NAMEs
334	P9971	10804	0.99	813653.72	4550389.10	310	EBRO
335	P9972	10783	0.98	805538.71	4551436.56	34	EBRO
336	P9973	10929	1.00	805278.67	4549818.95	30	EBRO
337	P9974	10409	0.95	803023.89	4550034.32	25	EBRO
338	P9975	10890	0.99	802543.91	4545225.28	180	EBRO
339	P9979	8278	0.76	784737.33	4514765.53	340	EBRO
340	P9979E	8463	0.77	794091.93	4534748.29	12	EBRO
341	P9981A	10957	1.00	794466.24	4524784.59	48	EBRO
342	P9984	10329	0.94	793159.37	4506197.23	167	EBRO
343	P9985	10288	0.94	795355.65	4513080.65	79	EBRO
344	P9987	10851	0.99	802317.77	4512990.66	8	EBRO
345	P9990	9825	0.90	817566.00	4734970.00	0	
346	P9991	10681	0.97	811050.97	4735849.00	940	
347	P9993I	8888	0.81	805398.07	4738409.74	890	
348	P9997E	8010	0.73	621155.88	4545758.05	1043	GALLOCANTA
349	P9998	10775	0.98	631680.07	4535759.57	1018	GALLOCANTA

A.2 Temperature

TABLE A.2: Temperature gauging stations selected for the analysis, with more than 65% of days with information within the control period 01/Jan/1661-31/Dec/1990

N°	ID	Data N° in CTRL	% Data in CTRL	Easting, [m] (ED_50, Z30N)	Northing, [m] (ED_50, Z30N)	Elevation [m.a.s.l.]	CHE_BASIN_NAMEs
1	T9001	9226	0.84	407235.94	4761652.30	855	EBRO
2	T9019	8563	0.78	423070.09	4739829.28	716	EBRO
3	T9041	7286	0.67	453311.97	4754458.00	595	NELA
4	T9044	8887	0.81	459162.26	4754914.26	595	NELA
5	T9069	10760	0.98	503641.60	4725180.88	520	EBRO
6	T9069A	8766	0.80	505779.39	4727156.48	475	BAYAS
7	T9076	8274	0.76	531848.61	4753170.00	570	ZADORRA
8	T9080	8591	0.78	528480.54	4756332.54	540	ZADORRA
9	T9087	7787	0.71	528212.31	4744393.36	521	ZADORRA
10	T9105	10422	0.95	483360.05	4685964.84	960	TIRON
11	T9107	10558	0.96	484276.55	4696573.22	770	TIRON
12	T9121	10644	0.97	512151.16	4713715.95	479	TIRON
13	T9131I	8614	0.79	508811.46	4668153.84	900	NAJERILLA
14	T9136	10680	0.97	510567.23	4675558.67	1020	NAJERILLA
15	T9145	8751	0.80	529041.86	4703401.84	437	EBRO
16	T9145A	10914	1.00	529384.08	4703464.97	430	EBRO
17	T9170	10957	1.00	555027.80	4700227.03	352	EBRO
18	T9174	9425	0.86	578022.20	4690944.77	310	EBRO
19	T9194O	7418	0.68	594731.90	4676713.09	285	EBRO
20	T9198	10644	0.97	703136.38	4735971.44	1160	ARAGON (TRAMO SUPERIOR)
21	T9201	7548	0.69	700794.44	4722565.23	885	ARAGON (TRAMO SUPERIOR)
22	T9204	7297	0.67	696060.12	4719064.64	855	ARAGON (TRAMO SUPERIOR)
23	T9205	7877	0.72	694779.50	4728105.05	1040	ARAGON (TRAMO SUPERIOR)
24	T9206	7509	0.69	690754.63	4710427.35	820	ARAGON (TRAMO SUPERIOR)
25	T9206E	7750	0.71	688972.83	4712971.83	762	ARAGON (TRAMO SUPERIOR)
26	T9208	7508	0.69	690554.56	4730981.97	980	ARAGON (TRAMO SUPERIOR)
27	T9210E	7364	0.67	680587.50	4714168.96	595	ARAGON (TRAMO SUPERIOR)
28	T9212	7135	0.65	677641.57	4735577.14	820	ARAGON (TRAMO SUPERIOR)
29	T9215	9985	0.91	665056.82	4718597.70	510	ARAGON (TRAMO SUPERIOR)
30	T9219I	7598	0.69	662259.09	4726093.46	580	ARAGON (TRAMO SUPERIOR)
31	T9220	7547	0.69	662706.99	4721566.91	495	ARAGON (TRAMO SUPERIOR)
32	T9223	10836	0.99	648334.28	4720133.60	515	IRATI
33	T9224	10341	0.94	646380.79	4717654.12	455	IRATI
34	T9236E	7825	0.71	648292.59	4748556.40	1060	IRATI
35	T9246	10957	1.00	626316.19	4692544.43	340	ARAGON (AGUAS ABAJO YESA)
36	T9248	7350	0.67	619463.47	4687888.54	354	ARAGON (AGUAS ABAJO YESA)
37	T9252	10938	1.00	610583.18	4705113.03	395	ARAGON (AGUAS ABAJO YESA)
38	T9255	10670	0.97	611004.81	4688613.33	304	ARAGON (AGUAS ABAJO YESA)
39	T9257E	8381	0.77	620598.39	4757827.62	615	ARGA

Continued on next page...

Table A.2 – Continued

N°	ID	Data N° in CTRL	% Data in CTRL	Easting, [m] (ED_50, Z30N)	Northing, [m] (ED_50, Z30N)	Elevation [m.a.s.l.]	CHE_BASIN_NAMEs
40	T9262	10900	0.99	611480.01	4741535.65	442	ARGA
41	T9269	10120	0.92	566824.30	4748886.38	525	ARGA
42	T9279	9360	0.85	586298.70	4728154.89	475	ARGA
43	T9283	7905	0.72	606445.45	4673795.50	268	EBRO
44	T9301	10941	1.00	608518.94	4646246.52	410	QUEILES
45	T9305	9585	0.88	628741.72	4648559.02	242	EBRO
46	T9311B	7446	0.68	621396.16	4632448.29	448	HUECHA
47	T9322	8736	0.80	669963.73	4695011.72	760	ARBA
48	T9331F	9068	0.83	643318.72	4672227.99	360	ARBA
49	T9333	8246	0.75	646773.26	4666127.53	321	ARBA
50	T9350A	9254	0.84	579125.03	4574113.71	700	JALON
51	T9371	10510	0.96	607751.35	4575839.19	570	JALON
52	T9375	8624	0.79	642199.75	4491995.71	983	JILOCA
53	T9381	7387	0.67	642874.90	4525263.63	932	JILOCA
54	T9388	9137	0.83	637989.77	4544698.24	793	JILOCA
55	T9390	10954	1.00	633427.76	4552788.84	779	JILOCA
56	T9425I	8425	0.77	649140.04	4585272.25	496	JALON
57	T9433O	8034	0.73	653781.12	4625605.65	235	EBRO
58	T9434	10888	0.99	665849.88	4614241.49	247	EBRO
59	T9443E	7514	0.69	676504.05	4612952.65	233	HUERVA
60	T9446	8935	0.81	718417.16	4739248.04	1285	GALLEGO
61	T9448E	7240	0.66	719753.28	4735152.51	1170	GALLEGO
62	T9451	9670	0.88	726344.97	4738237.47	1660	GALLEGO
63	T9454A	7124	0.65	719932.63	4723053.30	855	GALLEGO
64	T9455	7265	0.66	725273.58	4722205.71	1132	GALLEGO
65	T9460	10925	1.00	716824.35	4710851.11	790	GALLEGO
66	T9461	7425	0.68	723488.60	4707479.87	910	GALLEGO
67	T9470E	7732	0.71	698504.41	4706136.70	920	GALLEGO
68	T9470I	7195	0.66	692971.63	4707061.79	940	GALLEGO
69	T9481	10668	0.97	684090.64	4662279.91	400	GALLEGO
70	T9489	10712	0.98	692654.20	4664422.05	413	GALLEGO
71	T9491	9579	0.87	699581.87	4655970.85	390	GALLEGO
72	T9492	7522	0.69	686242.09	4649526.78	335	GALLEGO
73	T9495	8914	0.81	694761.53	4638704.86	298	GALLEGO
74	T9495F	7731	0.71	698549.50	4630258.97	415	GALLEGO
75	T9522E	7329	0.67	721948.44	4573153.73	140	EBRO
76	T9523	10879	0.99	721889.09	4575096.83	143	EBRO
77	T9544	7849	0.72	709274.58	4555492.12	342	MARTIN
78	T9562	8459	0.77	745224.09	4500662.51	990	GUADALOPE
79	T9573	8611	0.79	740952.01	4548501.81	325	GUADALOPE
80	T9575	7728	0.70	730453.90	4611611.00	466	EBRO
81	T9585	7950	0.73	906833.31	4698752.80	1704	SEGRE
82	T9619	8274	0.76	867279.56	4699100.82	692	SEGRE
83	T9621	10957	1.00	862114.88	4695150.07	642	SEGRE
84	T9638	10785	0.98	855931.20	4668077.50	480	SEGRE
85	T9649	9284	0.85	848072.44	4650305.40	360	SEGRE
86	T9650	7896	0.72	835842.48	4646222.35	320	SEGRE
87	T9657	8187	0.75	838326.77	4727420.40	940	NOGUERA PALLARESA
88	T9669	8186	0.75	848642.09	4729416.62	1100	NOGUERA PALLARESA
89	T9675	10775	0.98	846137.95	4713671.70	850	NOGUERA PALLARESA
90	T9688	8989	0.82	828730.88	4714002.49	2120	NOGUERA PALLARESA
91	T9689	10957	1.00	828154.38	4709244.50	1270	NOGUERA PALLARESA
92	T9690	10712	0.98	826886.13	4702599.10	1020	NOGUERA PALLARESA
93	T9695	10869	0.99	824387.22	4692743.55	660	NOGUERA PALLARESA
94	T9696A	10349	0.94	827672.43	4685290.61	550	NOGUERA PALLARESA
95	T9700	10804	0.99	822814.39	4676532.82	425	NOGUERA PALLARESA
96	T9704	10898	0.99	822360.99	4668845.17	380	NOGUERA PALLARESA
97	T9708	10877	0.99	822458.79	4662666.77	399	NOGUERA PALLARESA
98	T9710	10622	0.97	818369.28	4640812.39	245	SEGRE
99	T9713	7407	0.68	840588.09	4634420.03	349	SEGRE
100	T9720	7670	0.70	844725.03	4619157.89	375	SEGRE
101	T9729	10742	0.98	821966.29	4614266.65	268	SEGRE
102	T9729A	7184	0.66	823929.73	4615993.30	250	SEGRE
103	T9734	8097	0.74	806480.62	4717005.05	1093	NOGUERA RIBAGORZANA
104	T9736	9373	0.85	805020.74	4707544.19	960	NOGUERA RIBAGORZANA
105	T9738	7937	0.72	814808.87	4717346.48	1280	NOGUERA RIBAGORZANA
106	T9744A	7422	0.68	809282.06	4707453.79	1000	NOGUERA RIBAGORZANA
107	T9745	9285	0.85	807571.64	4701597.83	845	NOGUERA RIBAGORZANA
108	T9749	7561	0.69	808690.08	4692343.13	717	NOGUERA RIBAGORZANA
109	T9760E	8232	0.75	797094.96	4642890.21	315	NOGUERA RIBAGORZANA
110	T9767	7336	0.67	822425.26	4604024.98	304	SEGRE
111	T9770	7292	0.67	802741.22	4613677.35	221	SEGRE

Continued on next page...

Table A.2 – Continued

N°	ID	Data N° in CTRL	% Data in CTRL	Easting, [m] (ED_50, Z30N)	Northing, [m] (ED_50, Z30N)	Elevation [m.a.s.l.]	CHE_BASIN_NAMEs
112	T9770E	10951	1.00	804070.80	4614042.57	150	SEGRE
113	T9771	7277	0.66	801497.48	4614026.73	199	SEGRE
114	T9772	7599	0.69	830089.20	4588823.00	665	SEGRE
115	T9822	8857	0.81	752215.98	4703920.02	643	CINCA
116	T9829	9923	0.91	763900.85	4690141.65	504	CINCA
117	T9833	10712	0.98	767032.47	4671662.78	425	CINCA
118	T9841	7503	0.69	784803.30	4716206.43	930	ESERA
119	T9842	8579	0.78	784918.57	4715624.02	928	ESERA
120	T9843	10528	0.96	782486.58	4708541.19	816	ESERA
121	T9849	10804	0.99	777108.98	4680826.39	498	ESERA
122	T9878E	7366	0.67	759534.30	4623197.23	186	CINCA
123	T9885	7129	0.65	733599.86	4677022.17	650	ALCANADRE
124	T9895	9799	0.89	717471.40	4685613.61	990	FLUMEN
125	T9897	7519	0.69	714191.98	4678133.48	680	FLUMEN
126	T9898	10897	0.99	721151.39	4662570.85	541	FLUMEN
127	T9904I	7666	0.70	720632.68	4648197.38	335	FLUMEN
128	T9907I	10175	0.93	727763.58	4641444.32	365	FLUMEN
129	T9910	10804	0.99	732032.00	4620832.30	356	FLUMEN
130	T9911	7289	0.67	756901.56	4618531.16	215	ALCANADRE
131	T9914	7768	0.71	788741.13	4636490.07	282	CINCA
132	T9915	8779	0.80	773874.84	4639703.09	285	CINCA
133	T9918	9489	0.87	780362.89	4630934.32	218	CINCA
134	T9923	7153	0.65	783603.13	4617437.38	265	CINCA
135	T9941	9888	0.90	760544.98	4549079.80	359	MATARRANA
136	T9951	10764	0.98	796229.13	4570456.91	56	EBRO
137	T9951A	10894	0.99	797262.57	4570282.77	42	EBRO
138	T9961	8665	0.79	812467.31	4573144.82	357	MONTSANT
139	T9967	7243	0.66	814482.95	4554503.89	230	MONTSANT
140	T9968	8250	0.75	809648.06	4556584.33	110	EBRO
141	T9971	10850	0.99	813653.72	4550389.10	310	EBRO
142	T9981A	10771	0.98	794466.24	4524784.59	48	EBRO
143	T9990	9855	0.90	817566.00	4734970.00	0	
144	T9991	10834	0.99	811050.97	4735849.00	940	
145	T9993I	8888	0.81	805398.07	4738409.74	890	
146	T9998	7860	0.72	631680.07	4535759.57	1018	GALLOCANTA

A.3 Streamflow

TABLE A.3: Streamflow gauging stations selected for the analysis, with more than 65% of days with information within the control period 01/Jan/1661-31/Dec/1990

N°	ID	Data N° in CTRL	% Data in CTRL	Easting, [m] (ED_50, Z30N)	Northing, [m] (ED_50, Z30N)	CHE_BASIN_NAMEs
1	q001	10950	1.00	503750.00	4726339.00	EBRO
2	q002	10950	1.00	607902.00	4670804.00	EBRO
3	q003	10574	0.96	586644.00	4692045.00	EGA
4	q004	10950	1.00	598901.00	4685628.00	ARGA
5	q005	10825	0.99	611221.00	4689020.00	ARAGON (AGUAS ABAJO YESA)
6	q006	10914	1.00	545858.00	4719917.00	EGA
7	q007	10542	0.96	586579.00	4572511.00	JALON
8	q008	9582	0.88	601319.00	4561596.00	PIEDRA
9	q009	10409	0.95	617175.00	4581867.00	JALON
10	q010	10950	1.00	632826.00	4551974.00	JILOCA
11	q011	10950	1.00	676533.00	4614247.00	EBRO
12	q012	10762	0.98	685725.00	4671825.00	GALLEGO
13	q013	10605	0.97	776307.00	4678241.00	ESERA
14	q015	10950	1.00	741168.00	4549056.00	GUADALOPE
15	q017	9735	0.89	779339.00	4602598.00	CINCA
16	q018	10900	0.99	700817.00	4717118.00	ARAGON (TRAMO SUPERIOR)
17	q019	8101	0.74	802266.19	4743764.00	-
18	q020	9758	0.89	903828.00	4711283.00	SEGRE
19	q021	10262	0.94	905987.00	4708819.00	SEGRE
20	q022	9391	0.86	866536.00	4699087.00	SEGRE

Continued on next page...

Table A.3 – Continued

N°	ID	Data N° in CTRL	% Data in CTRL	Easting, [m] (ED_50, Z30N)	Northing, [m] (ED_50, Z30N)	CHE_BASIN_NAMEs
21	q023	9395	0.86	867444.00	4698760.00	SEGRE
22	q024	10220	0.93	803594.00	4614488.00	SEGRE
23	q025	10915	1.00	785454.00	4594800.00	SEGRE
24	q026	10950	1.00	413877.00	4758537.00	EBRO
25	q027	10721	0.98	797039.00	4524278.00	EBRO
26	q030	10740	0.98	722311.00	4513402.00	GUADALOPE
27	q032	8395	0.77	738321.00	4643896.00	ALCANADRE
28	q033	8395	0.77	738512.00	4644293.00	ALCANADRE
29	q034	10873	0.99	507822.00	4667930.00	NAJERILLA
30	q035	10662	0.97	528765.00	4664016.00	IREGUA
31	q036	10950	1.00	539186.00	4685361.00	IREGUA
32	q038	10429	0.95	526047.00	4705367.00	NAJERILLA
33	q039	10669	0.97	527231.00	4669025.00	IREGUA
34	q040	10851	0.99	753313.00	4703003.00	CINCA
35	q041	10813	0.99	646619.00	4532671.00	JILOCA
36	q042	10857	0.99	643199.00	4531928.00	JILOCA
37	q043	10854	0.99	564246.00	4652197.00	ALHAMA
38	q044	10883	0.99	555320.00	4661829.00	CIDACOS
39	q046	9179	0.84	751189.00	4678726.00	VERO
40	q047	10369	0.95	780464.00	4677088.00	ISABENA
41	q048	10704	0.98	518412.00	4678452.00	NAJERILLA
42	q049	10918	1.00	587585.19	4639991.00	ALHAMA
43	q050	10915	1.00	502460.00	4709966.00	TIRON
44	q051	10950	1.00	758499.00	4701828.00	CINCA
45	q052	10817	0.99	768746.00	4524361.00	MATARRANA
46	q055	8450	0.77	618695.00	4567865.00	JILOCA
47	q057	9855	0.90	585145.00	4582454.00	JALON
48	q058	10950	1.00	555463.00	4561056.00	JALON
49	q059	10872	0.99	685574.00	4682474.00	GALLEGO
50	q062	9687	0.88	681568.00	4725166.00	ARAGON (TRAMO SUPERIOR)
51	q063	10942	1.00	663000.00	4722000.00	ARAGON (TRAMO SUPERIOR)
52	q064	10790	0.98	650702.00	4730926.00	IRATI
53	q065	10764	0.98	639939.00	4720644.00	IRATI
54	q066	10816	0.99	642407.00	4756508.00	IRATI
55	q067	10365	0.95	613868.00	4749492.00	ARGA
56	q068	8970	0.82	598988.00	4743135.00	ARGA
57	q069	8494	0.78	599073.00	4738504.00	ARGA
58	q070	9269	0.85	578011.44	4727397.50	EGA
59	q071	10950	1.00	579083.00	4724990.00	EGA
60	q073	10846	0.99	643344.00	4712744.00	ARAGON (AGUAS ABAJO YESA)
61	q074	10950	1.00	508565.00	4725201.00	ZADORRA
62	q075	10449	0.95	509604.00	4725577.00	ZADORRA
63	q078	10950	1.00	611419.00	4717013.00	ARAGON (AGUAS ABAJO YESA)
64	q079	10950	1.00	628101.00	4736883.00	IRATI
65	q080	9957	0.91	678169.00	4748074.00	ARAGON (TRAMO SUPERIOR)
66	q083	10364	0.95	855163.00	4668850.00	SEGRE
67	q085	8122	0.74	585083.94	4735622.50	ARGA
68	q086	10950	1.00	610830.00	4717489.00	ARAGON (AGUAS ABAJO YESA)
69	q087	7482	0.68	651824.00	4621939.00	JALON
70	q088	9746	0.89	703113.00	4500242.00	GUADALOPE
71	q090	10220	0.93	601030.00	4637100.00	QUEILES
72	q091	9371	0.85	739160.00	4663736.00	ALCANADRE
73	q092	9582	0.88	465581.84	4742488.50	NELA
74	q093	10477	0.96	465605.00	4731645.00	HOMINO
75	q095	8943	0.82	759376.00	4657956.00	VERO
76	q096	10761	0.98	816451.00	4634016.00	SEGRE
77	q097	10920	1.00	797069.00	4642522.00	NOGUERA RIBAGORZANA
78	q100	10944	1.00	717321.00	4526852.00	GUADALOPE
79	q101	10950	1.00	646828.00	4719928.00	IRATI
80	q102	10265	0.94	833074.13	4689398.00	NOGUERA PALLARESA
81	q103	7969	0.73	821833.00	4644519.00	SEGRE
82	q104	7970	0.73	828440.00	4647751.00	SEGRE
83	q105	10713	0.98	660814.00	4588056.00	HUERVA
84	q106	10585	0.97	726779.00	4517766.00	GUADALOPE
85	q109	7703	0.70	764231.00	4524156.00	MATARRANA
86	q110	10880	0.99	764084.00	4521342.00	MATARRANA
87	q111	10430	0.95	858548.00	4684601.00	SEGRE
88	q112	10950	1.00	719782.00	4578748.00	EBRO
89	q113	10950	1.00	763049.00	4521618.00	MATARRANA
90	q114	7791	0.71	847890.63	4650210.50	SEGRE
91	q115	10128	0.92	805381.00	4673284.00	NOGUERA RIBAGORZANA
92	q116	9459	0.86	814974.38	4718349.00	NOGUERA RIBAGORZANA

Continued on next page…

Table A.3 – Continued

N°	ID	Data N° in CTRL	% Data in CTRL	Easting, [m] (ED_50, Z30N)	Northing, [m] (ED_50, Z30N)	CHE_BASIN_NAMEs
93	q117	10493	0.96	815265.63	4717547.50	NOGUERA RIBAGORZANA
94	q118	10950	1.00	694203.92	4540492.77	MARTIN
95	q120	10917	1.00	565478.00	4696449.00	EBRO
96	q121	10663	0.97	797636.69	4570260.50	EBRO
97	q122	10950	1.00	676498.21	4545071.81	AGUAS VIVAS
98	q123	10585	0.97	693373.00	4697534.00	GALLEGO
99	q124	10950	1.00	660496.00	4573702.00	HUERVA
100	q125	10919	1.00	600731.00	4569241.00	PIEDRA
101	q126	10770	0.98	600483.00	4575511.00	JALON
102	q127	10009	0.91	693539.00	4536469.00	MARTIN
103	q130	9947	0.91	805382.00	4711766.00	NOGUERA RIBAGORZANA
104	q131	9947	0.91	808913.50	4706979.50	NOGUERA RIBAGORZANA
105	q135	8283	0.76	855407.00	4720486.00	NOGUERA PALLARESA
106	q136	8852	0.81	801221.50	4707329.50	NOGUERA RIBAGORZANA
107	q137	10251	0.94	808017.00	4701188.00	NOGUERA RIBAGORZANA
108	q138	10919	1.00	681509.00	4555757.00	AGUAS VIVAS
109	q139	10942	1.00	581895.00	4658733.00	ALHAMA
110	q142	10950	1.00	531356.00	4661174.00	IREGUA
111	q143	9840	0.90	817457.56	4735108.00	-
112	q144	10353	0.94	848683.00	4729299.00	NOGUERA PALLARESA
113	q145	9102	0.83	785007.00	4720109.00	ESERA
114	q146	10532	0.96	828362.00	4685745.00	NOGUERA PALLARESA
115	q147	10795	0.98	574058.00	4573689.00	JALON
116	q148	9734	0.89	855408.00	4677290.00	SEGRE
117	q149	10950	1.00	538703.00	4703909.00	EBRO
118	q150	10465	0.95	588002.00	4733510.00	ARGA
119	q151	10521	0.96	587166.00	4733748.00	ARGA
120	q152	9713	0.89	621226.00	4758784.00	ARGA
121	q153	9320	0.85	775723.00	4537187.00	MATARRANA
122	q154	8229	0.75	755368.81	4514293.50	MATARRANA
123	q155	8237	0.75	649237.00	4680494.00	ARBA
124	q157	7281	0.67	497343.00	4679139.00	TIRON
125	q158	7626	0.70	482615.00	4694425.00	TIRON
126	q159	8485	0.77	615391.00	4744456.00	ARGA
127	q161	9490	0.87	478589.00	4737110.00	EBRO
128	q162	9398	0.86	619613.00	4653288.00	EBRO
129	q166	8607	0.79	470572.00	4737909.00	JEREA
130	q171	9217	0.84	774640.00	4723554.00	CINCA
131	q172	9217	0.84	762660.00	4715281.00	CINCA
132	q181	8512	0.78	827165.44	4684944.00	NOGUERA PALLARESA
133	q182	7939	0.72	817801.06	4635182.00	SEGRE
134	q183	8852	0.81	809747.00	4621140.00	SEGRE
135	q196	8487	0.78	737270.00	4724039.00	CINCA
136	q198	8336	0.76	855348.00	4720604.00	NOGUERA PALLARESA
137	Q801	10916	1.00	414344.53	4758210.50	EBRO
138	Q802	10949	1.00	797607.19	4570947.50	EBRO
139	Q803	9569	0.87	773989.38	4585107.50	EBRO
140	Q804	7757	0.71	787729.19	4571660.50	EBRO
141	Q809	10850	0.99	507355.06	4667519.50	NAJERILLA
142	Q811	10920	1.00	527073.63	4669289.00	IREGUA
143	Q812	9581	0.87	600792.31	4568764.50	PIEDRA
144	Q814	10493	0.96	660188.94	4573367.00	HUERVA
145	Q815	10585	0.97	681948.63	4561422.00	AGUAS VIVAS
146	Q816	10126	0.92	704415.13	4574277.50	AGUAS VIVAS
147	Q817	10217	0.93	694097.81	4539719.50	MARTIN
148	Q818	10949	1.00	726561.31	4517337.00	GUADALOPE
149	Q819	9954	0.91	735250.00	4550190.00	GUADALOPE
150	Q820	10311	0.94	718065.69	4528405.00	GUADALOPE
151	Q821	10583	0.97	764339.13	4523632.00	MATARRANA
152	Q827	10219	0.93	531397.63	4753098.00	ZADORRA
153	Q828	10220	0.93	528204.63	4756206.00	ZADORRA
154	Q829	10920	1.00	649104.06	4719975.50	IRATI
155	Q830	10948	1.00	586751.50	4728942.00	ARGA
156	Q831	10828	0.99	650307.25	4760953.00	IRATI
157	Q832	10865	0.99	716753.56	4736208.50	GALLEGO
158	Q833	10948	1.00	718728.88	4740999.50	GALLEGO
159	Q834	10950	1.00	726043.00	4737604.00	GALLEGO
160	Q835	7380	0.67	720013.50	4729060.00	GALLEGO
161	Q836	10778	0.98	686488.63	4694973.00	GALLEGO
162	Q837	10801	0.99	685561.31	4672672.00	GALLEGO
163	Q838	10950	1.00	692342.88	4664274.50	GALLEGO
164	Q845	10950	1.00	762630.63	4725465.00	CINCA

Continued on next page...

Table A.3 – Continued

N°	ID	Data N° in CTRL	% Data in CTRL	Easting, [m] (ED_50, Z30N)	Northing, [m] (ED_50, Z30N)	CHE_BASIN_NAMEs
165	Q846	7392	0.68	764790.06	4689698.00	CINCA
166	Q847	8852	0.81	767340.00	4671826.00	CINCA
167	Q848	10950	1.00	773781.44	4669077.50	ESERA
168	Q849	10896	0.99	771044.44	4718532.00	CINCA
169	Q850	10950	1.00	808680.06	4692912.50	NOGUERA RIBAGORZANA
170	Q851	9214	0.84	799316.13	4653672.50	NOGUERA RIBAGORZANA
171	Q852	10647	0.97	797130.50	4643060.50	NOGUERA RIBAGORZANA
172	Q853	10585	0.97	821239.50	4731694.00	-
173	Q854	10585	0.97	826530.69	4716900.50	NOGUERA PALLARESA
174	Q856	10924	1.00	835288.75	4730690.50	NOGUERA PALLARESA
175	Q857	10919	1.00	840031.63	4722261.00	NOGUERA PALLARESA
176	Q858	10865	0.99	823258.81	4677372.00	NOGUERA PALLARESA
177	Q859	10947	1.00	822367.19	4662716.50	NOGUERA PALLARESA
178	Q860	10918	1.00	822539.38	4647039.00	NOGUERA PALLARESA
179	Q861	10950	1.00	818545.19	4640772.50	SEGRE
180	Q862	10950	1.00	855248.25	4669157.00	SEGRE
181	Q863	10311	0.94	816386.38	4722163.00	NOGUERA RIBAGORZANA
182	Q864	7757	0.71	785910.44	4720647.00	ESERA

B

Projected Values of Annual, Seasonal and Monthly Precipitation and Temperature

B.1 Entire Ebro River basin

This Appendix present annual, seasonal and monthly projected values of precipitation and air temperature for the entire Ebro River basin during the control period 1961-1990 and the six future climate scenarios (2071-2100) described in Table 4.1.

B.1.1 Annual and Seasonal Projections

TABLE B.1: Annual and **seasonal** mean precipitation and temperature on the Ebro River basin, for the CTRL period 1961-1990 and for 6 RCMs during 2071-2100. Values computed averaging over the 349 and 146 **gauging stations** of precipitation and temperature, respectively.

	Mean Precipitation, [mm]					Mean Temperature, [°C]				
Scenario	Annual	DJF	MAM	JJA	SON	Annual	DJF	MAM	JJA	SON
CTRL	608.9	144.5	171.0	121.4	170.9	12.2	4.8	10.7	20.5	13.1
DMI.HS1	586.0	175.2	146.9	83.0	177.7	16.4	8.1	13.9	26.0	17.5
DMI.ecscA2	572.4	166.6	136.6	101.5	165.7	17.8	8.8	15.9	27.6	18.6
HC.adhfa	555.4	161.1	145.6	72.4	192.8	16.8	8.2	14.3	26.7	17.9
CNRM.DE6	519.3	157.8	134.0	72.7	154.4	16.3	7.7	14.4	25.7	17.1
SMHI.HCA2	566.2	164.8	149.1	66.4	183.0	16.5	7.9	13.9	26.7	17.3
SMHI.MPIA2	476.3	140.5	111.0	78.6	142.4	18.5	9.0	16.9	29.2	18.6
RCMs.Average	546.0	161.0	137.2	79.1	169.3	17.0	8.3	14.9	27.0	17.8

TABLE B.2: Annual and **seasonal** mean precipitation and temperature on the Ebro River basin, for the CTRL period 1961-1990 and for 6 RCMs during 2071-2100. Values computed averaging the **IDW** interpolated values in squared cells of 1km^2

	Mean Precipitation, [mm]					Mean Temperature, [°C]				
Scenario	Annual	DJF	MAM	JJA	SON	Annual	DJF	MAM	JJA	SON
CTRL	545.3	126.9	156.2	108.9	152.2	12.7	5.3	11.2	21.0	13.6
DMI.HS1	525.9	155.3	133.1	75.0	159.8	16.9	8.5	14.5	26.5	17.9
DMI.ecscA2	518.2	149.1	125.6	92.8	148.8	18.2	9.3	16.3	28.1	19.0
HC.adhfa	503.8	143.4	133.8	65.9	175.9	17.3	8.7	14.7	27.2	18.4
CNRM.DE6	466.1	139.6	122.0	65.0	138.9	16.8	8.2	14.9	26.2	17.5
SMHI.HCA2	509.6	145.3	136.7	59.8	165.2	17.0	8.4	14.4	27.2	17.8
SMHI.MPIA2	431.3	125.6	104.1	71.0	127.2	19.0	9.4	17.4	29.7	19.1
RCMs.Average	492.5	143.0	125.9	71.6	152.6	17.5	8.8	15.4	27.5	18.3

TABLE B.3: Annual and **seasonal** mean precipitation and temperature on the Ebro River basin, for the CTRL period 1961-1990 and for 6 RCMs during 2071-2100. Values computed averaging the **OK** interpolated values in squared cells of $1km^2$

	Mean Precipitation, [mm]					Mean Temperature, [°C]				
Scenario	Annual	DJF	MAM	JJA	SON	Annual	DJF	MAM	JJA	SON
CTRL	544.6	126.5	156.3	109.4	151.6	12.7	5.3	11.1	20.9	13.5
DMI.HS1	525.3	155.1	133.2	76.0	158.7	16.9	8.6	14.4	26.4	17.9
DMI.ecscA2	518.1	149.3	125.9	93.9	147.7	18.2	9.3	16.3	28.0	18.9
HC.adhfa	504.5	143.4	134.3	66.5	175.4	17.2	8.7	14.7	27.1	18.3
CNRM.DE6	465.4	139.5	122.0	65.6	138.1	16.7	8.3	14.8	26.1	17.5
SMHI.HCA2	508.5	145.2	136.8	60.1	164.1	17.0	8.4	14.4	27.1	17.7
SMHI.MPIA2	430.9	125.5	104.0	71.9	126.8	18.9	9.4	17.3	29.6	19.0
RCMs.Average	492.1	143.0	126.0	72.3	151.8	17.5	8.8	15.3	27.4	18.2

B.1.2 Monthly Projections

The monthly **precipitation** over the entire Ebro River basin during the future period 2071-2100 are presented in tables B.4, B.5 and B.6 for the 6 RCMs described in Table 4.1.

TABLE B.4: Monthly mean precipitation, [mm], on the Ebro River basin, for the CTRL period 1961-1990 and for 6 RCMs during 2071-2100. Values computed averaging over the 349 **gauging stations** of precipitation.

Scenario	Jan	Feb	Mar	Apr	May	Jun	Jul	Aug	Sep	Oct	Nov	Dec
CTRL	48.6	44.3	43.8	61.0	66.2	53.0	30.2	38.3	47.6	56.6	66.6	52.9
DMI.HS1	64.1	48.6	43.7	58.3	44.9	38.0	17.9	27.1	53.5	55.7	68.5	65.7
DMI.ecscA2	57.1	43.9	45.9	42.5	48.2	41.6	22.5	37.3	49.4	43.3	73.0	67.7
HC.adhfa	54.2	51.0	55.3	44.3	46.1	32.9	16.5	23.0	41.3	63.5	87.9	57.9
CNRM.DE6	58.6	51.9	39.0	54.1	40.9	30.6	16.9	25.2	42.8	53.4	58.2	47.7
SMHI.HCA2	57.4	48.2	45.4	63.6	40.1	35.5	15.2	15.8	62.3	51.5	69.2	61.9
SMHI.MPIA2	54.2	35.4	33.3	37.4	40.3	30.3	16.8	31.5	43.0	42.4	57.0	54.8
RCMs.Average	57.6	46.5	43.7	50.0	43.4	34.8	17.6	26.6	48.7	51.6	69.0	59.3

TABLE B.5: Monthly mean precipitation, [mm], on the Ebro River basin, for the CTRL period 1961-1990 and for 6 RCMs during 2071-2100. Values computed averaging the **IDW** interpolated values in squared cells of 1km^2

Scenario	Jan	Feb	Mar	Apr	May	Jun	Jul	Aug	Sep	Oct	Nov	Dec
CTRL	42.7	39.3	39.7	56.0	60.5	48.3	26.9	33.7	42.8	50.6	58.9	46.0
DMI.HS1	56.8	43.2	39.5	52.9	40.7	34.6	16.0	24.3	49.0	50.0	60.8	58.1
DMI.ecscA2	51.1	39.3	42.1	39.0	44.4	38.0	20.7	34.1	45.5	38.6	64.6	60.5
HC.adhfa	47.4	45.5	51.1	40.3	42.4	30.8	14.9	20.2	38.6	58.6	78.7	52.2
CNRM.DE6	51.4	47.2	35.2	49.3	37.5	28.1	15.0	22.0	38.3	48.5	52.1	41.6
SMHI.HCA2	50.2	42.7	41.3	58.3	37.1	32.7	13.5	13.5	56.4	45.8	63.0	54.9
SMHI.MPIA2	48.8	32.1	31.1	34.6	38.4	28.4	15.0	27.6	39.3	38.5	49.5	48.1
RCMs.Average	50.9	41.7	40.1	45.7	40.1	32.1	15.8	23.6	44.5	46.7	61.5	52.6

TABLE B.6: Monthly mean precipitation, [mm], on the Ebro River basin, for the CTRL period 1961-1990 and for 6 RCMs during 2071-2100. Values computed averaging the **OK** interpolated values in squared cells of $1km^2$

Scenario	Jan	Feb	Mar	Apr	May	Jun	Jul	Aug	Sep	Oct	Nov	Dec
CTRL	42.6	39.2	39.8	56.0	60.5	48.5	27.0	33.8	42.6	50.5	58.5	45.8
DMI.HS1	56.8	43.3	39.5	52.8	40.9	35.0	16.3	24.5	48.6	49.8	60.4	57.9
DMI.ecscA2	51.2	39.4	42.3	39.0	44.7	38.4	21.2	34.3	45.2	38.5	64.1	60.6
HC.adhfa	47.4	45.5	51.3	40.4	42.7	31.3	15.0	20.2	38.4	58.6	78.2	52.3
CNRM.DE6	51.4	47.2	35.2	49.2	37.5	28.4	15.1	22.1	38.0	48.5	51.7	41.5
SMHI.HCA2	50.1	42.9	41.4	58.2	37.3	32.9	13.6	13.6	56.1	45.6	62.6	54.8
SMHI.MPIA2	48.7	32.1	31.1	34.5	38.4	28.7	15.2	28.0	39.1	38.6	49.2	48.1
RCMs.Average	50.9	41.7	40.1	45.7	40.2	32.4	16.1	23.8	44.2	46.6	61.0	52.5

The monthly mean **temperature** over the entire Ebro River basin during the future period 2071-2100 are presented in tables B.7, B.8 and B.9 for the 6 RCMs described in Table 4.1.

TABLE B.7: Monthly mean temperature, [$^{\circ}$C], on the Ebro River basin, for the CTRL period 1961-1990 and for 6 RCMs during 2071-2100. Values computed averaging over the 146 **gauging stations** of temperature.

Scenario	Jan	Feb	Mar	Apr	May	Jun	Jul	Aug	Sep	Oct	Nov	Dec
CTRL	4.1	5.6	7.8	10.2	14.1	18.3	21.8	21.3	18.3	13.3	7.8	4.6
DMI.HS1	7.3	8.7	10.2	13.2	18.4	23.4	27.1	27.5	23.6	17.7	11.3	8.1
DMI.ecscA2	8.0	10.1	11.8	15.5	20.3	24.3	29.6	29.1	24.8	18.6	12.3	8.4
HC.adhfa	7.5	9.0	10.5	13.8	18.5	24.0	28.2	27.9	24.7	17.4	11.7	8.2
CNRM.DE6	7.5	8.4	11.0	13.6	18.6	23.4	27.3	26.4	22.6	17.1	11.5	7.3
SMHI.HCA2	7.2	8.6	10.1	13.2	18.4	23.6	28.2	28.4	23.5	17.4	11.1	8.0
SMHI.MPIA2	8.3	10.0	12.9	16.6	21.1	26.0	31.0	30.7	25.3	18.4	12.1	8.7
RCMs.Average	7.6	9.1	11.1	14.3	19.2	24.1	28.6	28.3	24.1	17.8	11.7	8.1

TABLE B.8: Monthly mean temperature, [$^{\circ}$C], on the Ebro River basin, for the CTRL period 1961-1990 and for 6 RCMs during 2071-2100. Values computed averaging the **IDW** interpolated values in squared cells of 1km^2

	Jan	Feb	Mar	Apr	May	Jun	Jul	Aug	Sep	Oct	Nov	Dec
CTRL	4.6	6.1	8.3	10.7	14.6	18.9	22.3	21.8	18.8	13.8	8.2	5.0
DMI.HS1	7.8	9.3	10.7	13.7	18.9	23.9	27.6	28.0	24.0	18.1	11.7	8.5
DMI.ecscA2	8.5	10.5	12.2	16.0	20.7	24.7	30.0	29.5	25.3	19.0	12.7	8.8
HC.adhfa	7.9	9.5	10.9	14.3	19.0	24.5	28.7	28.4	25.1	17.9	12.1	8.6
CNRM.DE6	8.1	8.9	11.5	14.0	19.1	23.9	27.8	26.9	23.1	17.6	11.9	7.8
SMHI.HCA2	7.7	9.1	10.7	13.7	18.9	24.2	28.7	28.8	24.0	17.8	11.6	8.4
SMHI.MPIA2	8.8	10.5	13.4	17.1	21.7	26.5	31.4	31.1	25.8	18.9	12.5	9.2
RCMs.Average	8.1	9.6	11.6	14.8	19.7	24.6	29.0	28.8	24.6	18.2	12.1	8.6

TABLE B.9: Monthly mean temperature, [°C], on the Ebro River basin, for the CTRL period 1961-1990 and for 6 RCMs during 2071-2100. Values computed averaging the **OK** interpolated values in squared cells of 1km^2

Scenario	Jan	Feb	Mar	Apr	May	Jun	Jul	Aug	Sep	Oct	Nov	Dec
CTRL	4.6	6.1	8.2	10.7	14.5	18.7	22.2	21.7	18.7	13.7	8.2	5.1
DMI.HS1	7.9	9.3	10.7	13.7	18.8	23.8	27.5	27.9	23.9	18.1	11.7	8.6
DMI.ecscA2	8.5	10.5	12.2	15.9	20.6	24.6	29.9	29.4	25.2	18.9	12.7	8.9
HC.adhfa	8.0	9.5	10.9	14.2	18.9	24.4	28.5	28.3	25.0	17.8	12.1	8.6
CNRM.DE6	8.1	8.9	11.4	14.0	19.0	23.8	27.7	26.8	23.0	17.5	11.9	7.8
SMHI.HCA2	7.7	9.1	10.6	13.6	18.9	24.0	28.6	28.7	23.9	17.7	11.5	8.4
SMHI.MPIA2	8.8	10.5	13.4	17.0	21.6	26.4	31.3	31.0	25.7	18.8	12.5	9.2
RCMs.Average	8.2	9.6	11.5	14.8	19.6	24.5	28.9	28.7	24.5	18.2	12.1	8.6

B.2 Ebro River basin, by elevation bands

This Appendix presents bias-corrected mean annual/seasonal/monthly precipitation and air temperature over each one of the four elevation bands described in Table 4.14 for the entire Ebro River basin, during the future period 2071-2100, for the six future climate scenarios described in Table 4.1.

B.2.1 Annual and Seasonal Projections

TABLE B.10: Bias-corrected mean **annual** precipitation and temperature for different elevation bands, on the Ebro River basin, for the CTRL period 1961-1990 and for 6 RCMs during 2071-2100. Values computed averaging over the 349 and 146 gauging stations of precipitation and temperature, respectively.

	Mean Precipitation, [mm]				Mean Temperature, [°C]			
Scenario	Low	Med.Low	Med.High	High	Low	Med.Low	Med.High	High
CTRL	388.0	571.6	743.3	947.3	14.0	12.4	10.7	8.4
DMI.HS1	371.5	552.8	714.4	911.0	18.1	16.5	15.1	13.0
DMI.ecscA2	382.0	535.1	694.1	866.9	19.4	17.9	16.4	14.4
HC.adhfa	364.2	531.9	676.6	818.9	18.5	16.9	15.4	13.4
CNRM.DE6	342.4	479.4	637.2	797.5	18.1	16.3	14.8	12.7
SMHI.HCA2	375.7	531.6	685.2	858.3	18.3	16.6	15.1	13.0
SMHI.MPIA2	326.1	442.8	575.1	713.9	20.2	18.7	17.1	15.1
RCMs.Average	360.3	512.2	663.7	827.7	18.8	17.1	15.6	13.6

TABLE B.11: Bias-corrected mean **winter** (DJF) precipitation and temperature for different elevation bands, on the Ebro River basin, for the CTRL period 1961-1990 and for 6 RCMs during 2071-2100. Values computed averaging over the 349 and 146 gauging stations of precipitation and temperature, respectively.

	Mean Precipitation, [mm]				Mean Temperature, [°C]			
Scenario	Low	Med.Low	Med.High	High	Low	Med.Low	Med.High	High
CTRL	78.6	142.8	182.5	225.9	6.1	5.1	3.6	2.0
DMI.HS1	91.3	178.4	219.4	273.0	9.3	8.3	7.0	5.5
DMI.ecscA2	97.5	166.0	205.7	249.9	10.0	9.1	7.8	6.4
HC.adhfa	92.7	160.1	205.1	236.2	9.3	8.5	7.2	5.9
CNRM.DE6	96.2	151.4	199.3	235.6	9.1	7.9	6.5	5.0
SMHI.HCA2	87.3	165.0	207.7	258.0	9.2	8.1	6.8	5.3
SMHI.MPIA2	86.2	136.1	173.0	213.0	10.2	9.2	7.8	6.4
RCMs.Average	91.9	159.5	201.7	244.3	9.5	8.5	7.2	5.8

TABLE B.12: Bias-corrected mean **spring** (MAM) precipitation and temperature for different elevation bands, on the Ebro River basin, for the CTRL period 1961-1990 and for 6 RCMs during 2071-2100. Values computed averaging over the 349 and 146 gauging stations of precipitation and temperature, respectively.

	Mean Precipitation, [mm]				Mean Temperature, [°C]			
Scenario	Low	Med.Low	Med.High	High	Low	Med.Low	Med.High	High
CTRL	113.3	164.4	205.0	253.4	12.8	10.9	8.9	6.4
DMI.HS1	91.3	140.4	178.7	228.7	15.8	14.1	12.4	10.0
DMI.ecscA2	91.2	130.0	164.8	202.6	17.6	16.1	14.4	12.1
HC.adhfa	95.1	142.7	174.9	211.9	16.1	14.4	12.8	10.5
CNRM.DE6	88.3	127.3	163.2	199.1	16.3	14.4	12.9	10.7
SMHI.HCA2	98.6	144.3	178.9	218.8	15.9	14.1	12.3	9.9
SMHI.MPIA2	86.2	106.0	126.7	149.7	18.7	17.2	15.3	13.0
RCMs.Average	91.8	131.8	164.5	201.8	16.7	15.0	13.3	11.0

TABLE B.13: Bias-corrected mean **summer** (JJA) precipitation and temperature for different elevation bands, on the Ebro River basin, for the CTRL period 1961-1990 and for 6 RCMs during 2071-2100. Values computed averaging over the 349 and 146 gauging stations of precipitation and temperature, respectively.

	Mean Precipitation, [mm]				Mean Temperature, [°C]			
Scenario	Low	Med.Low	Med.High	High	Low	Med.Low	Med.High	High
CTRL	76.2	107.3	150.3	204.1	22.8	20.4	18.6	15.9
DMI.HS1	52.5	71.5	104.8	139.9	28.1	25.9	24.5	22.0
DMI.ecscA2	68.7	86.4	127.4	164.5	29.7	27.6	26.1	23.7
HC.adhfa	43.9	66.1	92.8	114.4	29.1	26.5	25.0	22.4
CNRM.DE6	45.4	60.0	91.7	130.4	28.0	25.5	24.0	21.3
SMHI.HCA2	43.8	57.7	83.3	108.0	28.9	26.7	25.1	22.6
SMHI.MPIA2	50.9	67.2	100.5	128.9	31.3	29.2	27.7	25.3
RCMs.Average	50.8	68.1	100.1	131.0	29.2	26.9	25.4	22.9

TABLE B.14: Bias-corrected mean **autumn** (SON) precipitation and temperature for different elevation bands, on the Ebro River basin, for the CTRL period 1961-1990 and for 6 RCMs during 2071-2100. Values computed averaging over the 349 and 146 gauging stations of precipitation and temperature, respectively.

	Mean Precipitation, [mm]				Mean Temperature, [°C]			
Scenario	Low	Med.Low	Med.High	High	Low	Med.Low	Med.High	High
CTRL	119.5	155.7	204.0	262.3	14.8	13.3	11.7	9.4
DMI.HS1	134.1	159.7	207.9	264.6	19.1	17.6	16.2	14.3
DMI.ecscA2	123.3	150.5	193.6	246.6	20.1	18.8	17.2	15.4
HC.adhfa	144.0	178.7	223.5	279.8	19.5	18.1	16.5	14.6
CNRM.DE6	112.1	140.2	182.5	232.0	18.8	17.2	15.6	13.6
SMHI.HCA2	144.1	162.1	211.9	268.9	19.0	17.5	16.0	14.1
SMHI.MPIA2	100.8	129.6	169.8	216.2	20.3	18.8	17.2	15.3
RCMs.Average	126.4	153.5	198.2	251.3	19.5	18.0	16.5	14.5

B.2.2 Monthly Projections

TABLE B.15: Bias-corrected mean **January** (JAN) precipitation and temperature for different elevation bands on the Ebro River basin, for the CTRL period 1961-1990 and for 6 RCMs during 2071-2100. Values computed averaging over the 349 and 146 gauging stations of precipitation and temperature, respectively.

	Mean Precipitation, [mm]				Mean Temperature, [°C]			
Scenario	Low	Med.Low	Med.High	High	Low	Med.Low	Med.High	High
CTRL	26.2	48.5	60.8	76.2	5.3	4.3	2.9	1.7
DMI.HS1	32.2	66.2	80.3	99.8	8.5	7.5	6.3	5.1
DMI.ecscA2	34.8	56.7	69.8	84.6	9.1	8.2	7.0	5.8
HC.adhfa	26.8	55.1	69.8	84.7	8.4	7.7	6.5	5.5
CNRM.DE6	39.7	52.9	75.5	84.5	8.8	7.6	6.4	5.0
SMHI.HCA2	29.1	57.1	72.9	92.9	8.3	7.3	6.1	4.8
SMHI.MPIA2	34.5	53.1	65.7	79.7	9.4	8.5	7.3	6.0
RCMs.Average	32.9	56.8	72.3	87.7	8.8	7.8	6.6	5.4

TABLE B.16: Bias-corrected mean **February** (FEB) precipitation and temperature for different elevation bands on the Ebro River basin, for the CTRL period 1961-1990 and for 6 RCMs during 2071-2100. Values computed averaging over the 349 and 146 gauging stations of precipitation and temperature, respectively.

	Mean Precipitation, [mm]				Mean Temperature, [°C]			
Scenario	Low	Med.Low	Med.High	High	Low	Med.Low	Med.High	High
CTRL	23.7	43.8	56.7	68.5	7.2	6.0	4.1	2.1
DMI.HS1	23.2	50.3	62.0	76.3	10.2	9.0	7.4	5.5
DMI.ecscA2	23.7	43.3	55.6	68.6	11.4	10.4	8.8	7.0
HC.adhfa	25.2	52.9	67.0	74.9	10.4	9.3	7.7	5.9
CNRM.DE6	32.2	51.5	63.4	75.7	10.0	8.6	7.1	5.1
SMHI.HCA2	23.7	49.3	61.7	75.8	10.2	8.8	7.2	5.2
SMHI.MPIA2	23.0	33.4	43.5	53.5	11.4	10.3	8.7	6.9
RCMs.Average	25.2	46.8	58.9	70.8	10.6	9.4	7.8	5.9

TABLE B.17: Bias-corrected mean **March** (MAR) precipitation and temperature for different elevation bands on the Ebro River basin, for the CTRL period 1961-1990 and for 6 RCMs during 2071-2100. Values computed averaging over the 349 and 146 gauging stations of precipitation and temperature, respectively.

	Mean Precipitation, [mm]				Mean Temperature, [°C]			
Scenario	Low	Med.Low	Med.High	High	Low	Med.Low	Med.High	High
CTRL	27.3	43.8	53.3	62.9	9.6	8.1	6.1	3.8
DMI.HS1	25.2	44.6	53.2	65.0	12.0	10.4	8.7	6.5
DMI.ecscA2	30.5	46.3	54.4	63.5	13.4	12.1	10.4	8.2
HC.adhfa	36.6	57.3	65.6	72.9	12.1	10.8	9.1	7.0
CNRM.DE6	24.3	38.3	48.1	56.5	12.7	11.1	9.6	7.5
SMHI.HCA2	28.3	46.6	54.3	63.8	12.0	10.3	8.6	6.3
SMHI.MPIA2	22.7	34.1	38.9	44.7	14.5	13.3	11.5	9.4
RCMs.Average	27.9	44.5	52.4	61.1	12.8	11.3	9.6	7.5

TABLE B.18: Bias-corrected mean **April** (APR) precipitation and temperature for different elevation bands on the Ebro River basin, for the CTRL period 1961-1990 and for 6 RCMs during 2071-2100. Values computed averaging over the 349 and 146 gauging stations of precipitation and temperature, respectively.

	Mean Precipitation, [mm]				Mean Temperature, [°C]			
Scenario	Low	Med.Low	Med.High	High	Low	Med.Low	Med.High	High
CTRL	39.5	60.0	73.4	88.8	12.3	10.4	8.4	5.9
DMI.HS1	36.2	56.8	70.9	88.0	15.1	13.4	11.7	9.3
DMI.ecscA2	26.2	41.3	52.4	64.0	17.3	15.8	14.1	11.7
HC.adhfa	27.3	44.3	52.3	67.0	15.6	14.0	12.4	10.1
CNRM.DE6	35.8	51.7	66.1	79.1	15.5	13.6	12.0	9.9
SMHI.HCA2	42.4	61.3	76.3	93.2	15.1	13.4	11.6	9.2
SMHI.MPIA2	26.8	36.1	43.8	52.3	18.4	16.9	15.0	12.6
RCMs.Average	32.4	48.6	60.3	73.9	16.2	14.5	12.8	10.5

TABLE B.19: Bias-corrected mean **may** (MAY) precipitation and temperature for different elevation bands on the Ebro River basin, for the CTRL period 1961-1990 and for 6 RCMs during 2071-2100. Values computed averaging over the 349 and 146 gauging stations of precipitation and temperature, respectively.

	Mean Precipitation, [mm]				Mean Temperature, [°C]			
Scenario	Low	Med.Low	Med.High	High	Low	Med.Low	Med.High	High
CTRL	46.4	60.6	78.3	101.7	16.4	14.2	12.1	9.6
DMI.HS1	29.8	39.0	54.6	75.6	20.4	18.5	16.8	14.3
DMI.ecscA2	34.5	42.4	58.1	75.0	22.1	20.5	18.7	16.3
HC.adhfa	31.2	41.1	57.0	72.0	20.6	18.5	16.8	14.4
CNRM.DE6	28.2	37.2	49.0	63.5	20.8	18.5	17.0	14.6
SMHI.HCA2	27.9	36.4	48.2	61.8	20.5	18.5	16.7	14.1
SMHI.MPIA2	36.7	35.8	44.0	52.7	23.1	21.3	19.5	17.0
RCMs.Average	31.4	38.7	51.8	66.8	21.3	19.3	17.6	15.1

TABLE B.20: Bias-corrected mean **June** (JUN) precipitation and temperature for different elevation bands on the Ebro River basin, for the CTRL period 1961-1990 and for 6 RCMs during 2071-2100. Values computed averaging over the 349 and 146 gauging stations of precipitation and temperature, respectively.

	Mean Precipitation, [mm]				Mean Temperature, [°C]			
Scenario	Low	Med.Low	Med.High	High	Low	Med.Low	Med.High	High
CTRL	35.6	47.6	64.9	83.0	20.8	18.3	16.3	13.7
DMI.HS1	24.3	33.4	47.9	61.6	25.6	23.4	21.8	19.2
DMI.ecscA2	28.5	35.4	52.0	67.6	26.4	24.2	22.6	20.0
HC.adhfa	22.2	30.0	40.9	49.4	26.4	23.8	22.1	19.5
CNRM.DE6	19.9	26.3	38.1	51.4	26.0	23.1	21.5	18.8
SMHI.HCA2	26.1	31.4	43.1	52.6	25.9	23.6	21.8	19.2
SMHI.MPIA2	21.4	27.9	37.5	43.3	28.3	26.0	24.3	21.8
RCMs.Average	23.7	30.7	43.2	54.3	26.4	24.0	22.4	19.8

TABLE B.21: Bias-corrected mean **July** (JUL) precipitation and temperature for different elevation bands on the Ebro River basin, for the CTRL period 1961-1990 and for 6 RCMs during 2071-2100. Values computed averaging over the 349 and 146 gauging stations of precipitation and temperature, respectively.

	Mean Precipitation, [mm]				Mean Temperature, [°C]			
Scenario	Low	Med.Low	Med.High	High	Low	Med.Low	Med.High	High
CTRL	16.1	25.9	38.8	56.3	24.2	21.7	20.0	17.2
DMI.HS1	9.5	14.9	23.4	33.8	29.2	26.9	25.6	22.9
DMI.ecscA2	12.3	18.8	29.8	41.1	31.6	29.5	28.1	25.7
HC.adhfa	8.5	14.5	22.1	29.2	30.6	27.9	26.4	23.8
CNRM.DE6	9.5	13.1	22.0	33.9	29.6	27.0	25.7	22.9
SMHI.HCA2	7.9	12.7	20.0	28.8	30.4	28.1	26.6	24.0
SMHI.MPIA2	8.6	13.9	22.7	31.3	33.0	30.9	29.5	27.2
RCMs.Average	9.4	14.7	23.3	33.0	30.8	28.4	27.0	24.4

TABLE B.22: Bias-corrected mean **August** (AUG) precipitation and temperature for different elevation bands on the Ebro River basin, for the CTRL period 1961-1990 and for 6 RCMs during 2071-2100. Values computed averaging over the 349 and 146 gauging stations of precipitation and temperature, respectively.

	Mean Precipitation, [mm]				Mean Temperature, [°C]			
Scenario	Low	Med.Low	Med.High	High	Low	Med.Low	Med.High	High
CTRL	24.5	33.7	46.6	64.9	23.6	21.3	19.5	16.7
DMI.HS1	18.6	23.1	33.5	44.5	29.5	27.4	26.1	23.8
DMI.ecscA2	27.9	32.2	45.6	55.8	30.9	29.0	27.7	25.4
HC.adhfa	13.1	21.6	29.9	35.8	30.2	27.7	26.3	23.8
CNRM.DE6	16.0	20.6	31.6	45.1	28.6	26.3	24.8	22.2
SMHI.HCA2	9.7	13.6	20.2	26.6	30.4	28.3	26.9	24.6
SMHI.MPIA2	20.8	25.4	40.3	54.3	32.7	30.7	29.2	26.9
RCMs.Average	17.7	22.7	33.5	43.7	30.4	28.2	26.8	24.5

TABLE B.23: Bias-corrected mean **September** (SEP) precipitation and temperature for different elevation bands on the Ebro River basin, for the CTRL period 1961-1990 and for 6 RCMs during 2071-2100. Values computed averaging over the 349 and 146 gauging stations of precipitation and temperature, respectively.

	Mean Precipitation, [mm]				Mean Temperature, [°C]			
Scenario	Low	Med.Low	Med.High	High	Low	Med.Low	Med.High	High
CTRL	37.6	40.6	55.4	73.2	20.3	18.4	16.6	14.0
DMI.HS1	48.1	45.2	59.8	74.8	25.3	23.7	22.2	19.9
DMI.ecscA2	47.9	40.7	53.7	67.1	26.6	25.0	23.4	21.2
HC.adhfa	35.0	36.6	46.7	57.5	26.6	24.8	23.1	20.8
CNRM.DE6	34.2	35.9	49.9	66.2	24.7	22.7	21.0	18.6
SMHI.HCA2	53.3	52.6	70.8	91.1	25.4	23.6	22.0	19.8
SMHI.MPIA2	38.0	35.8	49.1	61.1	27.2	25.5	23.8	21.4
RCMs.Average	42.7	41.1	55.0	69.6	26.0	24.2	22.6	20.3

TABLE B.24: Bias-corrected mean **October** (OCT) precipitation and temperature for different elevation bands on the Ebro River basin, for the CTRL period 1961-1990 and for 6 RCMs during 2071-2100. Values computed averaging over the 349 and 146 gauging stations of precipitation and temperature, respectively.

	Mean Precipitation, [mm]				Mean Temperature, [°C]			
Scenario	Low	Med.Low	Med.High	High	Low	Med.Low	Med.High	High
CTRL	41.5	51.4	66.7	84.8	15.1	13.6	11.7	9.5
DMI.HS1	40.4	50.7	65.3	84.5	19.3	17.8	16.3	14.3
DMI.ecscA2	33.6	38.4	49.4	65.6	20.1	18.9	17.2	15.2
HC.adhfa	52.6	58.4	69.1	90.3	19.1	17.6	16.0	13.9
CNRM.DE6	40.7	48.3	62.0	78.3	18.9	17.3	15.6	13.5
SMHI.HCA2	38.9	45.4	60.2	78.6	19.1	17.5	15.9	13.9
SMHI.MPIA2	32.4	39.4	48.2	61.7	20.1	18.7	17.0	15.0
RCMs.Average	39.8	46.8	59.0	76.5	19.4	18.0	16.3	14.3

TABLE B.25: Bias-corrected mean **november** (NOV) precipitation and temperature for different elevation bands on the Ebro River basin, for the CTRL period 1961-1990 and for 6 RCMs during 2071-2100. Values computed averaging over the 349 and 146 gauging stations of precipitation and temperature, respectively.

	Mean Precipitation, [mm]				Mean Temperature, [°C]			
Scenario	Low	Med.Low	Med.High	High	Low	Med.Low	Med.High	High
CTRL	40.3	63.7	81.9	104.4	9.1	8.0	6.6	4.9
DMI.HS1	45.6	63.8	82.8	105.2	12.5	11.4	10.2	8.7
DMI.ecscA2	41.9	71.5	90.5	113.9	13.6	12.4	11.1	9.6
HC.adhfa	56.4	83.7	107.8	132.0	12.9	11.8	10.5	9.1
CNRM.DE6	37.2	56.0	70.7	87.6	12.9	11.6	10.3	8.7
SMHI.HCA2	51.9	64.0	81.0	99.2	12.4	11.3	10.0	8.6
SMHI.MPIA2	30.5	54.5	72.6	93.4	13.4	12.3	11.0	9.4
RCMs.Average	43.9	65.6	84.2	105.2	13.0	11.8	10.5	9.0

TABLE B.26: Bias-corrected mean **december** (DEC) precipitation and temperature for different elevation bands on the Ebro River basin, for the CTRL period 1961-1990 and for 6 RCMs during 2071-2100. Values computed averaging over the 349 and 146 gauging stations of precipitation and temperature, respectively.

	Mean Precipitation, [mm]				Mean Temperature, [°C]			
Scenario	Low	Med.Low	Med.High	High	Low	Med.Low	Med.High	High
CTRL	29.1	52.0	66.4	82.8	5.6	4.9	3.5	2.2
DMI.HS1	38.2	64.7	80.7	101.7	9.1	8.3	7.1	6.0
DMI.ecscA2	40.3	68.1	82.9	100.1	9.5	8.6	7.4	6.3
HC.adhfa	41.4	54.0	71.1	80.5	9.1	8.4	7.3	6.4
CNRM.DE6	24.8	47.4	60.8	75.8	8.5	7.5	6.2	5.0
SMHI.HCA2	36.4	61.2	76.6	94.0	9.0	8.2	7.0	5.9
SMHI.MPIA2	30.8	53.5	68.9	85.9	9.8	8.9	7.7	6.6
RCMs.Average	35.3	58.2	73.5	89.7	9.2	8.3	7.1	6.0

C

Detailed Plots of Hydrological Impacts

This Appendix presents 29-years daily flow duration curves (FDCs) for the control period and each one of the six future climate scenarios described in Table 4.1, along with the corresponding 95% of predictive uncertainty (95PPU) derived from hydrological parameterisation. An individual figure is used for each for each scenario, in order to look a the individual uncertainties derived from hydrological parameterisation.

C.1 Overall Impacts

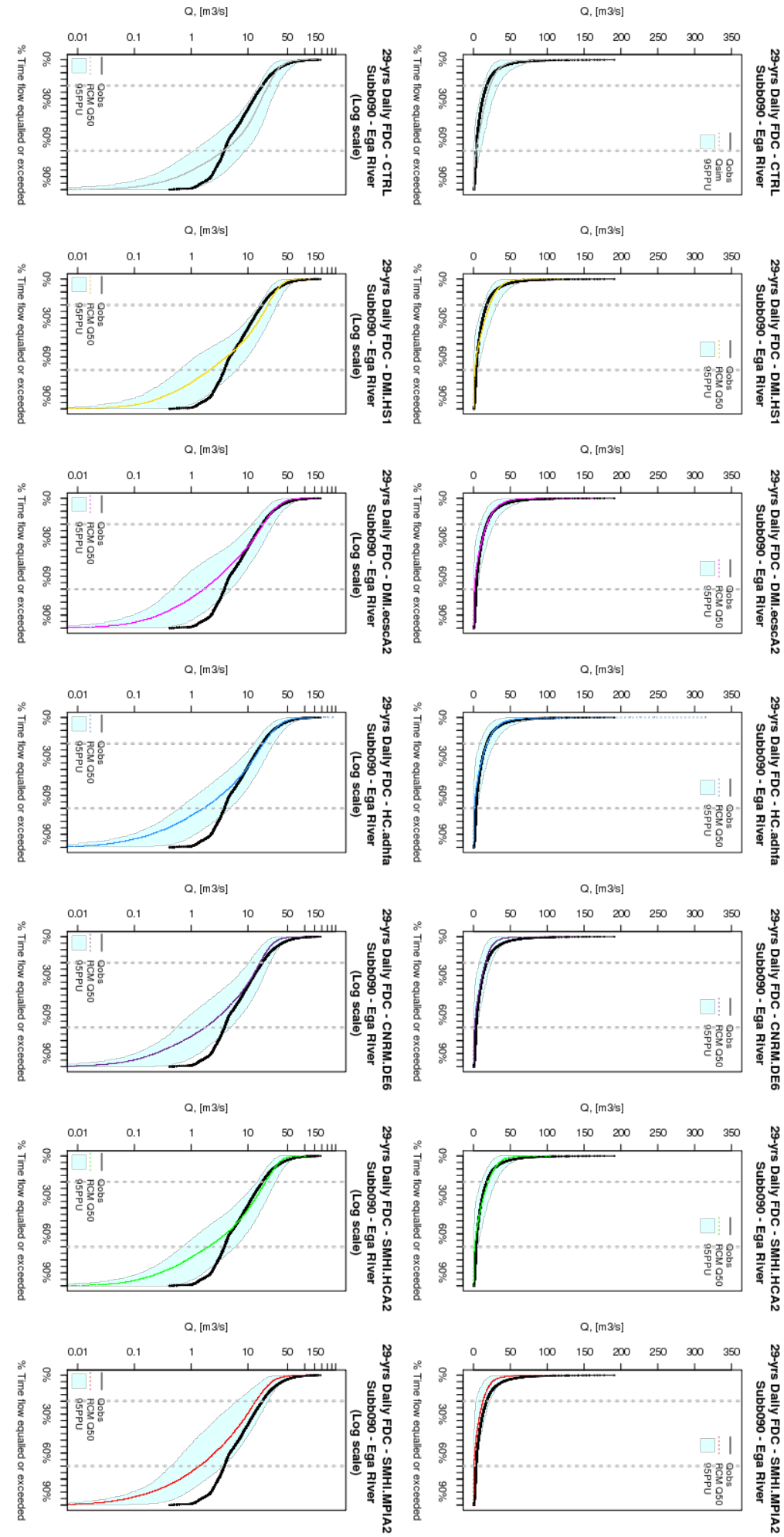

FIGURE C.1: 29-years flow duration curve (FDC) for subcatchment 090 (Ega River). Figures in the upper panel represent the FDCs with a normal vertical scale for each climate scenario, and figures on the bottom panel show the same FDC but using logarithmic vertical scale (removing zero values). Black continuous line is the observed FDC during the period 1962-1990, grey dotted line represent the median of the GLUE simulations for the same control period, and coloured dotted lines show the median of the simulations corresponding to different climate scenarios during the period 2072-2100. Shaded area represent the uncertainty due to the hydrological parameterisation adopted during GLUE simulations for each climate scenario.

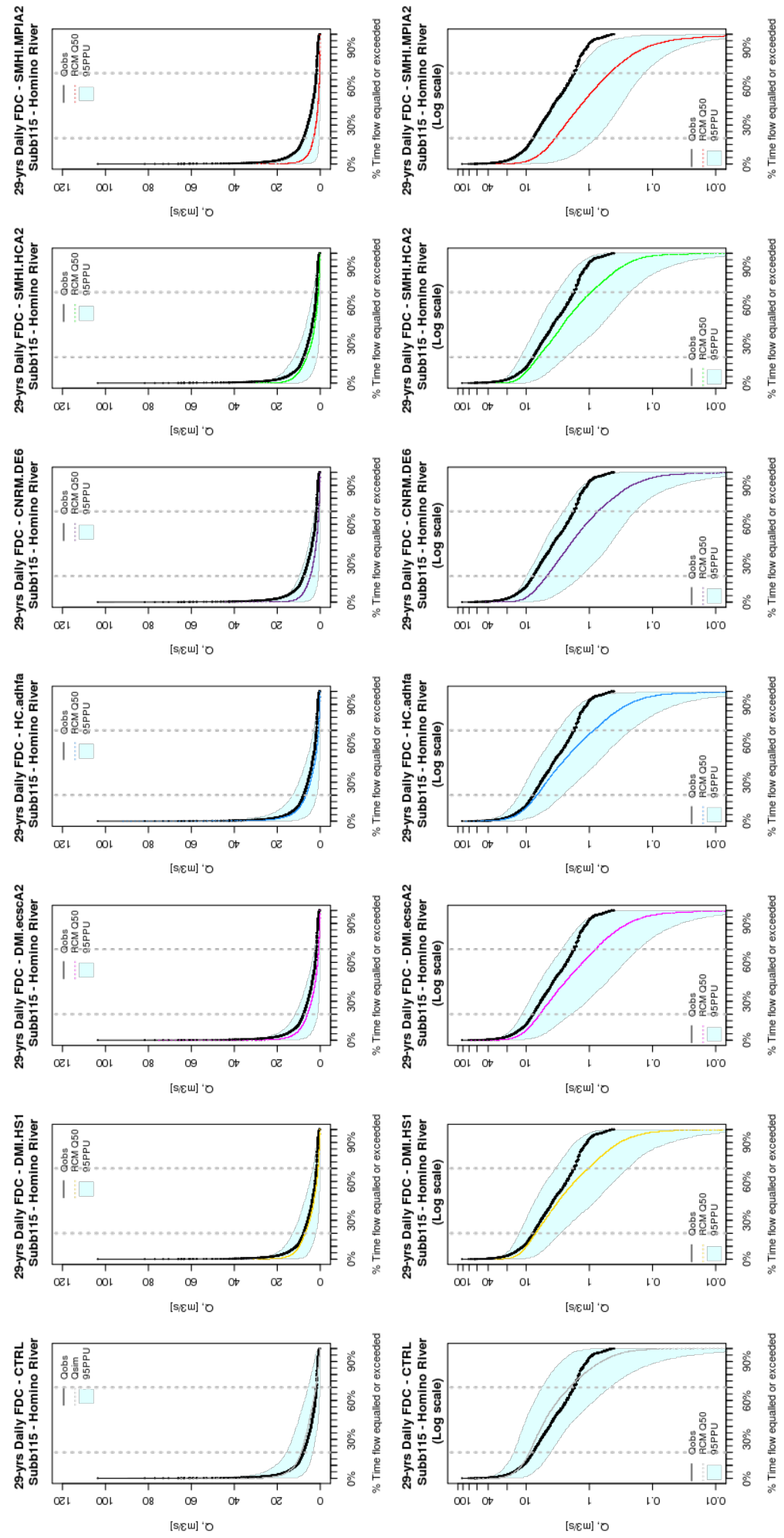

FIGURE C.2: 29-years flow duration curve (FDC) for subcatchment 115 (Homino River). Figures in the upper panel represent the FDCs with a normal vertical scale for each climate scenario, and figures on the bottom panel show the same FDC but using logarithmic vertical scale (removing zero values). Black continuous line is the observed FDC during the period 1962-1990, grey dotted line represent the median of the GLUE simulations for the same control period, and coloured dotted lines show the median of the simulations corresponding to different climate scenarios during the period 2072-2100. Shaded area represent the uncertainty due to the hydrological parameterisation adopted during GLUE simulations for each climate scenario.

C.2 Seasonal Impacts

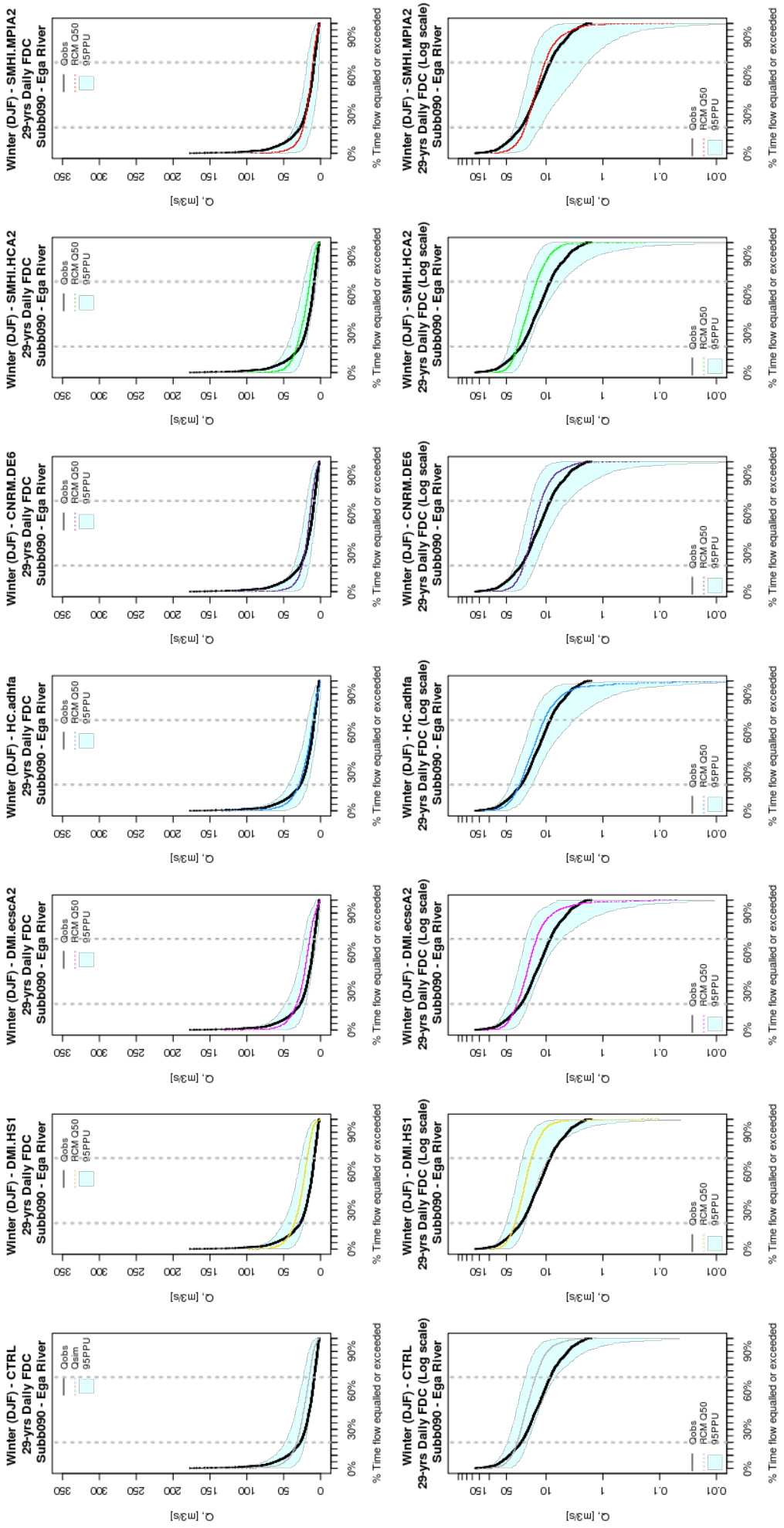

FIGURE C.3: 29-years winter (DJF) flow duration curve (FDC) for subcatchment 090 (Ega River). Figures in the upper panel represent the FDCs with a normal vertical scale for each climate scenario, and figures on the bottom panel show the same FDC but using logarithmic vertical scale (removing zero values). Black continuous line is the observed FDC during the period 1962-1990, grey dotted line represent the median of the GLUE simulations for the same control period, and coloured dotted lines show the median of the simulations corresponding to different climate scenarios during the period 2072-2100. Shaded area represent the uncertainty due to the hydrological parameterisation adopted during GLUE simulations for each climate scenario.

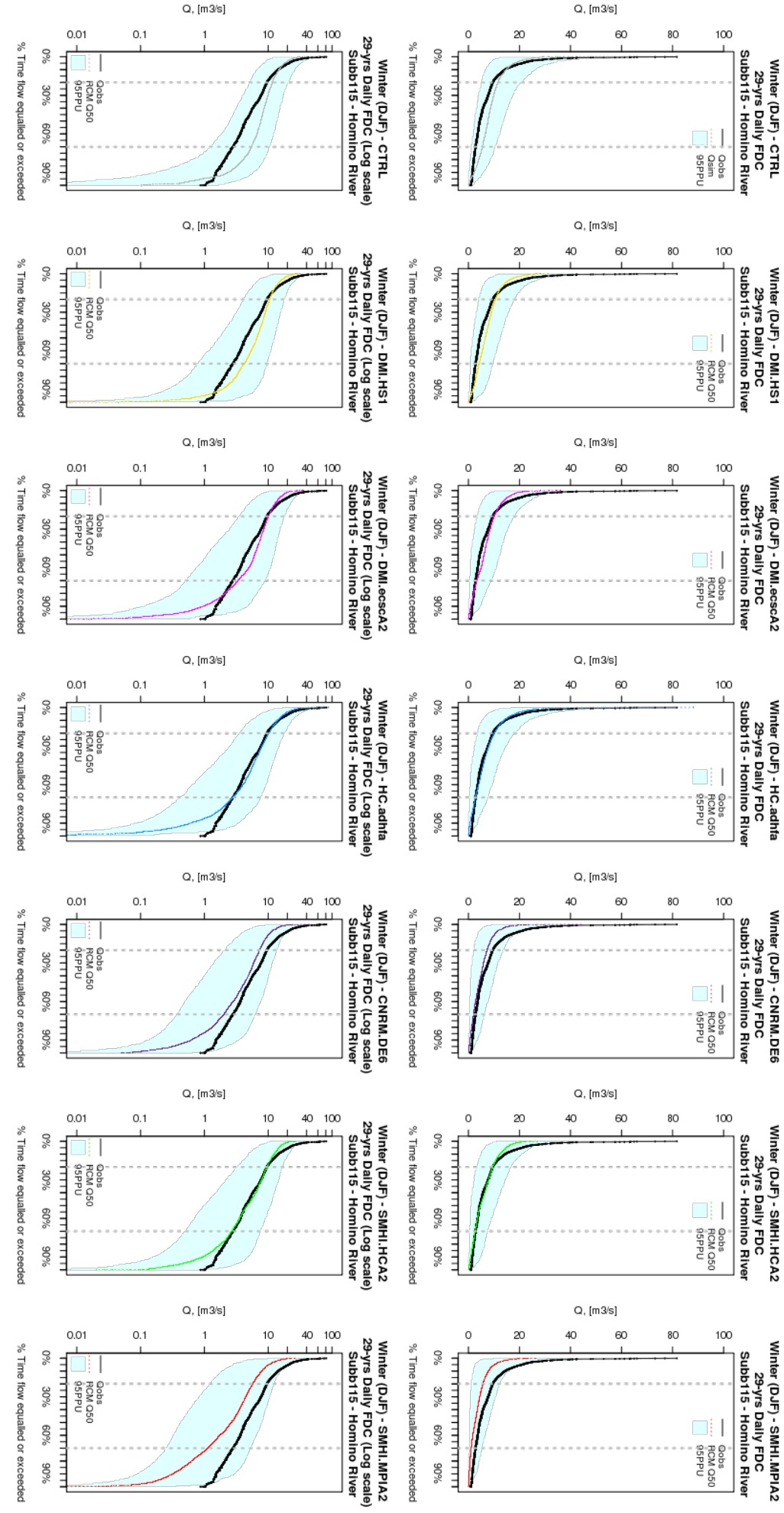

FIGURE C.4: 29-years winter (DJF) flow duration curve (FDC) for subcatchment 115 (Homino River). Figures in the upper panel represent the FDCs with a normal vertical scale for each climate scenario, and figures on the bottom panel show the same FDC but using logarithmic vertical scale (removing zero values). Black continuous line is the observed FDC during the period 1962-1990, grey dotted line represent the median of the GLUE simulations for the same control period, and coloured dotted lines show the median of the simulations corresponding to different climate scenarios during the period 2072-2100. Shaded area represent the uncertainty due to the hydrological parameterisation adopted during GLUE simulations for each climate scenario.

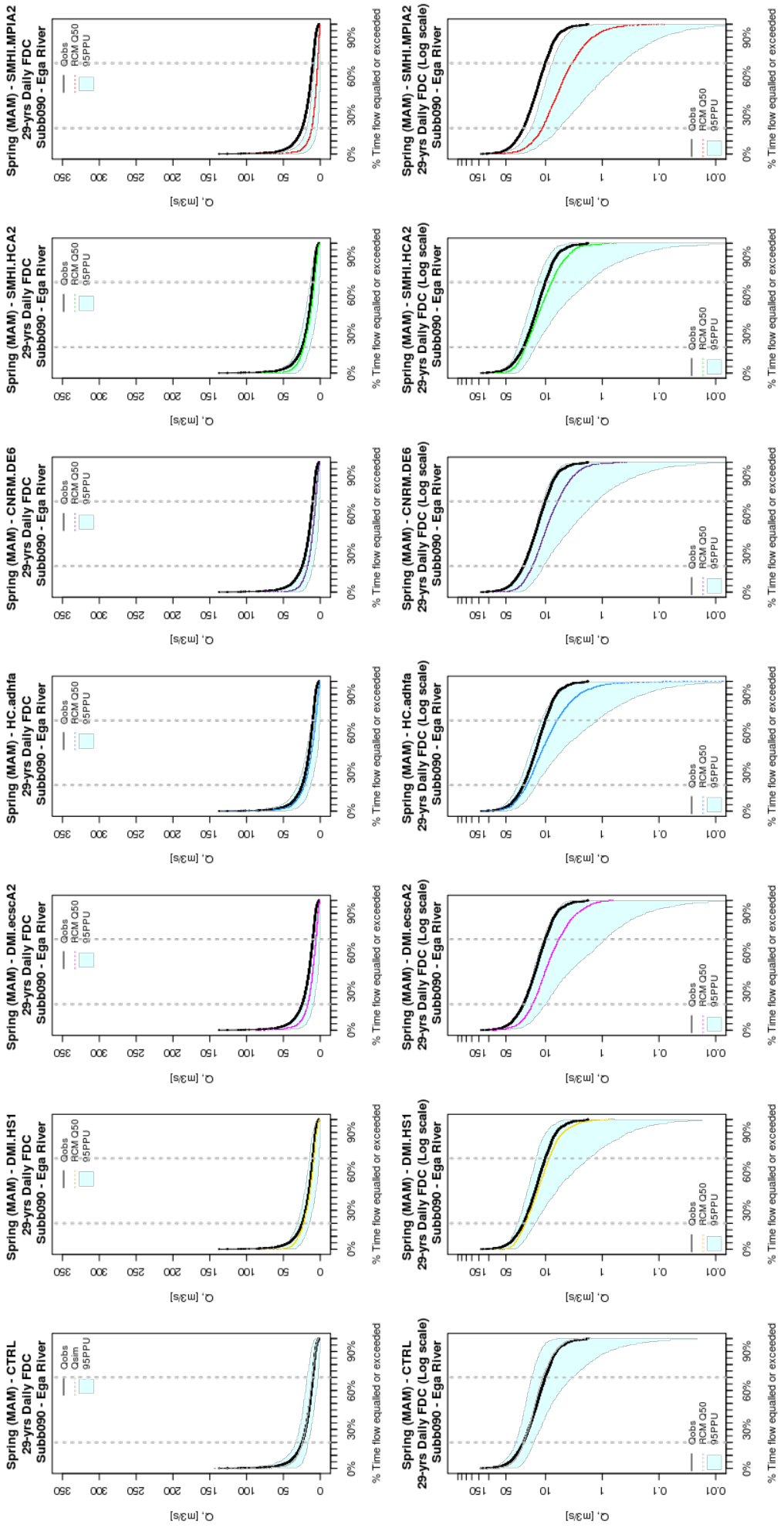

FIGURE C.5: 29-years spring (MAM) flow duration curve (FDC) for subcatchment 090 (Ega River). Figures in the upper panel represent the FDCs with a normal vertical scale for each climate scenario, and figures on the bottom panel show the same FDC but using logarithmic vertical scale (removing zero values). Black continuous line is the observed FDC during the period 1962-1990, grey dotted line represent the median of the GLUE simulations for the same control period, and coloured dotted lines show the median of the simulations corresponding to different climate scenarios during the period 2072-2100. Shaded area represent the uncertainty due to the hydrological parameterisation adopted during GLUE simulations for each climate scenario.

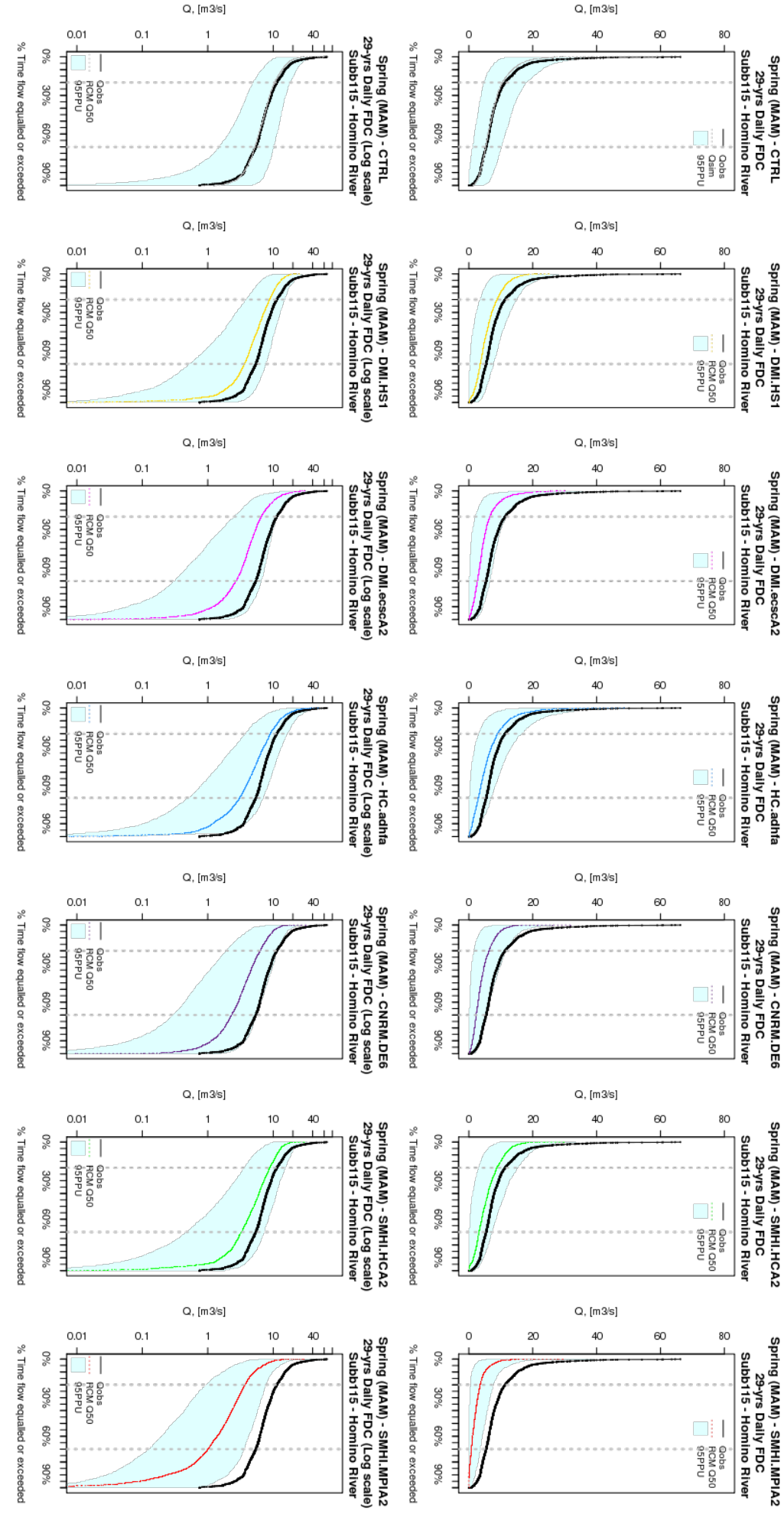

FIGURE C.6: 29-years spring (MAM) flow duration curve (FDC) for subcatchment 090 (Ega River). Figures in the upper panel represent the FDCs with a normal vertical scale for each climate scenario, and figures on the bottom panel show the same FDC but using logarithmic vertical scale (removing zero values). Black continuous line is the observed FDC during the period 1962-1990, grey dotted line represent the median of the GLUE simulations for the same control period, and coloured dotted lines show the median of the simulations corresponding to different climate scenarios during the period 2072-2100. Shaded area represent the uncertainty due to the hydrological parameterisation adopted during GLUE simulations for each climate scenario.

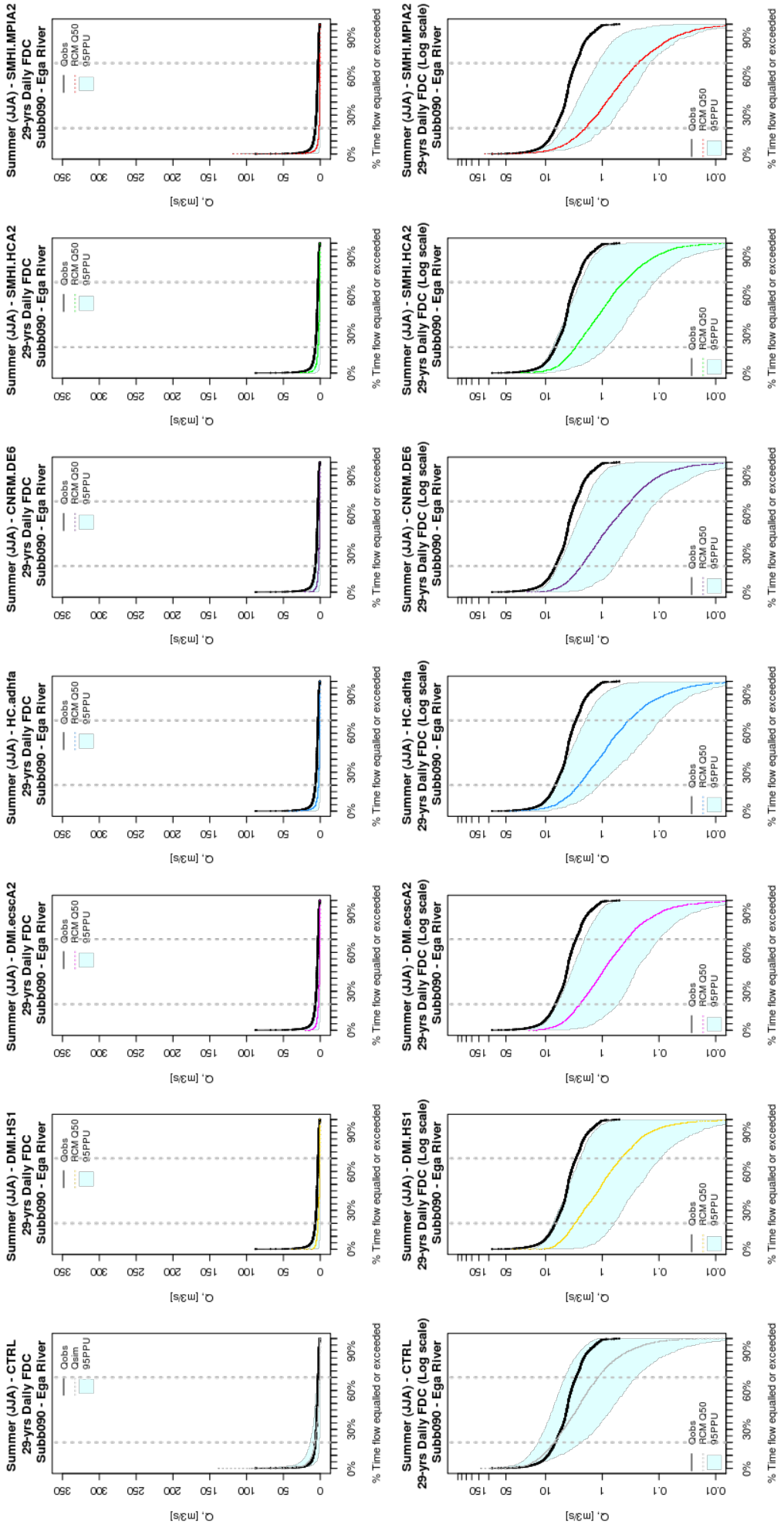

FIGURE C.7: 29-years summer (JJA) flow duration curve (FDC) for subcatchment 090 (Ega River). Figures in the upper panel represent the FDCs with a normal vertical scale for each climate scenario, and figures on the bottom panel show the same FDC but using logarithmic vertical scale (removing zero values). Black continuous line is the observed FDC during the period 1962-1990, grey dotted line represent the median of the GLUE simulations for the same control period, and coloured dotted lines show the median of the simulations corresponding to different climate scenarios during the period 2072-2100. Shaded area represent the uncertainty due to the hydrological parameterisation adopted during GLUE simulations for each climate scenario.

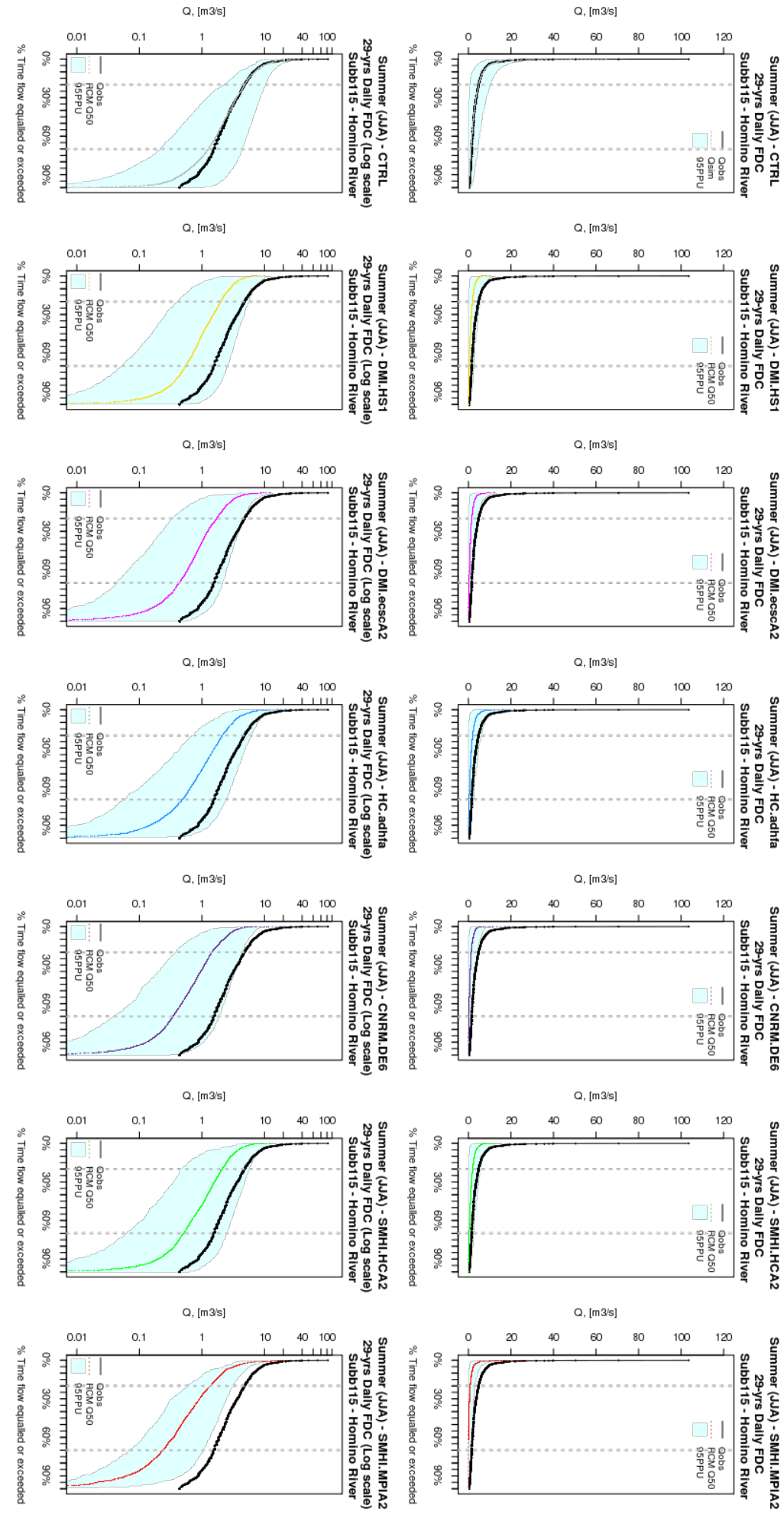

FIGURE C.8: 29-years summer (JJA) flow duration curve (FDC) for subcatchment 115 (Homino River). Figures in the upper panel represent the FDCs with a normal vertical scale for each climate scenario, and figures on the bottom panel show the same FDC but using logarithmic vertical scale (removing zero values). Black continuous line is the observed FDC during the period 1962-1990, grey dotted line represent the median of the GLUE simulations for the same control period, and coloured dotted lines show the median of the simulations corresponding to different climate scenarios during the period 2072-2100. Shaded area represent the uncertainty due to the hydrological parameterisation adopted during GLUE simulations for each climate scenario.

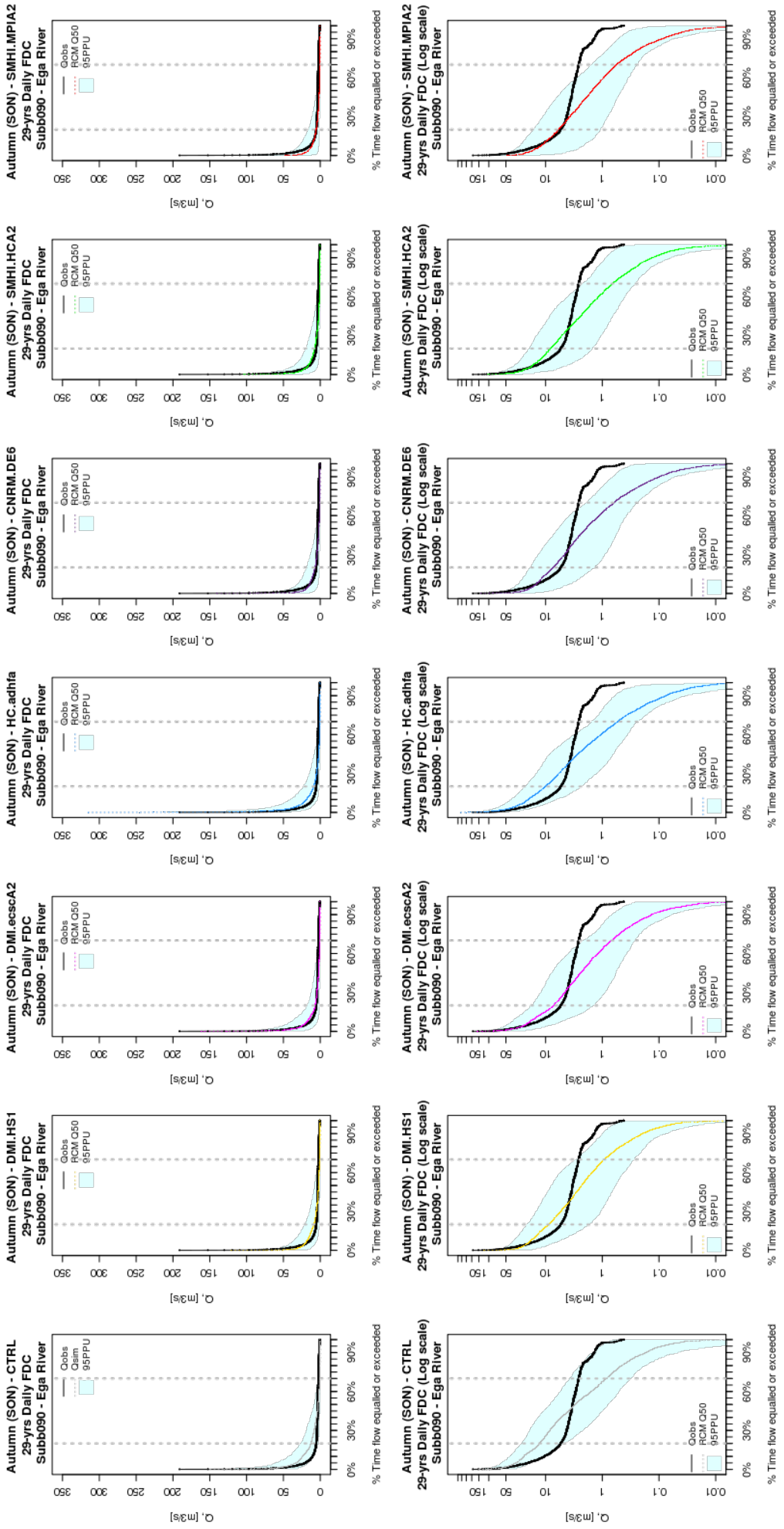

FIGURE C.9: 29-years autumn (SON) flow duration curve (FDC) for subcatchment 090 (Ega River). Figures in the upper panel represent the FDCs with a normal vertical scale for each climate scenario, and figures on the bottom panel show the same FDC but using logarithmic vertical scale (removing zero values). Black continuous line is the observed FDC during the period 1962-1990, grey dotted line represent the median of the GLUE simulations for the same control period, and coloured dotted lines show the median of the simulations corresponding to different climate scenarios during the period 2072-2100. Shaded area represent the uncertainty due to the hydrological parameterisation adopted during GLUE simulations for each climate scenario.

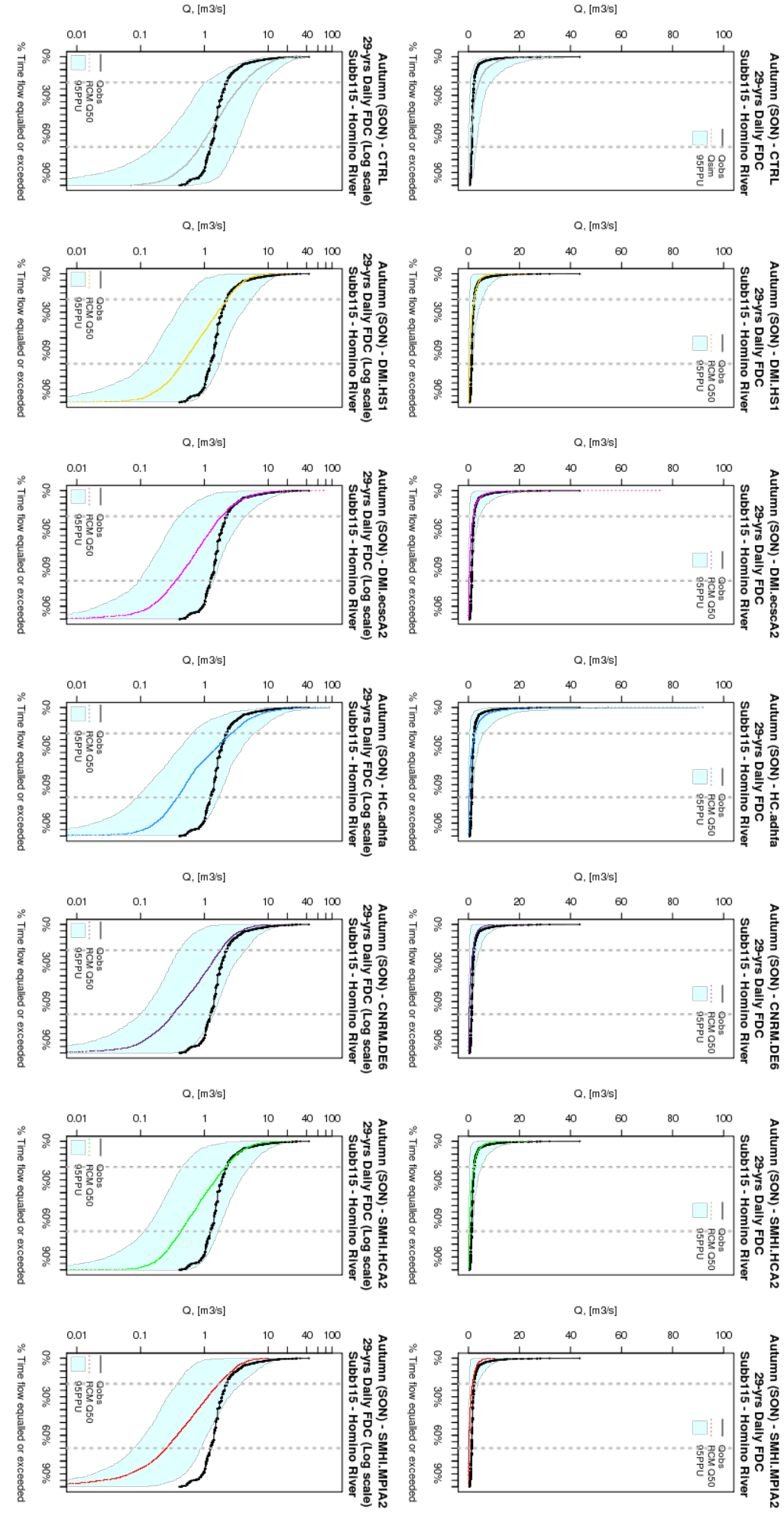

FIGURE C.10: 29-years autumn (SON) flow duration curve (FDC) for subcatchment 115 (Homino River). Figures in the upper panel represent the FDCs with a normal vertical scale for each climate scenario, and figures on the bottom panel show the same FDC but using logarithmic vertical scale (removing zero values). Black continuous line is the observed FDC during the period 1962-1990, grey dotted line represent the median of the GLUE simulations for the same control period, and coloured dotted lines show the median of the simulations corresponding to different climate scenarios during the period 2072-2100. Shaded area represent the uncertainty due to the hydrological parameterisation adopted during GLUE simulations for each climate scenario.

Package 'hydroTSM'

December 1, 2009

Type Package

Title Time Series Management and Interpolation for Hydrological Modelling

Version 0.1.6

Date 2009-12-01

Author Mauricio Zambrano Bigiarini

Maintainer Mauricio Zambrano Bigiarini <mauricio.zambrano@ing.unitn.it>

Description Functions for time series management and interpolation for hydrological modelling. So far, it works only with daily/monthly/seasonal/annual time series.

License LGPL-2

Depends R (>= 2.8.0), zoo

Suggests gstat, automap, maptools, sp, e1071, lattice

URL http://www.r-project.org, http://www.another.url

LazyLoad yes

R topics documented:

`hydroTSM-package` *Time Series Management and Interpolation for Hydrological Modelling.*

Description

Functions for time series management and interpolation for hydrological modelling. So far, it works only with daily/monthly/annual/seasonal time series.

Details

Package:	hydroTSM
Type:	Package
Version:	0.1.6
Date:	2009-12-01
License:	LGPL-2
LazyLoad:	yes

Author(s)

Mauricio Zambrano-Bigiarini

Maintainer: Mauricio Zambrano-Bigiarini <mauricio.zambrano@ing.unitn.it>

Examples

```
## Loading temperature data ##
data(EbroTEMPts)

## Ex1) Graphical correlation between the ts of daily temperature of the first
## 3 stations in 'EbroTEMPts'
hydropairs(EbroTEMPts[,2:4])

# Ex2) Annual values of temperature at the station "T9105", stored in EbroTEMPts.
sname2ts(EbroTEMPts, sname="T9105", dates=1, var.type="Temperature", tstep.out="annual")

# Ex3) Monthly and annual plots
sname2plot(EbroTEMPts, sname="T9105", var.type="Temperature", dates=1, pfreq="ma")


## Ex4) IDW interpolation and plot

## Loading the gis data
data(EbroTEMPgis)

## Loading the shapefile with the subcatchments
data(EbroSubcatch)

## Projection for the Subcatchments file
require(sp)
p4s <- CRS("+proj=utm +zone=30 +ellps=intl +units=m +no_defs")


## Selecting the first day of 'EbroTEMPts' for all the stations
x.ts <- as.numeric(EbroTEMPts[1, 2:ncol(EbroTEMPts)])

## Setting the name of the stations
names(x.ts) <- colnames(EbroTEMPts[1,2:ncol(EbroTEMPts)])
```

```
# Computing the interpolated values and plotting them
# Probably you will need to resize your window
## Not run:
x.idw <- hydrokrige(x.ts= x.ts, x.gis=EbroTEMPgis,
    X="EAST_ED50" , Y="NORTH_ED50" , sname="ID",
    bname= "CHE_BASIN_NAME", elevation="ELEVATION",
    IDW.type= "both",
    SubCatchments.fname= EbroSubcatch,
    p4s= p4s,
    cell.size= 1000,
    ColorRamp= "Temperature",
    col.nintv= 40, col.at= "auto")

## End(Not run)
```

`annualfunction` *Annual Function*

Description

Generic function for applying any R function to ALL the values in 'x' belonging to a given year

Usage

```
annualfunction(x, FUN, na.rm = TRUE, ...)

## Default S3 method:
annualfunction(x, FUN, na.rm = TRUE, ...)

## S3 method for class 'data.frame':
annualfunction(x, FUN, na.rm = TRUE, dates, date.fmt = "%Y-%m-%d",
        verbose = TRUE, ...)
```

Arguments

`x`	Daily, monthly or annual 'zoo' or 'data.frame' object
`FUN`	Function that will be applied to ALL the values in 'x' belonging to each weather season of the year (e.g., Fun can be some of c('mean', 'max', 'min', 'sd'))
`na.rm`	Logical. Should missing values be removed?. -) TRUE : the annual values are computed considering only those values different from NA -) FALSE: if there is AT LEAST one NA within a year, the annual values are NA
`dates`	"numeric", "factor", "Date" indicating how to obtain the dates correponding to the 'sname' station. If 'dates' is a number, it indicates the index of the column in 'x' that stores the

	dates If 'dates' is a factor, it have to be converted into 'Date' class, using the date format specified by 'date.fmt' If 'dates' is already of Date class, the code verifies that the number of days in 'dates' be equal to the number of element in 'x'
`date.fmt`	character indicating the format in which the dates are stored in 'dates', e.g. "%Y-%m-%d" ONLY required when class(dates)=="factor" or "numeric"
`verbose`	Logical; if TRUE, progress messages are printed
`...`	further arguments passed to or from other methods

Note

'FUN' is first applied to all the values of 'x' belonging to the same year and then it is applied to all the previously computed annual values to get the final result. Its final value will depend on the smapling frequency of 'x' and the type of fucntion provided by 'FUN' (e.g., 'mean' or 'max')

Author(s)

Mauricio Zambrano-Bigiarini, <mauricio.zambrano@ing.unitn.it>

See Also

`monthlyfunction`, `daily2annual`, `monthly2annual`

Examples

```
## Loading temperature data ##
data(EbroTEMPts)
x     <- EbroTEMPts[,2]
dates <- EbroTEMPts[,1]

## From 'character' to 'Date' class
dates <- as.Date(dates)

## From 'numeric' to 'zoo' class
x <- vector2zoo(x, dates)

## Daily to Monthly
daily2monthly(x, FUN=mean, na.rm=TRUE)

## Annual Mean values of temperature
annualfunction(x, FUN=mean, na.rm=TRUE)
```

`daily2annual` *Daily -> Annual*

Description

Generic function for transforming a DAILY/MONTHLY regular time series into an ANNUAL one

Usage

```
daily2annual(x, ...)

## Default S3 method:
daily2annual(x, FUN, na.rm = TRUE, out.fmt = "%Y", ...)

## S3 method for class 'data.frame':
daily2annual(x, FUN, na.rm = TRUE, out.fmt = "%Y", dates,
        date.fmt = "%Y-%m-%d", out.type = "data.frame", verbose = TRUE, ...)
```

Arguments

`x`	Daily zoo object which values will be converted into an Annual one.
`FUN`	Function that have to be applied for transforming from Daily/Monthly to Annual time step (e.g., For precipitation FUN=sum and for temperature and flow ts, FUN=mean) (e.g., For precipitation FUN=sum and for temperature and flow ts, FUN=mean)
`na.rm`	Logical. Should missing values be removed? -) TRUE : the monthly and annual values are computed considering only those values different from NA -) FALSE: if there is AT LEAST one NA within a year, the annual values are NA
`out.fmt`	Character indicating the format for the output time series. Possible values are: -) "%Y" : only the year will be used for the time. Default option. (e.g., "1961" "1962"...) -) "%Y-%m-%d": a complete date format will be used for the time. Default option. (e.g., "1961" "1962"...)
`dates`	"numeric", "factor", "Date" indicating how to obtain the dates for correponding to the 'sname' station If 'dates' is a number, it indicates the index of the column in 'x' that stores the dates If 'dates' is a factor, it have to be converted into 'Date' class, using the date format specified by 'date.fmt' If 'dates' is already of Date class, the code verifies that the number of days in 'dates' be equal to the number of element in 'x'
`date.fmt`	character indicating the format in which the dates are stored in 'dates', e.g. "%Y-%m-%d". ONLY required when class(dates)=="factor" or "numeric"

out.type	Character that defines the desired type of output. Valid values are: -) "data.frame": a data.frame, with as many columns as stations are included in 'x', and an additional column indicating the Year -) "db" : a data.frame, with 3 colums will be produced. The first column will store the Year The second column will store the ID of the station, The third column will contain the seasonal value corresponding to that year and that
verbose	logical; if TRUE, progress messages are printed
...	further arguments passed to or from other methods.

Author(s)

Mauricio Zambrano-Bigiarini, <mauricio.zambrano@ing.unitn.it>

See Also

vector2zoo, as.Date, daily2monthly, monthly2annual

Examples

```
## Loading temperature data ##
data(EbroTEMPts)
x     <- EbroTEMPts[,2]
dates <- EbroTEMPts[,1]

## From 'character' to 'Date' class
dates <- as.Date(dates)

## From 'numeric' to 'zoo' class
x <- vector2zoo(x, dates)

## Daily to Monthly
daily2monthly(x, FUN=mean, na.rm=TRUE)

## Monthly to Annual
monthly2annual(x, FUN=mean, na.rm=TRUE)
```

---

daily2monthly *Daily -> Monthly*

Description

Generic function for transforming a DAILY regular time series into a Monthly one

Usage

```
daily2monthly(x, ...)

## Default S3 method:
daily2monthly(x, FUN, na.rm = TRUE, ...)

## S3 method for class 'data.frame':
daily2monthly(x, FUN, na.rm = TRUE, dates, date.fmt = "%Y-%m-%d",
        out.type = "data.frame", verbose = TRUE, ...)
```

Arguments

x	Daily zoo object to be converted into a Monthly one.
FUN	Function that have to be applied for transforming from Daily to Annual time step. (e.g., For precipitation FUN=sum and for temperature and flow ts, FUN=mean) (e.g., For precipitation FUN=sum and for temperature and flow ts, FUN=mean) ONLY needed when 'var.type' is missing
na.rm	Logical. Should missing values be removed? -) TRUE : the monthly and annual values are computed considering only those values different from NA -) FALSE: if there is AT LEAST one NA within a year, the monthly values are NA
dates	"numeric", "factor", "Date" indicating how to obtain the dates for correponding to the 'sname' station If 'dates' is a number, it indicates the index of the column in 'x' that stores the dates If 'dates' is a factor, it have to be converted into 'Date' class, using the date format specified by 'date.fmt' If 'dates' is already of Date class, the code verifies that the number of days in 'dates' be equal to the number of element in 'x'
date.fmt	character indicating the format in which the dates are stored in 'dates', e.g. "%Y-%m-%d". ONLY required when class(dates)=="factor" or "numeric"
out.type	Character that defines the desired type of output. Valid values are: -) "data.frame": a data.frame, with as many columns as stations are included in 'x' -) "db" : a data.frame, with 4 colums will be produced. The first column stores the ID of the station, The second column stores the Year The third column stores the Month The fourth colum stores the numerical values corresponding to the year and month specified in the two previous fields.
verbose	logical; if TRUE, progress messages are printed
...	further arguments passed to or from other methods.

Author(s)

Mauricio Zambrano-Bigiarini, <mauricio.zambrano@ing.unitn.it>

See Also

vector2zoo, as.Date, daily2annual

Examples

```
## Loading temperature data ##
data(EbroTEMPts)
x     <- EbroTEMPts[,2]
dates <- EbroTEMPts[,1]

## From 'character' to 'Date' class
dates <- as.Date(dates)

## From 'numeric' to 'zoo' class
x <- vector2zoo(x, dates)

## Daily to Monthly
daily2monthly(x, FUN=mean, na.rm=TRUE)
```

---

dip *Days in Period*

Description

Given any starting and ending dates, it generates:
1) a vector with all the days between the two dates, OR
2) the amount of days between the two dates

Usage

```
dip(from, to, date.fmt = "%Y-%m-%d", out.type = "seq")
```

Arguments

from	Character indicating the starting date for computing the number of days. It MUST have the date format specified by 'date.fmt'
to	Character indicating the ending date for computing the number of days. It MUST have the date format specified by 'date.fmt'
date.fmt	Character indicating the date format in which you provide 'from' and 'to' (e.g., "%d-%m-%Y")

out.type	Character indicating the type of result that is given by this function. Valid values are: -) type= "seq" => a vectorial sequence with all the days within the given time period -) type= "nmbr" => the number of days in the vectorial sequence with all the days within the given time period

Author(s)

Mauricio Zambrano-Bigiarini, <mauricio.zambrano@ing.unitn.it>

See Also

mip

Examples

```
## Sequence of daily dates between "1961-01-01" and "1961-12-31" ##
dip("1961-01-01", "1961-12-31")

## Number of days between "1961-01-01" and "1965-06-30", with the date format "%d-%m-%Y"
dip("01-01-1961", "30-06-1965", date.fmt= "%d-%m-%Y", out.type = "nmbr")
```

---

diy *Days in Year*

Description

Given a numeric value of a year, it generates: 1) a vector with all the days (dates) within the year, OR 2) the amount of days in the year

Usage

```
diy(year, out.type = "seq")
```

Arguments

year	numeric, the year for which the sequence of days will be generated
out.type	Character indicating the type of result that is given by this function. Valid values are: -) type= "seq" => a vectorial sequence with all the days within the given year -) type= "nmbr" => the number of days in the vectorial sequence with all the days within the given year

Author(s)

Mauricio Zambrano-Bigiarini, <mauricio.zambrano@ing.unitn.it>

See Also

dip, mip

Examples

```
## Sequence of daily dates for the year 1961
diy(1961)

## Computing the number of days between in 1961
diy(1961, out.type = "nmbr")
```

---

dm2seasonal *Daily/Monthly -> Seasonal Values*

Description

Generic function for computing seasonal values for every year of a daily/monthly zoo object

Usage

```
dm2seasonal(x, ...)

## Default S3 method:
dm2seasonal(x, season, FUN, na.rm = TRUE, ...)

## S3 method for class 'data.frame':
dm2seasonal(x, season, FUN, na.rm = TRUE, dates, date.fmt = "%Y-%m-%d",
        out.type = "data.frame", ...)
```

Arguments

x	object of type 'zoo' or 'data.frame', with daily or monthly frequency
season	character, indicating the weather season to be used for selecting the data. Valid values are: -) "DJF": December, January, February -) "MAM": March, April, May -) "JJA": June, July, August -) "SON": September, October, November
FUN	Function that will be applied to ALL the values of 'x' belonging to the given weather season
na.rm	Logical. Should missing values be removed? -) TRUE : the seasonal values are computed considering only those values different from NA -) FALSE: if there is AT LEAST one NA within a weather season, the corresponding seasonal values are NA

dates	"numeric", "factor", "Date" indicating how to obtain the dates correponding to each row of 'x' If 'dates' is a number, it indicates the index of the column in 'x' that stores the dates If 'dates' is a factor, it have to be converted into 'Date' class, using the date format specified by 'date.fmt' If 'dates' is already of Date class, the code verifies that the number of days in 'dates' be equal to the number of elements in 'x'
date.fmt	character indicating the format in which the dates are stored in 'dates', e.g. "%Y-%m-%d" ONLY required when class(dates)=="factor" or "numeric"
out.type	Character that defines the desired type of output. Possible values are -) "data.frame": a data.frame, with as many columns as stations are included in 'x' -) "db" : a data.frame, with 4 colums will be produced. The first column stores the ID of the station The second column stores the Year, The third column stores the season, The fourth column contains the sesonal value corresponding to the year specified in the second column
...	further arguments passed to or from other methods.

Note

-) FUN is applied over all the vlaues of 'x' belonging to each season, so, the results of htis function depends on the frequency sampling of 'x' and the type of function given by 'FUN'
-) For any year, the FUN value for the summer season (DJF), is computed considering only January and February, and the value of December is used for computing the summer value of the next year.

Author(s)

Mauricio Zambrano-Bigiarini, <mauricio.zambrano@ing.unitn.it>

See Also

time2season, daily2monthly, daily2annual, monthly2annual

Examples

```
## Loading temperature data ##
data(EbroTEMPts)
x     <- EbroTEMPts[,2]
dates <- EbroTEMPts[,1]

## From 'character' to 'Date' class
dates <- as.Date(dates)

## From 'numeric' to 'zoo' class
x <- vector2zoo(x, dates)

## Annual Mean values of temperature during the summer season (DJF) in station 'x'
dm2seasonal(x, FUN=mean, season="DJF")

## Annual Mean values of temperature during the summer season (DJF),
```

```
## for the first 3 stations in 'EbroTEMPts'
dm2seasonal(EbroTEMPts[,1:4], FUN=mean, season="DJF", dates=1)
```

---

dmc *Double-Mass Curve*

Description

Monthly Double-Mass Curve for daily precipitation or streamflow data. From daily time series, in a data.frame, it computes the monthly mean double-mass curves (Homogeneity test)

Usage

```
## S3 method for class 'data.frame':
dmc(x, target, dates, date.fmt, var.type, FUN, na.rm = TRUE,
        method = "pearson",  use = "pairwise.complete.obs",
        main = "Monthly Double-Mass Curve",
        screen = c(ceiling(sqrt(ncol(x) - 1)), (ncol(x) - 1) -
                   ceiling(sqrt(ncol(x) - 1))),
        xlab = "Target Station", ylab = "Reference Station",
        col = "blue", print.out = "both", ...)
```

Arguments

x	variable of type 'zoo' or 'data.frame'
target	"character" with the ID of the target station, It has to correspond to some of the column names in 'x'. It also can take tha value "all", in which case the double-mass curve is computed for all the stations in 'x'
dates	"numeric", "factor", "Date" indicating how to obtain the dates for correponding to the 'sname' station If 'dates' is a number, it indicates the index of the column in 'x' that stores the dates If 'dates' is a factor, it have to be converted into 'Date' class, using the date format specified by 'date.fmt' If 'dates' is already of Date class, the following line verifies that the number of days in 'dates' be equal to the number of element in the time series corresponding to the 'st.name' station
date.fmt	character indicating the format in which the dates are stored in 'dates'. ONLY required when class(dates)=="factor" or "numeric"
var.type	character representing the type of variable being plotted ONLY for determining the function used for computing the monthly values when 'FUN' is missing. Valid values are: -) "Precipitation" => FUN = sum -) "Flow" => FUN = mean

FUN	Function that have to be applied for transforming from Daily to Annual time step. (e.g., For precipitation FUN=sum and for temperature and flow ts, FUN=mean) (e.g., For precipitation FUN=sum and for temperature and flow ts, FUN=mean) ONLY needed when 'var.type' is missing.
na.rm	Logical. Should missing values be removed?. -) TRUE : the annual values are computed considering only those values different from NA -) FALSE: if there is AT LEAST one NA within a year, the annual values are NA
method	See '?cor'. a character string indicating which correlation coefficient (or covariance) is to be computed. Valid values are: '"pearson"', (default), '"kendall"', or '"spearman"', can be abbreviated
use	See '?cor'. an optional character string giving a method for computing covariances in the presence of missing values. This must be (an abbreviation of) one of the strings: c('"everything"', '"all.obs"', '"complete.obs"', '"na.or.complete"', or '"pairwise.complete.obs"')
main	See '?plot'. An overall title for the plot: see 'title'.
screen	
xlab	See '?plot'. A title for the x axis: see 'title'.
ylab	See '?plot'. A title for the y axis: see 'title'.
col	See '?plot.default'. The colors for lines and points. Multiple colors can be specified so that each point can be given its own color. If there are fewer colors than points they are recycled in the standard fashion. Lines will all be plotted in the first colour specified.
print.out	character. Valid values are: -) "data.frame" : a data.frame with the results (monthly values in the reference and target stations, and cumulative values in reference and target stations) are pinted out -) "plot" : only the plot with the double-mass curve is printeed out, NO data.frame -) "both" : a data.frame with the results and a plot is printed out. Equivalent to 'print.out' = "data.frame" + "both"
...	

Author(s)

Mauricio Zambrano-Bigiarini, <mauricio.zambrano@ing.unitn.it>

Examples

```
## Loading temperature data ##
data(EbroQts)
x     <- EbroQts[,2]
dates <- EbroQts[,1]

## From 'character' to 'Date' class
```

```
dates <- as.Date(dates)

## From 'numeric' to 'zoo' class
x <- vector2zoo(x, dates)
```

---

drawxaxis *Hydrological 'X' Axis*

Description

It draws an X axies with daily, monthly, or annual time marks

Usage

```
drawxaxis(x, tick.tstep = "months", lab.tstep = "months")
```

Arguments

x	time series that will be plotted using the X axis that will be draw class(x) must be 'ts' or 'zoo'
tick.tstep	Character indicating the time step that have to be used for putting the ticks ont he time axis. Possible values are: 'days', 'months', 'years'
lab.tstep	Character indicating the time step that have to be used for putting the labels ont he time axis. Possible values are: 'days', 'months', 'years'

Author(s)

Mauricio Zambrano-Bigiarini, <mauricio.zambrano@ing.unitn.it>

Examples

```
data(EbroTEMPts)

## Daily values of temperature at the station "T9105", stored in EbroTEMPts.
x <-sname2ts(EbroTEMPts, sname="T9105", dates=1, var.type="Temperature", tstep.out="daily")

## Plotting the daily ts without an 'x' axis
plot.zoo(x, xaxt = "n" )

## Draws monthly ticks in the X axis, but labels only in years
drawxaxis(x, tick.tstep="months", lab.tstep="years")
```

`drty.dcs2zoo` *Downscaled Climate Scenario to Zoo*

Description

Reads the 360-days-in-a-year Downscaled Climate information on a single Station and generates a new time series with 365/366 values per year

Usage

```
drty.dcs2zoo(drty, var.type = "Precipitation", has360dpy = TRUE,
             file.ext = "out", from = "1961-01-01", to = "1990-12-31",
             date.fmt = "%Y-%m-%d", write2disk = TRUE,
             out.fname = paste(drty, "/", var.type, "-Downscaled.csv", sep = ""),
             verbose = TRUE)
```

Arguments

`drty`	Character indicating the directory where are located all the files that will be read. It HAS to finish with a "/". It is very important that this directory does not contain any subdirectory with the same extension of the data files (ex, files '*.out' and a subdirectory 'Temp.out'), because it'll try to read also the directory itself as a file
`var.type`	string representing the type of variable being analysed. Used for determining how to assign the vlaues to the missing dates when 'has360dpy' = TRUE Valid values are: -) "Precipitation": A zero value is assigned, for "almost" preserving the mean monthly value -) "Temperature" : The mean monthly value is assigned, for preserving the mean monthly value
`has360dpy`	Logical. If true (default) mean that the GCM used for generating the file uses 360 days oper year instead of the 365/366. Valid values are: "Precipitation", "Temperature"
`file.ext`	Character indicating the extension of the files that will be read, without the dot (e.g., for out daily files is "out")
`from`	Character indicating the starting date for the values stored in all the files that will be read. It HAs to be in the format indicated by 'date.fmt'
`to`	Character indicating the ending date for the values stored in all the files that will be read. It HAs to be in the format indicated by 'date.fmt'
`date.fmt`	Character indicating the date format in which you provide 'from' and 'to', e.g. "
`write2disk`	Logical. Indicates if the output have to be written into a CSV file, default=TRUE
`out.fname`	Character with the filename (with path) of the output file. Only needed if 'write2disk'=TRUE
`verbose`	logical; if TRUE, progress messages are printed

Details

This procedure reads the downscaled data of precipitation or temperature in a gauging station, in which all the years have 360 days (30 days in each month, including Febraury)and generates a new time series (zoo object) with 365/366 days, in which the new values are generates in the following way:

1) The first 90 original values are equally distributed among Jan, Feb, and March, and if the year is leap, a new value is added to February 29, with the procedure indicated below 2) May, Jul, Ago, Oct, Dic: the value corresponding to the 31 day is equal to the MEAN value of all the corresponding values within the month when the analysed time series is Temperature, and with a ZERO value when the analysed time series is Precipitation, in order of preserving the mean values in each month

The Starting date used by this algorithm is the 1st of January of the year specified in the first row of the file. The Ending date used by this algorithm is the 31th of December of the year specified in the last row of the file

Note

All the files that will be read HAVE TO have values within the time window defined by 'from' and 'to', and this procedure DO NOT VERIFY any inconsistence related to this

Author(s)

Mauricio Zambrano-Bigiarini

See Also

dcs2zoo

Examples

```
##---- Should be DIRECTLY executable !! ----
##-- ==>  Define data, use random,
##--or do  help(data=index)  for the standard data sets.
```

`dwi` *Days with Information*

Description

This function generates a table indicating the number of days with information (<>NA's) within a zoo object, aggregated by: Year, Month or Month per Year

Usage

```
dwi(x, ...)

## Default S3 method:
dwi(x, out.unit = "years", from = range(time(x))[1], to = range(time(x))[2],
        date.fmt = "%Y-%m-%d", ...)

## S3 method for class 'data.frame':
dwi(x, out.unit = "years", from, to, date.fmt = "%Y-%m-%d", dates = 1,
        verbose = TRUE, ...)
```

Arguments

x	variable of type 'zoo'
out.unit	aggregation time for the computation of the amount of days with info. Valid values are: -) "month": monthly; -) "year" : annual; -) "mpy" : month per year
from	Character indicating the starting date for the values stored in all the files that will be read. It HAs to be in the format indicated by 'date.fmt'
to	Character indicating the ending date for the values stored in all the files that will be read. It HAs to be in the format indicated by 'date.fmt'
date.fmt	Character indicating the date format in which you provide 'from' and 'to', e.g. "%d-%m-%Y"
dates	"numeric", "factor", "Date" indicating how to obtain the dates for correponding to the 'sname' station If 'dates' is a number, it indicates the index of the column in 'x' that stores the dates If 'dates' is a factor, it have to be converted into 'Date' class, using the date format specified by 'date.fmt' If 'dates' is already of Date class, the code verifies that the number of days in 'dates' be equal to the number of element in 'x'
verbose	logical; if TRUE, progress messages are printed
...	further arguments passed to or from other methods.

Author(s)

Mauricio Zambrano-Bigiarini, <mauricio.zambrano@ing.unitn.it>

See Also

matrixplot

Examples

```
## Loading temperature data ##
data(EbroTEMPts)

## Selecting the first station (the 1st column stores the dates)
x     <- EbroTEMPts[,2]
dates <- EbroTEMPts[,1]

## From 'character' to 'Date' class
dates <- as.Date(dates)

## From 'numeric' to 'zoo' class
x <- vector2zoo(x, dates)

## Days with information per year
dwi(x)

## Days with information per month per year at station 'x'
dwi(x, out.unit="mpy")

## Days with information per month per year in the 4 first stations of 'EbroTEMPts'
a <- dwi(EbroTEMPts[,1:5], out.unit="years", dates=1)

## Plotting the amount of days with information per year in each station
matrixplot(a, var.type="Days")
```

`EbroDEM1000m` *Digital Elevation Model (DEM) of the Ebro River Basin (Spain)*

Description

Digital Elevation Model of the Ebro River Basin (Spain), with cells of 1000x1000 [m]

Usage

```
EbroDEM1000m
```

Format

'SpatialGridDataFrame'

Details

Provided by the Confederacion Hidrografica del Ebro (CHE), 2008

Source

Confederacion Hidrografica del Ebro (CHE), 2008

EbroPPgis *Ebro Spatial Precipitation*

Description

Spatial location of the 349 stations of Daily Precipitation on the Ebro River Basin, Spain, with more than 70

Usage

```
EbroPPgis
```

Format

A data.frame with 7 fields: "ID", "STATION_NAME", "EAST_ED50", "NORTH_ED50", "ELEVATION", "CHE_BASIN_ID", "CHE_BASIN_NAME"

Details

Provided by the Confederacion Hidrografica del Ebro (CHE), 2008

Source

Confederacion Hidrografica del Ebro (CHE), 2008

EbroPPts *Ebro Daily Precipitation ts*

Description

Daily Precipitation time series on 349 stations of the Ebro River Basin, Spain, with more than 70

Usage

```
EbroPPts
```

Format

A data.frame with 349 time series

Details

Provided by the Confederacion Hidrografica del Ebro (CHE), 2008

Source

Confederacion Hidrografica del Ebro (CHE), 2008

EbroQgis *Ebro Spatial Streamflows*

Description

Spatial location of the 182 stations of Daily Streamflows on the Ebro River Basin, Spain, with more than 65

Usage

```
EbroQgis
```

Format

A data.frame with 10 fields: "ID", "CHE_BASIN_NAME", "STATION_NAME", "DATE_INI", "DATE_FIN", "Qmonthly_mean_m3s", "Qannual_mean_hm3s", "BASIN_ID", "EAST_ED50", "NORTH_ED50"

Details

Provided by the Confederacion Hidrografica del Ebro (CHE), 2008

Source

Confederacion Hidrografica del Ebro (CHE), 2008

EbroQts *Ebro Daily Streamflows ts*

Description

Daily streamflow time series on 182 stations of the Ebro River Basin, Spain, with more than 65

Usage

```
EbroQts
```

Format

A data.frame with 146 time series

Details

Provided by the Confederacion Hidrografica del Ebro (CHE), 2008

Source

Confederacion Hidrografica del Ebro (CHE), 2008

EbroSubcatch *Subcatchments of first order on the Ebro River Basin (Spain)*

Description

Shapefile wit the 37 subcatchments of first order on the Ebro River Basin (Spain)

Usage

```
EbroSubcatch
```

Format

Spatial object

Details

Provided by the Confederacion Hidrografica del Ebro (CHE), 2008

Source

Confederacion Hidrografica del Ebro (CHE), 2008

EbroTEMPgis *Ebro Spatial Temperature*

Description

Spatial location of the 146 stations of Daily Temperature on the Ebro River Basin, Spain, with more than 65

Usage

```
EbroTEMPgis
```

Format

A data.frame with 7 fields: "ID", "STATION_NAME", "EAST_ED50", "NORTH_ED50", "ELEVATION", "CHE_BASIN_ID", "CHE_BASIN_NAME"

Details

Provided by the Confederacion Hidrografica del Ebro (CHE), 2008

Source

Confederacion Hidrografica del Ebro (CHE), 2008

`EbroTEMPts` *Ebro Daily Temperature ts*

Description

Daily temperature time series on 146 stations of the Ebro River Basin, Spain, with more than 65

Usage

```
EbroTEMPts
```

Format

A data.frame with 146 time series

Details

Provided by the Confederacion Hidrografica del Ebro (CHE), 2008

Source

Confederacion Hidrografica del Ebro (CHE), 2008

`fdc` *Flow duration curve*

Description

Computes and plots the Flow Duration Curve in the original time units of 'x' and also gives the probability of exceedence of each element. If 'x' is a data.frame

Usage

```
fdc(x, ...)

## Default S3 method:
fdc(x, plot = TRUE, col = "black", main = "Flow Duration Curve",
        xlab = "% Time flow equalled or exceeded", ylab = "Q, [m3/s]",
        pch = 1, lty = 1, cex = 0.6, verbose=TRUE, ...)

## S3 method for class 'data.frame':
fdc(x, plot = TRUE, col = palette("default")[1:ncol(x)],
        main = "Flow Duration Curve",
        leg.txt = paste("Q", 1:ncol(x), sep = ""),
        xlab = "% Time flow equalled or exceeded", ylab = "Q, [m3/s]",
        pch = 1:ncol(x), lty = 1:ncol(x), cex = rep(0.6, ncol(x)),
```

```
        verbose=TRUE, ...)

## S3 method for class 'matrix':
fdc(x, plot = TRUE, col = palette("default")[1:ncol(x)],
        main = "Flow Duration Curve",
        leg.txt = paste("Q", 1:ncol(x), sep = ""),
        xlab = "% Time flow equalled or exceeded", ylab = "Q, [m3/s]",
        pch = 1:ncol(x), lty = 1:ncol(x), cex = rep(0.6, ncol(x)),
        verbose=TRUE, ...)
```

Arguments

x	'numeric, 'matrix' or 'data.frame' whose columns contains the values of the ts that be used for computing the flow duration curves.
plot	logical. Indicates if the flow duration curve should be plotted or not
col	See '?plot.default'. The colors for lines and points. Multiple colors can be specified so that each point can be given its own color. If there are fewer colors than points they are recycled in the standard fashion. Lines will all be plotted in the first colour specified.
main	See '?plot'. An overall title for the plot: see 'title'.
leg.txt	
xlab	See '?plot'. A title for the x axis: see 'title'.
ylab	See '?plot'. A title for the y axis: see 'title'.
pch	See '?plot.default'. A vector of plotting characters or symbols: see 'points'.
lty	See '?plot.default'. The line type, see 'par'.
cex	See '?plot.default'. A numerical vector giving the amount by which plotting characters and symbols should be scaled relative to the default. This works as a multiple of 'par("cex")'. 'NULL' and 'NA' are equivalent to '1.0'. Note that this does not affect annotation
verbose	logical; if TRUE, progress messages are printed
...	further arguments passed to or from other methods

Author(s)

Mauricio Zambrano-Bigiarini, <mauricio.zambrano@ing.unitn.it>

Examples

```
## Loading temperature data ##
data(EbroQts)

# Getting the daily values of the station 1 (the first column stores the dates)
x <- EbroQts[,2]

## Daily Flow Duration Curve
fdc(x)
```

`fillin` *Fill In*

Description

Fills in all the 'NA' values in 'x' with the corrensponding values in 'sim'.

Usage

```
fillin(x, ...)
## Default S3 method:
fillin(x, sim, ...)
## S3 method for class 'matrix':
fillin(x, sim, ...)
## S3 method for class 'data.frame':
fillin(x, sim, ...)
```

Arguments

`x`	'numeric', data.frame' or 'matrix' in which some values are 'NA'
`sim`	'numeric', 'data.frame' or 'matrix', with the same dimension of 'x', that contains the values that will be used for filling in the 'NA' values in 'x'
`...`	further arguments passed to or from other methods.

Author(s)

Mauricio Zambrano-Bigiarini, <mauricio.zambrano@ing.unitn.it>

Examples

```
obs <- c(1, NA, 3, 4, NA, 5)
sim <- rep(2, 6)

## Filling in the missing values in 'x' with the corresponding values in 'sim'
fillin(x=obs, sim)
```

`gists2spt` *Time Series and GIS Info -> (pseudo)Spatio-temporal Object*

Description

Given a data.frame (x.gis) with the spatial coordinates of a set of gauging stations, and a set of measurements in that stations (x.ts) this function adds the measurements in 'x.ts' to the corresponding stations in 'x.gis', even if they are not in the same order.
If 'X' and 'Y are given, the resulting object will be a 'SpatialPointsDataFrame' with coordinates given by the 'X' and 'Y' fields
If 'p4s' is given, the resulting object will be projected according to the specification provided by 'p4s'

Usage

```
gists2spt(x.ts, x.gis, sname, bname, X, Y, elevation,
          catchment.name="all", na.rm=TRUE, p4s)
```

Arguments

`x.ts`	numeric or data.frame with the measured value at each station for a given time. Each value of 'x.ts' has to have as name (names(x)) the ID of the station. 1) CAN contain as many stations as you want, e.g., all the stations in the your database, but 2) AT LEAST, HAVE TO contain some stationsof 'x.gis'
`x.gis`	'data.frame' with the spatial information (GIS) for the gauging stations. The names of each station, stored in the field 'sname', have to be equal to the corresponding ID used in 'x.ts' 1) It MAY contain as many stations as you want, e.g., all the stations in your database, but 2) AT LEAST, it HAVE TO contain the location of some stations in 'x.ts' The MINIMUM fields that HAVE TO be present in this file, and their corresponding colum index are those described by: X, Y, *sname*, *bname*, *elevation*
`sname`	character, field name in 'x.gis' that stores the name of the stations (have to start by a letter)
`bname`	OPTIONAL. character, field name in 'x.gis' that stores the name of the subcatchment in 'x.gis' that will be analysed ONLY necessary when 'catchment.name' is not "all"
`X`	character, field name in 'x.gis' that stores the EAST coordinate of the stations. The expected name is 'x', but if the value provided by the user is different, a new 'x' field is created and is used as the esting coordinate of 'x.gis'
`Y`	character, field name in 'x.gis' that stores the NORTH coordinate of the stations.The expected name is 'y', but if the value provided by the user is different, a new 'y' field is created and is used as the northing coordinate of 'x.gis'
`elevation`	OPTIONAL. character, field name in the shapefile 'SubCatchments.fname' that stores the elevation of the stations (m.a.s.l.).
`catchment.name`	name of the catchment that will be analized. Posble values are: -)"all" : ALL the stations in the 'x.gis' will be used

	-)other string: ONLY those stations in 'x.gis' with a 'BASIN_NAME' field value == 'catchment.name' will be used
`p4s`	Character with information about the projection of the GIS files, usually created by the CRS function of the 'sp' package
`na.rm`	a logical value indicating whether 'NA' values should be stripped before delivering the resulting object.

Value

SpatialPixelsDataFrame If 'p4s' is given, the returning object will be a 'SpatialPointsDataFrame', if not, it will be a 'data.frame'

Author(s)

Mauricio Zambrano-Bigiarini, <mauricio.zambrano@ing.unitn.it>

References

Applied Spatial Data Analysis with R. Series: Use R. Bivand, Roger S., Pebesma, Edzer J., Gomez-Rubio, Virgilio. 2008. ISBN: 978-0-387-78170-9
http://r-spatial.sourceforge.net/gallery/

See Also

krige, spplot

Examples

```
## Loading the ts data
data(EbroTEMPts)
## Loading the gis data
data(EbroTEMPgis)
## Loading the shapefile with the subcatchments
data(EbroSubcatch)

## Projection for the Subcatchments file
require(sp)

p4s <- CRS("+proj=utm +zone=30 +ellps=intl +units=m +no_defs")

## Field name in 'x.gis' with the ID of the station
sname <- "ID"
## Field name in 'x.gis'with the name of the catchment to which each station belongs
bname <- "CHE_BASIN_NAME"
## Field name in 'x.gis' with the Easting spatial coordinate
X     <- "EAST_ED50"
## Field name in 'x.gis' with the Northing spatial coordinate
Y     <- "NORTH_ED50"
## Field name in 'x.gis' with the Elevation
elevation <- "ELEVATION"
```

```
## Putting the measurements of the first row of 'EbroTEMPts' into their corresponding
## spatial location given by 'x.gis'
x.spt <- gists2spt(x.ts=EbroTEMPts[1,], x.gis=EbroTEMPgis, X=X, Y=Y,
                   elevation=elevation, sname=sname, bname=bname)
```

`hydrokrige` *Krige for Hydrological Time Series*

Description

Automatic interpolation for hydrological ts, with optional plot.
The (Block) Inverse Distance Weighted (IDW) interpolation is a wrapper to the 'idw' function of the 'gstat' package (so, requires the 'gstat' package).
The automatic kriging (OK and KED have been tested) is a wrapper to the 'autoKrige' function of the 'automap' package (so, requires the 'automap' package).

Usage

```
hydrokrige(x.ts, x.gis, ...)

## Default S3 method:
hydrokrige(x.ts, x.gis, X= "x", Y= "y", sname, bname,
        elevation, predictors, catchment.name = "all", IDW.type="cells",
        formula, SubCatchments.fname, IDvar = NULL, p4s, cell.size = 1000,
        grid.type = "regular", nmin = 0, nmax = Inf, maxdist = Inf,
        ColorRamp = "PCPAnomaly", sp.plot = TRUE, col.nintv = 10,
        col.at = "auto", main, stations.plot = FALSE, stations.offset,
        arrow.plot = FALSE, arrow.offset, arrow.scale,
        scalebar.plot = FALSE, sb.offset, sb.scale, verbose = TRUE, ...)

## S3 method for class 'data.frame':
hydrokrige(x.ts, x.gis, X= "x", Y= "y", sname, bname,
        elevation, predictors, catchment.name = "all", IDW.type = "block",
        formula, SubCatchments.fname, IDvar= "SUBBASIN", p4s, cell.size = 1000,
        grid.type = "regular", nmin = 0, nmax = Inf, maxdist = Inf,
        ColorRamp = "PCPAnomaly", sp.plot = FALSE, col.nintv = 10,
        col.at = "auto", main, stations.plot = FALSE, stations.offset,
        arrow.plot = FALSE, arrow.offset, arrow.scale,
        scalebar.plot = FALSE, sb.offset, sb.scale,
        verbose = TRUE,
        dates, from, to, date.fmt = "%Y-%m-%d", write2disk = TRUE,
        fname = paste(ColorRamp, "by_Subcatch.csv", sep = ""), ...)
```

Arguments

`x.ts`	numeric or data.frame with the measured value at each station. Each value of 'x.ts' has to have as name (names(x)) the ID of the station.

1) CAN contain as many stations as you want, e.g., all the stations in the your database
2) AT LEAST, HAVE to contain the stations that will be used for the interpolations

When 'x.ts' is a data.frame, the structure of this file is the following: -) 1st column: its name of HAS TO BE 'Date', ans it HAS TO contain the dates corresponding to the values of the stations stored in the other columns
-) 2nd...Nth column: The name of the columns is used as the ID of each station **-starting with a letter!!-** , and all the row values of each column have to contain the measured values by the station.

`x.gis` 'data.frame' with the spatial information (GIS) for the gauging stations. The names of each station, stored in the field 'NAME', have to be equal to the corresponding ID used in 'x.ts'
1) It MAY contain as many stations as you want, e.g., all the stations in your database
2) AT LEAST, it HAVE to contain the location of those stations that will be used for the interpolations
The MINIMUM fields that Have to be present in this file, and their corresponding column index are those described by: *X*, *Y*, *sname*, *bname*, *elevation*

`X` character, field name in 'x.gis' that stores the EAST coordinate of the stations

`Y` character, field name in 'x.gis' that stores the NORTH coordinate of the stations

`sname` character, field name in 'x.gis' that stores the name of the stations (have to start by a letter)

`bname` OPTIONAL. character, field name in 'x.gis' that stores the name of the subcatchment in 'x.gis' that will be analysed ONLY necessary when 'catchment.name' is not "all"

`elevation` OPTIONAL. character, field name in the shapefile 'SubCatchments.fname' that stores the elevation of the stations (m.a.s.l.).

`predictors` OPTIONAL. SpatialGridDataFrame object, with prediction/simulation locations. Must not contain NA's. Usually, a digital elevation model (DEM) read with the 'readGDAL' function of the 'rgdal' package.
See the 'newdata' argument in 'gstat::?krige'.
It should contain attribute columns with the independent variables (if present) and (if locations is a formula) the coordinates with names as defined in 'locations
If 'predictors' is missing, the grid to be used as prediction/simulation locations is generated from sampling the polygon specified by the user in 'SubCatchments.fname', according to the arguments provided by 'cells.size' and 'grid.type'

`catchment.name`
name of the catchment that will be analized. Posble values are:
-)"all" : ALL the stations in the 'x.gis' will be used
-)other string: ONLY those stations in 'x.gis' with a 'BASIN_NAME' field value == 'catchment.name' will be used .

`IDW.type` Character, indicating the type of plot required by the user. When 'x.ts' is a data.frame, the ONLY possible value is 'block'. For all the other cases, possible values are:
-) "cells" : the interpolated values are shown by each cell individually
-) "block" : the interpolated values are show by each catchment, where the value for each catchment is computed as the mean value over all the cells that belong to each subcatchment
-) "both" : "cells" and "block" are plotted in the same window

`formula` OPTIONAL. Formula to be used in case of ordinary kriging or kriging with external drift. Requieres the 'automap' package. All the variables to be used within 'formula' has to be present both in 'x.gis' and 'predictors'. See the 'formula' argument in '?gstat::krige'.
'formula' defines the dependent variable as a linear model of independent variables; suppose the dependent variable has name 'z', for ordinary and simple kriging use the formula 'z~1'; for simple kriging also define 'beta' (see below); for universal kriging, suppose 'z' is linearly dependent on 'x' and 'y', use the formula 'z~x+y

`SubCatchments.fname`
It can be:
1) Character with the filename (with path) of the shapefile with all the subcatchments within the Catchment. It HAS TO BE of 'polygon' type
2) Spatial object resulting from reading the shapefile with all the subcatchments within the Catchment

`IDvar` (from '?readShapePoly') a character string the name of a column in the 'SubCatchments.shp' shapefile DBF containing the ID values of the shapes - the values will be converted to a character vector

`p4s` Character with information about the projection of the GIS files, usually created by the 'CRS' function of the 'sp' package

`cell.size` Size of the cells to be used in the regular interpolation grid, [m]

`grid.type` See '?sp::spsmaple'. Character, indicating the yype of grid to be computed over the area defined by 'SubCatchments.shp'
Valid values are: -) 'regular' : for regular (systematically aligned) sampling; Default option
-) 'random' : for completely spatial random;
-) 'stratified' : for stratified random (one single random location in each "cell"
-) 'nonaligned' : for nonaligned systematic sampling (nx random y coordinates, ny random x coordinates);
-) 'hexagonal' : for sampling on a hexagonal lattice;
-) 'clustered' : for clustered sampling

`nmin` OPTIONAL. See '?gstat::krige'. For local interpolation: if the number of nearest observations within distance maxdist is less than 'nmin', a missing value will be generated; see 'maxdist'. By default 'nmin=0'

`nmax` OPTIONAL. See '?gstat::krige'. For local interpolation: the number of nearest observations that should be used for a kriging prediction, where nearest is defined in terms of the space of the spatial locations. By default, all observations are used

`maxdist` OPTIONAL. See '?gstat::krige'. For local interpolation: only observations within a distance of Max.Dist from the prediction location are used for prediction or simulation; if combined with 'nmax', both criteria apply. By default, all observations are used

`ColorRamp` Function defining the colour ramp to be used for plotting the maps OR character representing the colours to be used in the plot. In the latter case, valid values are: c('Precipitation', 'Temperature', 'PCPAnomaly', 'PCPAnomaly2', 'TEMPAnomaly', 'TEMPAnomaly2', 'TEMPAnomaly3')

`sp.plot` Logical, indicating if the interpolated values have to be ploted or not

`col.nintv` integer, number of colors that have to be used for plotting the interpolated values

`col.at` Specify at which interpolated values colours change. Valid values are:
-) "R" : uses the default setting of 'spplot'
-) "auto": default option.
at <- seq(min, max,length.out=col.nintv)
min <- floor(min(idw["var1.pred"]@data, na.rm=TRUE))
max <- ceiling(max(idw["var1.pred"]@data, na.rm=TRUE))
-) numeric: vector of reals giving the exact values in which the colors have to change. Useful when the user desires the same color for the same value when comparing to maps with different range of values

`main` Character with the title to be used for the plot

`stations.plot`
Logical, indicating if the gauging stations, defined by 'gis.fname' have to be plotted

`stations.offset`
2D list with the numeric coordinates in which the label with the amount of gauging stations have to be plotted. e.g., stations.offset = c(450000, 4600000)

`arrow.plot` Logical, indicating if a North Arrow have to be plotted

`arrow.offset` 2D list with the numeric coordinates in which the North Arrow have to be plotted. e.g., arrow.offset = c(690000,4760000)

`arrow.scale` Scale (in the map units) to be used for plotting the North Arrow, e.g., scale = 20000

`scalebar.plot`
Logical, indicating if a Scale Bar have to be plotted

`sb.offset` 2D list with the numeric coordinates in which the North Arrow have to be plotted. e.g., sb.offset = c(400000,4490000)

`sb.scale` Scale (in the map units) to be used for plotting the Scale Bar, e.g., scale = 100000, means that the scale bar will have a length of 100km

`verbose` logical; if TRUE, progress messages are printed

`dates` "numeric", "factor", "Date" indicating how to obtain the dates corresponding to each row of 'x' If 'dates' is a number, it indicates the index of the column in 'x' that stores the dates
If 'dates' is a factor, it have to be converted into 'Date' class, using the date format specified by 'date.fmt'
If 'dates' is already of Date class, the code verifies that the number of days in 'dates' be equal to the number of elements in 'x'

from	Character indicating the starting date for the values stored in all the files that will be read. It HAS TO be in the format indicated by 'date.fmt'
to	Character indicating the ending date for the values stored in all the files that will be read. It HAS TO be in the format indicated by 'date.fmt'
date.fmt	character indicating the format in which the dates are stored in 'dates', Default value is "%Y-%m-%d"
write2disk	Logical. Indicates if we want to write the output into a CSV file, default=TRUE
fname	OPTIONAL. Character with the filename of the output file. Only needed when 'write2disk'=TRUE
...	further arguments passed to or from other methods.

Details

The automatic kriging is carried out using a variogram generated automatically with the 'autofitVariogram' function of the 'automap' package.

Value

When 'IDW.type' is 'cells' or 'both':

Cells	SpatialPixelsDataFrame. The slot 'data' has two variables: 'var1.pred' and 'var1.var' with the predictions and its variances, respectively

When 'IDW.type' is 'block' or 'both, the following element is added:

Block	SpatialPolygonsDataFrame. The slot 'data' has four variables: 'x', 'y' with the easting and northing coordinate of the centroid of the catchments specified by 'SubCatchments.fname' , and 'var1.pred' and 'var1.var' with the predictions and its variances, respectively

Note

IMPORTANT: It is you responsibility to check the validity of the fitted variogram !!.

Author(s)

Mauricio Zambrano-Bigiarini, <mauricio.zambrano@ing.unitn.it>

References

N.A.C. Cressie, 1993, Statistics for Spatial Data, Wiley.
Applied Spatial Data Analysis with R. Series: Use R. Bivand, Roger S., Pebesma, Edzer J., Gomez-Rubio, Virgilio. 2008. ISBN: 978-0-387-78170-9
Pebesma, E.J., 2004. Multivariable geostatistics in S: the gstat package. Computers & Geosciences, 30: 683-691
http://www.gstat.org/
http://r-spatial.sourceforge.net/gallery/

See Also

krige, autoKrige, readShapePoly,spsample

Examples

```
## Loading the ts data
data(EbroTEMPts)
## Loading the gis data
data(EbroTEMPgis)
## Loading the shapefile with the subcatchments
data(EbroSubcatch)

## Projection for the Subcatchments file
require(sp)

# European Datum 50, Zone 30N
p4s <- CRS("+proj=utm +zone=30 +ellps=intl +units=m +no_defs")

## Field name in 'x.gis' with the ID of the station
sname <- "ID"
## Field name in 'x.gis'with the name of the catchment to which each station belongs
bname <- "CHE_BASIN_NAME"
## Field name in 'x.gis' with the Easting spatial coordinate
X     <- "EAST_ED50"
## Field name in 'x.gis' with the Northing spatial coordinate
Y     <- "NORTH_ED50"
## Field name in 'x.gis' with the Elevation
elevation <- "ELEVATION"

# Definition of the Arrow
arrow.offset = c(900000,4750000)
arrow.scale = 20000
# Definition of the scale bar
sb.offset = c(400000,4480000)
sb.scale = 100000

# Offset for writing the amount of stations used
stations.offset = c(450000, 4600000)

# Computing the number of stations
nstations <- nrow(EbroTEMPgis)

## Selecting the first day of 'EbroTEMPts' for all the stations
x.ts <- as.numeric(EbroTEMPts[1, 2:ncol(EbroTEMPts)])

## Setting the name of the stations
names(x.ts) <- colnames(EbroTEMPts[1,2:ncol(EbroTEMPts)])

ColorRamp= "Temperature"

nmax= 50
main <- paste("IDW Daily Mean Temperature on the Ebro. Stations=", nstations, sep="")
```

```
## IDW interpolation and plot
# Probably you will need to resize your window
x.idw <- hydrokrige(x.ts= x.ts, x.gis=EbroTEMPgis,
    X=X, Y=Y, sname=sname, bname=bname, elevation=elevation,
    IDW.type= "both",
    SubCatchments.fname= EbroSubcatch,
    p4s= p4s,
    cell.size= 1000,
    ColorRamp= ColorRamp,
    col.nintv= 40, col.at= "auto",
                   stations.plot=TRUE, stations.offset= stations.offset,
    arrow.plot= TRUE, arrow.offset= arrow.offset, arrow.scale= arrow.scale,
    scalebar.plot= TRUE, sb.offset= sb.offset, sb.scale= sb.scale)

## Not run:
## Ordinary Kriging interpolation and plot
# Probably you will need to resize your window
main <- "OK Daily Mean Temperature on the Ebro"
x.ok <- hydrokrige(x.ts= x.ts, x.gis=EbroTEMPgis,
                   X=X, Y=Y, sname=sname, bname=bname, elevation=elevation,
                   IDW.type= "both", formula=value~1,
                   SubCatchments.fname= EbroSubcatch,
                   p4s= p4s,
                   cell.size= 1000,
                   ColorRamp= ColorRamp,
                   col.nintv= 40, col.at= "auto",
                   arrow.plot= TRUE, arrow.offset= arrow.offset, arrow.scale= arrow.scale,
                   scalebar.plot= TRUE, sb.offset= sb.offset, sb.scale= sb.scale)



## Kriging with External Drift interpolation and plot
# Probably you will need to resize your window
main <- "KED Daily Mean Temperature on the Ebro"

#Loading the DEM
data(EbroDEM1000m)

#Giving a meaningful name to the predictor
EbroDEM1000m$ELEVATION <- EbroDEM1000m$band1

# Saving memory
EbroDEM1000m$band1 <- NULL

# Computing the KED
x.ked <- hydrokrige(x.ts= x.ts, x.gis=EbroTEMPgis,
                    X=X, Y=Y, sname=sname, bname=bname, elevation=elevation,
                    IDW.type= "cells", formula=value~ELEVATION,
                    SubCatchments.fname= EbroSubcatch,
                    p4s= p4s,
                    predictors=EbroDEM1000m,
```

```
                    cell.size= 4000,
                    ColorRamp= ColorRamp,
                    col.nintv= 40, col.at= "auto",
                    arrow.plot= TRUE, arrow.offset= arrow.offset, arrow.scale= arrow.scale,
                    scalebar.plot= TRUE, sb.offset= sb.offset, sb.scale= sb.scale)


## Block IDW interpolation and plot of 'EbroTEMPts' during 3 days
dates <- EbroTEMPts[, 1]
EbroTEMPts <- EbroTEMPts[, 2:ncol(EbroTEMPts)]
\dontrun{
x.idw <- hydrokrige(x.ts= EbroTEMPts, x.gis=EbroTEMPgis,
                  X=X, Y=Y, sname=sname, bname=bname, elevation=elevation,
  IDW.type= "cells", #'both'
  SubCatchments.fname= EbroSubcatch,
  p4s= p4s,
  cell.size= 1000,
  ColorRamp= ColorRamp,
  sp.plot= TRUE,
  col.nintv= 40, col.at= "auto",
  arrow.plot= TRUE, arrow.offset= arrow.offset, arrow.scale= arrow.scale,
  scalebar.plot= TRUE, sb.offset= sb.offset, sb.scale= sb.scale,
                  dates=dates, from="1961-01-10", to="1961-01-13")
}

## End(Not run)
```

`hydropairs` *Visual Correlation Matrix*

Description

Visualization of a Correlation Matrix.

Usage

```
hydropairs(x, dec = 3, use = "pairwise.complete.obs", method = "pearson",...)
```

Arguments

`x`	numeric vector, matrix or data frame
`dec`	decimal places to be used for showing the correlation values
`use`	See '?cor' an optional character string giving a method for computing covariances in the presence of missing values. This must be (an abbreviation of) one of the strings '"everything"', '"all.obs"', '"complete.obs"', '"na.or.complete"', or '"pairwise.complete.obs"'.
`method`	See '?cor' a character string indicating which correlation coefficient (or covariance) is to be computed. One of '"pearson"' (default), '"kendall"', or '"spearman"', can be abbreviated
`...`	further arguments passed to or from other methods.

Value

On top	the (absolute) value of the correlation plus the result of the cor.test as points
On botttom	the bivariate scatterplots, with a fitted line
On diagonal	histograms (from '?pairs')

Note

Original idea taken from: http://addictedtor.free.fr/graphiques/graphcode.php?graph=137
Histogram panel was taken from the R help of the original 'pairs' function

Author(s)

Mauricio Zambrano-Bigiarini, <mauricio.zambrano@ing.unitn.it>

See Also

cor, pairs

Examples

```
## Loading temperature data ##
data(EbroTEMPts)

## Annual Mean values of temperature during the summer season (DJF) for the first
## 3 stations in 'EbroTEMPts'
hydropairs(EbroTEMPts[,2:4])
```

---

hydroplot *Station Plot and hdydroplot*

Description

Given a data.frame whose columns contains the time series (without missing dates) of several gauging stations, it takes the name of one gauging station and plots 9 graphs (see 'hydroplot' description)

Usage

```
hydroplot(x, sname = "X", elevation = "", var.type = "Precipitation",
          FUN, na.rm = TRUE, var.unit = "mm", main, win.len1 = 365 * 1,
          win.len2 = 365 * 3, ptype = "ts+boxplot+hist", pfreq = "dma",
          tick.tstep= "months", lab.tstep= "years")

sname2plot(x, sname, elevation = "", var.type = "Precipitation",
           FUN, na.rm = TRUE, var.unit = "mm", main, win.len1 = 365 * 1,
           win.len2 = 365 * 3, ptype = "ts+boxplot+hist", pfreq = "dma",
           dates, date.fmt = "%Y-%m-%d", tick.tstep= "months", lab.tstep= "years")
```

Arguments

`x`	data.frame whose columns contains the time series (without missing values) for several gauging stations.
`sname`	character with the name of the station whose values will be ploted. This name MUST eixst as column name in 'x'
`dates`	"numeric", "factor", "Date" indicating how to obtain the dates correponding to the 'sname' station. If 'dates' is a number, it indicates the index of the column in 'x' that stores the dates If 'dates' is a factor, it have to be converted into 'Date' class, using the date format specified by 'date.fmt' If 'dates' is already of Date class, the code verifies that the number of days in 'dates' be equal to the number of element in 'x'
`date.fmt`	Character indicating format in which the dates are stored in 'dates', e.g, "%Y-%m-%d" ONLY required when class(dates)=="factor" or "numeric"
`elevation`	Character representing the elevation of the meteorological station, only for putting it on the plot ONLY used for labelling the title
`var.type`	character representing the type of variable being plotted. Used for determining the function used for computing the Monthly and Annual values when 'FUN' is missing. Valid values are: -) "Precipitation" => FUN = sum -) "Temperature" => FUN = mean -) "Flow" => FUN = mean
`FUN`	ONLY required when 'var.type' is missing. Function that have to be applied for transforming from daily to monthly or annual time step (e.g., For precipitation FUN=sum and for temperature and flow ts, FUN=mean)
`na.rm`	Logical. Should missing values be removed? -) TRUE : the annual values are computed considering only those values different from NA -) FALSE: if there is AT LEAST one NA within a year, the annual values are NA
`var.unit`	Character representing the measurement unit of the variable being plotted. ONLY used for labelling the axes. (e.g., "mm" for precipitation, "C" for temperature, and "m3/s" for flow.)
`main`	Character representing the main title of the plot. If the user did not provide a title, this is created automatically as: main= paste(var.type, "at", st.name, sep=" "),
`win.len1`	number of days for being used in the computation of the first moving average
`win.len2`	number of days for being used in the computation of the second moving average
`ptype`	Character indicating the type of plot that will be plotted. Valid values are: -) ptype= "ts" => only time series -) ptype= "ts+boxplot" => only time series + boxplot -) ptype= "ts+hist" => only time series + histogram -) ptype= "ts+boxplot+hist" => time series + boxplot + histogram

pfreq	Character indicating how many plots are desired by the user. Valid values are: -) 'dma': Daily, Monthly and Annual values are plotted -) 'ma' : Monthly and Annual values are plotted -) 'dm' : Daily and Monthly values are plotted
tick.tstep	string indicating the time step that have to be used for putting the ticks ont he time axis. Valid values are: -) 'days', -) 'months', -) 'years'
lab.tstep	string indicating the time step that have to be used for putting the labels ont he time axis. Valid values are: -) 'days' -) 'months' -) 'years'

Author(s)

Mauricio Zambrano-Bigiarini, <mauricio.zambrano@ing.unitn.it>

See Also

hydroplot, sname2ts

Examples

```
## Loading temperature data ##
data(EbroTEMPts)

## Plot of the monthly and annual values of temperature at station "T9105",
## stored in EbroTEMPts.
sname2plot(EbroTEMPts, sname="T9105", var.type="Temperature", dates=1, pfreq="ma")
```

---

hypsometricc *Hypsometric Curve*

Description

Computes and plots the hypsometric curve corresponding to the data provided by a digital elevation model (DEM)

Usage

```
hypsometricc(x, main="Hypsometric Curve",
             xlab="Basin Area Lower than Elevation, [%]",
             ylab="Elevation, [m.a.s.l.]", col="blue",...)
```

Arguments

x	Object of class 'SpatialGridDataFrame' with the elevations of the catchment. Possibly, a raster file already read with the 'readGDAL' function.
main	See '?plot'. An overall title for the plot: see 'title'.
xlab	See '?plot'. A title for the x axis: see 'title'.
ylab	See '?plot'. A title for the y axis: see 'title'.
col	See '?plot.default'. The colors for lines and points.
...	further arguments passed to or from other methods

Author(s)

Mauricio Zambrano-Bigiarini, <mauricio.zambrano@ing.unitn.it>

Examples

```
## Not run:
require(rgdal)
data(EbroDEM1000m)
dem <- EbroDEM1000m
hypsometricc(dem)
require(sp)
spplot(dem, scales=list(draw=TRUE, y=list(rot=90)))

## End(Not run)
```

---

interpol1 *Interpolation*

Description

Interpolates the value at the station "s" on the day "i", using all the other gauging stations.

Usage

```
interpol1(x.ts.catch, cc, i, s, method = "cc-neighs", n.neighs)
```

Arguments

x.ts.catch	data.frame with the time series of all the stations involved in the computations. The name of each column in 'x.ts.catch' have to correspond to the names of the gauging station. 'x.ts.catch' doesn't need to have a column with Dates or any other thing, ONLY the time series (with some missing values)
cc	Matrix with the coefficient of correlation among all the time series in 'x.ts.catch'. This value can be computed within this procedure, but it is a waste of time, because it is a unique value for all the iterations, so it only needs to be computed ONE time

i	counter corresponding to the day that it is being interpolated, so, it corresponds to the position of the row of 'x.ts.catch' that is is being used for the computation
s	counter corresponding to the station in which the interpolation is being computed, so, it corresponds to the position of the column of 'x.ts.catch' that is receiving the computations
method	Character with the name of the method that will be used for the interpolations. Valid values are: -) "cc-normal": normal coefficient correlation method, where all the stations with values are used for computing the interoplated value in the target station -) "cc-neighs": modified coefficient correlation method, where only a number of stations (provided by the user) with the highest coefficient of correlation with the target station are used for computing the interoplated value in the target station
n.neighs	Integer with the number of neighbors, with valid values (NON-'NA'), that will be considered on the computation of the interpolated values. ONLY required when 'mehtod'= "cc-neighs"

Details

Given a data.frame whose columns contains the time series (without missing dates) of several gauging stations, it interpolates the value at the station "s" on the day "i", using all the other gauging stations.
The interpolation method is a modified IDW, where the Pearson's product-momenet coefficient of correlation between the time series of all teh stations is used instead of the spatial distance, following the paper of Teegavarapu and Chandramouli 2005 (See 'references')

Two methods can be used for carrying out interpolations:
1) "cc-normal": normal coefficient correlation method, where all the stations are used
2) "cc-neighs": modified coefficient correlation method, where only the stations with the highest coefficient of correlation with the target station are used

Note

The overall performance of this method was better than the overall performance of the traditional IDW, considering 146 stations of temperature and 349 stations of precipitation with daily data during 30 years.
This was assessed with a posterior cross-validation for each station (comparing the observed with the interpolated values)

Author(s)

Mauricio Zambrano-Bigiarini, <mauricio.zambrano@ing.unitn.it>

References

Teegavarapu R.S.V., Chandramouli V. 2005. Improved weighting methods, deterministic and stochastic data-driven models for estimation of missing precipitation records. Journal of Hydrology, 312 (1-4), pp. 191-206.

Examples

```
##---- Should be DIRECTLY executable !! ----
##-- ==>  Define data, use random,
##--or do  help(data=index)  for the standard data sets.
```

`istdx` *Inverse Standarization*

Description

This function back transforms a standarized vector/matrix into their original values, i.e., re-scales all the values in the [0,1] interval to the original range of values z = re-scale(x) = x*[xmax - xmin] + xmin

Usage

```
istdx(x, ...)
## Default S3 method:
istdx(x, xmin, xrange, ...)
```

Arguments

`x`	standarized vector or matriz to be re-scaled, all the values have to be in the range [0,1]
`xmin`	numeric with the minimum value(s) in the original 'x' -) if 'z' is a vector, 'xmin' has to be a real -) if 'z' is a matrix/data.frame, 'xmin' has to be a vector, with the minimum values for each column of the original 'x'. In this case, the vector of minimums can be otained as: xmin <- apply(x, 2, min, na.rm=TRUE)
`xrange`	numeric with the range of value(s) in the original 'x' -) if 'z' is a vector, 'xrange' has to be a real -) if 'z' is a matrix/data.frame, 'xrange' has to be a vector, with the range of values for each column of the original 'x'. In this case, the vector of ranges can be otained as: xrange <- apply(x, 2,range, na.rm=TRUE) xrange <- apply(xrange, 2, diff, na.rm=TRUE)
`...`	further arguments passed to or from other methods

Author(s)

Mauricio Zambrano-Bigiarini, `<mauricio.zambrano@ing.unitn.it>`

See Also

`stdx`

Examples

```
## Loading temperature data ##
data(EbroTEMPts)

x     <- EbroTEMPts[,2]
dates <- EbroTEMPts[,1]

## From 'character' to 'Date' class
dates <- as.Date(dates)

## From 'numeric' to 'zoo' class
x <- vector2zoo(x, dates)

## Computing xmin and the range of 'x'
xmin <- min(x, na.rm=TRUE)
r <- diff(range(x, na.rm=TRUE))

## Standarized variable
s <- stdx(x)

## Inverse of the standarized variable
si <- istdx(s, xmin, xrange=r)

## 'si' and 'x' should be the same
summary(x-si)

############
### Standarizing a subset of the stations 9 to 12 in 'EbroTEMPts'
n <- EbroTEMPts[1:70,10:13]
xmin   <- apply(n, 2, min, na.rm=TRUE)
xrange <- apply(n, 2, range, na.rm=TRUE)
xrange <- apply(xrange, 2, diff, na.rm=TRUE)

## Standarized variable
s <- stdx(as.matrix(n))

## Inverse of the standarized variable
si <- istdx(s, xmin, xrange)

## 'si' and 'n' should be the same
summary(n - si)
```

`izoo2rzoo` *Irregular Zoo -> Regular Zoo*

Description

This function takes a time series of (very likely) irregular (with missing dates) daily time series and then transforms it into a variable regulary spaced, filling the voids with some value (by default: NA)

Usage

```
izoo2rzoo(x, date.fmt = "%Y-%m-%d", from = range(time(x))[1],
          to = range(time(x))[2], tstep = "day")
```

Arguments

x	time series of type zoo (very likely with some missing days)
date.fmt	character indicating the format in which the dates are stored in 'dates', e.g. "%Y-%m-%d" ONLY required when class(dates)=="factor" or "numeric"
from	Character indicating the starting date for the values stored in all the files that will be read. It HAS to be in the format indicated by 'date.fmt'
to	Character indicating the ending date for the values stored in all the files that will be read. It HAS to be in the format indicated by 'date.fmt'
tstep	time step in which are stored the values of 'x'

Author(s)

Mauricio Zambrano-Bigiarini, <mauricio.zambrano@ing.unitn.it>

See Also

vector2zoo

Examples

```
x <- 1:9

## February 29th is missing:
dates <- c("1964-02-25", "1964-02-26", "1964-02-27", "1964-02-28",
           "1964-03-01", "1964-03-02", "1964-03-03", "1964-03-04", "1964-03-05")

## From 'character' to 'Date' class
dates <- as.Date(dates)

## From 'numeric' to 'zoo' class
x <- vector2zoo(x, dates) #Feb 29th is still missing

## Feb 29th is added to 'y' with a missing value
y <- izoo2rzoo(x, from=dates[1], to=dates[length(dates)])
```

---

ma *Moving Average*

Description

Generic function for computing a Moving (sliding) Average of ts

Usage

```
ma(x, ...)

## Default S3 method:
ma(x, win.len, FUN = mean, ...)

## S3 method for class 'zoo':
ma(x, win.len, FUN = mean, ...)
```

Arguments

x	ts or zoo object with n elements
win.len	number of terms that will be considered in the mean. It have to be odd
FUN	Function that have to be applied for computing the moving average. Usually, FUN MUST be 'mean'
...	further arguments passed to or from other methods.

Value

a vector with the moving average termns. The length of the resulting vector is the same of 'x', but the first and last (win.len-1)/2 elements will be NA.

Author(s)

Mauricio Zambrano-Bigiarini, <mauricio.zambrano@ing.unitn.it>

Examples

```
## Loading temperature data ##
data(EbroQts)
x     <- EbroQts[,2]
dates <- EbroQts[,1]

## From 'character' to 'Date' class
dates <- as.Date(dates)

## From 'numeric' to 'zoo' class
x <- vector2zoo(x, dates)

## Daily to Monthly ts
m <- daily2monthly(x, FUN=mean, na.rm=FALSE)

# Plotting the monthly values
plot(m)

## Plotting the annual moving average in station 'x'
lines(ma(m, win.len=12), col="blue")
```

`matrixplot` *Plot Days with Information*

Description

Plots a color matrix representing the amount of days with information in a set of gauging stations

Usage

```
matrixplot(x, ColorRamp, ncolors = 70, main = "", var.type="Days", ...)
```

Arguments

`x`	'matrix', with the amount of days with information in each station -) The rows represent the gauging stations -) The columns represetn the years, and they stores the amount of days with information in each station
`ColorRamp`	OPTIONAL. Gives the possibility to the user to pass a personalized color ramp for ploting. When ColorRamp is missing, the color ramp is created according to the value of 'var.type'
`ncolors`	Number of color intervals that will be used for differentiating from 0 to 366 days with information
`main`	Main title for the plot
`var.type`	ONLY used when ColorRamp is missing. Character representing the type of variable being plotted. Used for determining the color ramp to be used for plotting the values in 'x'. Valid values are: c('Days', 'Precipitation', 'Temperature', 'PCPAnomaly', 'TEMPAnomaly', 'TEMPAnomaly2', 'TEMPAnomaly3')
`...`	further arguments passed to levelplot or from other methods

Note

Adapted (and thank you very much) from: http://www2.warwick.ac.uk/fac/sci/moac/currentstudents/peter_cock/r/matrix_contour/

Author(s)

Mauricio Zambrano-Bigiarini, <mauricio.zambrano@ing.unitn.it>

See Also

dwi

Examples

```
## Loading temperature data ##
data(EbroTEMPts)

## Selecting the first station (the 1st column stores the dates)
x     <- EbroTEMPts[,2]
dates <- EbroTEMPts[,1]

## From 'character' to 'Date' class
dates <- as.Date(dates)

## From 'numeric' to 'zoo' class
x <- vector2zoo(x, dates)

## Total number of days with information per month at station 'x'
dwi(x, out.unit="months")

## Mean number of months with information at station 'x'
dpm <- c(31, 28, 31, 30, 31, 30, 31, 31, 30, 31, 30, 31)
dwi(x, out.unit="months") / dpm

## Days with information per month per year in the first 4 stations in 'EbroTEMPts'
m <- dwi(EbroTEMPts[,1:5], out.unit="months", dates=1)

## Plotting the amount of days with information per month in each station
matrixplot(m/dpm, var.type="Days")
```

`mip` *Months in Period*

Description

Given any starting and ending dates, it generates: 1) a vector with all the months between the two dates, OR 2) the amount of months between the two dates

Usage

```
mip(from, to, date.fmt = "%Y-%m-%d", out.type = "seq")
```

Arguments

`from`	Character indicating the starting date for the values stored in all the files that will be read. It HAs to be in the format indicated by 'date.fmt'
`to`	Character indicating the ending date for the values stored in all the files that will be read. It HAs to be in the format indicated by 'date.fmt'
`date.fmt`	character indicating the format in which the dates are stored in 'dates', e.g. "%Y-%m-%d"

out.type	character indicating the type of result that is given by this function. Valid values are: -) type= "seq" => a vectorial sequence with all the months within the given year -) type= "nmbr" => the number of days in the vectorial sequence with all the months within the given year

Author(s)

Mauricio Zambrano-Bigiarini

See Also

dip, diy

Examples

```
# Sequence of monthly dates between "1961-01-01" and "1961-12-31" ##
mip("1961-01-01", "1961-12-31")

## Computing the number of months between "1961-01-01" and "1965-06-30",
## with the date format  "%d-%m-%Y" ##
mip("01-01-1961", "30-06-1965", date.fmt= "%d-%m-%Y", out.type = "nmbr")
```

---

monthlyfunction *Monthly Function*

Description

Generic function for applying any R function to ALL the values in 'x' belonging to a given month

Usage

```
monthlyfunction(x, ...)

## Default S3 method:
monthlyfunction(x, FUN, na.rm = TRUE, ...)

## S3 method for class 'data.frame':
monthlyfunction(x, FUN, na.rm = TRUE, dates, date.fmt = "%Y-%m-%d",
                out.type = "data.frame", verbose = TRUE, ...)
```

Arguments

x	Object of type 'zoo', 'matrix' or 'data.frame'. Can be a daily or monthly object.
FUN	Function that will be applied to ALL the values in 'x' belonging to each one of the 12 months of the year (e.g., Fun can be some of c('mean', 'max', 'min', 'sd'))

na.rm	Logical. Should missing values be removed? -) TRUE : the monthly values and FUN are computed considering only those values in 'x' different from NA -) FALSE: if there is AT LEAST one NA within a month, the corresponing monthly and FUN values are NA
dates	"numeric", "factor", "Date" indicating how to obtain the dates correponding to the 'sname' station. If 'dates' is a number, it indicates the index of the column in 'x' that stores the dates If 'dates' is a factor, it have to be converted into 'Date' class, using the date format specified by 'date.fmt' If 'dates' is already of Date class, the code verifies that the number of days in 'dates' be equal to the number of element in 'x'
date.fmt	Character indicating format in which the dates are stored in 'dates', e.g, "%Y-%m-%d" ONLY required when class(dates)=="factor" or "numeric"
out.type	Character defining the desired type of output. Valid values are: -) "data.frame": a data.frame, with 12 columns representing the months, and as many rows as stations are included in 'x' -) "db" : a data.frame, with 4 colums will be produced. Useful for a posterior boxplot The first column will store the ID of the station, The second column will store the year, The third column will store month, The fourth column will contain the seasonal value corresponding to that year and that station.
verbose	Logical; if TRUE, progress messages are printed
...	further arguments passed to or from other methods

Note

Due to the fact that 'FUN' is applied over all the elements in 'x' belongng to a given weather season, its result will depend on the smapling frequency of 'x' and the type of fucntion provided by 'FUN' (e.g., 'mean' or 'max')

Author(s)

Mauricio Zambrano-Bigiarini, <mauricio.zambrano@ing.unitn.it>

See Also

annualfunction, daily2monthly

Examples

```
## Loading temperature data ##
data(EbroTEMPts)
x     <- EbroTEMPts[,2]
dates <- EbroTEMPts[,1]
```

```
## From 'character' to 'Date' class
dates <- as.Date(dates)

## From 'numeric' to 'zoo' class
x <- vector2zoo(x, dates)

## Daily to Monthly
m <- daily2monthly(x, FUN=mean, na.rm=TRUE)

## Monthly Mean values of temperature
monthlyfunction(x, FUN=mean, na.rm=TRUE)

## Boxplot of monthly values
cmonth <- format(time(m), "%b")
months <- factor(cmonth, levels=unique(cmonth), ordered=TRUE)
boxplot(coredata(m)~months)

## Monthly mean values of temperature in the first 2 stations of 'EbroTEMPts'
## Not run:
m <- monthlyfunction.data.frame(EbroTEMPts[,2:3], FUN=mean, dates=1, var.type="Temperature",
m$Month <- factor(m$Month, levels=month.abb)
## boxplot of the monthly values in both stations
boxplot(Value ~ Month, m, col="lightyellow")

## End(Not run)
```

`mspplot` *Multiple spplot*

Description

Plots several maps of interpolated values in the same plot

Usage

```
mspplot(x, SubCatchments.fname, IDvar = NULL, p4s, var.type = "Precipitation",
        sp.plot = TRUE, col.nintv = 10, col.at = "auto", ColorRamp, main,
        stations.plot = FALSE, stations.gis, X, Y,
arrow.plot = FALSE, arrow.offset, arrow.scale,
        scalebar.plot = FALSE, sb.offset, sb.scale,
verbose = TRUE)
```

Arguments

`x`

`SubCatchments.fname`
: Character with the filename (with path) of the shapefile with all the Subcatchments within the Catchment. It has to be of 'polygon' type

`IDvar`
: (from ?readShapePoly) a character string the name of a column in the 'SubCatchments.shp' shapefile DBF containing the ID values of the shapes - the values will be converted to a character vector

`p4s`
: Character with information about the projection of the GIS files, usually created by the CRS function of the 'sp' package

`var.type`
: Character defining the colors to be used for plotting the maps. Valid values are: c('Precipitation', 'Temperature', 'PCPAnomaly', 'PCPAnomaly2', 'TEMPAnomaly', 'TEMPAnomaly2', 'TEMPAnomaly3')

`sp.plot`
: Logical, indicating if the interpolated values have to be ploted or not

`col.nintv`
: integer, number of colors that have to be used for plotting the interpolated values

`col.at`
: Specify at which interpolated values colours change. Valid values are:
-) "R" : uses the default setting of 'spplot'
-) "auto": default option.
at <- seq(min, max,length.out=col.nintv)
min <- floor(min(idw["var1.pred"]@data, na.rm=TRUE))
max <- ceiling(max(idw["var1.pred"]@data, na.rm=TRUE))
-) numeric: vector of reals giving the exact values in which the colors have to change. Useful when the user desires the same color for the same value when comparing to maps with different range of values

`ColorRamp`
: Function defining the color ramp to be used for plotting the maps. It is used when 'var.type' is missing.

`main`
: Character with the title to be used for the plot

`stations.plot`
: Logical, indicating if the gauging stations, defined by 'gis.fname' have to be plotted

`stations.gis`
: OPTIONAL. 'data.frame' with the stations that will be added to the plot. ONLY required when 'stations.plot' == TRUE

`X`
: OPTIONAL. character, field name in 'x.gis' that stores the easting coordinate of the stations. ONLY required when 'stations.plot' == TRUE

`Y`
: OPTIONAL. character, field name in 'x.gis' that stores the northing coordinate of the stations. ONLY required when 'stations.plot' == TRUE

`arrow.plot`
: Logical, indicating if a North Arrow have to be plotted

`arrow.offset`
: OPTIONAL. 2D list with the numeric coordinates in which the North Arrow have to be plotted. e.g., arrow.offset = c(690000,4760000). ONLY required when 'arrow.plot' == TRUE

`arrow.scale`
: OPTIONAL. Scale (in the map units) to be used for plotting the North Arrow, e.g., scale = 20000. ONLY required when 'arrow.plot' == TRUE

`scalebar.plot`
: Logical, indicating if a Scale Bar have to be plotted

`sb.offset`
: OPTIONAL. 2D list with the numeric coordinates in which the North Arrow have to be plotted. e.g., sb.offset = c(400000,4490000). ONLY required when 'scalebar.plot' == TRUE

sb.scale	OPTIONAL. Scale (in the map units) to be used for plotting the Scale Bar, e.g., scale = 100000, means that the scale bar will have a length of 100km. ONLY required when 'scalebar.plot' == TRUE
verbose	logical; if TRUE, progress messages are printed

Author(s)

Mauricio Zambrano-Bigiarini, <mauricio.zambrano@ing.unitn.it>

References

Applied Spatial Data Analysis with R. Series: Use R. Bivand, Roger S., Pebesma, Edzer J., Gomez-Rubio, Virgilio. 2008. ISBN: 978-0-387-78170-9
http://r-spatial.sourceforge.net/gallery/

See Also

spplot, krige

Examples

```
## Loading the ts data
data(EbroTEMPts)
## Loading the gis data
data(EbroTEMPgis)
## Loading the shapefile with the subcatchments
data(EbroSubcatch)

## Projection for the Subcatchments file
require(sp)

p4s <- CRS("+proj=utm +zone=30 +ellps=intl +units=m +no_defs")

## Field name in 'x.gis' with the ID of the station
sname <- "ID"
## Field name in 'x.gis'with the name of the catchment to which each station belongs
bname <- "CHE_BASIN_NAME"
## Field name in 'x.gis' with the Easting spatial coordinate
X     <- "EAST_ED50"
## Field name in 'x.gis' with the Northing spatial coordinate
Y     <- "NORTH_ED50"
## Field name in 'x.gis' with the Elevation
elevation <- "ELEVATION"

# Definition of the Arrow
arrow.offset = c(900000,4750000)
arrow.scale = 20000
# Definition of the scale bar
sb.offset = c(400000,4480000)
sb.scale = 100000

# Character the Time Window being analyzed
```

```
Time.Window.stg <- "1961-01-01"

# Character for the plot title
TimePeriod.stg <- "CTRL: "

# Computing the number of stations
nstations <- nrow(EbroTEMPgis)

## Selecting the first day in 1961 of 'EbroTEMPts' for all the stations
x.ts <- as.numeric(EbroTEMPts[1, 2:ncol(EbroTEMPts)])

## Setting the name of the stations
names(x.ts) <- colnames(EbroTEMPts[ ,2:ncol(EbroTEMPts)])

## Title of the plot
main <- paste("IDW Annual Mean Temperature on the Ebro, ", TimePeriod.stg,
      Time.Window.stg, ". Stations=", nstations, sep="")

## IDW interpolation and plot
x.idw <- hydrokrige(x.ts= x.ts, x.gis=EbroTEMPgis,
                    X=X, Y=Y, sname=sname, bname=bname, elevation=elevation,
    catchment.name= "all",
    IDW.type= "cells", #'both'
    SubCatchments.fname= EbroSubcatch,
    p4s= p4s,
    cell.size= 3000,
    nmax= 50,
    ColorRamp= "Temperature",
    col.nintv= 40, col.at= "auto",
    main= main,
    arrow.plot= TRUE, arrow.offset= arrow.offset, arrow.scale= arrow.scale,
    scalebar.plot= TRUE, sb.offset= sb.offset, sb.scale= sb.scale,
    verbose=TRUE)

## Storing the interpolated values
x.idw@data["Jan1961"]   <- x.idw@data["var1.pred"]
x.idw@data["var1.pred"] <- NULL
x.idw@data["var1.var"]  <- NULL


## Selecting the first of July 1961 of 'EbroTEMPts' for all the stations
x.ts <- as.numeric(EbroTEMPts[366, 2:ncol(EbroTEMPts)])

## Setting the name of the stations
names(x.ts) <- colnames(EbroTEMPts[ , 2:ncol(EbroTEMPts)])

## IDW interpolation and plot
x.idw2 <- hydrokrige(x.ts= x.ts, x.gis=EbroTEMPgis,
                     X=X, Y=Y, sname=sname, bname=bname, elevation=elevation,
     catchment.name= "all",
     IDW.type= "cells", #'both'
     SubCatchments.fname= EbroSubcatch,
     p4s= p4s,
```

```
      cell.size= 3000,
      nmax= 50,
      ColorRamp= "Temperature",
      sp.plot= TRUE,
      col.nintv= 40, col.at= "auto",
      main= main,
      arrow.plot= TRUE, arrow.offset= arrow.offset,
      arrow.scale= arrow.scale,
      scalebar.plot= TRUE, sb.offset= sb.offset,
      sb.scale= sb.scale,
      verbose=TRUE)

x.idw@data["Jan1962"] <- x.idw2@data["var1.pred"]

## Plotting in the same graph the 2 interpolated fileds
mspplot(x=x.idw, #x.gis.fname,
        SubCatchments.fname=EbroSubcatch,
IDvar=NULL, p4s,
        var.type="Temperature",
        sp.plot=TRUE, col.nintv=50,
col.at="auto",
main="IDW Annual Mean Precipitation on the Ebro River Basin, [mm/year]",
stations.plot=FALSE,
        arrow.plot=TRUE, arrow.offset=c(900000,4750000), arrow.scale=20000,
        scalebar.plot=TRUE, sb.offset=c(400000,4480000), sb.scale=100000,
        verbose=TRUE)
```

`plotbands` *Plot a ts with simulated values and two confidence bands*

Description

Plot a ts with simulated values and two confidence bands. Optionally can also add an observed time series.

Usage

```
plotbands(x, lband, uband, obs, x.col= "blue", bands.col="lemonchiffon",
          obs.col="red", main="Confidence Bands for 'x'", xlab="Time",
          tick.tstep= "months", lab.tstep= "years", ...)
```

Arguments

`x`	ts or 'zoo' object with the simulated values
`lband`	ts or 'zoo' object with the values of the lower band
`uband`	ts or 'zoo' object with the values of the upper band
`obs`	OPTIONAL. ts or 'zoo' object with the values of the observed values
`x.col`	color to be used for plotting the 'x' ts

bands.col	color to be used for filling th area between the lower and upper band
obs.col	OPTIONAL. color to be used for plotting the observed ts
main	an overall title for the plot: see 'title'
xlab	a title for the x axis: see 'title'
tick.tstep	string indicating the time step that have to be used for putting the ticks ont he time axis. Possible values are: 'days', 'months', 'years'
lab.tstep	string indicating the time step that have to be used for putting the labels ont he time axis. Possible values are: 'days', 'months', 'years'
...	further arguments passed to levelplot or from other methods

Author(s)

Mauricio Zambrano Bigiarini <mauricio.zambrano@ing.unitn.it>

---

rm1stchar *Remove First Character*

Description

Deletes the first characther of each element of 'x'

Usage

```
rm1stchar(snames, start.col = 1)
```

Arguments

snames	vector of character, where each element represents the name of a single gauging station
start.col	numeric, indicating the index of the colum in which the renaming process should start

Author(s)

Mauricio Zambrano-Bigiarini, <mauricio.zambrano@ing.unitn.it>

See Also

substr

Examples

```
## Loading temperature data ##
data(EbroTEMPts)

names <- colnames(EbroTEMPts)
rm1stchar(names)
```

`seasonalfunction` *Seasonal Function*

Description

Generic function for applying any R function to all the values of 'x' that belongs to a given weather sesason.

Usage

```
seasonalfunction(x, ...)

## Default S3 method:
seasonalfunction(x, FUN, na.rm = TRUE, ...)

## S3 method for class 'data.frame':
seasonalfunction(x, FUN, na.rm = TRUE, dates, date.fmt = "%Y-%m-%d",
                         out.type = "data.frame", verbose = TRUE, ...)
```

Arguments

`x`	Daily or monthly object of type 'zoo' or 'data.frame'
`FUN`	Function that will be applied to ALL the values in 'x' belonging to each one of the 4 weather seasons. (e.g., Fun can be some of c('mean', 'max', 'min', 'sd'))
`na.rm`	Logical. Should missing values be removed? -) TRUE : the monthly values are computed considering only those values in 'x' different from NA -) FALSE: if there is AT LEAST one NA within a month, the FUN and monthly values are NA
`dates`	"numeric", "factor", "Date" indicating how to obtain the dates for correponding to the 'sname' station If 'dates' is a number, it indicates the index of the column in 'x' that stores the dates If 'dates' is a factor, it have to be converted into 'Date' class, using the date format specified by 'date.fmt' If 'dates' is already of Date class, the code verifies that the number of days in 'dates' be equal to the number of element in 'x'
`date.fmt`	character indicating the format in which the dates are stored in 'dates', e.g. "%Y-%m-%d". ONLY required when class(dates)=="factor" or "numeric"
`out.type`	Character defining the desired type of output. Valid values are: -) "data.frame": a data.frame, with 4columns representing the weather seasons, and as many rows as stations are included in 'x' -) "db" : a data.frame, with 4 colums will be produced. Useful for a posterior boxplot The first column will store the ID of the station, The second column will store the Year, The third column will store the season,

	The fourth column will contain the seasonal value corresponding to that year and that station.
`verbose`	Logical; if TRUE, progress messages are printed
`...`	further arguments passed to or from other methods

Author(s)

Mauricio Zambrano-Bigiarini, <mauricio.zambrano@ing.unitn.it>

Examples

```
##---- Should be DIRECTLY executable !! ----
##-- ==>  Define data, use random,
##--or do  help(data=index)  for the standard data sets.
```

`sfreq` *Hydrological Sampling Frequency*

Description

Sampling Frequency of an hydrological ts/zoo object.

This function generates a table indicating the number of days with information (<>NA's) within a data.frame

Usage

```
sfreq(x, min.year = 1800)
```

Arguments

`x`	variable of type 'zoo' or 'ts', with AT LEAST 2 elements, AND with a daily, monthly or annual sampling frequency.
`min.year`	integer used for a correct identification of the sampling fequency when 'x' is an annual zoo (e.g.: time(x) = "1961") => the minimum possible years starts in 'min.year'

Value

Possible values are:
-) 'daily' : indicating that the sampling freqeuncy in 'x' is daily
-) 'monthly' : indicating that the sampling freqeuncy in 'x' is monthly
-) 'annual' : indicating that the sampling freqeuncy in 'x' is annual

Author(s)

Mauricio Zambrano-Bigiarini, <mauricio.zambrano@ing.unitn.it>

Examples

```
## Loading temperature data ##
data(EbroTEMPts)
x     <- EbroTEMPts[,2]
dates <- EbroTEMPts[,1]

## From 'character' to 'Date' class
dates <- as.Date(dates)

## From 'numeric' to 'zoo' class
d <- vector2zoo(x, dates)

## Daily to Monthly
m <- daily2monthly(d, FUN=mean, na.rm=TRUE)

## Daily to Annual
a <- daily2annual(d, FUN=mean, na.rm=TRUE)

sfreq(d)
sfreq(m)
sfreq(a)
```

`smry` *Summary*

Description

Extended summary function, with 13 summary statistics for numeric objects

Usage

```
smry(x, ...)

## Default S3 method:
smry(x, na.rm = TRUE, digits = 2,...)

## S3 method for class 'matrix':
smry(x, na.rm = TRUE, digits = 2,...)

## S3 method for class 'data.frame':
smry(x, na.rm = TRUE, digits = 2,...)
```

Arguments

`x`	a numeric object, vector, matrix or data.frame, for which a summary is desired.
`na.rm`	a logical value indicating whether 'NA' values should be stripped before the computation proceeds.

digits	numeric, with the amount of decimal places to be included in the result
...	further arguments passed to or from other methods.

Value

Computed summary statistics are:

Min	Minimum
1stQ	First quartile (lower-hinge)
Mean	Mean value
Median	Median
3rdQ	Third quartile (upper-hinge
Max	Maximum of the input values.
IQR	Interquartile Range of the 'x' values. 'IQR(x) = quantile(x,3/4) - quantile(x,1/4)'
sd	Standard deviation of the values in 'x'. It uses denominator 'n-1'.
cv	Coefficient of variation (cv= sd / |mean|)
skewness	Skewness (using e1071 package)
kurtosis	Kurtosis (using e1071 package)
n	total number of data in 'x'
NA's	amount of missing values in 'x'

Note

Skewness and Kurtosis are computed with the e1071 package

Author(s)

Mauricio Zambrano-Bigiarini <mauricio.zambrano@ing.unitn.it>

See Also

summary, fivenum, IQR, sd, skewness, kurtosis

Examples

```
## Loading temperature data ##
data(EbroTEMPts)

## Summary of daily temperature values for the first 3 stations in 'EbroTEMPts'
smry(EbroTEMPts[,2:4])
```

sname2ts *Station Name -> Time Series*

Description

This function takes a data.frame whose columns contains the time series (without missing dates) of several gauging stations, it takes the name of one gauging station and extracts a time series with daily, monthly or annual time step

Usage

```
sname2ts(x, sname, dates, date.fmt = "%Y-%m-%d", var.type,
         tstep.out = "daily", FUN, na.rm = TRUE)
```

Arguments

x	data.frame containing the complete (without missing dates) times series of all the stations. It can also contain 1 column with the dates of the measurements, or they can be provided in a separated way
sname	string representing the name of the station, which have to correspond with one column name in 'x'
dates	"numeric", "factor", "Date" indicating how to obtain the dates correponding to the 'sname' station. If 'dates' is a number, it indicates the index of the column in 'x' that stores the dates If 'dates' is a factor, it have to be converted into 'Date' class, using the date format specified by 'date.fmt' If 'dates' is already of Date class, the code verifies that the number of days in 'dates' be equal to the number of element in 'x'
date.fmt	Character indicating format in which the dates are stored in 'dates', e.g, "%Y-%m-%d". ONLY required when class(dates)=="factor" or "numeric"
var.type	character representing the type of variable being plotted. Used for determining the function used for computing the monthly or/and annual values when 'FUN' is missing. Valid values are: -) "Precipitation" => FUN = sum -) "Temperature" => FUN = mean -) "Flow" => FUN = mean
tstep.out	character that defines the time step of the desired output time series. Valid values are: -) "daily" : daily time series -) "monthly": monthly time series -) "annual" : annual time series

FUN	ONLY required when 'var.type' is missing and 'tstep' is in c('monthly', 'annual') Function that have to be applied for transforming from daily to monthly or annual time step (e.g., For precipitation FUN=sum and for temperature and flow ts, FUN=mean)
na.rm	Logical. Should missing values be removed? -) TRUE : the annual values are computed considering only those values different from NA -) FALSE: if there is AT LEAST one NA within a year, the annual values are NA

Author(s)

Mauricio Zambrano-Bigiarini, <mauricio.zambrano@ing.unitn.it>

Examples

```
## Loading temperature data ##
data(EbroTEMPts)

## Annual values of temperature at the station "T9105", stored in EbroTEMPts.
sname2ts(EbroTEMPts, sname="T9105", dates=1, var.type="Temperature", tstep.out="annual")
```

---

stdx *Standarization*

Description

Standarizes a vector or matrix, i.e., scales all the values in a way that the transformed values will be within the range [0,1].

Usage

```
stdx(x, ...)
```

Arguments

x	vector, matrix or data.frame to be scaled
...	further arguments passed to or from other methods

Details

$$z = \frac{x - x_{min}}{x_{max} - x_{min}} z = scale(x) = [x - xmin]/[xmax - xmin]$$

Author(s)

Mauricio Zambrano-Bigiarini, <mauricio.zambrano@ing.unitn.it>

See Also

scale

Examples

```
## Loading temperature data ##
data(EbroTEMPts)

stdx(as.matrix(EbroTEMPts[1:70,10:13]))
```

---

subset.zoo *Subset*

Description

Extracts from a zoo object, all the values belonging to a given month, year or weather season

Usage

```
extractzoo(x, trgt, ...)
```

Arguments

x	'zoo' object
trgt	numeric or character indicating elements to extract from 'x'. Valid values are: 1) integer from 1 to 12: 'trgt' is considered as a month, and all the vaues in 'x' belonging to the month specified by 'trgt' will be extracted (1=JAN, 2=FEB,...., 12=DEC) 2) integer > 12: 'trgt' is considered as a year, and all the values in 'x' belonging to the year specified by 'trgt' will be extracted 3) character: 'trgt' is considered as a weather season, and all the values in 'x' belonging to the season specified by 'trgt' will be extracted. Valid values are: -) "DJF": December, January, February -) "MAM": March, April, May -) "JJA": June, July, August -) "SON": September, October, November
...	further arguments passed to or from other methods

Author(s)

Mauricio Zambrano-Bigiarini, <mauricio.zambrano@ing.unitn.it>

See Also

time2season, daily2annual, daily2monthly

Examples

```
### Loading temperature data ##
data(EbroTEMPts)

## Annual values of temperature at the station "T9105", stored in EbroTEMPts.
x <- sname2ts(EbroTEMPts,sname="T9105",dates=1,var.type="Temperature", tstep.out="daily")

## Extracting all the values belonging to February (FEb=2)
extractzoo(x, trgt=2)

## Extracting all the values belonging to the year 1970
extractzoo(x, trgt=1970)

## Extracting all the values belonging to the autumn
extractzoo(x, trgt="SON")
```

---

time2season *Time character -> Seasonal character*

Description

This function transforms a vector of dates into a vector of seasons (summer, winter, autumm, spring), considering that:

-) winter = DJF: December, January, February
-) spring = MAM: March, April, May
-) summer = JJA: June, July, August
-) autumm = SON: September, October, November

Usage

```
time2season(x, out.fmt = "months")
```

Arguments

x	vector with the dates that have to be transformed. class(x) must be "Date"
out.fmt	format of the output seasons. Possible values are: -) 'seasons' => "winter", "spring", "summer", autumm" -) 'months' => "DJF", "MAM", "JJA", SON"

Value

vector with the wheater season to which each date in 'x' belongs

Author(s)

Mauricio Zambrano-Bigiarini, <mauricio.zambrano@ing.unitn.it>

See Also

dip

Examples

```
## Sequence of daily dates between "1961-01-01" and "1961-12-31" ##
t <- dip("1961-01-01", "1961-12-31")
time2season(t)

## Sequence of monthly dates between "1961-01-01" and "1961-12-31" ##
t <- mip("1961-01-01", "1961-12-31")
time2season(t)
time2season(t, out.fmt="seasons")
```

---

vector2zoo *Vector -> Zoo*

Description

Transform a numericl vectorial and its corresponding dates into a 'zoo' variable, for being used by other procedures of this library

Usage

```
vector2zoo(x, dates, date.fmt = "%Y-%m-%d")
```

Arguments

x	numeric vector
dates	vector with the dates corresponding to each elemnt of 'x'
date.fmt	Character indicating format in which the dates are stored in 'dates', e.g, "%Y-%m-%d" ONLY required when class(dates)=="factor" or "numeric"

Author(s)

Mauricio Zambrano-Bigiarini, <mauricio.zambrano@ing.unitn.it>

Examples

```
## Loading temperature data ##
data(EbroQts)
x     <- EbroQts[,2]
dates <- EbroQts[,1]

## From 'character' to 'Date' class
dates <- as.Date(dates)

## From 'numeric' to 'zoo' class
x <- vector2zoo(x, dates)
```

zoo2RHtest *Hydrological Sampling Frequency*

Description

It creates the input file to the 'RHtest_dlyPrcp.r' script, used for testing the homogeneity of climatological time series (http://ccma.seos.uvic.ca)

This function generates a table indicating the number of days with information (<>NA's) within a data.frame

Usage

```
zoo2RHtest(x, fname="pcp.txt", tstep.out="daily", dec=".", na="-999.0")
```

Arguments

x	time series that will be written. class(x) must be 'zoo'
fname	filename of the precipitation time series
tstep.out	Character indicating the time step that have to be used for writting 'x' into the output file
dec	the string to use for decimal points in numeric or complex columns: must be a single character.
na	the string to use for missing values in the data

Author(s)

Mauricio Zambrano-Bigiarini, <mauricio.zambrano@ing.unitn.it>

References

http://ccma.seos.uvic.ca

Examples

```
## Loading precipitation data ##
data(EbroPPts)

# station ID
sname <- "P9056"

#Getting the monthly ts
pcp.m <- sname2ts(EbroPPts, sname, dates=1,  tstep.out="monthly", FUN=sum, na.rm=FALSE)

# From zoo to the input format required by 'FindU.dlyPrcp' function
zoo2RHtest(x=pcp.m, fname="pcp-monthly.txt", tstep.out="monthly", na="-999.0")

## Not run:
```

```
# Homogeneity analysis
FindU.dlyPrcp(InSeries="pcp-monthly.txt", output="pcp-monthly", MissingValueCode="-999.0", G

## End(Not run)
```

Index

Package 'hydroGOF'

December 1, 2009

Type Package

Title Goodness-of-fit for hydrological modelling

Version 0.1.3

Date 2009-12-01

Author Mauricio Zambrano Bigiarini

Maintainer Mauricio Zambrano Bigiarini <mauricio.zambrano@ing.unitn.it>

Description Both statistical and graphical goodness-of-fit measures between observed and simulated values, mainly oriented to hydrological modelling tasks

License LGPL-2

Depends R (>= 2.8.0)

Suggests zoo, hydroTSM

URL http://www.r-project.org

LazyLoad yes

R topics documented:

`hydroGOF-package` *Goodnes of Fit*

Description

Both statistical and graphical model evaluation techniques for assessing the goodnes-of-fit between observed and simulated values, for being used during the calibration, validation, and application of hydrological models.
Missing values in observed and/or simulated values can removed before the computations.

Quantitative statistics included are: Mean Error (**me**), Mean Absolute Error (**mae**), Root Mean Square Error (**rms**), Normalized Root Mean Square Error (**nrms**), Pearson Correltation coefficient (**r.Pearson**), Spearman Correltation coefficient (**r.Spearman**), Coefficient of Determination (**R2**), Ratio of Standard Deviations (**rSD**), Nash-Sutcliffe efficiency (**NSeff**), Modified Nash-Sutcliffe efficiency (**NSeff1**), Index of Agreement (**d**), Persistence Index (**PI**), Percent Bias (**pbias**) and the coef. of determination multiplied by the slope of the linear regresion between 'sim' and 'obs' (**bR2**)

Details

Package:	hydroGOF
Type:	Package
Version:	0.1.3
Date:	2009-12-01
License:	LGPL-2
LazyLoad:	yes

Author(s)

Mauricio Zambrano Bigiarini <mauricio.zambrano@ing.unitn.it>

Maintainer: Mauricio Zambrano Bigiarini <mauricio.zambrano@ing.unitn.it>

References

Boyle, D. P., H. V. Gupta, and S. Sorooshian (2000), Toward Improved Calibration of Hydrologic Models: Combining the Strengths of Manual and Automatic Methods, Water Resour. Res., 36(12),

3663–3674

Krause, P., Boyle, D. P., and Base, F.: Comparison of different efficiency criteria for hydrological model assessment, Adv. Geosci., 5, 89–97, 2005

Legates, D. R., and G. J. McCabe Jr. (1999), Evaluating the Use of "Goodness-of-Fit" Measures in Hydrologic and Hydroclimatic Model Validation, Water Resour. Res., 35(1), 233–241

Moriasi, D.N., Arnold, J.G., Van Liew, M.W., Bingner, R.L., Harmel, R.D., Veith, T.L. 2007. Model evaluation guidelines for systematic quantification of accuracy in watershed simulations Transactions of the ASABE. 50(3):885-900

Kitanidis, P. K., and R. L. Bras (1980), Real-Time Forecasting With a Conceptual Hydrologic Model 2. Applications and Results, Water Resour. Res., 16(6), 1034–1044

J.E. Nash and J.V. Sutcliffe, River flow forecasting through conceptual models. Part 1: a discussion of principles, J. Hydrol. 10 (1970), pp. 282–290

Yapo P. O., Gupta H. V., Sorooshian S., 1996. Automatic calibration of conceptual rainfall-runoff models: sensitivity to calibration data. Journal of Hydrology. v181 i1-4. 23–48

Examples

```
sim <- 2:11
obs <- 1:10
## Not run:
ggof(sim, obs)

## End(Not run)
```

`br2` *br2*

Description

Coefficient of determination (r2) multiplied by the slope of the regression line between 'sim' and 'obs', with treatment of missing values.

Usage

```
br2(sim, obs)
```

Arguments

`sim`	'numeric', 'vector', 'matrix' or 'data.frame' with simulated values
`obs`	'numeric', 'vector', 'matrix' or 'data.frame' with observed values

Details

$$br2 = \mid b \mid R2, \mid b \mid \leq 1; br2 = \mid b \mid R2, \mid b \mid > 1$$

A model that sistematically over or underpredicts all the time will still result in "good" 'r2' (close to 1), even if allpredctions were wrong (Krause et al., 2005). The 'br2' coefficient allows accounting for the discrepancy ibn the magnitude of two signals (depicted by 'b') as well as their dynamics (depicted by 'r2')

Note

The missing values in 'obs' and 'sim' are removed before the computation proceeds, and only those positions with non-missing values in 'obs' and 'sim' are considered in the computation

The slope 'b' is computed as the coefficient of the linear regression between 'sim' and 'obs', forcing the intercept be equal to zero.

Author(s)

Mauricio Zambrano Bigiarini <mauricio.zambrano@ing.unitn.it>

References

Krause, P., Boyle, D. P., and Base, F.: Comparison of different efficiency criteria for hydrological model assessment, Adv. Geosci., 5, 89-97, 2005

See Also

gof, cor, lm

Examples

```
sim <- 1:10
obs <- 1:10
br2(sim, obs)

sim <- 2:11
obs <- 1:10
br2(sim, obs)
```

ggof *Graphical Goodness of Fit*

Description

Graphical comparision bewtween two vectors (numeric, ts or zoo), with several numerical goodness of fit printed as a legend.
Missing values in observed and/or simulated values can removed before the computations.

Usage

```
ggof(sim, obs, dates, date.fmt = "%Y-%m-%d", var.names = c("Obs", "Sim"),
     var.units = c("m3/s", "m3/s"), main, xlab = "Time", ylab = "",
     ftype = "o", pt.style = "ts", ts.col = c("black", "blue"),
     ts.lwd = c(1, 1), ts.lty = c(1, 2), ts.pch = c(1, 9), ts.cex = c(0.6, 0.6),
     tick.tstep = "months", lab.tstep = "years", leg.gof = TRUE,  digits=2,
     leg.cex=1, FUN, na.rm = TRUE, cal.ini=NA, val.ini=NA)
```

Arguments

sim	'numeric', 'vector', 'matrix' or 'data.frame' with simulated values
obs	'numeric', 'vector', 'matrix' or 'data.frame' with observed values
dates	'character', 'factor", 'Date' indicating how to obtain the dates for the correponding values in the 'sim' and 'obs' time series If 'dates' is a factor, it have to be converted into 'Date' class, using the date format specified by 'date.fmt' If 'dates' is already of Date class, the following line verifies that the number of days in 'dates' be equal to the number of element in the time series corresponding to the 'st.name' station
date.fmt	OPTIONAL. Character indicating the format in which the dates entered are stored in 'dates', 'cal.ini' and 'val.ini'. Default value is "%Y-%m-%d" ONLY required when class(dates)== "character" or "factor" or when 'cal.ini' or 'val.ini' is provided.
var.names	string representing the type of variable being plotted (e.g., "Precipitation", "Temperature", "Flow",...). ONLY used for labelling the axes
var.units	string representing the measurement unit of the variable being plotted (e.g., "mm" for precipitation, "C" for temperature, "m3/s" for flow,...). ONLY used for labelling the axes
main	string representing the main title of the plot
xlab	label for the 'x' axis
ylab	label for the 'y' axis

ftype	string indicating how many plots are desired by the user. Valid values are: -) 'o' : only the original 'sim' and 'obs' time series are plotted -) 'dm' : it assumes that 'sim' and 'obs' are daily time series and Daily and Monthly values are plotted -) 'ma' : it assumes that 'sim' and 'obs' are monthly time series and Monthly and Annual values are plotted -) 'dma': it assumes that 'sim' and 'obs' are daily time series and Daily, Monthly and Annual values are plotted
pt.style	Character indicating if the 2 ts have to be plotted as lines or bars. When 'ftype' is NOT 'o', it only applies for the annual values. Valid values are: -) "ts" : (default) each ts is ploted as a lines along the 'x' axis -) "bar": the 2 series are plotted as a barplot.
ts.col	vector with the colors of 'sim' and 'obs'
ts.lwd	vector with the line width of sim' and 'obs'
ts.lty	vector with the line type of sim' and 'obs'
ts.pch	vector with the type of symbol for 'x' and 'y'. (e.g., 1: whithe circle; 9: white rhombus with a cross inside)
ts.cex	vector with the values controlling the size of text and symbols of 'x' and 'y' with respect to the default
tick.tstep	string indicating the time step that have to be used for putting the ticks ont he time axis. Valid values are: -) 'days', -) 'months', -) 'years'
lab.tstep	string indicating the time step that have to be used for putting the labels ont he time axis. Valid values are: -) 'days', -) 'months', -) 'years'
leg.gof	logical, indicating if several numerical goodness of fit have to be computed between 'sim' and 'obs', and ploted as a legend on the graph. If leg.gof=TRUE, then 'x' is considered as observed and 'y' as simulated values (for some gof functions this is important).
digits	OPTIONAL, only used when 'leg.gof=TRUE'. Decimal places used for rounding the goodness-of-fit indexes.
leg.cex	OPTIONAL. ONLY used when 'leg.gof' is TRUE. Character expansion factor *relative* to current 'par("cex")'. Used for text, and provides the default for 'pt.cex' and 'title.cex'. Default value = 1
FUN	OPTIONAL, ONLY required when 'ftype' is in c('dm', 'ma', 'dma'). Function that have to be applied for transforming from daily to monthly or annual time step (e.g., for precipitation FUN MUST be "sum", for temperature and flow time series, FUN MUST be "mean")

na.rm	Logical. ONLY matters when 'step.out' is "monthly' or 'annual' -) TRUE : the annual mean value is computed considering only those values different from NA -) FALSE: if there is AT LEAST one NA within a year, the monthly mean value is NA
cal.ini	OPTIONAL. Character with the date in which the calibration period started. ONLY used for drawing a vertical red line at this date.
val.ini	OPTIONAL. Character with the date in which the validation period started. ONLY used for drawing a vertical red line at this date.

Details

Plots observed and simulated alues in the same graph.

If 'leg.cex' is TRUE, it computes It computes the numerical values of:
'me', 'mae', 'rms', 'nrms', 'r.Pearson', 'r.Spearman', 'r2', 'rSD', 'NSeff', 'NSeff1', 'd', 'PI', 'PBIAS', 'r.Pearson', 'r.Spearman'

Value

me	Mean Error
mae	Mean Absolute Error
rms	Root Mean Square Error
nrms	Normalized Root Mean Square Error
r.Pearson	Pearson Correltation coefficient (-1 <= r <= 1)
r.Spearman	Spearman Correltation coefficient (-1 <= r <= 1)
R2	Coefficient of Determination (0 <= R2 <= 1). Gives the proportion of the variance of one variable that is predictable from the other variable
rSD	Ratio of Standard Deviations, rSD = SD(sim) / SD(obs)
NSeff	Nash-Sutcliffe Efficiency (-Inf <= NSeff <= 1)
NSeff1	Modified Nash-Sutcliffe Efficiency
d	Index of Agreement (0 <= d <= 1)
PI	Persistence Index (0 <= PI <= 1)
PBIAS	Percent Bias (-1 <= PBIAS <= 1)
bR2	r2 multiplied by the coefficient of the regression line between 'sim' and 'obs' (0 <= bR2 <= 1)

Author(s)

Mauricio Zambrano Bigiarini <mauricio.zambrano@ing.unitn.it>

References

Legates, D. R., and G. J. McCabe Jr. (1999), Evaluating the Use of "Goodness-of-Fit" Measures in Hydrologic and Hydroclimatic Model Validation, Water Resour. Res., 35(1), 233–241.

Krause P., Boyle D.P., and B\"ase F., Comparison of different efficiency criteria for hydrological model assessment, Advances in Geosciences 5 (2005), pp. 89–97

Moriasi, D.N., Arnold, J.G., Van Liew, M.W., Bingner, R.L., Harmel, R.D., Veith, T.L. 2007. Model evaluation guidelines for systematic quantification of accuracy in watershed simulations Transactions of the ASABE. 50(3):885-900

Boyle, D. P., H. V. Gupta, and S. Sorooshian (2000), Toward Improved Calibration of Hydrologic Models: Combining the Strengths of Manual and Automatic Methods, Water Resour. Res., 36(12), 3663–3674

Kitanidis, P. K., and R. L. Bras (1980), Real-Time Forecasting With a Conceptual Hydrologic Model 2. Applications and Results, Water Resour. Res., 16(6), 1034–1044

J.E. Nash and J.V. Sutcliffe, River flow forecasting through conceptual models. Part 1: a discussion of principles, J. Hydrol. 10 (1970), pp. 282–290

Yapo P. O., Gupta H. V., Sorooshian S., 1996. Automatic calibration of conceptual rainfall-runoff models: sensitivity to calibration data. Journal of Hydrology. v181 i1-4. 23–48

See Also

gof, plot2

Examples

```
sim <- 2:11
obs <- 1:10
## Not run:
ggof(sim, obs)

## End(Not run)
```

---

gof *Numerical Goodness of Fit*

Description

Numerical goodness of fit between 'sim and 'obs', with treatment of missing values. Several performance indexes for comparing two vectors, matrix or data.frames

Usage

```
gof(sim, obs, do.spearman = FALSE, na.rm = TRUE, digits=2, ...)
```

Arguments

`sim`	'numeric', 'vector', 'matrix' or 'data.frame' with simulated values
`obs`	'numeric', 'vector', 'matrix' or 'data.frame' with observed values
`do.spearman`	logical. Indicates if the Spearman correltation have to be computed. The default is FALSE
`na.rm`	a logical value indicating whether 'NA' values should be stripped before the computation proceeds.
`digits`	decimal places used for rounding the goodness-of-fit indexes.
`...`	further arguments passed to or from other methods.

Value

`me`	Mean Error
`mae`	Mean Absolute Error
`rms`	Root Mean Square Error
`nrms`	Normalized Root Mean Square Error
`r.Pearson`	Pearson Correltation coefficient (-1 <= r <= 1)
`r.Spearman`	Spearman Correltation coefficient (-1 <= r <= 1)
`R2`	Coefficient of Determination (0 <= R2 <= 1). Gives the proportion of the variance of one variable that is predictable from the other variable
`rSD`	Ratio of Standard Deviations, rSD = SD(sim) / SD(obs)
`NSeff`	Nash-Sutcliffe Efficiency (-Inf <= NSeff <= 1)
`NSeff1`	Modified Nash-Sutcliffe Efficiency
`d`	Index of Agreement (0 <= d <= 1)
`PI`	Persistence Index (0 <= PI <= 1)
`PBIAS`	Percent Bias (-1 <= PBIAS <= 1)
`bR2`	R2 multiplied by the coefficient of the regression line between 'sim' and 'obs' (0 <= bR2 <= 1)

Note

Missing values in 'obs' and/or 'sim' can be removed before the computations, depndeing on the value of 'na.rm'.

Although 'r.Pearson' and 'r2' have been widely used for model evaluation, these statistics are oversensitive to outliers and insensitive to additive and proportional differences between model predictions and measured data (Legates and McCabe, 1999)

Author(s)

Mauricio Zambrano Bigiarini <mauricio.zambrano@ing.unitn.it>

References

Legates, D. R., and G. J. McCabe Jr. (1999), Evaluating the Use of "Goodness-of-Fit" Measures in Hydrologic and Hydroclimatic Model Validation, Water Resour. Res., 35(1), 233–241.

Krause P., Boyle D.P., and B\"ase F., Comparison of different efficiency criteria for hydrological model assessment, Advances in Geosciences 5 (2005), pp. 89–97

Moriasi, D.N., Arnold, J.G., Van Liew, M.W., Bingner, R.L., Harmel, R.D., Veith, T.L. 2007. Model evaluation guidelines for systematic quantification of accuracy in watershed simulations Transactions of the ASABE. 50(3):885-900

Boyle, D. P., H. V. Gupta, and S. Sorooshian (2000), Toward Improved Calibration of Hydrologic Models: Combining the Strengths of Manual and Automatic Methods, Water Resour. Res., 36(12), 3663–3674

Kitanidis, P. K., and R. L. Bras (1980), Real-Time Forecasting With a Conceptual Hydrologic Model 2. Applications and Results, Water Resour. Res., 16(6), 1034–1044

J.E. Nash and J.V. Sutcliffe, River flow forecasting through conceptual models. Part 1: a discussion of principles, J. Hydrol. 10 (1970), pp. 282–290

Yapo P. O., Gupta H. V., Sorooshian S., 1996. Automatic calibration of conceptual rainfall-runoff models: sensitivity to calibration data. Journal of Hydrology. v181 i1-4. 23–48

See Also

me, mae, rms, nrms, rSD, NSeff, NSeff1, IoA, PI, pbias, br2

Examples

```
sim <- 1:10
obs <- 1:10
gof(sim, obs)

sim <- 2:11
obs <- 1:10
gof(sim, obs)
```

`IoA` *Index of Agreement*

Description

This function computes the Index of Agreement between 'sim' and 'obs, with treatment of missing values.

If 'x' is a matrix or a data frame, a vector of the Index of Agreement of the columns is returned.

Usage

```
IoA(sim, obs, ...)
```

Arguments

`sim`	'numeric', 'vector', 'matrix' or 'data.frame' with simulated values
`obs`	'numeric', 'vector', 'matrix' or 'data.frame' with observed values
`...`	further arguments passed to or from other methods.

Details

$$d = \frac{1 - \sum_{i=1}^{N} (O_i - S_i)^2}{\sum_{i=1}^{N} \left|S_i - \bar{O}\right| + \left|O_i - \bar{O}\right|}$$

The Index of Agreement (d) developed by Willmott (1981) as a standardized measure of the degree of model prediction error and varies between 0 and 1. A value of 1 indicates a perfect match, and 0 indicates no agreement at all (Willmott, 1981).

The index of agreement can detect additive and proportional differences in the observed and simulated means and variances; however, it is overly sensitive to extreme values due to the squared differences (Legates and McCabe, 1999).

Note

The missing values in 'obs' and 'sim' are removed before the computation proceeds, and only those positions with non-missing values in 'obs' and 'sim' are considered in the computation.

Author(s)

Mauricio Zambrano Bigiarini <mauricio.zambrano@ing.unitn.it>

References

Willmott, C.J. 1981. On the validation of models. Physical Geography, 2, 184–194

Willmott, C. J. (1984). On the evaluation of model performance in physical geography. Spatial Statistics and Models, G. L. Gaile and C. J. Willmott, eds., 443-460

Legates, D. R., and G. J. McCabe Jr. (1999), Evaluating the Use of "Goodness-of-Fit" Measures in Hydrologic and Hydroclimatic Model Validation, Water Resour. Res., 35(1), 233–241

Examples

```
sim <- 1:10
obs <- 1:10
IoA(sim, obs)

sim <- 2:11
obs <- 1:10
IoA(sim, obs)
```

`mae.data.frame` *Mean Absolute Error*

Description

Mean Absolute Error between 'sim' and 'obs', in the same units of 'sim' and 'obs', with treatment of missing values.

Usage

```
mae(sim, obs, na.rm = TRUE, ...)
```

Arguments

`sim`	'numeric', 'vector', 'matrix' or 'data.frame' with simulated values
`obs`	'numeric', 'vector', 'matrix' or 'data.frame' with observed values
`na.rm`	a logical value indicating whether 'NA' values should be stripped before the computation proceeds.
`...`	further arguments passed to or from other methods.

Author(s)

Mauricio Zambrano Bigiarini <mauricio.zambrano@ing.unitn.it>

References

http://en.wikipedia.org/wiki/Mean_absolute_error

See Also

me

Examples

```
sim <- 1:10
obs <- 1:10
mae(sim, obs)

sim <- 2:11
obs <- 1:10
mae(sim, obs)
```

---

me *Mean Error*

Description

Mean Error between 'sim' and 'obs', in the same units of 'sim' and 'obs', with treatment of missing values.

Usage

```
me(sim, obs, na.rm = TRUE, ...)
```

Arguments

sim	'numeric', 'vector', 'matrix' or 'data.frame' with simulated values
obs	'numeric', 'vector', 'matrix' or 'data.frame' with observed values
na.rm	a logical value indicating whether 'NA' values should be stripped before the computation proceeds.
...	further arguments passed to or from other methods.

Author(s)

Mauricio Zambrano Bigiarini <mauricio.zambrano@ing.unitn.it>

See Also

mae

Examples

```
sim <- 1:10
obs <- 1:10
me(sim, obs)

sim <- 2:11
obs <- 1:10
me(sim, obs)
```

---

nrms *Normalized Root Mean Square Error*

Description

Normalized Root Mean Square Error between 'sim' and 'obs', with treatment of missing values.

Usage

```
nrms(sim, obs, na.rm = TRUE, ...)
```

Arguments

sim	'numeric', 'vector', 'matrix' or 'data.frame' with simulated values
obs	'numeric', 'vector', 'matrix' or 'data.frame' with observed values
na.rm	a logical value indicating whether 'NA' values should be stripped before the computation proceeds.
...	further arguments passed to or from other methods.

Details

$$nrms = 100 \frac{\sqrt{\frac{1}{N}\sum_{i=1}^{N}(S_i - O_i)^2}}{O_{max} - O_{min}}$$

Note

The result is given in percentage (%)

Author(s)

Mauricio Zambrano Bigiarini <mauricio.zambrano@ing.unitn.it>

See Also

rms

Examples

```
sim <- 1:10
obs <- 1:10
nrms(sim, obs)

sim <- 2:11
obs <- 1:10
nrms(sim, obs)
```

`NSeff` *Nash-Sutcliffe Efficiency*

Description

Nash-Sutcliffe efficiency between 'sim' and 'obs', with treatment of missing values.

Usage

```
NSeff(sim, obs, ...)
```

Arguments

`sim`	'numeric', 'vector', 'matrix' or 'data.frame' with simulated values
`obs`	'numeric', 'vector', 'matrix' or 'data.frame' with observed values
`...`	further arguments passed to or from other methods.

Details

$$NSeff = 1 - \frac{\sum_{i=1}^{N} (S_i - O_i)^2}{\sum_{i=1}^{N} \left(O_i - \bar{O}\right)^2}$$

The Nash-Sutcliffe efficiency (NSeff) is a normalized statistic that determines the relative magnitude of the residual variance ("noise") compared to the measured data variance ("information") (Nash and Sutcliffe, 1970). NSeff indicates how well the plot of observed versus simulated data fits the 1:1 line.

Nash-Sutcliffe efficiencies range from -Inf to 1. Essentially, the closer to 1, the more accurate the model is.

-) NSeff = 1, corresponds to a perfect match of modeled to the observed data.
-) NSeff = 0, indicates that the model predictions are as accurate as the mean of the observed data,
-) -Inf < NSeff < 0, indicates that the observed mean is better predictor than the model.

Author(s)

Mauricio Zambrano Bigiarini <mauricio.zambrano@ing.unitn.it>

References

Nash, J. E. and J. V. Sutcliffe (1970), River flow forecasting through conceptual models part I -A discussion of principles, Journal of Hydrology, 10 (3), 282-290.

http://en.wikipedia.org/wiki/Nash%E2%80%93Sutcliffe_model_efficiency_coefficient

See Also

NSeff1

Examples

```
sim <- 1:10
obs <- 1:10
NSeff(sim, obs)

sim <- 2:11
obs <- 1:10
NSeff(sim, obs)
```

NSeff1 *Modified Nash-Sutcliffe Efficiency*

Description

Modified Nash-Sutcliffe Efficiency between 'sim' and 'obs', with treatment of missing values.

Usage

```
NSeff1(sim, obs, ...)
```

Arguments

sim	'numeric', 'vector', 'matrix' or 'data.frame' with simulated values
obs	'numeric', 'vector', 'matrix' or 'data.frame' with observed values
...	further arguments passed to or from other methods.

Details

$$NSeff = 1 - \frac{\sum_{i=1}^{N} |S_i - O_i|}{\sum_{i=1}^{N} |O_i - \bar{O}|}$$

The modified NSeff is not inflated by the squared values of the differences, because the squares are replaced by absolute values.

Author(s)

Mauricio Zambrano Bigiarini <mauricio.zambrano@ing.unitn.it>

References

Legates, D. R., and G. J. McCabe Jr. (1999), Evaluating the Use of "Goodness-of-Fit" Measures in Hydrologic and Hydroclimatic Model Validation, Water Resour. Res., 35(1), 233-241.

See Also

NSeff

Examples

```
sim <- 1:10
obs <- 1:10
NSeff1(sim, obs)

sim <- 2:11
obs <- 1:10
NSeff1(sim, obs)
```

---

pbias *Percent Bias*

Description

Percent Bias between 'sim' and 'obs', with treatment of missing values.

Usage

```
pbias(sim, obs, ...)
```

Arguments

sim	'numeric', 'vector', 'matrix' or 'data.frame' with simulated values
obs	'numeric', 'vector', 'matrix' or 'data.frame' with observed values
...	further arguments passed to or from other methods.

Details

$$PBIAS = 100 \frac{\sum_{i=1}^{N} (S_i - O_i)}{\sum_{i=1}^{N} O_i}$$

Percent bias (PBIAS) measures the average tendency of the simulated values to be larger or smaller than their observed ones.

The optimal value of PBIAS is 0.0, with low-magnitude values indicating accurate model simulation. Positive values indicate overestimation bias, whereas negative values indicate model underestimation bias

Note

The result is given in percentage (%)

Author(s)

Mauricio Zambrano Bigiarini <mauricio.zambrano@ing.unitn.it>

References

Yapo P. O., Gupta H. V., Sorooshian S., 1996. Automatic calibration of conceptual rainfall-runoff models: sensitivity to calibration data. Journal of Hydrology. v181 i1-4. 23-48.

Examples

```
sim <- 1:10
obs <- 1:10
pbias(sim, obs)

sim <- 2:11
obs <- 1:10
pbias(sim, obs)
```

PI *Persistence Index*

Description

Persistence Index between 'sim' and 'obs', with treatment of missing values.

Usage

```
PI(sim, obs, ...)
```

Arguments

sim	'numeric', 'vector', 'matrix' or 'data.frame' with simulated values
obs	'numeric', 'vector', 'matrix' or 'data.frame' with observed values
...	further arguments passed to or from other methods.

Details

$$PI = 1 - \frac{\sum_{i=2}^{N} (S_i - O_i)^2}{\sum_{i=1}^{N-1} (O_{i+1} - O_i)^2}$$

Persistence Index (Kitadinis and Bras, 1980; Corradini et al., 1986) is used to compare the model performance against a simple model using the observed value of the previous day as the prediction for the current day.

The coefficient of persistence compare the predictions of the model with the predictions obtained by assuming that the process is a Wiener process (variance increasing linearly with time), in which case, the best estimate for the future is given by the latest measurement (Kitadinis and Bras, 1980).

Persistence model efficiency (PI) is a normalized model evaluation statistic that quantifies the relative magnitude of the residual variance (noise) to the variance of the errors obtained by the use of a simple persistence model (Moriasi et al., 2007).

Value

PI ranges from 0 to 1, with PME = 1 being the optimal value and it should be larger than 0.0 to indicate a minimally acceptable model performance.

Author(s)

Mauricio Zambrano Bigiarini <mauricio.zambrano@ing.unitn.it>

References

Kitanidis, P.K., and Bras, R.L. 1980. Real-time forecasting with a conceptual hydrologic model. 2. Applications and results. Water Resources Research, Vol. 16, No. 6, pp. 1034:1044.

Moriasi, D. N. et al. (2007). Model Evaluation Guidelines for Systematic Quantification of Accuracy in Watershed Simulations. Transactions of the ASABE, 50:(3), 885-900

Examples

```
sim <- 1:10
obs <- 1:10
PI(sim, obs)

sim <- 2:11
obs <- 1:10
PI(sim, obs)
```

`plot2` *Plot 2 Time Series*

Description

Plot 2 Time Series

Usage

```
plot2(x, y, plot.type = "single", var.names = c("Observed", "Simulated"),
      var.units = c("", ""), main, tick.tstep = "months", lab.tstep = "years",
      ts.col = c("black", "blue"), ts.lwd= c(1,2), ts.lty=c(1,9),
      ts.pch = c(1, 2), ts.cex = c(0.6, 0.6), xlab = "Year", ylab = "Observed",
      pt.style = "ts", add = FALSE, leg.gof = FALSE, digits=2, leg.cex = 1,
      cal.ini=NA, val.ini=NA, date.fmt="%Y-%m-%d")
```

Arguments

x	time series that will be plotted. class(x) must be 'ts' or 'zoo'. If leg.gof=TRUE, then 'x' is considered as observed (for some gof functions this is important)
y	time series that will be plotted. class(x) must be 'ts' or 'zoo'. If leg.gof=TRUE, then 'y' is considered as simulated values (for some gof functions this is important)
plot.type	character that indicates if the 2 ts have to be ploted in the same window or in two different vertical ones. Valid values are: -) "single" : (default) superimposes the 2 ts on a single plot -) "multiple": plots the 2 series on 2 multiple vertical plots
var.names	character vector with the types (names) of variables being plotted, (e.g, "Precipitation", "Temperature" or "Flow"). ONLY used for labelling the axes
var.units	character representing the measurement unit of the variable being plotted, e.g., "mm" for precipitation, "C" for temperature, and "m3/s" for flow.
main	an overall title for the plot: see 'title'
tick.tstep	string indicating the time step that have to be used for putting the ticks ont he time axis. Valid values are: -) 'days', -) 'months', -) 'years'
lab.tstep	string indicating the time step that have to be used for putting the labels ont he time axis. Valid values are: -) 'days' -) 'months' -) 'years'
ts.col	vector with the colors of 'x' and 'y'
ts.lwd	vector with the line width of 'x' and 'y'
ts.lty	vector with the line type of 'x' and 'y'
ts.pch	vector with the type of symbol for 'x' and 'y'. (e.g.: 1: whithe circle; 9: white rhombus with a cross inside)
ts.cex	vector with the values controlling the size of text and symbols of 'x' and 'y' with respect to the default
xlab	label for the 'x' axis
ylab	label for the 'y' axis
pt.style	Character that indicates if the 2 ts have to be plotted as lines or bars. Valid values are: -) "ts" : (default) each ts is ploted as a lines along the 'x' axis -) "bar": the 2 series are plotted as a barplot.
add	logical indicating if other plots will be added in further calls to this function. -) 'add=FALSE' => the plot and the legend are plotted on the same graph -) 'add=TRUE' => the legend is plotted in a new graph, usually when called from another function (e.g.: 'ggof')

leg.gof	logical, indicating if several numerical goodness of fit have to be computed between 'sim' and 'obs', and ploted as a legend on the graph. If leg.gof=TRUE (default value), then 'x' is considered as observed and 'y' as simulated values (for some gof functions this is important). This legend is ONLY plotted when 'plot.type' is 'single'
digits	OPTIONAL, only used when 'leg.gof=TRUE'. Decimal places used for rounding the goodness-of-fit indexes.
leg.cex	OPTIONAL. ONLY used when 'leg.gof' is TRUE. Character expansion factor *relative* to current 'par("cex")'. Used for text, and provides the default for 'pt.cex' and 'title.cex'. Default value = 1
cal.ini	OPTIONAL. Character with the date in which the calibration period started. ONLY used for drawing a vertical red line at this date.
val.ini	OPTIONAL. Character with the date in which the validation period started. ONLY used for drawing a vertical red line at this date.
date.fmt	OPTIONAL. Character indicating the format in which the dates entered are stored in 'cal.ini' and 'val.ini'. Default value is "%Y-%m-%d" ONLY required when 'cal.ini' or 'val.ini' is provided.

Author(s)

Mauricio Zambrano Bigiarini <mauricio.zambrano@ing.unitn.it>

See Also

ggof

Examples

```
sim <- 2:11
obs <- 1:10
## Not run:
plot2(sim, obs)

## End(Not run)
```

---

rms *Root Mean Square Error*

Description

Root Mean Square (RMS) Error between 'sim' and 'obs', in the same units of 'sim' and 'obs', with treatment of missing values.

Usage

```
rms(sim, obs, na.rm = TRUE, ...)
```

Arguments

sim	'numeric', 'vector', 'matrix' or 'data.frame' with simulated values
obs	'numeric', 'vector', 'matrix' or 'data.frame' with observed values
na.rm	a logical value indicating whether 'NA' values should be stripped before the computation proceeds.
...	further arguments passed to or from other methods.

Details

$$rms = \sqrt{\frac{1}{N}\sum_{i=1}^{N}(S_i - O_i)^2}$$

Value

RMS gives the standard deviation of the model prediction error. A samller value indicates better model performance.

Author(s)

Mauricio Zambrano Bigiarini <mauricio.zambrano@ing.unitn.it>

References

http://en.wikipedia.org/wiki/Root_mean_square_deviation

See Also

nrms, ssq

Examples

```
sim <- 1:10
obs <- 1:10
rms(sim, obs)

sim <- 2:11
obs <- 1:10
rms(sim, obs)
```

rSD *Ratio of Standard Deviations*

Description

Ratio of Standard Deviations between 'sim' and 'obs', with treatment of missing values.

Usage

```
rSD(sim, obs, na.rm = TRUE, ...)
```

Arguments

sim	'numeric', 'vector', 'matrix' or 'data.frame' with simulated values
obs	'numeric', 'vector', 'matrix' or 'data.frame' with observed values
na.rm	a logical value indicating whether 'NA' values should be stripped before the computation proceeds.
...	further arguments passed to or from other methods.

Author(s)

Mauricio Zambrano Bigiarini <mauricio.zambrano@ing.unitn.it>

See Also

sd

Examples

```
sim <- 1:10
obs <- 1:10
rSD(sim, obs)

sim <- 2:11
obs <- 1:10
rSD(sim, obs)
```

ssq *Sum of the Squared Residuals*

Description

Sum of the Squared Residuals between 'sim' and 'obs', with treatment of missing values. Its units are the squared measurement units of 'sim' and 'obs'

Usage

```
ssq(sim, obs, ...)

## Default S3 method:
ssq(sim, obs, na.rm = TRUE, ...)
```

Arguments

sim	'numeric', 'vector', 'matrix' or 'data.frame' with simulated values
obs	'numeric', 'vector', 'matrix' or 'data.frame' with observed values
na.rm	a logical value indicating whether 'NA' values should be stripped before the computation proceeds.
...	further arguments passed to or from other methods.

Author(s)

Mauricio Zambrano Bigiarini <mauricio.zambrano@ing.unitn.it>

Examples

```
sim <- 1:10
obs <- 1:10
ssq(sim, obs)

sim <- 2:11
obs <- 1:10
ssq(sim, obs)
```

`valid.indexes` *Validation of Indexes*

Description

Identify the indexes that are valid (not missing) simulataneously in 'obs' and 'sim'.

Usage

```
valid.indexes(obs, sim)
```

Arguments

`obs`	'numeric', 'vector', 'matrix' or 'data.frame' with observed values
`sim`	'numeric', 'vector', 'matrix' or 'data.frame' with simulated values

Note

This function is used for the treatment of missing values.

Author(s)

Mauricio Zambrano Bigiarini <mauricio.zambrano@ing.unitn.it>

Examples

```
sim <- 1:5
obs <- c(1, NA, 3, NA, 5)
valid.indexes(sim, obs)
```

Index